

POLYIMIDES FOR ADVANCED APPLICATIONS

by

David C. Rich

S.B., Chemical Engineering
Massachusetts Institute of Technology, 1992

Submitted to the Department of Materials Science and Engineering
in Partial Fulfillment of the Requirements for the Degree of

DOCTOR OF PHILOSOPHY
in Polymers

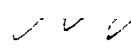
at the
Massachusetts Institute of Technology
May 3, 1996

©Massachusetts Institute of Technology. All rights reserved.

Signature of Author.....

David Rich
Department of Materials Science and Engineering

Certified by.....

 Professor Peggy Cebe
Thesis Supervisor

Accepted by.....

.....
PROFESSOR MICHAEL RUBNER
Chairman, Departmental Committee on Graduate Studies

MASSACHUSETTS INSTITUTE
OF TECHNOLOGY

JUN 24 1996 Science

POLYIMIDES FOR ADVANCED APPLICATIONS

by

DAVID C. RICH

Submitted to the Department of Materials Science and Engineering
on May 3, 1996 in partial fulfillment of the requirements for the
Degree of Doctor of Philosophy in Polymers

Thesis Supervisor: Professor Peggy Cebe

ABSTRACT

The processing, structure, and properties of aromatic polyimides are investigated for their use as liquid crystal alignment layers and in other advanced applications. Probimide 32 polyamide-imide and Probimide 412 inherently photosensitive polyimide are the primary materials which are evaluated. The physical and chemical changes that occur in the polyimide films as the materials undergo cloth brushing, UV irradiation, and thermal curing treatments are of chief interest. Polyimide films are studied by conventional characterization techniques, by property prediction methods, and by a new technique called "alignment layer relaxation," which can be used to detect thermal transitions in polymer surface layers. The alignment relaxation technique is based upon the observation that as alignment layers are cured above their glass transition temperatures, their liquid crystal aligning properties are irreversibly destroyed. The aligning performance of polymer films is evaluated by the phase-sensitive laser optical transmission of parallel-aligned nematic liquid crystal cells placed between crossed polarizers. A non-contact method of alignment of surface aligning liquid crystals is also introduced, in which polyamide-imide alignment films are irradiated with linearly polarized short wavelength ultraviolet light ($\lambda=254$ nm). The technique produces alignment that appears to be comparable with that achieved by conventional contact brushing. The photo-aligned polyamide-imide is believed to develop its aligning properties via a chain scission process that occurs in the alignment films as a consequence of the UV exposure, though the exact mechanism of the alignment is not completely understood at this time. The removal of solvent from polyimide films upon

curing is investigated by thermogravimetric analysis and Fourier transform infrared spectroscopy. Solvent is found to be rapidly eliminated from polyamide-imide thin films ($\sim 450\text{\AA}$) at low temperatures ($\sim 110^\circ\text{C}$). High temperature cures are found to chemically crosslink the polyimides, especially if the treatment proceeds in an air environment. Also, comparison of predicted and measured refractive indices of polyimides materials indicate that, upon thermal imidization, non-fluorinated polyimides undergo chain packing and/or charge transfer processes that appear to be substantially mitigated in polyimides with bulky fluorinated spacer groups.

Table of Contents

Abstract.....	2
Table of Contents.....	4
List of Figures.....	9
List of Tables.....	19
Acknowledgments.....	21
Chapter 1. Introduction and Theory.....	22
1.1. Synthesis and Processing.....	22
1.1.1. General scheme.....	22
1.1.2. Photosensitive polyimide precursors.....	24
1.1.3. Preimidized polyimides.....	24
1.1.4. Preimidized, photosensitive polyimides.....	26
1.2. Structure.....	26
1.2.1. Macroscopic orientation of polymer films.....	26
1.2.2. Crystalline packing.....	26
1.2.3. Chain-chain interactions.....	28
1.2.4. Liquid crystalline nematic order and alignment.....	29
1.3. Properties.....	30
1.3.1. Quantitative relationship between polymer chemistry and refractive index.....	30
1.3.2. Property changes associated with charge transfer complexation.....	37
1.3.3. Anisotropy of optical properties.....	39
1.3.4. Measurement of index of refraction.....	45
1.3.5. Optical transmission model for liquid crystal alignment.....	46
1.4. Performance: Liquid Crystal Alignment Layers.....	53
1.4.1. Liquid crystal surface alignment on brushed polymer films.....	53
1.4.2. Alternative treatments to polymer layers for liquid crystal alignment.....	55

1.4.3. An LCD device: the TN-LCD.....	58
1.5. References.....	60
Chapter 2. Refractive Indices of Aromatic Polyimides.....	72
2.1. Introduction.....	72
2.2. Experimental Techniques.....	74
2.2.1. Polyimide film preparation.....	74
2.2.2. Zone drawing.....	74
2.2.3. Refractive index measurement.....	75
2.2.4. Refractive index prediction.....	76
2.3. Relationship Between Polyimide Chemistry and Refractive Index.....	76
2.3.1. Amorphous, non-fluorinated polyimides.....	76
2.3.2. Semicrystalline polyimides.....	77
2.3.3. Polyimides containing hexafluoroisopropylidene (6F).....	77
2.3.4. Polyimides containing fluorinated alkoxy side chains.....	78
2.3.5. Polyimides containing pentafluorosulfanyl (SF5).....	79
2.4. Relationship Between Polyimide Processing and Refractive Index.....	89
2.4.1. In-plane birefringence in polyimide films.....	89
2.4.2. Birefringence in zone drawn films.....	90
2.4.3. Effect of cure temperature on refractive index.....	91
2.4.4. Effect of post-cure annealing on NEW-TPI polyimide.....	96
2.5. Conclusions.....	96
2.6. References.....	99

Chapter 3. Curing Study of Probimide® 412 Preimidized Photosensitive Polyimide.....	104
3.1. Introduction.....	104
3.2. Experimental.....	105
3.2.1. Polymer film samples.....	105
3.2.2. Measurement techniques.....	106
3.3. Results and Discussion.....	108
3.3.1. Coloration and brittleness.....	108
3.3.2. Thermogravimetric analysis.....	108
3.3.3. Dynamic mechanical analysis.....	116
3.3.4. Index of refraction.....	124
3.3.5. Fourier transform infrared spectroscopy.....	124
3.4. Conclusions.....	128
3.5. References.....	139
Chapter 4. Effect of Cure Conditions on Probimide® 32 Polyamide-imide.....	141
4.1. Introduction.....	141
4.2. Experimental.....	142
4.2.1. Polymer film processing.....	142
4.2.2. Measurement techniques.....	143
4.3. Results and Discussion.....	143
4.3.1. Coloration and brittleness.....	143
4.3.2. Thermogravimetric analysis.....	144
4.3.3. Dynamic mechanical analysis.....	152
4.3.4. Index of refraction.....	153
4.3.5. Fourier transform infrared spectroscopy.....	160

4.3.6. Differential scanning calorimetry.....	167
4.4. Conclusions.....	185
4.5. References.....	185
Chapter 5. Alignment of Liquid Crystals on Brushed Polymer Layers.....	187
5.1. Introduction.....	187
5.2. Experimental Section.....	188
5.2.1. Construction of LC alignment cells.....	189
5.2.2. Evaluation of alignment cells.....	195
5.3. Results and Discussion.....	205
5.3.1. Brushing-induced alignment in Probimide 32 polyamide-imide.....	205
5.3.2. Brushing-induced alignment in other polymers.....	207
5.3.3. FTIR spectra of Probimide 32 polyamide-imide alignment films.....	209
5.3.4. Atomic force microscopy of brushed polyamide-imide alignment films.....	210
5.3.5. <i>In situ</i> thermal stability of LC alignment on brushed Probimide 32 polyamide-imide layers.....	216
5.3.6. “Liquid crystal alignment relaxation” - a new technique for measuring thermal transitions in surface layers.....	217
5.4. Experimental Error.....	227
5.5. Conclusions.....	228
5.6. References.....	229

Chapter 6. Liquid Crystal Surface Alignment on Photo-irradiated Polymer Layers.....	232
6.1. Introduction.....	232
6.2. Experimental Section.....	232
6.2.1. Photo-alignment technique.....	232
6.2.2. Comments regarding the methodology by which the PAI was selected.....	234
6.3. Results and Discussion.....	234
6.3.1. Evidence of liquid crystal alignment upon LP-UV exposure.....	234
6.3.2. Effect of unpolarized UV exposure.....	237
6.3.3. Effects of linearly polarized UV exposure.....	240
6.4. Conclusions.....	250
6.5. Subjects for further work.....	250
6.6. References.....	252
Appendix A. Description of Nematic Alignment in Terms of the Poincare Sphere.....	253
A.1. The Poincare sphere.....	253
A.2. Changes in polarization state of the Poincare sphere.....	254
A.3. Examples of nematic LC orientation.....	257
A.4. Effect of misalignment of the LCs.....	259
A.5. References.....	259

List of Figures

Figure 1.1.	General synthesis of polyimides.....	23
Figure 1.2.	Processing scheme of photosensitive polyimide precursors.....	25
Figure 1.3.	Types of orientation in polymer films. a.) isotropic orientation, b.) in-plane orientation, and c.) uniaxial orientation.....	27
Figure 1.4.	Charge transfer interactions in polyimides.....	28
Figure 1.5.	A nematic liquid crystalline phase with director D'	29
Figure 1.6.	Representations of nematic liquid crystalline material. a.) no alignment and b.) bulk alignment along director D'	31
Figure 1.7.	Sample calculation of the index of refraction of polystyrene using the van Krevelen / Vogel technique.....	35
Figure 1.8.	Bicerano prediction for the refractive index of polystyrene.....	38
Figure 1.9.	Examples of optical anisotropy. a.) birefringence on the molecular level, b.) birefringence on the microscopic level in a polymer spherulite, c.) birefringence on the microscopic level in a nematic grain, d.) bulk birefringence in an in-plane oriented film, and e.) bulk birefringence in a film of aligned liquid crystals.....	41
Figure 1.10.	A thick semicrystalline polymer block that is microscopically birefringent but has $n_x=n_y=n_z$	44
Figure 1.11.	Prism coupling technique for measuring index of refraction.....	45
Figure 1.12.	Graphical representation of a parallel-aligned liquid crystal plate between a polarizer (p) and an analyzer (A).....	46

Figure 1.13.	Plot of $I(\phi)/I(45^\circ)$ vs ϕ	48
Figure 1.14.	Elliptically polarized light with handedness (left or right), azimuth (α), and ellipticity ($\beta = a/b$).....	49
Figure 1.15.	Parallel-aligned liquid crystals with inhomogeneities.....	50
Figure 1.16.	Rays of light passing through different points 1 or 2 of the inhomogenous liquid crystal sample and emerging at 1' or 2' with different polarization states.....	51
Figure 1.17.	Alignment of liquid crystals on brushed polymer surfaces.....	53
Figure 1.18.	A polymer surface being rubbed by a brushing wheel.....	54
Figure 1.19.	The photochemical reaction in polyvinylmethoxycinnamate and the oriented structure, proposed by Schadt, that is formed by exposure to linearly polarized UV.....	56
Figure 1.20.	Anisotropic chain degradation proposed to occur in a polyimide film during exposure to linearly polarized UV.....	57
Figure 1.21.	States of a twisted nematic liquid crystal display (TN-LCD) device. a.) off state and b.) on state.....	59
Figure 2.1.	Zone drawing method.....	75
Figure 2.2.	Experimental and predicted refractive indices of non-fluorinated polyimides in Table 2.1.....	79
Figure 2.3.	Wide angle X-ray scattering (WAXS) of: a.)PMDA-ODA and b.) ODPA-PDA.....	80
Figure 2.4.	Measured and predicted refractive indices of semicrystalline polyimides in Table 2.2.....	82

Figure 2.5.	Measured and predicted refractive indices of 6F polyimides in Table 2.3.....	84
Figure 2.6.	Predicted refractive indices (Bicerano's method) of polyimides with fluorinated alkoxy side chains.....	86
Figure 2.7.	Refractive index vs. draw ratio for 6FDA-4BDAP in the direction of the draw and normal to the draw.....	91
Figure 2.8.	Refractive indices of several polyimides as a function of cure temperature.....	93
Figure 2.9.	Predicted (Bicerano's method) vs. measured refractive indices of several polyimides. a.) Predicted values of the polyamic acid precursors vs. measured values of the films after only 100°C cure and b.) Predicted values of the polyimides vs. measured values after 300°C cure.....	94
Figure 2.10.	a.) Average refractive index of NEW-TPI vs. post-cure annealing temperature and b.) Birefringence vs. post-cure annealing temperature.....	97
Figure 2.11.	a.) Average refractive index vs. post-cure annealing time at 290°C and b.) Birefringence vs. post-cure annealing time at 290°C.....	98
Figure 3.1.	Preparation of bulk films. a.) Coating and blading process for optimization of film smoothness and thickness uniformity. b.) Pre-cure air-drying chamber.....	107
Figure 3.2.	Thermogravimetric weight loss and derivative of weight loss vs. temperature for Probimide [®] 412 thick films with highest cure temperature: (a) room temperature, (b) 100°C, (c) 140°C, (d) 200°C, and (e) 300°C.....	110

Figure 3.3.	Thermogravimetric weight loss vs. temperature for Probimide [®] 412 thick films baked at 100°C, UV irradiated or unirradiated.....	115
Figure 3.4.	1 Hz dynamic Young's modulus and loss factor, $\tan\delta$, vs. temperature for Probimide [®] 412 thick films with highest cure temperature: (a) 100°C, (b) 200°C, (c) 300°C (in nitrogen), (d) 400°C (in nitrogen).....	118
Figure 3.5.	1 Hz dynamic Young's modulus and loss factor, $\tan\delta$, vs. temperature for Probimide [®] 412 thick films cured at 100°C, UV irradiated (dashed line) or unirradiated (solid line).....	122
Figure 3.6.	1 Hz dynamic Young's modulus and loss factor, $\tan\delta$, vs. temperature for Probimide [®] 412 thick films cured at 300°C, in air (dashed line) or in nitrogen (solid line).....	123
Figure 3.7.	Indices of refraction of spin coated Probimide [®] 412 films as a function of highest cure temperature.....	125
Figure 3.8.	Indices of refraction of spin coated Probimide 412 films as a function of UV exposure time.....	126
Figure 3.9.	Relative IR absorbance vs. wavenumber for spin coated Probimide [®] 412 films softbaked 15 minutes at 100°C and exposed to UV: (a) 0 minutes (no irradiation), (b) 2 minutes, (c) 10 minutes, (d) 50 minutes.....	130
Figure 3.10.	Relative IR absorbance vs. wavenumber (2000-4000 cm^{-1} range) for spin coated Probimide [®] 412 films with highest cure temperature treatment: (a) 300°C (3 hours in nitrogen), (b) 300°C (1 hour in air), (c) 300°C (3 hours in air), (d) 400°C (1 hour in nitrogen).....	134

- Figure 3.11. Relative IR absorbance vs. wavenumber (400-2000 cm^{-1} range) for spin coated Probimide[®] 412 films with highest cure temperature treatment: (a) 300°C (3 hours in nitrogen), (b) 300°C (1 hour in air), (c) 300°C (3 hours in air), (d) 400°C (1 hour in nitrogen)..... 135
- Figure 4.1. Weight loss and derivative of weight loss vs. temperature for N-methyl pyrrolidone (NMP)..... 145
- Figure 4.2. Weight loss and derivative of weight loss vs. temperature for Probimide[®] 32 thick films: a.) dried under an air current at room temperature, b.) then baked 6 hours at 100°C, c.) then 3 hours at 200°C, d.) then 3 hours at 300°C..... 146
- Figure 4.3. Weight loss and derivative of weight loss vs. temperature for Probimide[®] 32 thick films baked at 100°C for 1, 6, or 24 hours..... 151
- Figure 4.4. Young's modulus and dissipation factor, $\tan\delta$, for Probimide[®] 32 thick films: a.) cured 6 hours at 100°C, b.) then 3 hours at 200°C, c.) then 3 hours at 300°C in either air or, d.) nitrogen..... 154
- Figure 4.5. a.) Indices of refraction of spin coated Probimide[®] 32 films vs. highest cure temperature in air. Cure cycle was 15 minutes at 100°C, 1 hour at 200°C, 1 hour at 300°C. b.) Refractive indices for different cure conditions at 300°C..... 158
- Figure 4.6. Relative absorbance vs. wavenumber (400-2000 cm^{-1}) for spin coated Probimide[®] 32 films: a.) baked 10 min. at 100°C, b.) 10 min. at 120°C, c.) 10 min. at 140°C, d.) 10 min. at 160°C, e.) 10 min. at 180°C, f.) 10 min. at 200°C..... 168
- Figure 4.7. Relative absorbance vs. wavenumber (2000-4000 cm^{-1}) for spin coated Probimide[®] 32 films: a.) baked 10 minutes at 100°C, b.) then 10 minutes at 120°C, c.) then 10 minutes at 140°C, d.) then 10 minutes at 160°C, e.) then 10 minutes at 180°C, f.) then 10 minutes at 200°C..... 174

Figure 4.8.	Relative absorbance vs. wavenumber (400-2000 cm^{-1}) for spin coated Probimide [®] 32 films: a.) baked 15 minutes at 100°C, b.) then 1 hour at 200°C, c.) then 1 hour at 300°C in either air or, d.) nitrogen.....	175
Figure 4.9.	Relative absorbance vs. wavenumber (2000-4000 cm^{-1}) for spin coated Probimide [®] 32 films: a.) baked 15 minutes at 100°C, b.) then 1 hour at 200°C, c.) then 1 hour at 300°C in either air or, d.) nitrogen.....	179
Figure 4.10.	Ratio of relative absorbance of peak at 1680 cm^{-1} to that of the 1370 cm^{-1} vs. highest cure temperature.....	180
Figure 4.11.	Endothermic heat flow vs. temperature for Probimide [®] 32 thick films: a.) baked 6 hours at 100°C, b.) then 3 hours at 200°C, c.) then 3 hours at 300°C in either air or, d.) nitrogen.....	181
Figure 5.1.	Alignment film brushing technique.....	191
Figure 5.2.	Cell construction procedure. (a.) alignment film formation, (b.) empty cell construction, (c.) cell filling, (d.) cell annealing, and (e.) cell sealing.....	193
Figure 5.3.	Qualitative observations of liquid crystal alignment cells between crossed polarizers.....	196
Figure 5.4.	Optical transmission apparatus with phase-sensitive detection.....	198
Figure 5.5.	Instrument connections for phase-sensitive detection.....	199
Figure 5.6.	Measure relative intensity vs. expected relative intensity for phase-sensitive detection of neutral density filtered light. a.) linear scale, and b.) log-log scale.....	201

- Figure 5.7. Measure relative intensity vs. expected relative intensity for phase-sensitive detection of light diminished by two consecutive polarizers with their polarizing axes lying at an angle χ . a.) linear scale, and b.) log-log scale..... 202
- Figure 5.8. Adjustment made for a cell with small degree of twist distortion q . The first liquid crystal surface director N is oriented parallel to polarizer P . The second surface director is N' . The analyzer is adjusted by q from A to A' such that A' is perpendicular to N' 204
- Figure 5.9. a.) Intensity / intensity at 45° vs. rotation angle for a nematic liquid crystal cell aligned with brushed Probimide 32 polyamide-imide layers. The x-axis is the azimuth of the alignment director with respect to the polarizer. b.) Relative intensity vs. rotation angle for nematic liquid crystal cell with untreated Probimide 32 polyamide-imide layers. The x-axis represents the azimuth of an arbitrary reference axis with respect to the polarizer..... 206
- Figure 5.10. Values of Φ , the effective angle of misalignment, for liquid crystal cells produced with alignment films of brushed PMDA-APB polyimide (PI), PMDA-APB poly(amic acid) (PAA), polyamide-imide (PAI), poly(phenylene ether sulfone) (PPES), poly(vinyl alcohol) (PVA), poly(methyl methacrylate) (PMMA), and polycarbonate (PC). All cells but those produced with PMMA and PC appear to have very strong macroscopic alignment..... 209
- Figure 5.11. Relative absorbance vs. wavenumber for Probimide 32 polyamide-imide coated from 3wt% solids content and softbaked at 110°C , with final film thickness approximately 450\AA 211

Figure 5.12.	Relative absorbance vs. wavenumber for a brushed Probimide 32 polyamide-imide thin film. a.) Incident infrared electric field polarized parallel to the brushing direction. b.) Incident infrared electric field polarized perpendicular to the brushing direction.....	212
Figure 5.13.	Atomic force microscopy (AFM) images of polyamide-imide films. a.) brushed, and b.) unbrushed.....	214
Figure 5.14.	$I(0^\circ)/I(45^\circ)$ vs. temperature for a polyamide-imide aligned liquid crystal cell undergoing an annealing cycle of systematically increasing temperature treatments.....	216
Figure 5.15.	$I(0^\circ)/I(45^\circ)$ vs. post-brush cure temperature for LC alignment cells produced with Probimide 32 polyamide-imide alignment films.....	218
Figure 5.16.	Depiction of the structure of the alignment layer films during alignment relaxation process of the polyamide-imide. The amorphous chains begin randomly coiled in the plane of the film (a). They are oriented by the brushing process (b). The orientation is reversed by annealing above T_g (c).....	219
Figure 5.17.	$I(0^\circ)/I(45^\circ)$ vs. post-brush cure temperature for liquid crystal alignment cells produced with brushed polyamide-imide that were either softbaked (filled circles) or cured at 300°C in air (open circles) prior to brushing.....	220
Figure 5.18.	$I(0^\circ)/I(45^\circ)$ vs. post-brush cure temperature for liquid crystal alignment cells produced with brushed poly(phenylene ether sulfone) alignment films.....	221
Figure 5.19.	$I(0^\circ)/I(45^\circ)$ vs. post-brush cure temperature for liquid crystal alignment cells produced with brushed PMDA-APB alignment films. a.) PMDA-APB poly(amic acid) softbaked only, b.) PMDA-APB hard baked 275°C 1 hour, and c.) PMDA-APB cured at 221°C for 30 minutes.....	223

Figure 5.20.	$I(0^\circ)/I(45^\circ)$ vs. post-brush cure temperature for liquid crystal alignment cells produced with poly(vinyl alcohol) alignment layers.....	226
Figure 6.1.	Exposure technique for irradiating alignment films with linearly polarized ultraviolet light (LP-UV).....	233
Figure 6.2.	$I(\phi)/I(45^\circ)$ vs. rotation angle for liquid crystal alignment cell produced with polyamide-imide alignment layers that have been irradiated with LP-UV for 25 minutes.....	235
Figure 6.3.	$I(0^\circ)/I(45^\circ)$ vs. LP-UV exposure time for liquid crystal cells produced with LP-UV irradiated polyamide-imide alignment films.....	236
Figure 6.4.	Relative absorbance vs. wavenumber for a Probimide 32 polyamide-imide film. a.) unexposed to UV, and b.) UV exposed.....	238
Figure 6.5.	$I(0^\circ)/I(45^\circ)$ vs. post-brush curing temperature for liquid crystal cells produced with UV exposed (squares) and unexposed (circles) polyamide-imide alignment layers.....	240
Figure 6.6.	Relative absorbance vs. wavenumber for polyamide-imide layers exposed to linearly polarized ultraviolet ($\lambda=245$ nm). a.) 2 hour exposure, UV axis parallel to incident IR axis, b.) 2 hour exposure, UV axis perpendicular to incident IR axis, c.) 4 hour exposure, UV axis parallel to incident IR axis, and d.) 4 hour exposure, UV axis perpendicular to incident IR axis.....	242
Figure 6.7	$I(0^\circ)/I(45^\circ)$ vs. post-aligning cure temperature for liquid crystals cells produced with polyamide-imide alignment films that have been exposed to LP-UV (triangles) or brushed (circles).....	246
Figure 6.8.	Atomic force microscopy (AFM) image of LP-UV irradiated polyamide-imide films.....	247

Figure 6.9.	$I(0^\circ)/I(45^\circ)$ vs. post-aligning unpolarized UV exposure time for liquid crystal cells produced from polyamide-imide alignment films that were exposed to LP-UV (open circles) or brushed (filled circles).....	249
Figure A.1.	Lines of latitude (l) on the Poincare sphere representing ellipticity (β).....	253
Figure A.2.	Lines of longitude (L) on the Poincare sphere representing azimuth (α).....	254
Figure A.3.	Movement along the Poincare sphere from reference point P along the small circle of the sphere centered on OS, where O is the center of the sphere and S represents the azimuthal angle parallel to the fast vibration axis of the crystal.....	255
Figure A.4.	The relative change in polarization state induced by the analyzer is a longitudinal shift through the arc length between the analyzer (A) and the point of reference (P). X1 moves to X2.....	256
Figure A.5.	The arc length from reference state P1 to final state P3 is given by 2ρ . The intensity transmitted by the system is $\cos^2\rho$ where full intensity is unity.....	257
Figure A.6.	Parallel aligned LC plate with nematic vector parallel to P.....	258
Figure A.7.	LC cell with nematic vector 45° with respect to P and A. The light is elliptically polarized by the sample as it moves along the prime meridian to point E.....	258
Figure A.8.	Effect of random inhomogenous region on the Poincare sphere analysis. The shaded region represents a distribution of polarization states deviating from A.....	259

List of Tables

Table 1.1.	Meaning of the ratio of transmitted intensity at 0° (MIN) to transmitted intensity at 45° (MAX).....	52
Table 2.1.	Dianhydride (R) and diamine (Z) elements of polyimides in Figure 2.2.....	81
Table 2.2.	Dianhydride (R) and diamine (Z) elements of polyimides in Figure 2.4.....	83
Table 2.3.	Dianhydride (R) and diamine (Z) elements of the 6F polyimides in Figure 2.5.....	85
Table 2.4.	Dianhydride (R) and diamine (Z) elements of polyimides with fluorinated alkoxy side chains.....	87
Table 2.5.	Measured and predicted refractive indices of SF ₅ polyimides.....	88
Table 2.6.	Optical properties of PMDA-ODA.....	89
Table 2.7.	Refractive indices of optically transparent polyimides.....	90
Table 3.1.	Color and brittleness of Probimide® 412 films cured at progressively higher temperatures.....	108
Table 3.2.	IR absorption regions of Probimide® 412.....	129
Table 4.1.	Color and brittleness of Probimide® 32 films cured at progressively higher temperatures.....	144
Table 4.2.	IR absorption regions of NMP and xylene.....	161

Table 4.3.	Partial list of IR absorption bands in Probimide [®] 32 polyamide-imide.....	163
Table 5.1	Composition of Merck E7 nematic liquid crystals from Cognard's chromatographic analysis.....	194
Table 5.2.	Physical properties of Merck E7 nematic liquid crystals.....	195
Table 5.3.	Settings for EG&G lock-in amplifier used for phase- sensitive detection of chopped light.....	200
Table 5.4.	List of polymers which were examined as liquid crystal aligning agents and some of their characteristics.....	208
Table 5.5.	Relative ratios of the heights of the imide N-C (1370 cm^{-1}) peaks to the imide C=O (1720 cm^{-1}) peaks for brushed Probimide 32 layers.....	216

ACKNOWLEDGMENTS

There are so very many people I would like to acknowledge for helping this project go forward, but knowing where to begin is not difficult at all. First, I would like to thank my advisor Professor Peggy Cebe for seeing this project through to the end, and for her ceaseless commitment to my graduate education. Peggy has been an immense source of inspiration to me, as she has been to so many other students.

I would also like to thank other individuals whose work has provided direct help in seeing this research go forward. I would like to thank Dr. Enid Sichel, not only for the contributions she has made to the project, but also for her never-ending support and career advice. I would also like to acknowledge UROP student Roland Desrochers for his contributions to the project.

I am also grateful to the Minnesota Mining and Manufacturing Company for providing funding for this project. Specifically, I would like to thank Dr. David Cross, Dr. Robert Wenz, and Dr. Timothy Gardner for their consultations and advice.

I also thank the various individuals and institutions who donated materials and supplies. First, I would like to thank Dr. Anne St. Clair of the NASA Langley Research Center for providing numerous polyimide samples. I would also like to thank OCG Microelectronic Materials, Inc., Nippon Electric Glass, Amoco Chemical Company, and Nissan Chemical Company.

Next, I would like to express my appreciation to the following Professors and their research groups for allowing use of laboratory equipment: Professor Anne Mayes for the spin coater, Professor Michael Rubner for the FTIR, Professor Frederick McGarry for the curing furnace, and Professor Stephen Senturia for the Metricon prism coupler. I would also like to thank the individuals who helped instruct me in using the equipment. Specifically, I would like to thank Dr. Ken Zernach for help with the FTIR, and Dr. Greg Kellogg for help with the spin coater.

I also would like to acknowledge my thesis readers Professor Frederick McGarry, Professor David Roylance, and Professor Lionel Kimerling. I immensely appreciate their time and effort.

Finally, I would like to thank my colleagues, friends, and family for the love and support they have provided. I thank all recent members of Professor Cebe's Polymer Physics Group for providing a friendly and supportive work environment. I express my wishes for the best of success to all of them.

Chapter 1. Introduction and Theory

Polyimides are high temperature, high performance polymers with substantial technological importance [1-6]. They exhibit excellent mechanical, thermal, adhesive, and chemical-resistant properties that are highly advantageous for aerospace, electronic packaging, display, waveguide, and other high technology applications. Many polyimides with varying properties and behavior are available commercially.

In this thesis, I report the structure and properties of polyimides and examine their use in liquid crystal alignment applications. It is the goal of this chapter to introduce the reader to polyimides, and to introduce some of the main concepts that are essential for understanding the topics addressed in this thesis. First, I discuss in this chapter the **synthesis and processing** of polyimides. Then, I discuss the key material **structure** issues that are pertinent to this thesis. Third, I discuss material **properties**, with my focus on the optical properties of polyimides and nematic liquid crystals. Finally, I discuss the **performance** of polyimides in nematic liquid crystal alignment applications.

1.1. Synthesis and Processing

1.1.1. General scheme

One synthesizes polyimides by a step growth polymerization, followed by a ring closure reaction (see Figure 1.1) [7]. A polycondensation reaction between a dianhydride and a diamine forms a polyamic acid, the precursor to polyimide. This reaction generally proceeds in a polar, high boiling point solvent such as γ -butyrolactone (GBL, $T_b = 205^\circ\text{C}$ [8]), dimethylacetamide (DMAc, $T_b = 166^\circ\text{C}$ [9]), or N-methylpyrrolidone (NMP, $T_b = 202^\circ\text{C}$ [10]). A high temperature cure, usually 300°C or above, forges a ring closure, or imidization, reaction between the acid and amide groups of the polyamic acid precursor, converting the precursor to polyimide. One can also carry out a chemical imidization at low temperature by adding an acetic anhydride/pyridine solution [7]. Water is removed from the polymer chain during the imidization step.

Polyimides usually serve as film coatings. Spin coating, solvent casting, and doctor blading are common processing techniques. Manufacturers also produce thick extruded polyimide films. Subsequent processing of the films depends on the application.

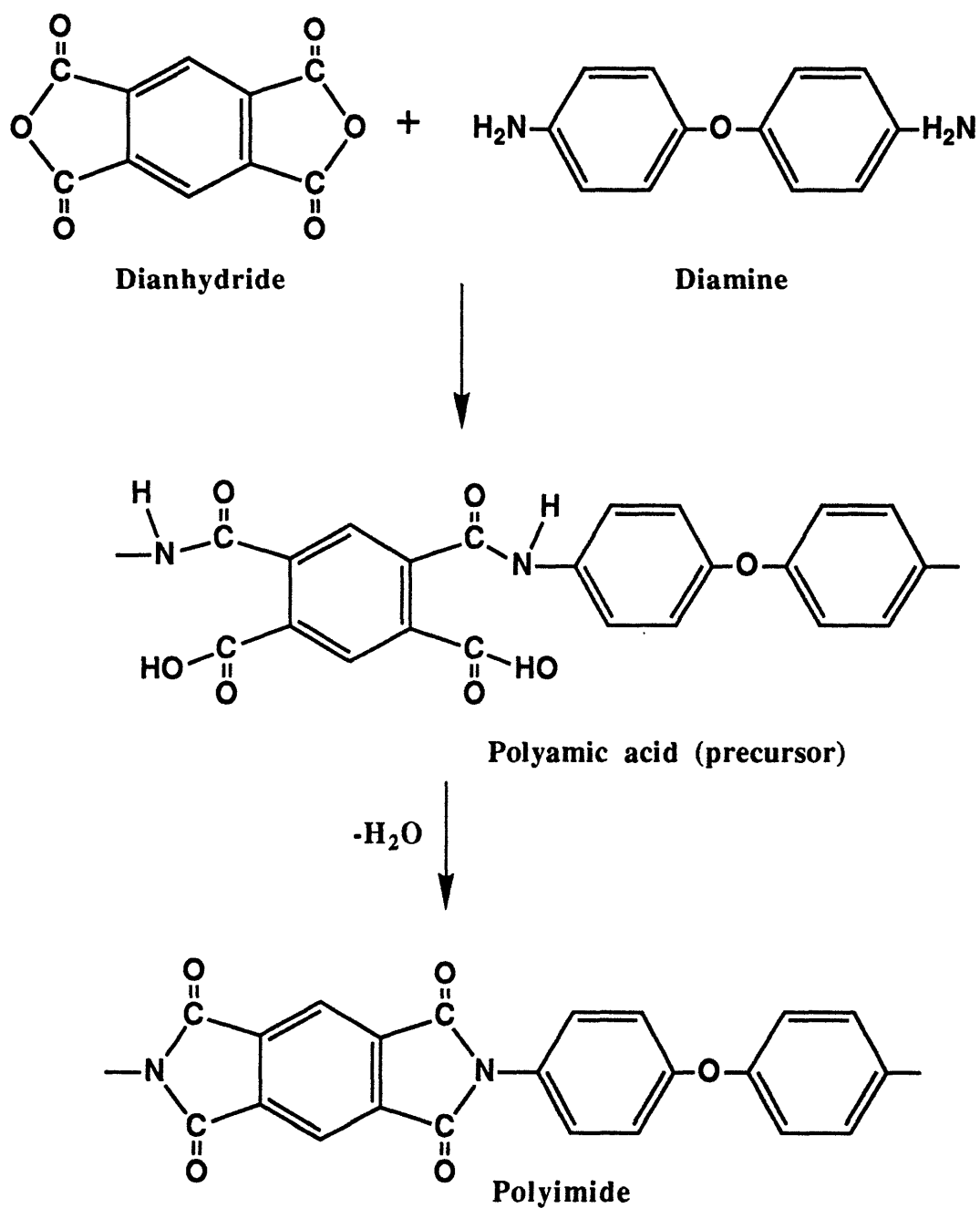


Figure 1.1. General synthesis scheme of polyimides. PMDA-ODA shown here.

1.1.2. Photosensitive polyimide precursors

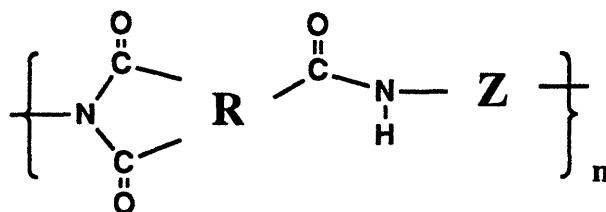
Photosensitive polyimides [11] which can be patterned by photolithography are of tremendous interest to the electronics industry. Workers at Siemens [12,13] introduced polyimide precursors that could be processed as negative photoresists. The photo-processing scheme is shown in Figure 1.2. Soluble polyamic esters with photoreactive ester groups crosslink upon exposure to UV radiation. Development of unexposed regions yields an insoluble photopattern of crosslinked polyamic ester precursor. The precursor material requires a high temperature cure after photoprocessing in order to convert it to polyimide. During this step, the side chain crosslinks are released from the main chain. Since the polymer is converted from a soluble polymer (polyamic ester) to an insoluble polymer (polyimide), there is generally a great deal of solvent loss and film shrinkage during this step. In addition, organic molecules which can potentially plasticize the film are released from the polymer during the cure.

1.1.3. Preimidized polyimides

Polyimides in solution are generally in their preconverted (polyamic acid) form. That is because the fully converted materials are usually insoluble. Workers at NASA Langley Research Center [14] have investigated techniques of improving polyimide solubility, which include incorporating bridging groups between phenyl rings in the main chain and manipulating the isomeric points of attachment of the bridging groups to the phenyl rings.

Some polyimides are highly soluble in their fully converted form and can be coated directly from solution [15,16]. They do not need to be cured for the purpose of imidization, but for the removal of solvent. These fully converted materials are typically soluble in the same organic solvent as polyamic acids, i.e., NMP, GBL, etc.

One important class of polyimides are polyamide-imides [17,18], which have the general form:



where R and Z are, in general, aromatic groups. Although these polymers are not widely known to be soluble in the fully converted state [19], a fully imidized and soluble polyamide-imide is manufactured by OCG Microelectronic Materials [18]. This material, called Probimide 32, is of substantial importance to the research presented in this document.

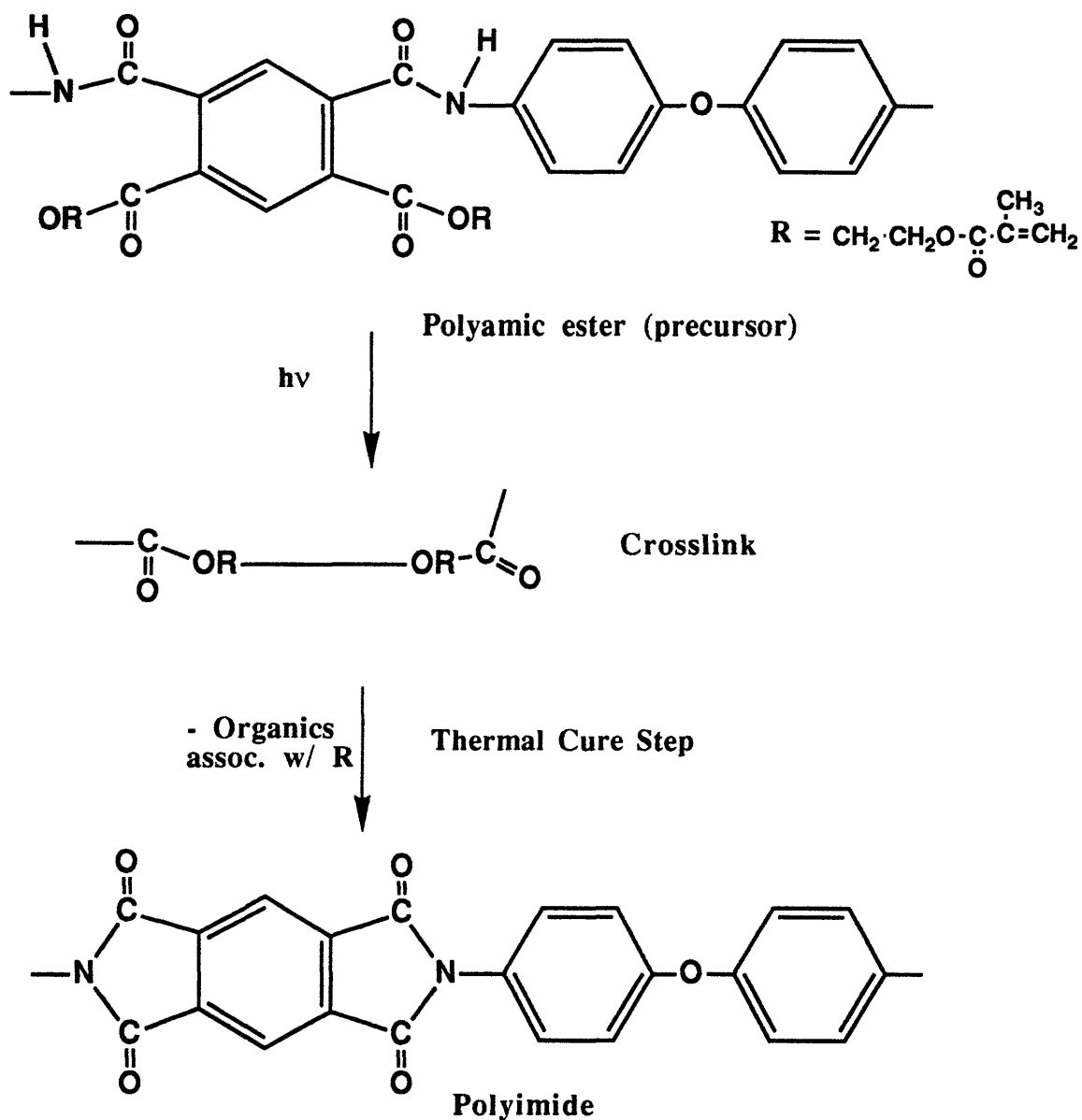


Figure 1.2. Processing scheme of photosensitive polyimide precursors.

1.1.4. Preimidized, photosensitive polyimides

Researchers at Ciba Geigy in 1985 introduced polyimides that are both photosensitive and soluble in the fully converted, imidized state [15,16]. There has been much work done since then investigating their properties [20-27] and photo-reaction mechanism [28-31]. Solubility in the converted state was achieved by the addition of alkyl substituents to the polymer's phenyl groups. These alkyl groups are also involved in the polymer's photochemical reaction. These materials can be processed as negative photoresists from the preimidized polymer in solution without the need for imidization. This material, unlike the photosensitive precursor, undergoes minimal shrinkage and does not contain organic by-products upon process completion. A material of this type, its properties, and its reaction mechanism are discussed in Chapter 3.

1.2. Structure

1.2.1. Macroscopic orientation of polymer films

Three levels of macroscopic orientation which might exist in polymer films are depicted in Figure 1.3. Figure 1.3(a) shows a polymer which is an unoriented random coil. This structure is completely isotropic. Figure 1.3(b), on the other hand, shows a structure that is in-plane oriented. That is, the molecular chains of the polymer preferentially lie parallel to the plane of the film. This structure is typical of thin coated films [32-42], especially those with rigid backbones. Polymeric films can also orient along one axis of the film, as shown in Figure 1.3(c). One way to induce this type of orientation in thick films is to draw the material [43-49]. In very thin films on the order of hundreds of Angstroms, this type of orientation can be produced by brushing [50-55] the films along one axis with a cloth. The significance of brushed polymer layers in the alignment of liquid crystals will be discussed in section 1.4.

1.2.2. Crystalline packing

Though most polyimides are amorphous, some can be semicrystalline [56-66]. Currently, it is difficult to know for certain, prior to synthesis and experimental determination, whether a polyimide with a certain chemical composition will readily crystallize. In addition, since, in general, the softening and melting temperatures of these polymers are extremely high, it is generally difficult to control crystallinity in these

materials. However, crystallinity is somewhat controllable in several thermoplastic polyimides [59,60,62-66] designed with low glass transition and melting temperatures.

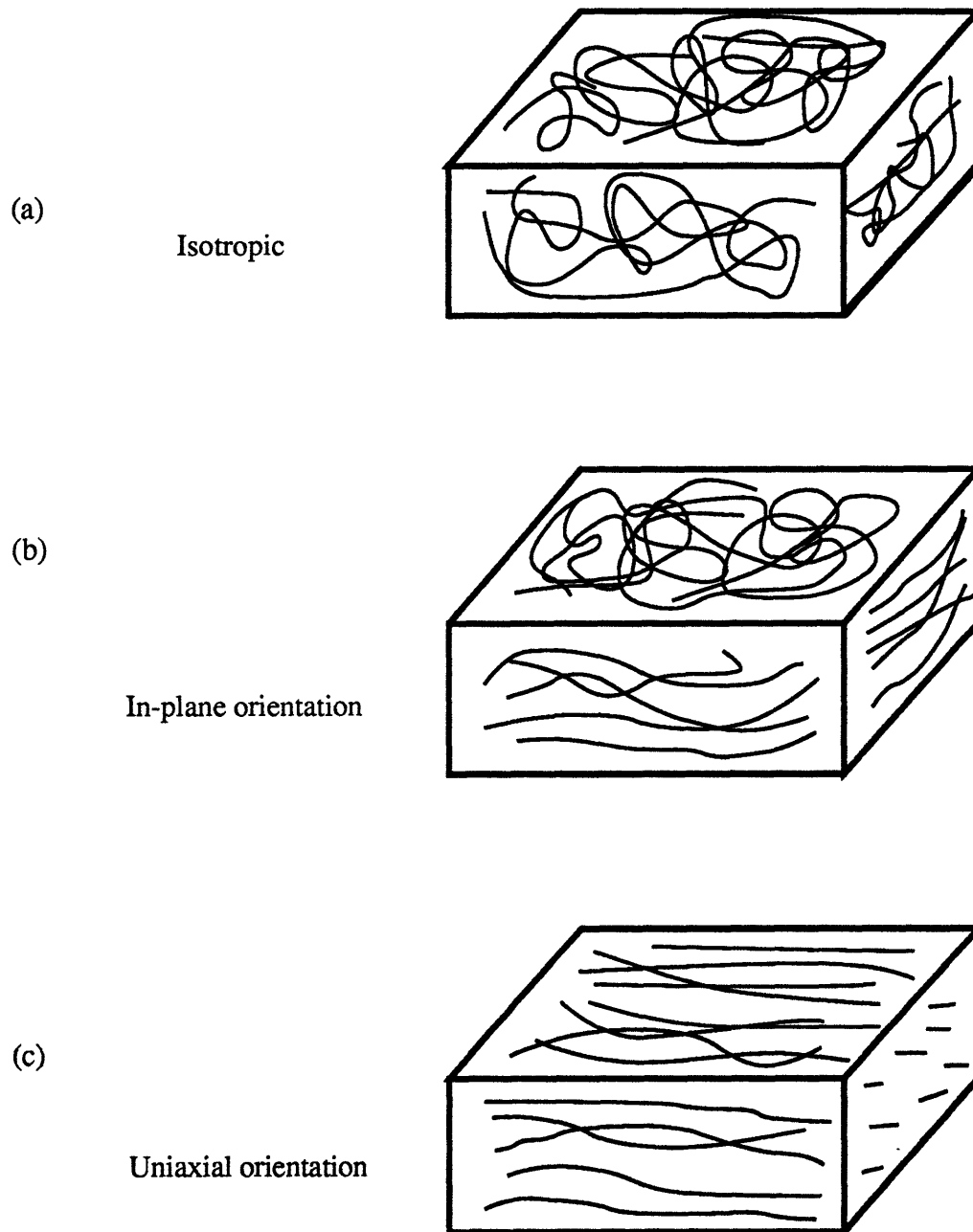


Figure 1.3. Types of orientation in polymer films: a.) isotropic orientation, b.) in-plane orientation, c.) uniaxial orientation.

1.2.3. Chain-chain interactions

Many workers believe that charge transfer complexation [67-74], a strong interchain electronic interaction, occurs in polyimides. Dine-Hart and Wright [67], in their early studies of model aromatic imide compounds, first suggested this interaction to take place. The phenomenon is demonstrated in the top portion of Figure 1.4. The lower portion of Figure 1.4 shows the staggered arrangement of adjacent polymer chains discussed by St. Clair [70]. Imide nitrogen donates electrons to their adjacent phenyl groups while the carbonyl groups withdraw electrons from their adjacent phenyl rings. Intermolecular charge transfer complexes result from the opposite partial charges on the aromatic rings of the polymer. Furthermore, it was suggested that this strong interchain interaction is associated with staggered packing of the phenyl rings, with rings of opposite partial charge in maximum contact.

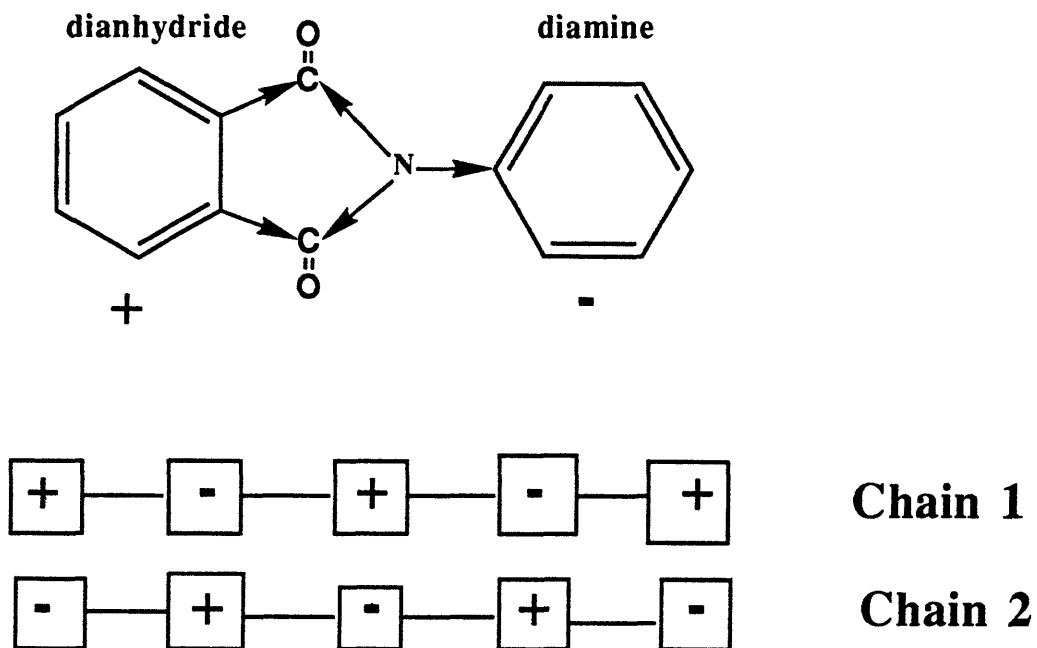
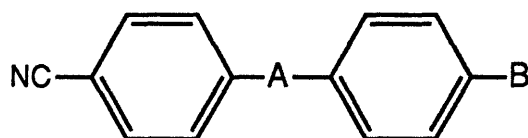


Figure 1.4. Charge transfer interactions in polyimides.

1.2.4. Liquid crystalline nematic order and alignment

Nematic order

Monomeric nematic liquid crystals [75-78] are very important materials for display applications. A typical chemical structure [77,78] of such a material is shown below:



In the above structure, "A" represents a chemical group such as an ester, a phenyl ring, or, perhaps, no group. "B" is typically a hydrocarbon chain 3-7 carbon atoms in length.

The nematic liquid crystalline state is a condition in which the molecules in a phase orient along a preferred axis known as the nematic director. The nematic state is depicted in Figure 1.5, where D' is the nematic director. Further discussion of the nematic phase can be found in many texts [75,76].

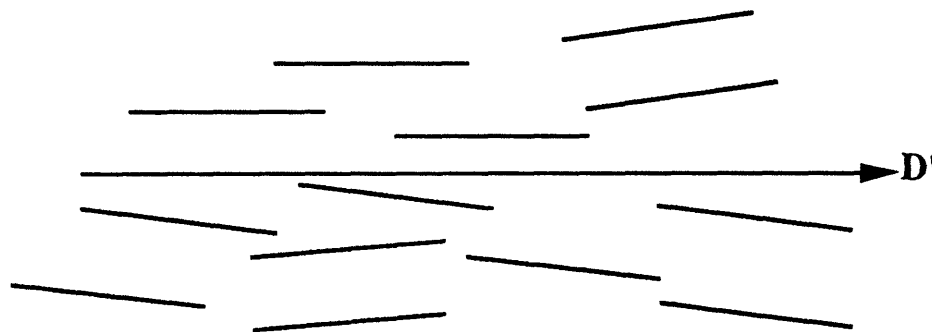


Figure 1.5. A nematic liquid crystalline phase with director D' .

Nematic alignment

The difference between nematic order and nematic alignment is a crucial distinction. A slab of nematic liquid crystalline material will form many nematic grains, each with its own nematic director. But without any external influence, the nematic directors of the

individual grains will have no preferential orientation with respect to the bulk. This is represented in Figure 1.6 (a).

Macroscopic “alignment” [77-81] is the condition in which the nematic directors of the liquid crystals in a slab of material are *non-random with respect to the bulk*. That is, the liquid crystals are preferentially oriented along a particular axis of the bulk. A “perfectly” or “ideally” aligned specimen will be entirely homogeneous, that is, have only one nematic director. This condition is represented in Figure 1.6(b). The ability to align liquid crystals on the macroscopic level is essential for using of liquid crystals as flat panel display materials.

Alignment can be produced, in a general sense, by a number of techniques [77-81]. Such techniques include applying an electromagnetic field, shearing, inducing flow, and treating adjacent surface layers. In this thesis, the treatment of adjacent surface layers to produce nematic liquid crystal alignment is of particular interest, and will be discussed later in this chapter (section 1.4) as well as in Chapters 5 and 6.

1.3. Properties

1.3.1. Quantitative relationships between polymer chemistry and refractive index

The index of refraction determines the speed of light in a material through the defining equation:

$$n(\omega) = v/c \quad (1)$$

where n is the refractive index, ω is frequency, v is the speed of light in the material, and c is the speed of light in a vacuum.

Refractive index is also a measure of the electronic polarizability of the material. The index of refraction is related to electronic polarizability (α) by the Lorentz-Lorenz equation:

$$[(n^2 - 1) / (n^2 + 2)] (M/\rho) = (N_{av}/3\epsilon_0) \alpha \quad (2)$$

where M is molecular weight, ρ is density, N_{av} is Avagadro’s number, ϵ_0 is relative permittivity in a vacuum. Refractive index is related to dielectric constant by:

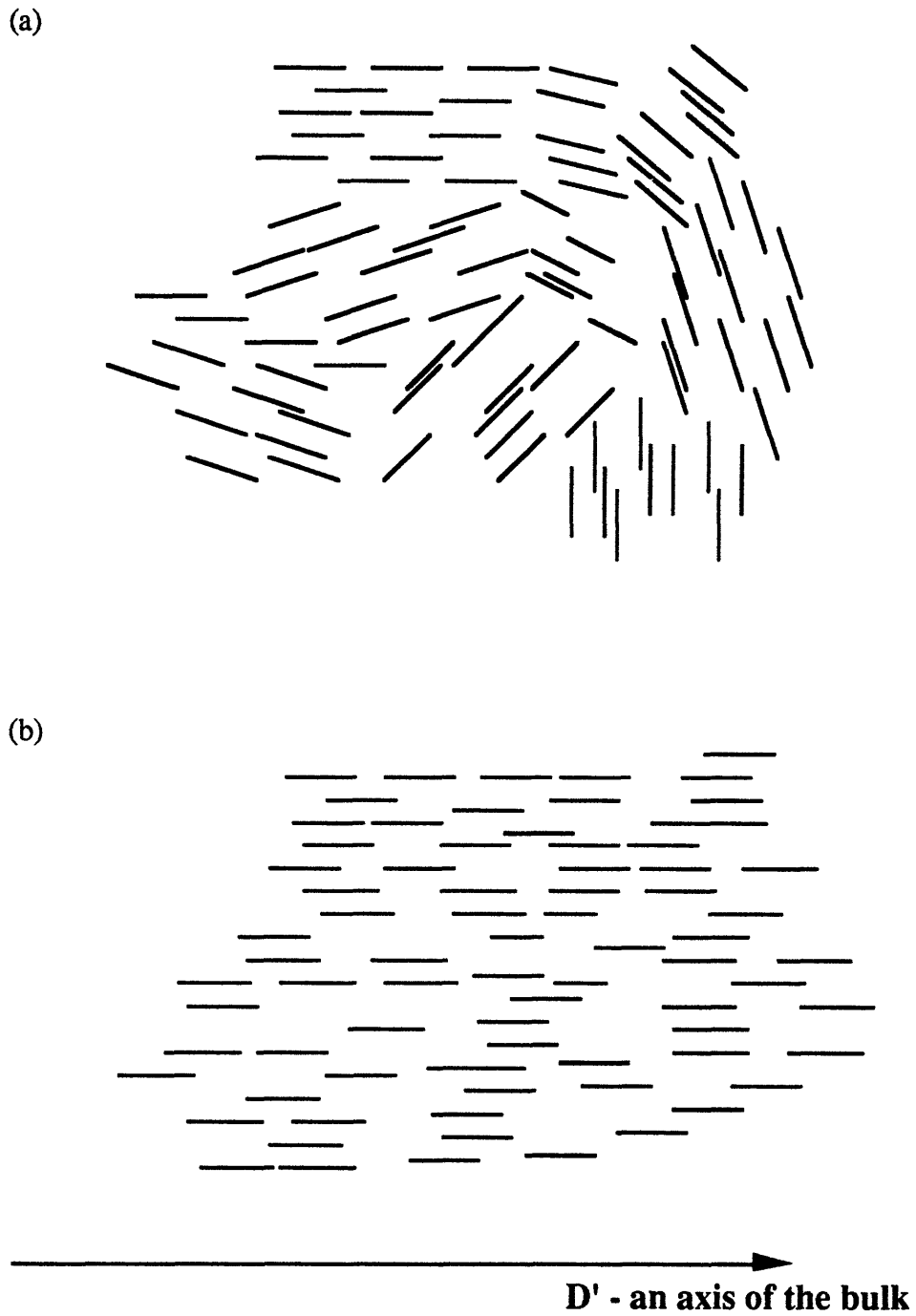


Figure 1.6. Representations of nematic liquid crystalline material. a.) no alignment, and b.) bulk alignment along axis D' .

$$\epsilon_{\infty} = n^2 \quad (3)$$

where ϵ_{∞} is the dielectric constant at optical frequency.

The refractive index is an important parameter for polyimide applications. For many electronic packaging applications, a low dielectric constant is required for minimizing crosstalk between the copper lines and maximizing signal propagation through the copper itself. The index of refraction is a particularly valuable measure of dielectric properties because it is easily obtained experimentally, even if the material is anisotropic. Polyimide electronic packaging layers have also been suggested to serve as waveguides for optical interconnect technologies [82]. The refractive index is an important parameter in evaluating their performance as waveguides.

Researchers have found that fluorinated polymers have low refractive indices. The index of refraction, for example, for polyethylene (-CH₂CH₂) is 1.51 [83], for poly(vinylidene fluoride) (-CF₂CH₂-) is 1.42 [83], and for polytetrafluoroethylene (-CF₂CF₂-) is 1.35 [83]. Groh and Zimmermann [84] predict that the intrinsic lower limit for the refractive index that can be introduced by fluorination is about 1.29. A tremendous amount of work has been done in reducing the refractive indices of polyimides by addition of fluorine to the polymer backbone [85-99].

Because the index of refraction is an important physical property of a material, the relationship between polymer chemical structure and index of refraction is of significant interest to polymer scientist. In addition, since polyimides with low refractive indices are of significant industrial interest, it is important to understand why the index of refraction is reduced. This is an important subject of Chapter 2 of this thesis.

Techniques have been developed to predict the index of refraction of a polymer, given its chemical structure. Two methods are discussed below. The first class of techniques discussed here are van Krevelen additive group contribution techniques [100]. The second type of approach is a prediction methodology developed by J. Bicerano [101] which utilizes the concept of atomic bond connectivity [102,103].

Van Krevelen

The underlying concept behind van Krevelen [100] group contribution techniques is that polymer properties are "in some way determined by a sum of contributions made by the structural and functional groups in the molecule or repeating unit of the polymer"[100]. The individual contributions, called "increments", that each of these groups makes to a physical property are assumed to be additive.

The additive physical property we are concerned with here is the "molar refraction", from which refractive index can be easily calculated. Van Krevelen offers three techniques for refractive index prediction [100]. The first is based on the Lorentz-Lorenz equation, previously shown in equation (2), and shown below in equation (4).

$$[(n^2 - 1) / (n^2 + 2)] (M/\rho) = (N_{av}/3\epsilon_0) \alpha \equiv P \equiv R_{LL} \quad (4)$$

P is the molar polarization defined here as equal to the molar refraction R_{LL} . The molar refractions of the individual van Krevelen groups (i) in the backbone are summed according to:

$$R_{LL} = \sum R_{LLi} \quad (5)$$

It is crucial to note that foreknowledge of the molar volume M/ρ is required in order to make this calculation.

The second technique is based on the equation of Gladstone and Dale [104]:

$$R_{GD} = (n - 1) (M/\rho) \quad (6)$$

The molar refraction R_{GD} is summed in the same way, using a different tabulated set of group contribution values for the groups that make up the backbone. The molar volume M/ρ is also required to make this calculation.

The third technique does not require experimental values for the density nor any other experimental measurement. This method is based on the equation of Vogel [105]:

$$R_V = n M \quad (7)$$

which states that the Vogel molar refraction R_V is simply the product of refractive index (n) and molecular weight (M) in grams/mole. The total R_V is the summation of the individual group contributions.

A limitation of this technique is that it does not explicitly take into account the density of the material. Nonetheless, this equation has been shown to give refractive index predictions which are as accurate as those obtained by the more theoretically-based equations of Lorentz-Lorenz and Gladstone-Dale. The Vogel technique is hence a convenient way to estimate refractive index without the need for experimental density data, which is often unavailable. This technique, however, does not factor in the possibility of

increased density due to semicrystallinity, chain packing, or other type of ordering. We might therefore expect this method to be more accurate for amorphous polymers with limited chain packing.

One limitation of this form of technique, in general, is that contributions of a particular group may differ in different surroundings. For example, the bonding environment around a particular group may differ if attached to an alkyl group as opposed to an aromatic group. However, the technique attempts to correct, as much as possible, for different bonding environments.

Another limitation of the van Krevelen method, in general, is that the functional groups are preselected and may not be appropriate or convenient for complicated novel polymers. A reasonable approach to assembling an appropriate set of contributing groups must be employed, and sometimes best guesses must be made. For example, correction factors for several ring structures have been calculated by van Krevelen, although no value is specifically available for the imide ring structure present in polyimides. Since most ring structures have very close correction factors, the value for a similar ring, a piperidyl ring, is used instead in Chapter 2. A sample van Krevelen/Vogel calculation for polystyrene is shown in Figure 1.7.

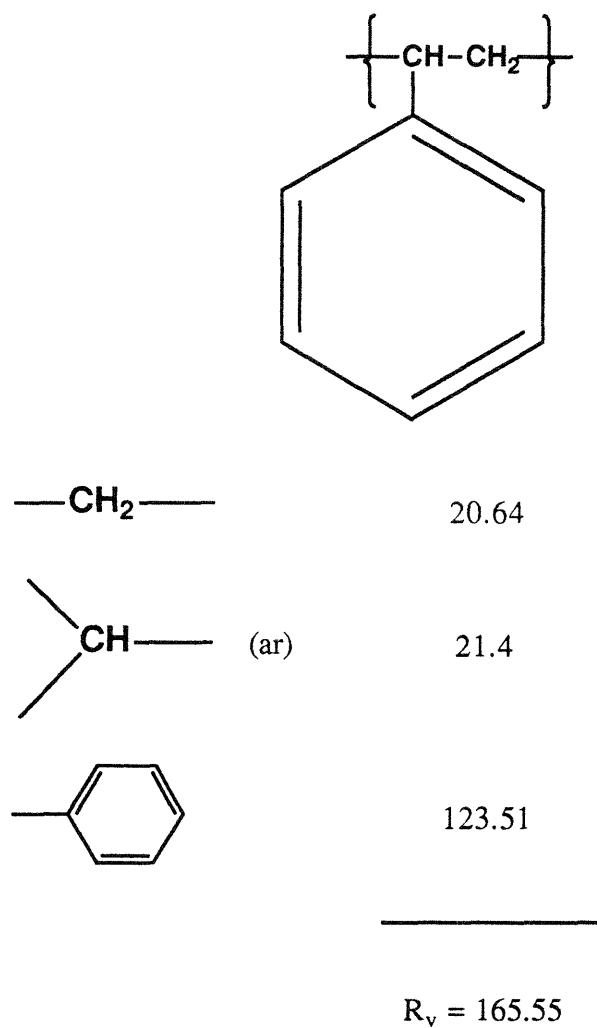
Bicerano

A new method for polymer property prediction developed by Jozef Bicerano of Dow Chemical Company has recently become available [101]. This is not a group contribution method, but a topological method that takes into account all of the atoms and bonds present in the material. It utilizes four connectivity indices [102,103] and other parameters which are calculated as described below and demonstrated for polystyrene in Figure 1.8. Because there is no preselection of chemical contribution groups, we should expect this technique to be especially useful for complex polymers such as polyimides.

The hydrogen suppressed repeat unit is drawn (with a bond drawn at only one end of the repeat unit connecting the unit to the next one). At the location of each atom, the number of non-hydrogen atoms to which it is connected is written. The value at each atom represents the zeroeth order simple connectivity index δ of the atom. The zeroeth order simple (atomic) connectivity index for the entire molecule ${}^0\chi$ is then the sum of the negative one-half powers of the connectivities of all its atoms:

$${}^0\chi = \sum (1/\sqrt{\delta}) \quad (8)$$

Van Krevelen Calculation (Polystyrene)



$$M = 104 \text{ g/mol}$$

$$n = R_v / M = 1.592$$

$$n_{\text{exp}} = 1.591$$

Figure 1.7. Sample calculation of the index of refraction of polystyrene using the van Krevelen / Vogel technique. The predicted value, 1.591, is in excellent agreement with the experimental value 1.592 [83].

The product of the atomic connectivities of every two adjacent atoms is then written at the bond line between the two atoms. The value at each bond line represents its bond index β . The first order simple (bond) connectivity index for the entire molecule is then calculated as shown in equation (9). This index, though used to predict other properties, is not present in Bicerano's refractive index correlation.

$${}^1\chi = \Sigma (1/\sqrt{\beta}) \quad (9)$$

Next, on a new hydrogen suppressed repeat unit, zeroeth order valence connectivity indices δ^v , given by equation (10), for each atom, are written at the location of each atom.

$$\delta^v \equiv (Z^v - N_H) / (Z - Z^v - 1) \quad (10)$$

In equation (10), Z^v is the number of valence electrons, N_H is the number of adjacent hydrogen atoms, and Z is the atomic number. For second row atoms carbon, nitrogen, oxygen, and fluorine, equation (10) reduces to $\delta^v = Z^v - N_H$, that is, the atom's valence minus the number of hydrogen atoms attached. First order valence connectivity indices for the bonds of the molecule are calculated as the products of the adjacent zeroeth order valence indices and are written at the bond lines. Atomic and bond valence connectivity indices for the entire atom are calculated as shown in equations (11) and (12).

$${}^0\chi^v = \Sigma (1/\sqrt{\delta^v}) \quad (11)$$

$${}^1\chi^v = \Sigma (1/\sqrt{\beta^v}) \quad (12)$$

In the development of correlations for property prediction [101], Bicerano uses these connectivity parameters, as well as additional correction factors which account for the overestimation or underestimation of the contribution of certain groups or atoms due to, for example, orbital conjugation, hydrogen bonding, or unusually low polarizability. Bicerano's correlation for predicting refractive index at room temperature is shown in equation (13).

$$n \approx 1.8853 + 0.024558 (17 {}^0\chi^v - 20 {}^0\chi - 12 {}^1\chi^v - 9N_{\text{rot}} + N_{\text{ref}}) / N \quad (13)$$

In equation (13), N is the total number of non-hydrogen atoms. N_{rot} is the number of rotatable, non-aromatic single bonds in the repeat unit that change the spacial coordinates of

one or more atoms upon rotation. Bonds in "floppy" rings contribute one-half to N_{rot} . N_{ref} is a correction factor given by equation (14).

$$N_{\text{ref}} = -11N_{\text{F}} - 3N_{\text{Cl-Ph}} + 18N_{\text{S}} + 9N_{\text{fused}} + 12N_{\text{HB}} + 32N_{\text{Si-Si}} \quad (14)$$

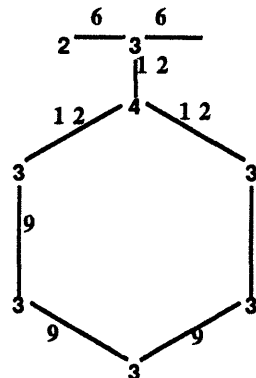
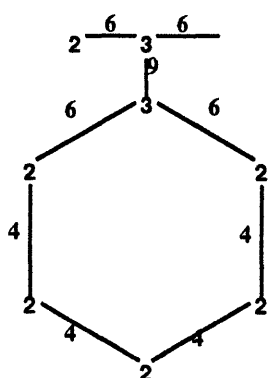
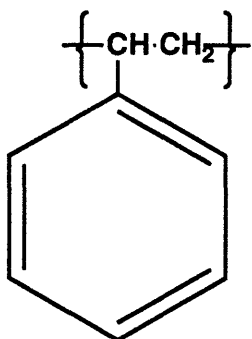
In equation (14), N_{F} is the number of fluorine atoms, N_{S} is the number of sulfur atoms, $N_{\text{Cl-Ph}}$ is the number of chlorine atoms bonded to phenyl rings, N_{fused} is the number of rings which are present in attached-edge multi-ring (e.g., aromatic imide) structures, N_{HB} is the number of hydrogen bonding moieties, and $N_{\text{Si-Si}}$ is the number of delocalized and conjugated silicon-silicon bonds. Only N_{fused} and N_{F} are relevant to the polyimides discussed in this work.

Using 183 polymers with refractive indices ranging from 1.34 to 1.69, a correlation coefficient of 0.977 and a standard deviation of 0.016 was obtained by Bicerano for equation (10). The standard deviation represents less than 1% of the average refractive index of the data set. Thus, we should expect this method to be highly accurate.

1.3.2. Property changes associated with charge transfer complexation

Charge transfer complexation (see section 1.2.3) is believed to have a substantial effect on the properties of polyimides [67-74,85-99]. Examples of property changes believed to be associated with charge transfer complexation include increased yellow coloration, glass transition temperature, dielectric constant, refractive index, and optical attenuation. Workers have found that charge transfer complexation is mitigated when separator groups, chain kinks, and bulky chemical substituents are introduced into the polyimide backbone [72-74,85-99]. Introduction of these chemical groups have marked effects on properties. For example, St. Clair *et al.* [73,74,89,96] have found that incorporation of charge transfer-reducing groups reduce coloration and dielectric constant. Fryd [72] found that addition of such groups reduce glass transition temperature. Feger *et al.* [98] have found that addition of bulky fluorinated groups reduces optical losses in waveguides.

Bicerano Calculation (Polystyrene)



Repeat unit

Simple Connectivity

Valence Connectivity

 $\delta = \# \text{ adjacent non-H atoms}$
 $\delta^v = \text{valence minus \# adjacent H}$

$$\beta_{ij} = \delta_i \times \delta_j$$

$$\beta_{ij}^v = \delta_i^v \times \delta_j^v$$

$$N = 8$$

$$N_{\text{rot}} = 3$$

$$N_{\text{ref}} = 0$$

$${}^0\chi = \sum (1/\sqrt{\delta}) \quad \text{atomic connectivity index}$$

$${}^1\chi = \sum (1/\sqrt{\beta}) \quad \text{bond connectivity index}$$

$${}^0\chi = (6/\sqrt{2}) + (2/\sqrt{3}) = 5.397$$

$${}^0\chi^v = (1/\sqrt{2}) + (6/\sqrt{3}) + (1/\sqrt{4}) = 4.671$$

$${}^1\chi = (4/\sqrt{4}) + (4/\sqrt{6}) + (1/\sqrt{9}) = 3.966$$

$${}^1\chi^v = (2/\sqrt{6}) + (4/\sqrt{9}) + (3/\sqrt{12}) = 3.016$$

$$N_{\text{ref}} = -11N_{\text{F}} - 3N_{\text{Cl-Ph}} + 18N_{\text{S}} + 9N_{\text{fused}} + 12N_{\text{HB}} + 32N_{\text{Si-Si}}$$

$$n \approx 1.885312 + 0.024558 \times (17 {}^0\chi^v - 20 {}^0\chi - 12 {}^1\chi^v - 9 N_{\text{rot}} + N_{\text{ref}}) / N$$

$$n \text{ (predicted)} = 1.604$$

$$n \text{ (experimental)} = 1.592$$

Figure 1.8. Bicerano prediction for the refractive index of polystyrene. The estimated value, 1.604, is within 0.75% of the experimental value, 1.592 [83].

1.3.3. Anisotropy of optical properties

Birefringence is a term which is defined as a difference in refractive index in a material along different spacial axes. However, it is very important that the term not be used loosely. That is, we must be precise in how we define the axes of comparison. In Figure 1.9(a-e), we review a number of ways in which birefringence can be defined. Examples of optical anisotropy on three different levels are presented: molecular, microscopic, and macroscopic.

Molecular birefringence

Optical anisotropy on the molecular level is shown in Figure 1.9(a). In the molecule in this figure, the refractive index along the chain axis $n_{//}$ is different from the refractive index perpendicular to the chain axis n_{\perp} . One might define the molecular birefringence Δn_{mol} as:

$$\Delta n_{\text{mol}} = n_{//} - n_{\perp} \quad (15)$$

In this particular example, $n_{//}$ should be greater than n_{\perp} . This is because the polarizability of the aromatic ring is greater in its plane than normal to it. The axis parallel to the main chain must always be in the plane of the phenyl rings of the polymer, while axes perpendicular to the main chain will, in general, not be. For a molecule in which the highly polarizable aromatic units are perpendicular to the main chain, e.g., polystyrene, $n_{//}$ will be less than n_{\perp} [33,34].

Microscopic birefringence

Birefringence on the microscopic level is shown in Figure 1.9(b,c). A polymer spherulite appears in Figure 1.9(b) in which the refractive index along the radial axis n_r is different from the refractive index along the tangential axis n_t . It might be convenient for the case in Figure 9(b) to define birefringence of the spherulite Δn_{sph} as:

$$\Delta n_{\text{sph}} = n_r - n_t \quad (16)$$

The relationship of n_r to n_t will depend upon the orientation of the main chain with respect to the radial axis, as well as the relationship between $n_{//}$ and n_{\perp} described above.

Figure 1.9(c) shows a nematic liquid crystalline grain in which the refractive index along the extraordinary axis n_e is different from the refractive index along the ordinary axis n_o . This is another form of microscopic birefringence. We might define birefringence of the liquid crystalline phase Δn_{LC} as:

$$\Delta n_{LC} = n_e - n_o \quad (17)$$

We can expect n_e to be, most often, greater than n_o because the molecules of organic liquid crystals typically have their primary polarizable groups along the long axis of the molecule.

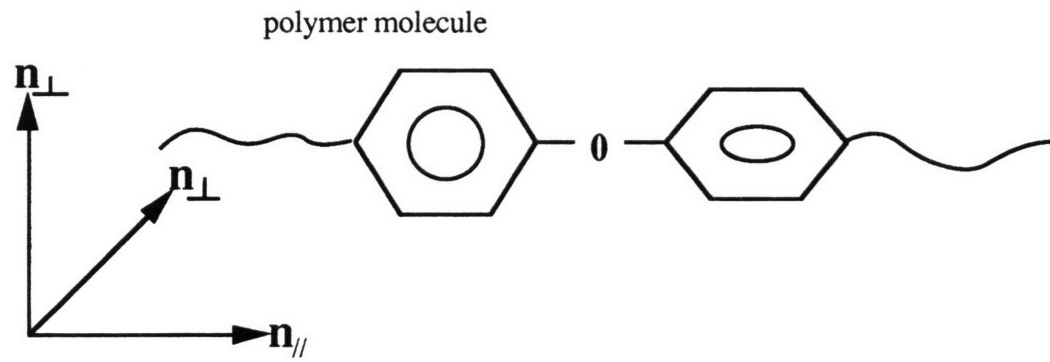
Macroscopic birefringence

Birefringence on the macroscopic level is shown in Figure 1.9(d,e). An in-plane oriented polymer film is shown in Figure 1.9(d) in which the bulk in-plane index n_{TE} is different from the bulk out-of-plane index n_{TM} . This film structure was previously shown in Figure 1.3(b). The difference between n_{TE} and n_{TM} will depend upon whether the main chain is more polarizable along its main chain or normal to its main chain. If, for example, the molecule is more polarizable along its main chain (e.g., polyimide), n_{TE} will be greater than n_{TM} , as the bulk film consequently will be more polarizable in the plane of the film. On the other hand, if the polymer is more polarizable normal to the main chain (e.g., polystyrene), n_{TM} will be greater than n_{TE} [33,34]. Here, we can define the birefringence of the film Δn_{film} as:

$$\Delta n_{film} = n_{TE} - n_{TM} \quad (18)$$

An aligned liquid crystal film is shown in Figure 1.9(e) with differing refractive indices $n_{TE,//}$, $n_{TE,\perp}$, and n_{TM} . The condition of macroscopic alignment was previously shown in Figure 1.6(b). In the case that the liquid crystals are *perfectly* aligned, $n_{TE,//}$ should be equal to n_o in Figure 1.9(c), while $n_{TE,\perp}$ and n_{TM} should be equal to n_e from Figure 1.9(c).

(a)



(b)

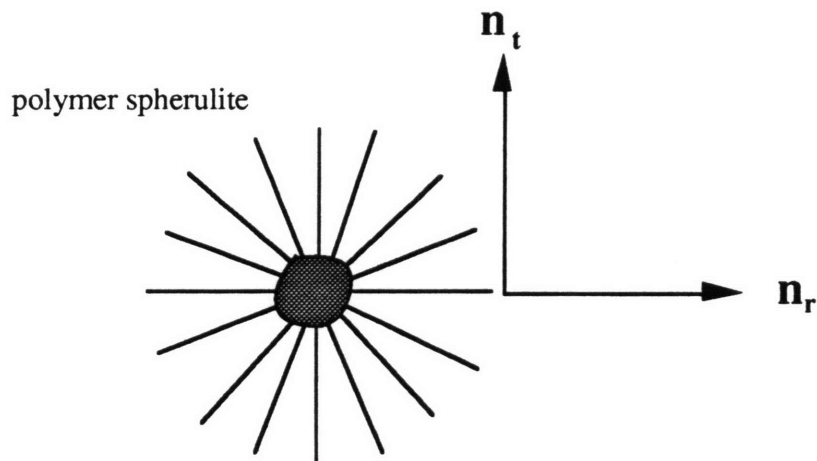


Figure 1.9. Examples of optical anisotropy. a.) birefringence on the molecular level, b.) birefringence on the microscopic level in a polymer spherulite,

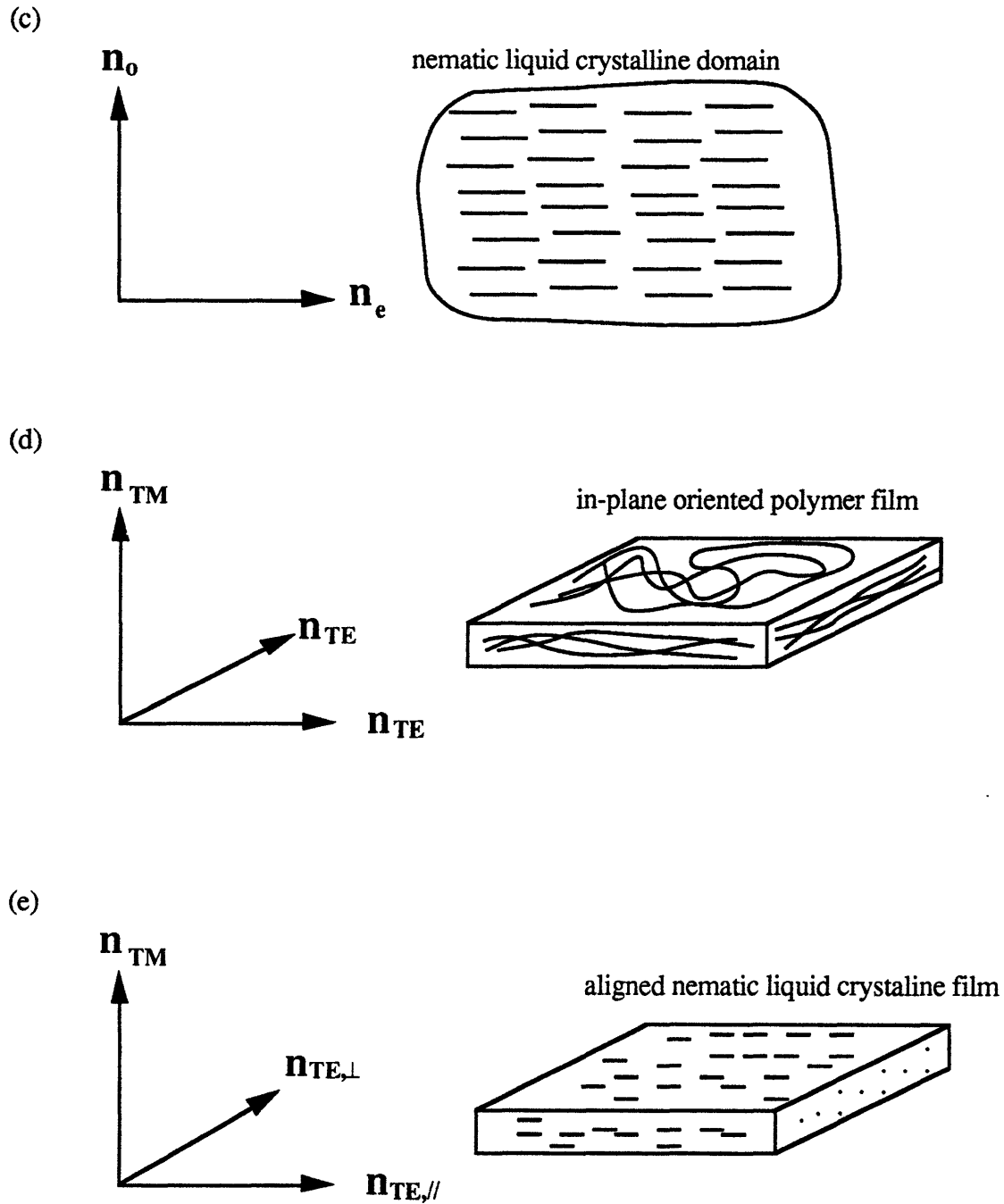


Figure 1.9. continued. Examples of optical anisotropy. c.) birefringence on the molecular level in a nematic grain, d.) bulk birefringence in an in-plane oriented film, e.) bulk birefringence in a film of aligned liquid crystals.

For the general case of a macroscopic birefringence, we can imagine a block of material in Cartesian axes as shown in Figure 1.10. We can define three refractive indices n_x , n_y , and n_z , as well as three macroscopic birefringences as shown in equations (19), (20), and (21):

$$\Delta n_{xy} = n_x - n_y \quad (19)$$

$$\Delta n_{xz} = n_x - n_z \quad (20)$$

$$\Delta n_{yz} = n_y - n_z = \Delta n_{xz} - \Delta n_{xy} \quad (21)$$

We can also define an average refractive index as:

$$n_{avg} = (1/3) (n_x + n_y + n_z) \quad (22)$$

For an in-plane oriented polymer film which is isotropic in the plane of the film, as shown in Figures 1.3(b) and 1.9(d), average refractive index is:

$$n_{avg} = (2n_{TE} + n_{TM}) / 3 \quad (23)$$

This focus of this thesis is macroscopic optical properties. However, others [106] have done extensive investigations of the relationships between intrinsic molecular birefringence, crystalline fraction, crystalline orientation function, and macroscopic birefringence.

Molecular vs. microscopic vs. macroscopic birefringence

It is important to realize that a material can be birefringent on either the molecular, microscopic, or macroscopic level, yet not be birefringent on any of the other two. For example, most polymers have refractive indices that are different along the main chain as compared to normal to the main chain. However, a film or block of such a polymer will not necessarily be birefringent on the macroscopic or even the microscopic level. It may be entirely amorphous and unoriented.

Likewise, a material can be birefringent on the microscopic level, but not on the macroscopic level. Figure 1.10 shows a block of polymer which is semicrystalline. The crystallites are perfectly spherical. Assuming that, for the spherulites, $n_r \neq n_t$, the material

will be highly birefringent on the *microscopic* level. When placed between crossed polarizers, a significant quantity of light will be transmitted. However, if one measures the *bulk refractive indices* along axes x , y , and z of the block, one will find that they are exactly the same! Between crossed polars, rotation of the block about the normal axis will not change the transmitted intensity. It does not matter whether, for example, the x -axis is 0° or 45° to the polarizer. That is, we have the situation in which the material is highly birefringent (microscopically), though the *bulk* refractive indices are identical in every direction.

The situation described above may occur for any situation in which there is microscopic birefringence, but no orientation with respect to the bulk. A slab of unaligned nematic liquid crystals, for example, will be “birefringent” locally, but “non-birefringent” if we define the optical axes with respect to the bulk sample. A slab of aligned liquid crystals, on the other hand, will be birefringent on both the microscopic and macroscopic levels.

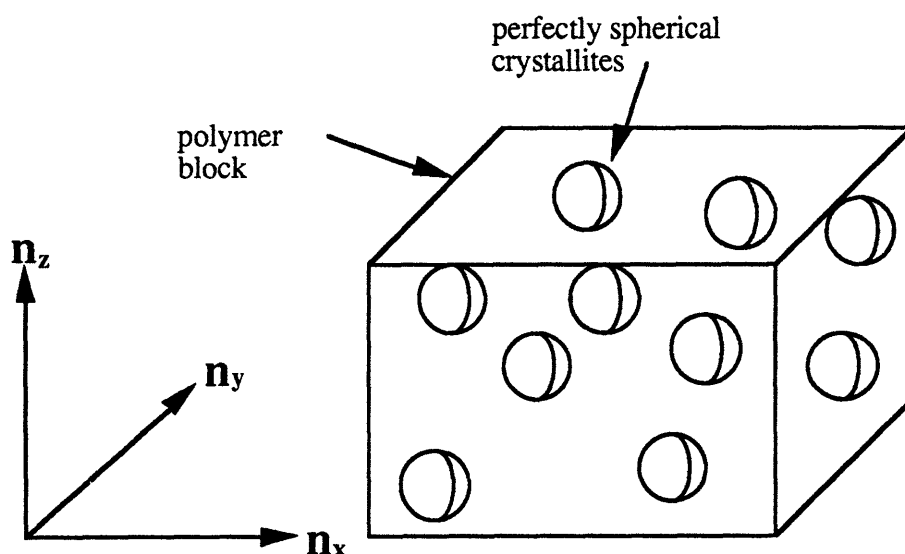


Figure 1.10. A thick semicrystalline polymer block that is microscopically birefringent but has $n_x=n_y=n_z$.

1.3.4. Measurement of index of refraction

There are many techniques in existence that can be used to measure the refractive index of a material [107-110]. These include ellipsometry, Abbe refractometry, and fluid matching. Another technique of recent interest is called waveguide mode prism coupling [108,109], and is discussed here.

The application of the prism coupling technique is shown in Figure 1.11. The film is pressed to the base of a high index prism. A polarized laser is focused on one face of the prism. The light refracts into the prism, totally internally reflects at the base of the prism, and is detected as it leaves the opposite face. When the angle of incidence Θ is equal to that of an allowed mode in the film, the light propagates into the film and there is a sharp drop in light intensity at the detector. Also, when Θ drops below the critical angle of the polymer film, the laser refracts into the film, and there is a large permanent drop in detected intensity. The refractive index of the material can be calculated from either the waveguide mode "coupling" angles or from the critical angle. The critical angle approach, while slightly less accurate than waveguide propagation method, is preferable to use in thick films in which waveguide modes are poorly pronounced.

Workers at Bell Labs developed the prism coupling method in the early 1970s [108]. Today, a commercial instrument, the Metricon prism coupler, applies this technique. Using the Metricon instrument, one can measure both the in-plane index (n_{TE}) and out-of-plane index (n_{TM}) of a thin film by changing the polarization of the incident light. The Metricon prism coupler is equipped with both waveguide mode and critical angle measurement capability. Many workers have used the prism technique to measure the refractive index and optical anisotropy of polyimide and other polymer films [32-41,43].

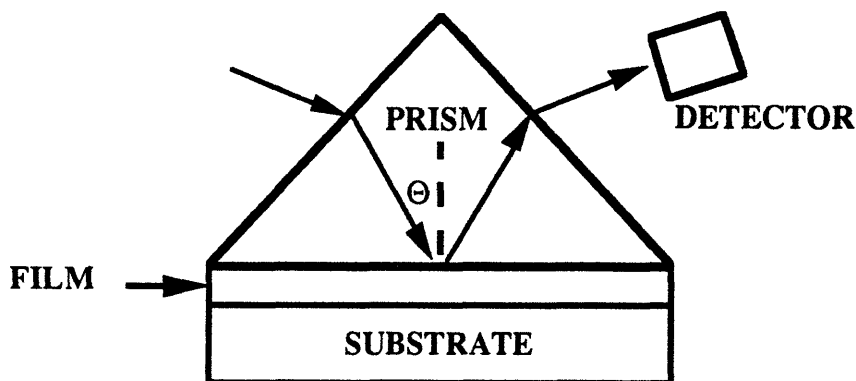


Figure 1.11. Prism coupling technique for measuring index of refraction.

1.3.5. Optical transmission model for liquid crystal alignment

This section is dedicated to the discussion of an adequate framework for evaluating the alignment of nematic liquid crystals in a film. Nematic liquid crystals are birefringent on a microscopic level. The molecules in each liquid crystalline domain are oriented preferentially along a director with the index of refraction greater along the ordinary axis than along the extraordinary axis. The microscopic birefringence of the liquid crystalline phase is a function of the material itself and is independent of any external forces which may act to align the liquid crystals with respect to the bulk. However, in this section, we are concerned with evaluating the macroscopic alignment of the liquid crystals, that is, how well they are oriented with respect to a given axis of the bulk.

Optical model for an aligned liquid crystal plate

Let \underline{D}' be the nematic director of an aligned liquid crystal plate (such as that found in Figure 1.9(e)), with \underline{D}'' the ordinary axis orthogonal to \underline{D}' and in the plane of the plate. Also, let OP be the axis of the polarizer, and OA be the axis of the analyzer. Let angle χ be the angle between the polarizer and analyzer, angle ϕ be the angle between the polarizer and nematic vector. These vector are shown in Figure 1.12 below.

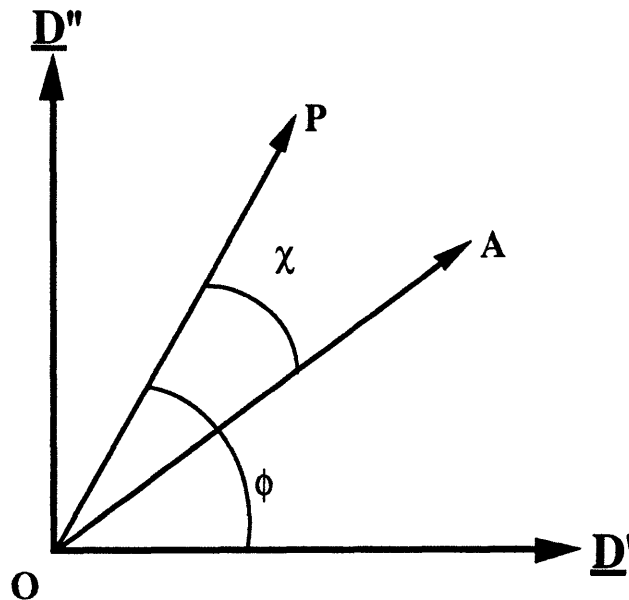


Figure 1.12. Graphical representation of a parallel-aligned liquid crystal plate between a polarizer (P) and analyzer (A).

An electric field plane wave passing through the polarizer enters the liquid crystal plate. When D' is not parallel or perpendicular to OP, the electric field vector is divided into two components that have mutually orthogonal displacement vectors but differing velocities of propagation. The two waves emerge from the plate with a phase difference δ given by [111]:

$$\delta = (2\pi / \lambda) (\Delta n) h \quad (24)$$

where:

$$\begin{aligned} \lambda &= \text{wavelength of light in free space} \\ \Delta n &= \text{difference between ordinary and} \\ &\quad \text{extraordinary refractive indices} \\ h &= \text{plate thickness} \end{aligned}$$

The intensity I of light passing through the crystal plate, polarizer, and analyzer is given by [111]:

$$I = E^2 \{ \cos^2 \chi - \sin 2\phi \sin 2(\phi - \chi) \sin^2(\delta/2) \} \quad (25)$$

When the polarizer and analyzer are crossed, i.e. $\chi = \pi/2$, intensity I_{\perp} is given by:

$$I_{\perp} = E^2 \sin^2 2\phi \sin^2(\delta/2) \quad (26)$$

When the nematic vector D' is aligned parallel or perpendicular to the polarizer axis OP, the value of I_{\perp} is identically zero. That is, according to equation (26):

$$I_{\perp} = I_{\perp, \min} = 0, \quad \text{when } \phi = 0, \pi/2, \pi, \dots \quad (27)$$

On the other hand, the angular position of the liquid crystal nematic vector which produces maximum intensity $I_{\perp, \max}$ is 45° with respect to the polarizer axis. The maximum intensity in equation (26) is given by:

$$I_{\perp} = I_{\perp, \max} = E^2 \sin^2(\delta/2), \quad \text{when } \phi = \pi/4, 3\pi/4, 5\pi/4, \dots \quad (28)$$

If we normalize the equation for $I_{\perp}(\phi)$ given by equation (26) by the maximum intensity $I_{\perp, \max}$ given by equation (28), we get the following simple expression for $I(\phi)/I(\pi/4)$, that is, the intensity at angle ϕ normalized by the maximum intensity found at $\phi=\pi/4$:

$$I(\phi) / I(\pi/4) = \sin^2(2\phi) \quad (29)$$

This relationship is plotted below in Figure 1.13.

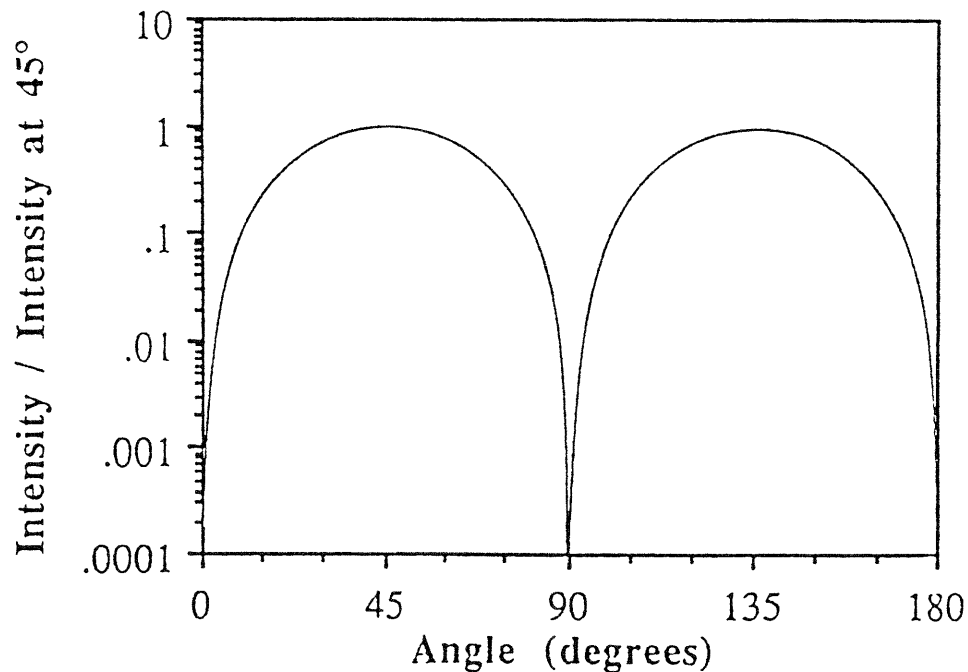


Figure 1.13. Plot of $I(\phi)/I(45^\circ)$ vs. ϕ from equation (29).

Elliptically polarized light

Figure 1.14 shows the most general case of elliptically polarized light [107,112,113]. The direction of polarization systematically changes in an elliptical pattern as it propagates. The polarization state of the electric field can be described by three

parameters, which are represented in Figure 1.14. The first parameter is the handedness, right (clockwise) or left (counterclockwise). The second parameter is the azimuth α , that is, the angle between the semimajor axis of the ellipse and the defined reference axis. The third parameter is the ellipticity β , which is the ratio between the lengths of the semimajor and semiminor axes of the ellipse, or b/a in Figure 1.14.

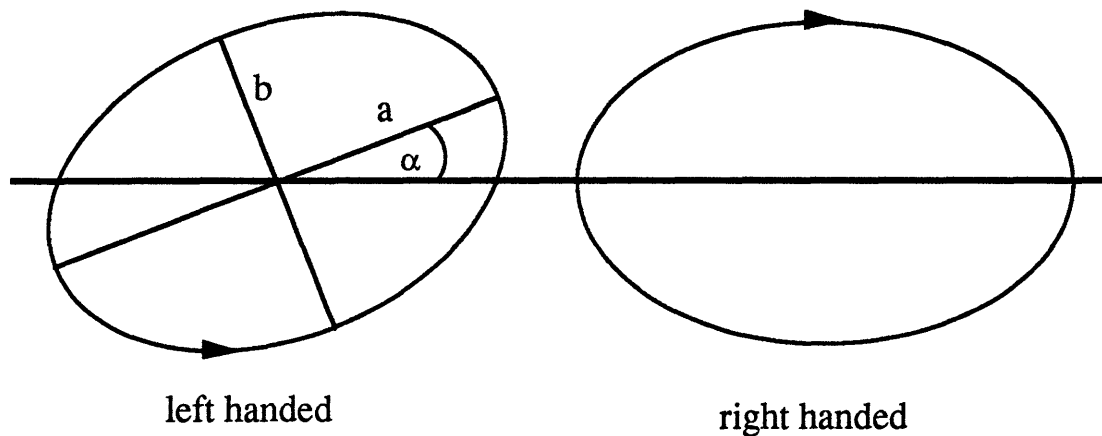


Figure 1.14. Elliptically polarized light with handedness (left or right), azimuth (α), and ellipticity ($\beta = a / b$).

Linearly and circularly polarized light are special cases of elliptically polarized light. Linearly polarized light is the case where $\beta = 0$. It can possess any value of α , but has no handedness. Circularly polarized light, on the other hand, is the case where $|\beta| = 1$. It can be left or right handed, but has no azimuth.

Misalignment

In the case of a perfectly aligned specimen, polarized light passing through the specimen will move from an original state of linear polarization ($\alpha = 0$ and $\beta = 0$) to another state of elliptical polarization depending upon the thickness of the film and the orientation with respect to the polarizer. This is true except for the case where the liquid crystals are aligned 0 or 90° with respect to the polarizer and in which there is no change in the alignment state. Now consider a film of liquid crystals in which the liquid crystals are not in a perfect state of alignment. A case in which there are regions of liquid crystals misoriented with respect to the bulk alignment axis is depicted below in Figure 1.15.

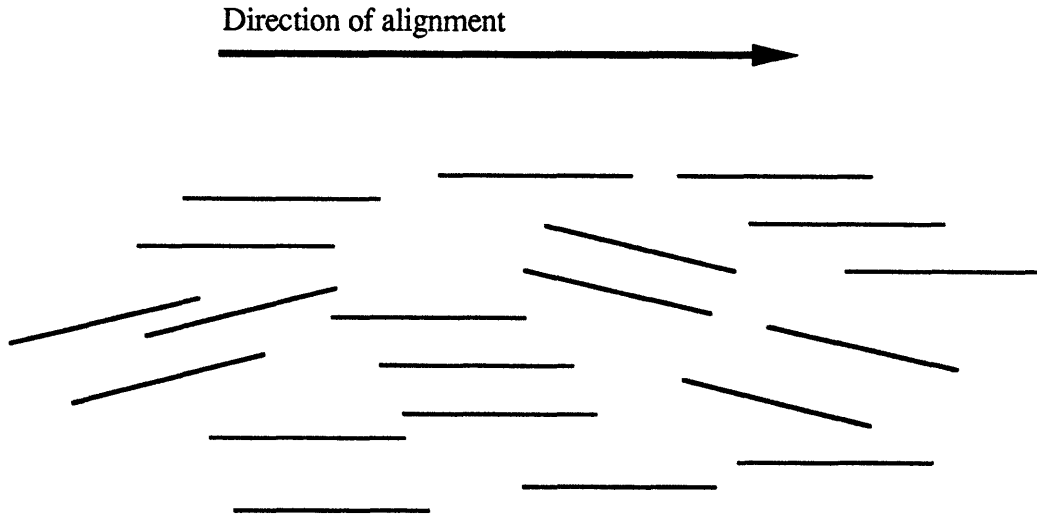


Figure 1.15. Parallel-aligned liquid crystals with inhomogeneities.

Consider only the case in which the polarizer and analyzer are crossed and the liquid crystal alignment director is parallel to the polarizer. We showed previously that under these conditions in an ideally aligned system, no light is transmitted, i.e., intensity is zero. However, if the system has misaligned liquid crystal domains, some light can be transmitted as a consequence of random elliptical polarization produced as light travels through the unaligned regions. Thus, unlike the ideal case, transmitted intensity will be greater than zero.

Each distinct misaligned nematic domain will have its own orientation with respect to the polarizer. The following exercise will clarify this concept. Imagine a linearly polarized laser beam in azimuth α_0 passing through a LC specimen with random inhomogeneities “a”, “b”, “c”, “d”, and “e”. This is shown in Figure 1.16. As the laser penetrates the liquid crystalline sample at point “1”, the light passes through inhomogeneous phases “a” and “b”. Both “a” and “b” have unique nematic directors and unique optical path lengths. Light incident at point “2” of the specimen, however, travels through inhomogeneous phases “c”, “d”, and “e”, which have their own unique directors and optical path lengths. The light emerging at points 1’ and 2’ will have unique ellipticities β_1 and β_2 and unique azimuths α_1 and α_2 different from the initial polarization.

A large beam of light, hence, will emerge from the sample with a distribution of polarization states depending upon the significance of the misalignment. Consequently, some light will not be blocked by the analyzer. Furthermore, since there is no specific relationship between β_1 and β_2 or between α_1 and α_2 , there is no compensator, e.g., a 1/4 wave plate, that can single-handedly negate the ellipticity of the emanating light.

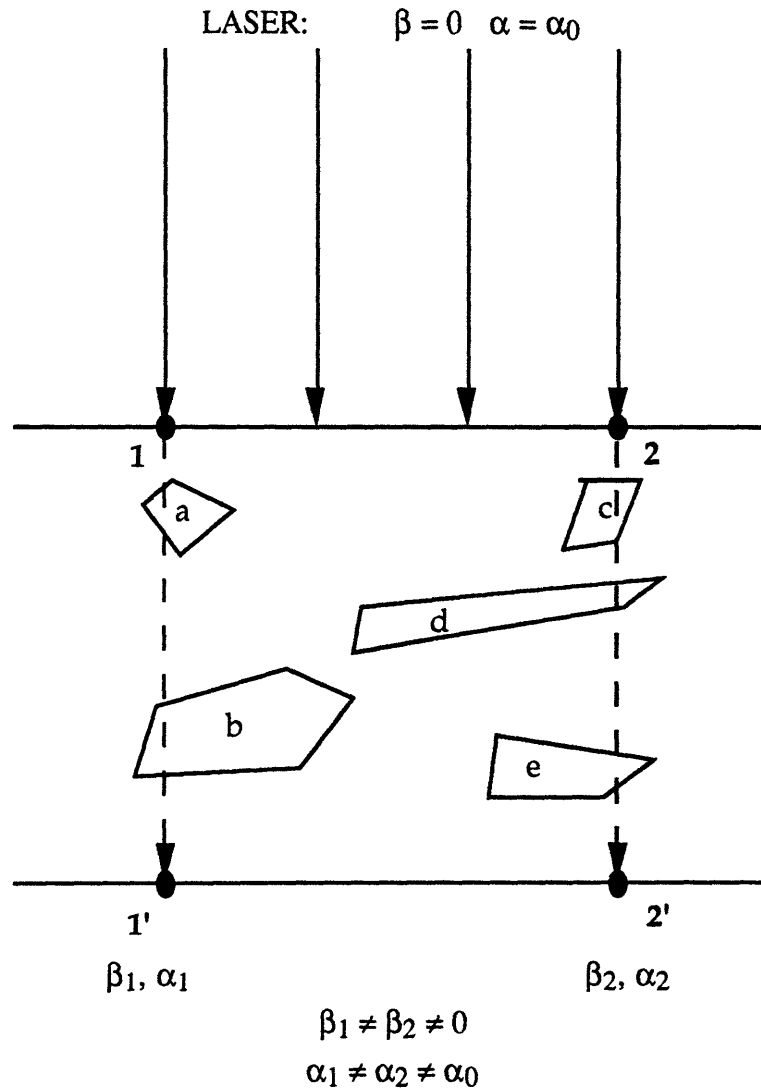


Figure 1.16. Rays of light passing through different points 1 or 2 of the liquid crystal sample and emerging at 1' or 2' with different polarization states. Domains a-e represent regions of differing optical retardation.

Characterizing the Misaligned State

Let us suppose that a liquid crystal film is placed between a crossed polarizer and analyzer with the alignment axis at an angle ϕ with respect to the polarizer. Let us now define a liquid crystal alignment parameter "A", which is given by the ratio of the experimentally measured transmitted intensity at $\phi=0^\circ$ to the experimentally measured

transmitted intensity at $\phi=45^\circ$. The parameter “A” is, essentially, the ratio of minimum to maximum intensity.

$$A \equiv I(0^\circ) / I(45^\circ) \quad (30)$$

The meanings of the values of A are shown in Table 1.1. It has already been shown in equation (29) that the ideal value of A for a perfectly aligned liquid crystal film is zero. From the previous discussion of misalignment, it is clear that for a film with misalignment, A will be greater than zero. For the case that there is no alignment, A is unity, as there is no distinguishable difference between the 0° and 45° conditions. Hence, A will, in general, be a parameter between zero and one inclusively, with low values representing strong alignment, high values representing weak alignment, zero representing perfect alignment, and one representing no alignment. Note that a value of A greater than one would represent the case in which the material is aligned with a greater preference along the 45° axis than along the alignment director that was initially assumed.

Table 1.1. Meaning of the ratio of transmitted intensity at 0° (MIN) to transmitted intensity at 45° (MAX).

<u>MIN/MAX (A) ratio</u>	<u>Meaning</u>
A = 0	LCs perfectly aligned
$0 < A < 1$	LCs have intermediate level of alignment
e.g., A is small, but > 0	LCs strongly aligned
A is large, but < 1	LC weakly aligned
A = 1	LCs not aligned
A > 1	LCs aligned with preference to 45° axis

Using equations (29) and (30), we can also define an “effective angle of misalignment” Φ :

$$A \equiv \sin^2(2\Phi) \quad (31)$$

The parameter Φ represents the angle at which the liquid crystals appear to be misaligned with respect to the alignment (0°) axis. For the case that $A=0$, i.e., perfect alignment, $\Phi=0$. For the case that $A=1$, i.e., no alignment, $\Phi=45^\circ$. The $\Phi=45^\circ$ condition, means that the liquid crystal nematic phases have their directors oriented along any axis with equal probability. Equation (31) is not valid for the odd case that $A>1$.

1.4. Performance: Liquid Crystal Alignment Layers

Polyimides are important as electronic packaging materials, as engineering plastics for high technology applications, and as alignment films for liquid crystals. Much of this thesis focuses on their use as liquid crystal alignment films. A discussion of the alignment of liquid crystals on polymer surfaces follows.

1.4.1. Liquid crystal surface alignment on brushed polymer films

The surface alignment of liquid crystals is a crucial element in the performance of LCD technology [77-81]. “Alignment layers” at surfaces of liquid crystal films, as shown in Figure 1.17, define the axis of macroscopic liquid crystal orientation at that surface. Alignment layers are typically rubbed polyimides or obliquely evaporated SiO_x thin films. In the case of rubbed polyimides, it has been observed that liquid crystals that come in contact with a rubbed polymer film align in the direction the polymer is rubbed.

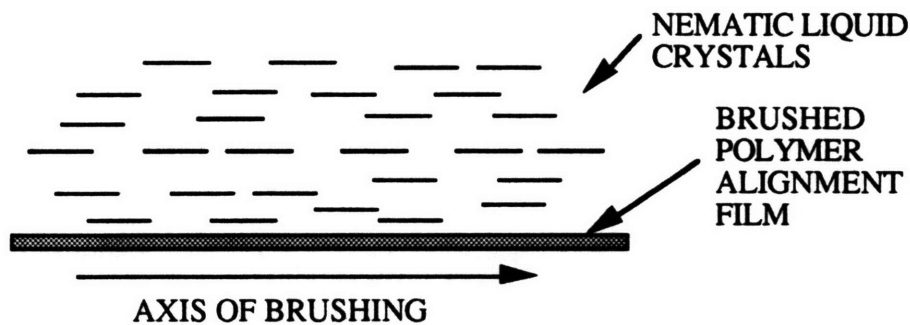


Figure 1.17. Alignment of liquid crystals on brushed polymer surfaces.

The liquid crystals can order in the direction of the rubbing at an inclination angle with respect to the horizontal surface. This is known as the angle of surface pretilt [114,115]. Depending upon the particular device technology, a specific pretilt angle can be desired for optimal switching performance. The liquid crystal pretilt angle is a function of the polymer alignment material, the nematic liquid crystal, and the way in which the alignment films are processed [116-119]. The generation and control of pretilt was not, however, investigated in this thesis.

The brushing process is accomplished industrially on a spinning wheel covered with a silk, rayon, or other cloth. This is shown in Figure 1.18. On the laboratory scale, however, films can be brushed by hand to create liquid crystal alignment, and complex apparatus is not required.

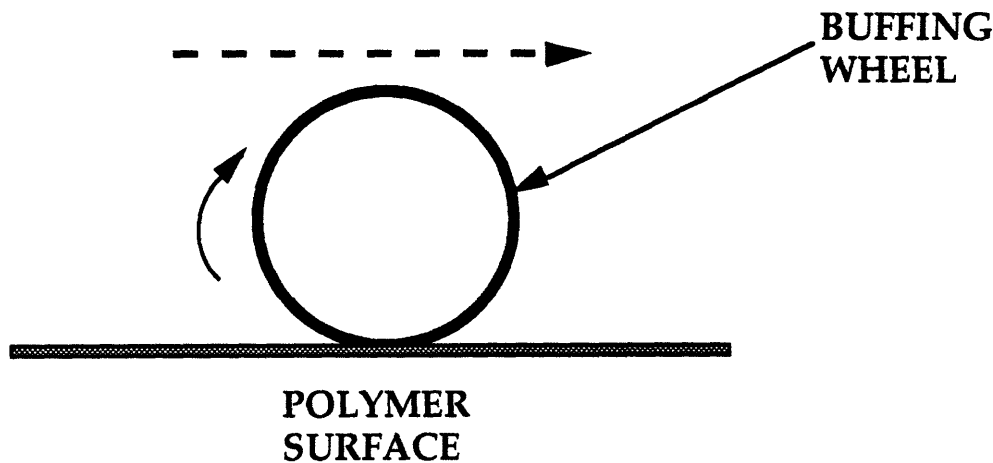


Figure 1.18. A polymer surface being rubbed by a brushing wheel.

Although rubbed polyimides perform as excellent liquid crystal alignment layers, the mechanism of alignment is not well understood. Brushing-induced surface alignment is often referred to as a “black art”, as it has both baffled and intrigued scientists for decades. Berreman and others [120-122] have postulated that liquid crystals align along surface grooves created by the rubbing process. More recently, workers have shown that liquid crystal alignment is more likely associated with the orientation of chemical groups in the alignment polymer [48-55]. Geary *et al.* [50] observed that polymers that are oriented and highly crystalline are effective liquid crystal alignment films. As to why liquid crystals would align on oriented surface is a matter of speculation, though it has been suggested [123] that intermolecular interactions between the polymer and the liquid crystal are involved.

1.4.2. Alternative treatments to polymer layers for liquid crystal alignment

There are a number of serious disadvantages of the brushing process as a means of inducing alignment of liquid crystals. First, the process can generate particulates which can affect the quality of display devices. Second, the buffing can create static charge, which can interfere with the device electronics. Third, the brushing can only be performed on planar surfaces. Notched or curved substrates can present difficulties in achieving brushing-induced alignment. Fourth, brushing is a costly and energy consuming mechanical process. Finally, brushing is a surface-uniform technique which cannot be used directly to pattern a device.

A number of alternative, non-contact liquid crystal surface alignment processes have been proposed and demonstrated. For example, workers have investigated the non-contact formation of surface grooves as a means of producing alignment [124,125]. Also, Langmuir-Blodgett films have also been used to align liquid crystals [126-128].

Recently, Schadt and others [129-131] have demonstrated the alignment of liquid crystals on films of a photosensitive cinnamate polymer (polyvinylmethoxycinnamate) [132] that have been exposed to linearly polarized ultraviolet light (LP-UV). Schadt [129] proposes that an anisotropic structure, as shown in Figure 1.19, is forged in the polymer alignment film during the exposure to LP-UV. The top portion of Figure 1.19 shows the chemical groups which react, while the bottom portion depicts the proposed oriented structure. The polymer, which crosslinks upon exposure to UV, is believed to crosslink in a preferential way upon exposure to LP-UV which results in an anisotropic distribution of crosslinked side chain molecules, exerts an orienting force upon the main chain of the polymer, and depletes uncrosslinked side chains oriented along the LP-UV axis. The authors believe that the induced orientation in the polymer is associated with the liquid crystal alignment, which was found to be perpendicular to the axis of the LP-UV.

Other researchers have investigated linearly polarized light as a way producing alignment in liquid crystals. One might refer to this class of techniques as “photo-alignment”. Ichimura *et al.* [133-135] have investigated the alignment of liquid crystals on azobenzene films that have been exposed to linearly polarized UV. The azobenzene dyes undergo a ‘trans-cis’ photoisomerization upon exposure to the linearly polarized light [136,137]. Gibbons *et al.* [138-142] have investigated the optical control of liquid crystal alignment using azo dye doped polyimide alignment films and exposing liquid crystal cells to linear polarized laser beams. Gibbons’ group is interested in photo-orientation processes not only for display applications, but also for holography, optical data storage, and other potential applications of liquid crystals which require their macroscopic alignment.

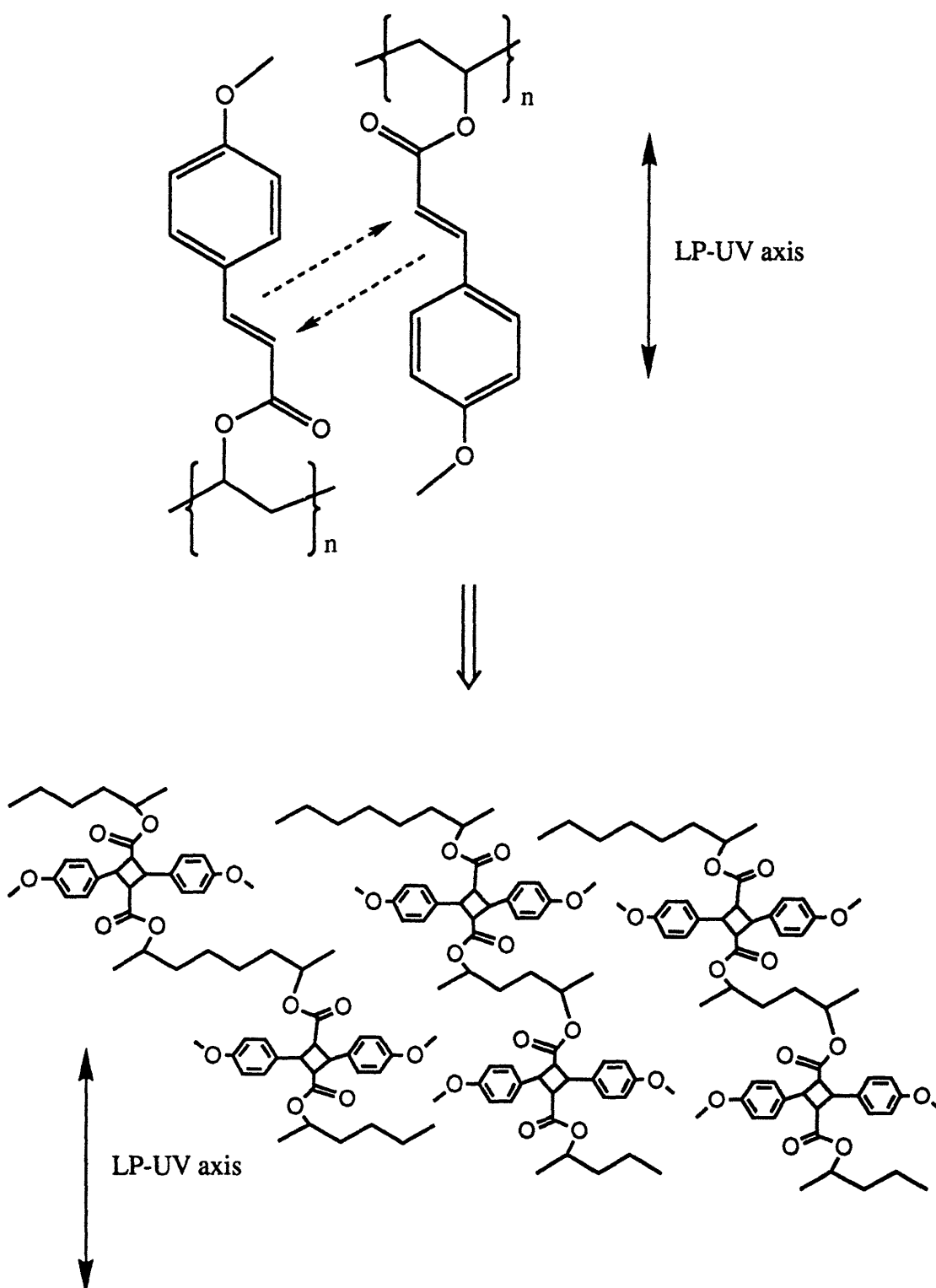


Figure 1.19. The photochemical reaction in polyvinylmethoxycinnamate and the oriented structure, proposed by Schadt [129], that is formed by exposure to linearly polarized UV.

Hasegawa and Taira [143] demonstrated the alignment of nematic liquid crystals on films of an aliphatic/aromatic polyimide that have been exposed to linearly polarized deep ultraviolet light. They found alignment to occur, however, in only a tiny window of exposure time, below and above which, no alignment was seen. The authors suggest that the anisotropic depolymerization of the polyimide film is responsible for the alignment. They argue that at short exposures, the polymer begins to degrade preferentially along the LP-UV axis, as shown in Figure 1.20. This process results in an oriented structure in the polymer film that is preferential to the axis in the plane of the film perpendicular to the LP-UV. At the exposure dosage critical for producing alignment, the polymer film is in a state of optimal orientation. At this point, chains parallel to the LP-UV become depleted and further exposure to LP-UV destroys chains perpendicular to the UV axis as well, thus, destroying the alignment.

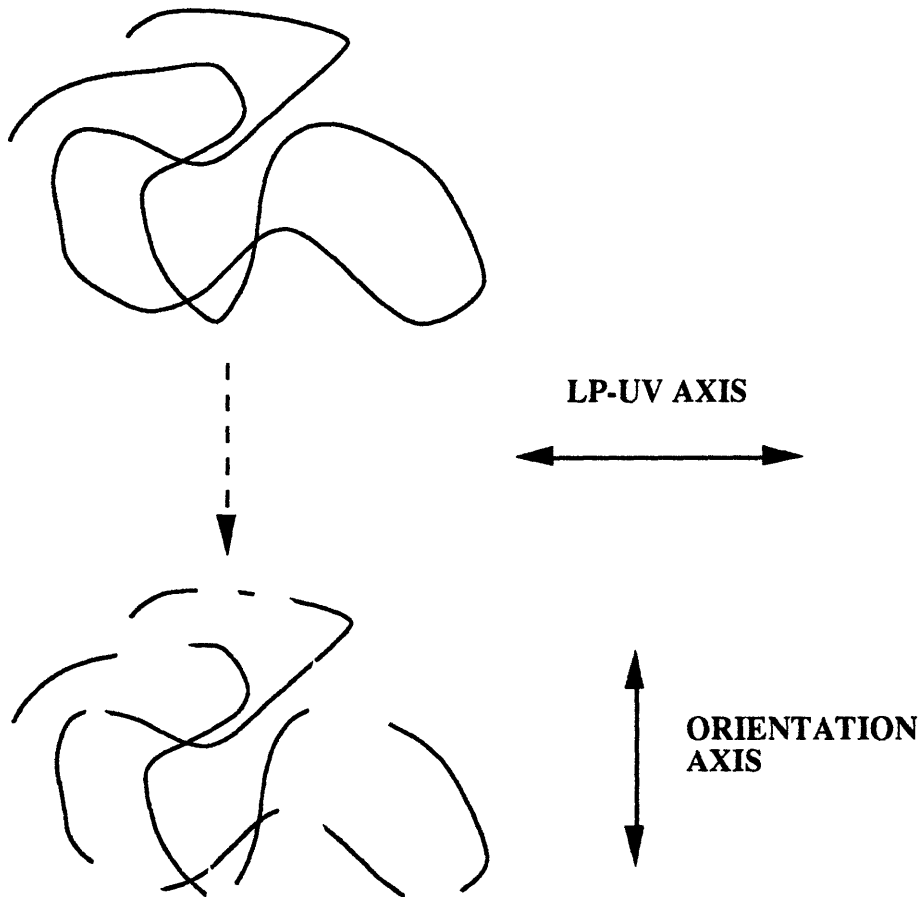


Figure 1.20. Anisotropic chain degradation proposed to occur [143] in a polyimide film during exposure to linearly polarized UV.

There is precedent for the belief that deep UV depolymerizes the polyimide. For example, Kambe [144] discusses the degradation of mechanical properties of aromatic polyimide, polyamide, and polyamide-imide films that have undergone very long exposures to deep UV. In addition, polyimides are well known to be destroyed during deep UV laser ablation processes [145-149]. In analogy, the LP-UV here might be thought of as a light, anisotropic surface ablation.

1.4.3. An LCD device: the TN-LCD

Liquid crystals displays are devices which take advantage of the optical properties of macroscopically oriented liquid crystalline materials in order to produce switchable pixels. So that it is clear why surface alignment is important in the display industry, an example of a simple liquid crystal device, known as the TN-LCD, or “twisted nematic liquid crystal display” [150], is briefly explained here, and also shown in Figure 1.21. It should be noted, however, that there are other types of LCDs [151], as well as other potential applications of liquid crystals.

A TN-LCD cell consists of a nematic liquid crystal phase which is gradually rotated by 90° . The 90° rotation is achieved by inducing surface-alignment directors at each liquid crystal-polymer interface that are perpendicular to each other. The twisted liquid crystal film is sandwiched between two substrates, each coated with the appropriately treated alignment film. Each substrate contains a polarizer with the axis of polarization parallel to alignment director defined by the adjacent alignment film. There are also electrodes atop each substrate so that an electric field can be applied to the cell.

In the “off” state, the twisted TN layer rotates the direction of polarization of the entering light by 90° . The second polarizer prevents light from passing through, and the cell appears dark. However, when voltage is applied to the two electrodes on each surface of the TN layer, the liquid crystals reorient parallel to the applied field. In that state, the layer no longer twists the direction of polarization of the light passing through, and the cell appears bright. When the electric field is removed, the liquid crystals return to their default alignment state, which is the twisted nematic state. Also note that if the two polarizers in the device were perpendicular instead of parallel, the cell would function in reverse, i.e., as off/on instead of on/off.

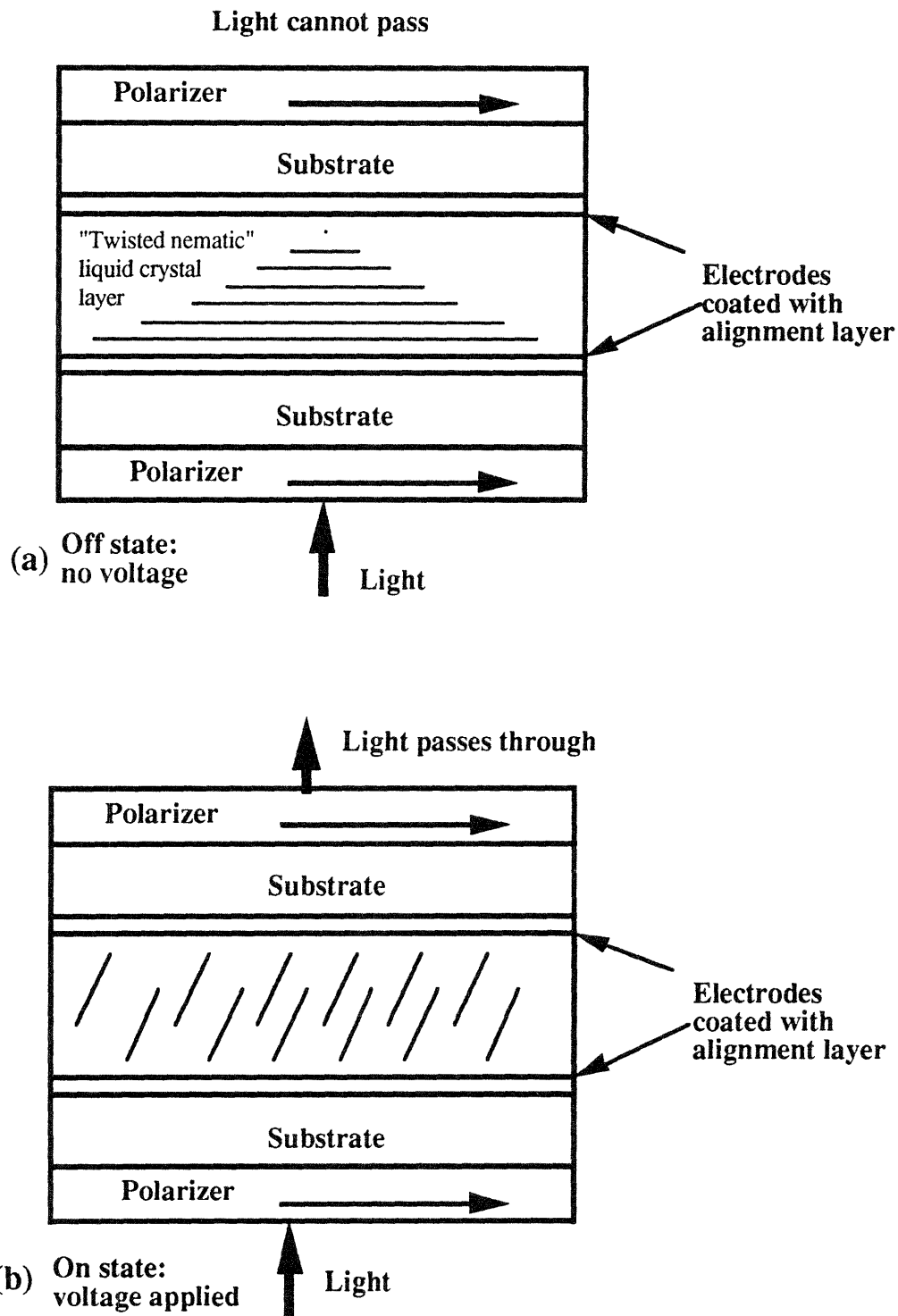


Figure 1.21. States of a twisted nematic liquid crystal display (TN-LCD) device. a.) on state and b.) off state.

1.5. References

1. K.L. Mittal, Ed., *Polyimides: Synthesis, Characterization, and Applications*, Plenum Press, New York (1984), Proceedings of the First Technical Conference on Polyimides, Ellenville, NY (1982).
2. W.D. Weber and M.R. Gupta, Eds., *Recent Advances in Polyimide Science and Technology*, SPE, Inc., Poughkeepsie, NY (1987), Proc. of the Second Tech. Conference on Polyimides, Ellenville, NY (1985).
3. C. Feger, M.M. Khojasteh, and J.E. McGrath, Eds., *Polyimides: Materials, Chemistry, and Characterization*, Elsevier, Amsterdam (1989), Proceedings of the Third Technical Conference on Polyimides, Ellenville, NY (1988).
4. D.Wilson, H. Stenzenberger, and P. Hergenrother, Eds., *Polyimides*, Chapman and Hall, NY, (1990).
5. S.D. Senturia, in *Polymers for High Technology - Electronics and Photonics*, M.J. Bowden and S.R. Turner, Eds., ACS, Washington, D.C., p 428 (1987), Symposium of the ACS Div. PMSE at the 192nd meeting of the ACS, Anaheim, CA (1986).
6. J.W. Verbicky, Jr., "Polyimides" in *Encyclopedia of Polymer Science and Engineering*, John Wiley and Sons, Inc., New York (1987).
7. F.W. Harris, in *Polyimides*, p.1, D.Wilson, H. Stenzenberger, and P. Hergenrother, Eds., Chapman and Hall, NY, (1990).
8. Amoco Chemical Company material safety data sheet, γ -butyrolactone (1993).
9. Baxter Healthcare Corporation material safety data sheet, dimethyl acetamide (1989).
10. Mallinckrodt, Inc., material safety data sheet, N-methyl pyrrolidone (1985).
11. H. Hiramoto, *Mat. Res. Soc. Symp. Proc.*, **167**, 87 (1990).

12. R. Rubner, H. Ahne, E. Kuhn, and G. Kolodziej, *Photogr. Sci. Eng.*, **23(5)**, 303 (1979).
13. H. Ahne, H. Kruger, E. Pammer, and R. Rubner, in *Polyimides: Synthesis, Characterization, and Applications*, p. 905, K.L. Mittal, Ed., Plenum Press, New York (1984).
14. T.L. St. Clair, A.K. St. Clair, and E.N. Smith, in *Structure-Solubility Relationships in Polymers*, p.199, F.W. Harris and R.B. Seymour, Eds., Academic Press, New York (1977).
15. J. Pfeifer and O. Rhode, in *Recent Advances in Polyimide Science and Technology*, p.336, W.D. Weber and M.R. Gupta, Eds., Society of Plastic Engineers, New York (1987).
16. O. Rhode, P. Smolka, P. Falcigno, and J. Pfeifer, *Polym. Eng. Sci.*, **32(21)**, 1623 (1992).
17. H.R. Slater, *Advanced Materials and Processes*, **1**, 19 (1995).
18. OCG Microelectronic Materials, Inc., product information, Probimide 32 polyamide-imide resin.
19. Personal communication. Dr. Doug Fjare, Amoco Chemical Company, and Dr. Brian Auman, DuPont Corporation.
20. K.K. Chakravorty and C.P. Chien, *SPIE Int. Conf. on Adv. in Intercon. and Packaging*, **1389**, 559 (1990).
21. C.P. Chien and K.K. Chakravorty, *SPIE Optical. Thin Films III: New Developments*, **1323**, 338 (1990).
22. R. Mo, T. Maw, A. Roza, K. Stefanisko, and R. Hopla, *Proc. 7th Int. IEEE VLSI Multilevel Intercon. Conf.*, 390 (1990).
23. T. Maw and R. Hopla, *MRS Symp. Proc.*, **203**, 71 (1991).

24. T. Maw and R. Hopla, *MRS Symp. Proc.*, **227**, 205 (1991).
25. T. Maw, M. Masola, and R. Hopla, *Polym. Mat. Sci. Eng.*, **66**, 247 (1992).
26. M. Ree and K. Chen, *Polym. Prep.*, **31(2)**, 594 (1990).
27. M. Ree, K. Chen, and G. Czornyj, *Polym. Eng. Sci.*, **32(14)**, 924 (1992).
28. H. Higuchi, T. Yamashita, K. Horie, and I. Mita, *Chem. Mater.*, **3**, 188 (1991).
29. J. Scaiano, A. Becknell, and R. Small, *J. of Photochem. Photobio. A*, **44**, 99 (1988).
30. A. Lin, V. Sastri, G. Tesoro, A. Reiser, and R. Eachus, *Macromol.*, **21(4)**, 1165 (1988).
31. J. Scaiano, J. Netto-Ferreira, A. Becknell, and R. Small, *Polym. Eng. Sci.*, **29(14)**, 942 (1989).
32. T.P. Sosnowski and H.P. Weber, *Appl. Phys. Lett.*, **21(7)**, 310 (1972).
33. W.M. Prest and D.J. Luca, *J. Appl. Phys.*, **50(10)**, 6067 (1979).
34. W.M. Prest and D.J. Luca, *J. Appl. Phys.*, **51(10)**, 5170 (1980).
35. T.P. Russell, H. Gugger, and J.D. Swallen, *J. Polym. Sci.: Polym. Phys.*, **21**, 1745 (1983).
36. S. Herminghaus, D. Boese, D.Y. Yoon, and B.A. Smith, *Appl. Phys. Lett.*, **59(9)**, 1043 (1991).
37. D. Boese, H. Lee, D.Y. Yoon, J.D. Swallen, and J.F. Rabolt, *J. Polym. Sci.: Polym. Phys.*, **30**, 1321 (1992).
38. S.C. Noe, Doctoral Thesis, Massachusetts Institute of Technology (1992).

39. S.C. Noe, J.Y. Pan, and S.D. Senturia, *Polym. Eng. Sci.*, **32(15)**, 1015 (1992).
40. R. Burzynski and P. Prasad, *Polymer*, **31(4)**, 627 (1990).
41. S. Bai, R. Spry, D. Zelmon, U. Ramabadran, and J. Jackson, *J. Polym. Sci.: Pt. B, Polym. Phys.*, **30**, 1507 (1992).
42. J. Machell, J. Greener, and B. Contestable, *Macromol.*, **23**, 186 (1990).
43. K. Nakagawa, *J. Appl. Polym. Sci.*, **41**, 2049 (1990).
44. V.E. Smirnova and M.I. Bessonov, in *Polyimides: Materials, Chemistry, and Characterization*, p.563, C. Feger, M.M. Khojasteh, and J.E. McGrath, Eds., Elsevier, Amsterdam (1989).
45. T. Kinugi, I. Aoki, M. Hashimoto, *Kobunshi Ronbunshyu*, **38**, 301 (1981).
46. Y. Aihara and P. Cebe, *Polym. Eng. Sci.*, **34(16)**, 1275 (1994).
47. J. Teverovsky, D. Rich, Y. Aihara, and P. Cebe, *J. Appl. Polym. Sci.*, **54**, 497 (1994).
48. H. Aoyama, Y. Yamazaki, N. Matsuura, H. Mada, and S. Kobayashi, *Mol. Cryst. Liq. Cryst.*, **72**, 127 (1981).
49. N. van Aerle and J. Tol, *Macromol.*, **27**, 6520 (1994).
50. J.M. Geary, J.W. Goodby, A.R. Kmetz, and J.S. Patel, *J. Appl. Phys.*, **62(10)**, 4100 (1987).
51. E. Lee, P. Vetter, T. Miyashita, and T. Uchida, *Jpn. J. Appl. Phys.*, **32**, L1339 (1993).
52. S. Kuniyasu, H. Fukuro, S. Maeda, K. Nakara, M. Nitta, N. Ozaki, and S. Kobayashi, *Jpn. J. Appl. Phys.*, **27(5)**, 827 (1988).

53. N. van Aerle, *J. of the SID*, **2(1)**, 41 (1994).
54. S. Ishihara, H. Wakemoto, K. Nakazima, Y. Matsuo, *Liquid Crystals*, **4(6)**, 669 (1989).
55. D. Seo, H. Matsuda, T. Oh-Ide, and S. Kobayashi, *Mol. Cryst. Liq. Cryst.*, **224**, 13 (1993).
56. N.P. Kuznetsov and M.I. Bessonov, *Vysokomol. soyed.*, **A28 (1)**, 100 (1986).
57. M. Ree, T.L. Nunes, and D.P. Kirby, *Polym. Prep.*, **33(1)**, 309 (1992).
58. T.L. St. Clair and A.K. St. Clair, *J. Polym Sci: Polym. Chem.*, **15**, 1529 (1977).
59. P.M. Hergenrother, N.T. Wakelyn, and S.J. Havens, *J. Polym Sci: Polym. Chem.*, **25**, 1093 (1987).
60. P.M. Hergenrother and S.J. Havens, *J. Polym Sci: Polym. Chem.*, **27**, 1161 (1989).
61. C.R. Gautreaux, J.R. Pratt, and T.L. St. Clair, *J. Polym. Sci.: Polym. Phys.*, **30**, 71 (1992).
62. D.C. Rich, P. Huo, C. Liu, and P. Cebe, *ACS Polym. Mat. Sci. Eng.*, **68**, 124 (1993).
63. J. Friler and P. Cebe, *Polym. Eng. Sci.*, **33(10)**, 588 (1993).
64. P.P. Huo and P. Cebe, *Polymer*, **34(4)**, 696 (1993).
65. P.P. Huo, J. Friler, and P. Cebe, *Polymer*, **34(21)**, 4387 (1993).
66. J. T. Muellerleile, B. G. Risch, D. E. Rodrigues and G. Wilkes. *Polymer*, **34(4)**, 789 (1993).

67. R.A. Dine-Hart and W.W. Wright, *Die Makromolek. Chem.*, **143**, 189 (1971).
68. B.V. Kotov, T.A. Gordina, V.S. Voishchev, O.V. Kolinov, and A.N. Pravednikov, *Vysokomol. Soyed.*, **A19(3)**, 614 (1977).
69. J.M. Salley, T. Miwa, and C.W. Frank, in *Materials Science of High Temperature Polymers for Microelectronics, Mater. Res. Soc. Proc.*, **227**, p.117, D.T. Grubb, I. Mita, and D.Y. Yoon, Eds. (1991).
70. T.L. St. Clair, in *Polyimides*, p. 58, D. Wilson, H.D. Stenzenberger, and P.M. Hergenrother, Eds., Blackie, Glasgow (1990).
71. YE. P. Krasnov, A.YE. Stepanyan, YU.I. Mitchenko, YU.A. Tolkachev, and N.V. Lukasheva, *Vysokomol. Soyed.*, **A19 (7)**, 1566 (1977).
72. M. Fryd, in *Polyimides: Synthesis, Characterization, and Applications*, K.L. Mittal, Ed., Plenum Press, New York (1984).
73. A.K. St. Clair, T.L. St. Clair, W.S. Slemp, and K.S. Ezzell, "Optically Transparent/Colorless Polyimides", NASA Technical Memorandum 87650 (1985).
74. A.K. St. Clair, T.L. St. Clair, and W.S. Slemp, in *Polyimides: Materials, Chemistry, and Characterization*, p. 16, C. Feger, M.M. Khojasteh, and J.E. McGrath, Eds., Elsevier, Amsterdam (1989).
75. P.G. de Gennes, *The Physics of Liquid Crystals*, Ch.3, Oxford University Press, London (1975).
76. F.C. Frank, in *Liquid Crystals: Their Physics, Chemistry, and Applications*, p. 1, C. Hilsum and E. Raynes, Eds., Royal Society of London (1983).
77. J. Cognard, *Mol. Cryst. Liq. Cryst.*, **78**, Suppl. 1 (1982).
78. T. Uchida and H. Seki, in *Liquid Crystals: Applications and Uses*, B. Bahador, Ed., Vol. 3, Ch. 5., World Scientific, Teaneck, NJ (1990).

79. J. Castellano, *Mol. Cryst. Liq. Cryst.*, **94**, 33 (1983).
80. S. Kobayashi, Y. Iimura, and M. Nishikawa, *Conf. Rec. SID Int. Displ. Res. Conf.*, 78 (1994).
81. O'Mara, *Liquid Crystal Flat Panel Displays Manufacturing Science and Technology*, Van Nostrand Reinhold, New York (1992).
82. R. Selvaraj, H. Lin, and J. McDonald, *J. Lightwave Tech.*, **6(6)**, 1034 (1988).
83. J. Bandrup and E. Immergut, Eds., *Polymer Handbook*, John Wiley & Sons, New York (1989).
84. W. Groh and A. Zimmermann, *Macromol.*, **24**, 6660 (1991).
85. S. Sasaki, T. Matsuura, S. Nishi, and S. Ando, in *Materials Science of High Temperature Polymers for Microelectronics*, D.T. Grubb, I. Mita, and D.Y. Yoon, Eds., *Mater. Res. Soc. Proc.*, **227** (1991).
86. J.W. Labadie, M.I. Sanchez, Y.Y. Cheng, and J.L. Hedrick, *ibid.*, p. 43.
87. H. Haider, E. Chenevey, R.H. Vora, W. Cooper, M. Glick, and M. Jaffe, *ibid.*, p. 35.
88. D.M. Stoakley and A.K. St. Clair, in *Optical and Electrical Properties of Polymers*, J.A. Emerson and J.M. Torkelson, Eds., *Mater. Res. Soc. Proc.*, **214**, 1990.
89. A.K. St. Clair, T.L. St. Clair, and W.P. Winfree, *Polym. Mat. Sci. Eng.*, **59**, 28 (1988).
90. G. Hougham, G. Tesoro, and J. Shaw, in *Polyimides: Materials, Chemistry, and Characterization*, p. 465, C. Feger, M.M. Khojasteh, and J.E. McGrath, Eds., Elsevier, Amsterdam (1989).
91. A. Misra, G. Tesoro, and G. Hougham, *Polymer*, **33(5)**, 1078 (1992).

92. T. Matsuura, Y Hasuada, S. Nishi, and N. Yamada, *Macromol.*, **24**, 5001 (1991).
93. T. Matsuura, M. Ishizawa, Y Hasuada, and S. Nishi, *Macromol.*, **25**, 3540 (1992). (1990).
94. D.M. Stoakley and A.K. St. Clair, in *Polymeric Materials for Electronic Packaging and Interconnection*, p. 87, J.H. Lupinski and R.S. Moore, Eds., ACS, Washington (1989).
95. D.L. Goff, E.L. Yuan, H. Long, and H.J. Neuhaus, *ibid.*, p. 93.
96. A.K. St. Clair and T.L. St. Clair, in *Polymers for High Technology - Electronics and Photonics*, p.437, M.J. Bowden and S. R. Turner, Eds., ACS, Washington (1987).
97. T. Inchino, S. Sasaki, T. Matsuura, and S. Nishi, *J. Polm. Sci: Polym Chem.*, **28**, 323 (1990).
98. R. Reuter, H. Franke, and C. Feger, *Applied Optics*, **27**(21), 4565 (1988).
99. G. Hougham, G. Tesoro, A. Viehbeck, and J. Chapple-Sokol, *Polym. Prep*, **34**(1), 371 (1993).
100. D.W. Van Krevelen, *Properties of Polymers: Their Correlation with Chemical Structure, Their Numerical Estimation and Prediction from Additive Group Contributions*, Ch. 10, Elsevier, Amsterdam (1990).
101. J. Bicerano, *Prediction of Polymer Properties*, Ch. 8, Marcel Dekker, New York (1993).
102. M. Randic, *J. Amer. Chem. Soc.*, **97**(23), 6609 (1975).
103. L. Kier, L. Hall, W. Murray, and M. Randic, *J. Pharm. Sci.*, **64**(12), 1971 (1975).
104. J. Gladstone and T. Dale, *Trans. Roy. Soc. (London)*, **148**, 887 (1858).

105. A. Vogel, W. Cresswell, and I. Leicester, *J. Phys. Chem.*, **58**, 174 (1954).
106. R. Stein and G. Wilkes, in *Structure and Properties of Oriented Polymers*, I. Ward, Ed., J. Wiley, New York (1975).
107. G. Meeten, in *Optical Properties of Polymers*, Ch. 1, G. Meeten, Ed., Elsevier Applied Science, New York (1986).
108. P. Tien, R. Ulrich, and R. Martin, *Appl. Phys. Lett.*, **14(9)**, 291 (1969).
109. G. Leclerc and A. Yelon, *Appl. Optics*, **23(16)**, 2760 (1984).
110. F. McCrackin, E. Passaglia, R. Stromberg, and H. Steinberg, *J. National Bureau Standards*, **67A(4)**, 363 (1963).
111. M. Born and E. Wolf, *Principles of Optics Fifth Edition*, p. 694, Pergamon Press, New York (1975).
112. C. Viney, *Transmitted Polarised Light Microscopy*, Mc Crone Research Institute, Chicago (1990).
113. H. Jerrard, *J. Opt. Soc. Am.*, **44(8)**, 634 (1954).
114. G. Baur, V. Wittwer, and D. Berreman, *Phys. Lett.*, **56A(2)**, 142 (1976).
115. T.J. Scheffer and J. Nehring, *J. Appl. Phys.*, **48(5)**, 1783 (1977).
116. M. Becker, R. Kilian, B. Kosmowski, and D. Mlynski, *Mol. Cryst. Liq. Cryst.*, **132**, 167 (1986).
117. B. Myrvold, K. Kondo, and S. Oh-Hara, *Liquid Crystals*, **15(3)**, 429 (1993).
118. B. Myrvold and K. Kondo, *Liquid Crystals*, **18(2)**, 271 (1995).
119. H. Fukuro and S. Kobayashi, *Mol. Cryst. Liq. Cryst.*, **163**, 157 (1988).

120. D. Berreman, *Phys. Rev. Lett.*, **28(26)**, 1683 (1972).
121. D. Berreman, *Mol. Cryst. Liq. Cryst.*, **23**, 215 (1973).
122. U. Wolff, W. Greubel, and H. Kruger, *Mol. Cryst. Liq. Cryst.*, **23**, 187 (1973).
123. E. Matsui, K. Nito, and A. Yasuda, *Liquid Crystals*, **17(3)**, 311 (1994).
124. E. Lee, P. Vetter, T. Miyashita, T. Uchida, M. Kano, M. Abe, and K. Sugawara, *Jpn. J. Appl. Phys.*, **32(10A)**, L1436 (1993).
125. Y. Kawata, K. Takatoh, M. Hasegawa, and M. Sakamoto, *Liquid Crystals*, **16(6)**, 1027 (1994).
126. Y. Zhu, Z. Lu, F. Quian, X. Yang, and Y. Wei, *Appl. Phys. Lett.*, **63(25)**, 3433 (1993).
127. K. Kawahara, Y. Nakajima, T. Udagawa, H. Fujii, and H. Morimoto, *Rec. SID Int. Disp. Res. Conf.*, 180 (1994).
128. Y. Nakajima, K. Saito, M. Murata, and M. Uekita, *Mol. Cryst. Liq. Cryst.*, **237**, 111 (1993).
129. M. Schadt, K. Schmitt, V. Kozinkov, and V. Chigrinov, *Jpn. J. Appl. Phys.*, **31(7)**, 2155 (1992).
130. S. Jain and H. Kitzerow, *Appl. Phys. Lett.*, **64(22)**, 2946 (1994).
131. S. Jain and H. Kitzerow, *Jpn. J. Appl. Phys.*, **33(5A)**, L656 (1994).
132. L. Minsk, J. Smith, W. van Deusen, and J. Wright, *J. Appl. Polym. Sci.*, **2(6)**, 302 (1959).
133. K. Ichimura, Y. Hayashi, K. Goto, and N. Ishizuki, *Thin Solid Films*, **235**, 101 (1993).

134. K. Ichimura, Y. Hayashi, H. Akiyama, and T. Ikeda, *Appl. Phys. Lett.*, **63(4)**, 449 (1993).
135. M. Sakuragi, T. Tamaki, T. Seki, Y. Suzuki, Y. Kawanishi, and K. Ichimura, *Chem. Lett.*, 1763 (1992).
136. Z. Sekkat, M. Buchel, H. Menzel, and W. Knoll, *Chem. Phys. Lett.*, **220**, 497 (1994).
137. Z. Sekkat and M. Dumont, *Synthetic Metals*, **54**, 373 (1993).
138. S. Sun, W. Gibbons, and P. Shannon, *Liquid Crystals*, **12(5)**, 869 (1992).
139. P. Shannon, W. Gibbons, and S. Sun, *Nature*, **368**, 532 (1994).
140. W. Gibbons, P. Shannon, and S. Sun, and B. Swetlin, *Nature*, **351**, 49 (1991).
141. W. Gibbons, A. Bell, P. Shannon, and S. Sun, *Rec. SID Int. Disp. Res. Conf.*, 157 (1994).
142. W. Gibbons, P. Shannon, and S. Sun, *SPIE*, **1665**, 184 (1992).
143. M. Hasegawa and Y. Taira, *Rec. SID Int. Disp. Res. Conf.*, 213 (1994).
144. H. Kambe, in *Aspects of Degradation and Stabilization of Polymers*, Ch. 8, H. Jellinek, Ed., Elsevier, Amsterdam (1978).
145. R. Srinivasan and B. Braren, *J. Polym. Sci.: Polym. Chem.*, **22**, 2601 (1984).
146. G. Pettit and R. Suaerbrey, *Appl. Phys. Lett.*, **58(8)**, 793 (1991).
147. R. Srinivasan, B. Braren, and R. Dreyfus, *J. Appl. Phys.*, **61(1)**, 372 (1987).
148. J. Brannon, J. Lankard, A. Baise, F. Burns, and J. Kaufman, *J. Appl. Phys.*, **58(5)**, 2036 (1985).

149. G. Pettit, M. Ediger, D. Hahn, B. Brinson, and R. Sauerbrey, *Appl. Phys. A*, **58**, 573 (1994).
150. M. Schadt and W. Helfrich, *Appl. Phys. Lett.*, **18**, 127 (1971).
151. T.J. Scheffer and J. Nehring, *Appl. Phys. Lett.*, **45(10)**, 1021 (1984).

Chapter 2. Refractive Indices of Polyimides

2.1. Introduction

The optical index of refraction is an important physical property of polyimides. The purpose of this chapter is to explore the fundamental factors that determine the indices of refraction of polyimides as a class of materials. The work focuses primarily on the relationship between polyimide chemistry and refractive index, but also investigates various processing effects.

Refractive index is a measure of the material's electronic polarizability, which is an important component of its dielectric behavior. In many electronic packaging applications, a low dielectric constant is required for minimizing crosstalk and maximizing signal propagation speed. Refractive index is related to the dielectric constant by:

$$\epsilon_{\infty} = n^2 \quad (1)$$

where n is refractive index and ϵ_{∞} is the dielectric constant at optical frequency. The index of refraction at optical frequencies, unlike the dielectric constant at electrical frequencies, is easily obtained experimentally, even if the material is anisotropic.

The index of refraction is also important as a waveguide parameter. Polyimide electronic packaging layers have been suggested to serve as waveguides for optical interconnect technologies [1].

It is well known that polyimides with high fluorine content [2-19] have low dielectric constants and refractive indices. Unfortunately, however, there is no adequate explanation in the literature as to why this is so. There are three possible explanations: reduced crystallinity, reduced electronic polarizability, and reduced charge transfer complexation.

First, it is possible that bulky fluorinated groups impede crystallization in polyimides. Index of refraction is related to density as shown in the Lorentz-Lorenz equation shown below:

$$[(n^2 - 1) / (n^2 + 2)] = (\rho/M) (N_{av}/3\epsilon_0) \alpha \quad (2)$$

where M is molecular weight, ρ is density, N_{av} is Avagadro's number, ϵ_0 is relative

permittivity in a vacuum. In equation (2), for the range of refractive indices typical of organic polymers, refractive index increases with (ρ/M) and with α . Crystalline polymers are more densely packed and would therefore, in general, be expected to have higher indices of refraction. Though crystallinity has been observed in some polyimides [20-29], polyimides are most frequently considered to be primarily amorphous. Thus, reduced crystallinity is probably not a fully adequate explanation for the reduced indices of refraction in fluorinated polyimides.

Another possible explanation is reduced electronic polarizability. Refractive index is related to electronic polarizability α as previously stated in equation (2). The carbon-fluorine bond has low electronic polarizability, and consequently, fluorinated polymers are known to have low indices of refraction [30].

A third explanation is the reduced charge transfer complexation associated with the incorporation of bulky fluorinated groups. The groups sterically hinder the intermolecular interactions in the polyimide. This theory was put forth by St. Clair *et al.* [2,10-12].

It is quite possible that all three of these explanations play some role in the reduced indices of refraction. However, it has been entirely unclear as to what are the relative contributions of these effects. Discussions of this issue in the literature are frustratingly inadequate.

For example, Inchino *et al.* [3] systematically increased the length of fluorinated alkoxy side chains in order to systematically reduce the dielectric constant of polyimides. The authors state, in agreement with St. Clair *et al.* [2,10-12], "the increase in length of the fluorinated alkoxy groups, leading to a more bulky separator which sterically hinders the [chain-chain] interaction, must reduce the dielectric constant" [3]. The authors then continue to state that "fluorine has low electronic polarizability which reduces the dielectric constant" [3]. However, it is unclear in this work what they believe is the main contributor.

The explanation put forth by Matsuura *et al.* [15,16] for the reduced dielectric constant in rigid rod fluorinated polyimides is more confusing. According to the authors, "the low dielectric constants of the fluorinated polyimides result from reduced chain-chain interaction due to the low electronic polarizability of the fluorine" [16]. This is, of course, a non-sensical explanation, as the low electronic polarizability of the C-F bonds and the reduced intermolecular interactions are different and unnecessarily related phenomena.

Hence, it is the goal of this chapter to gain better insight into the mechanisms of the refractive index reduction in polyimides that occurs as a result of fluorination. The optical

properties of a large number of polyimides are compared. Experimental refractive indices are then compared to indices calculated by the property prediction techniques described in Chapter 1. The effects of processing on the index of refraction in polyimides are also investigated later in the chapter.

2.2. Experimental Techniques

2.2.1. Polyimide film preparation

Two sources of polyimide refractive index data were used. The first was the literature [2-5,31-36]. Films preparation for these samples are described by the authors. The second source was polyimide films synthesized at and provided by Dr. Anne St. Clair of the NASA Langley Research Center, Hampton, Virginia. The chemical compositions of these and other polymers are presented in Tables 2.1-2.3. Polyimides ODPA-3,3'-ODA, ODPA-4-BDAF, 6FDA-3,3'-ODA, 6FDA-4-BDAF, 6FDA-DASP, BFDA-DASP, BPDA-DASP, ODPA-DASP, IPAN-DASP, BTDA-DASP, HQDEA-DASP, BDSDA-DASP, BTDA-1,3BABB, PMDA-ODA, and ODPA-PDA were obtained as thick free standing films. The polyamic acids were synthesized in N,N-dimethylacetamide, solution cast on glass, and cured in a low humidity environment at 100°C, 200°C, and 300°C for one hour at each temperature. PMDA-ODA was annealed an additional 20 minutes at 400°C. Regulus™ NEW-TPI, whose chemical composition is shown in Table 2.1, was received from the Mitsui Toatsu Chemical Co. Polyimides discussed in section 2.4.3, PMDA-ODA, PMDA-APB, PMDA-BDAF, 6FDA-ODA, 6FDA-APB, and 6FDA-BDAF, were received as 15% solids by weight solutions in N,N-dimethylacetamide. The solutions were spin coated on glass using a Headway Research spin coater at 4000 RPM for 30 seconds. The coated films were progressively cured at 100°C, 200°C, and 300°C for one hour at each temperature.

2.2.2. Zone drawing

The zone drawing technique has been described previously [37-40] and is depicted in Figure 2.1 below. The film is placed between two clamps with a weight pulling on one end. A zone heater passes over the film at a constant rate which heats the film above the glass transition temperature. The material is drawn at the site of heating. By varying the

drawing weight and temperature, films of various draw ratios (final length / initial length) were produced for 6FDA-4-BDAF fluorinated polyimide films.

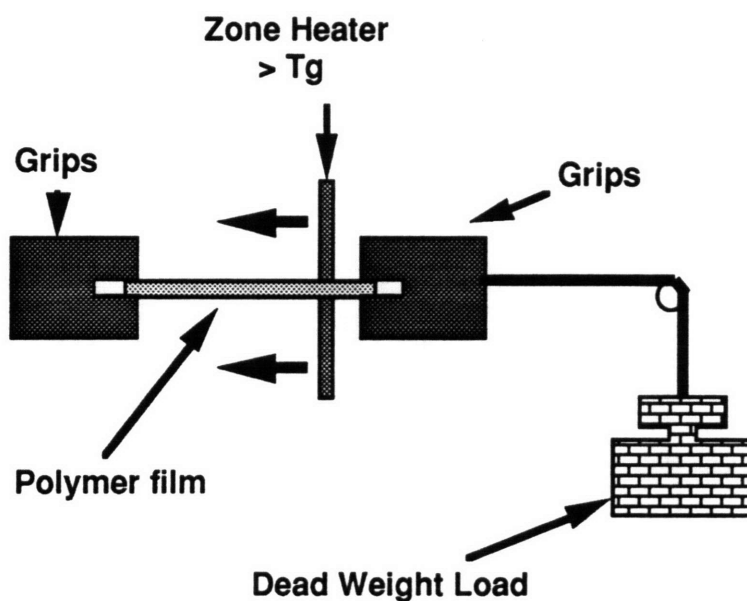


Figure 2.1. Film zone drawing method.

2.2.3. Refractive index measurement

Refractive index measurements were made for polyimide films using a Metricon PC-2000 prism coupler with $\lambda = 6328\text{\AA}$. Average refractive indices were calculated as:

$$n_{\text{avg}} = (1/3) (2n_{\text{TE}} + n_{\text{TM}}) \quad (3)$$

The prism coupling technique for measuring index of refraction is discussed in Chapter 1.

2.2.4. Refractive index prediction

Two property prediction techniques, which are discussed in Chapter 1, were utilized in order to estimate how varying chemical make-up should affect refractive index. It is assumed that these estimation techniques account for the intrachain electronic

polarizability of the polymer molecular repeat unit. The first is the group contribution method by van Krevelen [41] based on an equation used by Vogel [42]. The second is a topological technique by Bicerano [43]. Both methods, unlike two other techniques described by van Krevelen [41], require no measurement of the polymer density prior to the calculation. Only the chemical structure is needed. However, since polymer density is not used in these calculations, both methods are intended only for amorphous polymers. For details concerning these calculations, please refer back to Chapter 1 or the original references [41-43].

2.3. Relationship Between Polyimide Chemistry and Refractive Index

Experimental and predicted refractive indices of a large number of polyimides were compared. Three types of behavior were found. First, many amorphous, non-fluorinated polyimides were found to have refractive indices of around 1.68-1.70, deviating slightly, though systematically, above the predicted refractive index. Second, some polyimides were found to have refractive indices that were substantially higher than those predicted. Third, fluorinated polyimides had low refractive indices which generally compared favorably to predicted values.

2.3.1. Amorphous, non-fluorinated polyimides

A comparison between predicted and measured refractive indices in nonfluorinated polyimides is shown in Figure 2.2. The polyimides have generally been arranged from left to right in order of declining measured refractive index. The chemical structures of the polyimides are shown in Table 2.1.

Although the calculated refractive indices are close to experimental values, we notice a systematic underprediction, especially when using the presumably more accurate method of Bicerano. Refractive indices calculated by van Krevelen's method are good, underpredicting by only about 0.02-0.03. Bicerano's method underpredicts refractive index by about 0.05-0.06, which is three to four times the standard deviation in Bicerano's correlation. It is unlikely that such large deviations from experimental values in the Bicerano computations can be attributed solely to statistical error.

Charge transfer complexation [2,10-12,44-49] and/or molecular ordering might result in deviations of predicted from measured refractive indices. There has been no evidence of substantial crystal lattice ordering in these materials. However, as shown in Figure 2.3(a), PMDA-ODA may exhibit slight paracrystalline order when examined using

wide-angle X-ray scattering (WAXS). Alternatively, chain packing which might result from intermolecular complexation could be responsible for an increase in density of the amorphous phase and/or an increase in electronic polarizability. The property prediction techniques apparently do not account for the chain packing and/or charge transfer effects.

2.3.2. Semicrystalline polyimides

The index of refraction of a polymer is directly related to its density. Since crystalline phases are denser than amorphous phases, a measured refractive index that is substantially higher than that predicted by property prediction methods may be associated with polymer semicrystallinity. Figure 2.4 compares predicted and measured indices of polyimides with unusually high refractive indices. See Table 2.2 for the chemical structures.

There is substantial experimental evidence of crystal lattice ordering in these particular materials. Previous authors have shown that BPDA-PDA [22], ODPA-PDA [20], BTDA-1,3-BABB [21,23-27] are crystallizable. WAXS analysis, shown in Figure 2.3(b), confirms the presence of a crystalline phase in our ODPA-PDA sample. This material has exactly the same atoms and bonds as does PMDA-ODA (chemical structure Table 2.1, WAXS Figure 2.3(a)), but has a refractive index significantly greater. Thus, there is likely a strong structure-property relationship between crystallinity and refractive index in polyimides which is not taken into account in the van Krevelen and Bicerano predictions.

2.3.3. Polyimides containing hexafluoroisopropylidene (6F)

The optical properties of polyimides containing the hexafluoroisopropylidene (6F) group have been the subject of much investigation [2-19]. It has generally been observed that the refractive indices of polyimides decrease with increasing fluorine content. It is also believed by these authors that the 6F group, which consists of two trifluoromethyl groups bonded to carbon, sterically inhibits charge transfer complexation in the polyimides.

Figure 2.5 shows a comparison of predicted and measured refractive indices of polyimides containing the 6F group. For the chemical structures, see Table 2.3. Both property prediction methods estimate refractive index quite accurately. Bicerano's method is accurate when the 6F group appears in both the dianhydride and diamine portions of the repeat unit, but very slightly underpredicts refractive index when the 6F group exists in

only one segment. This demonstrates that the lower refractive indices that have been observed experimentally in 6F materials can be predicted from the modified chemical structure. Furthermore, the good agreement between measured refractive index and these predictions suggests that chain packing and charge transfer complexation may be reduced in these materials.

2.3.4. Polyimides containing fluorinated alkoxy side chains

The synthesis and characterization of novel polyimides containing fluorinated alkoxy side chains, shown in Table 2.4, have been reported [3]. Measured refractive indices and dielectric constants were shown to be reduced systematically with increasing fluorine content. The fluorine content of the polyimides was increased by increasing the length of the side chains.

In Figure 2.6, predicted refractive index (Bicerano technique) is shown as a function of fluorine content. The predicted indices compare fairly favorably to measurement. However, experimentally, a slight dependence on the dianhydride chemistry was found by the authors. Polyimides containing the 6FDA dianhydride, for example, had lower refractive indices than polyimides containing non-fluorinated dianhydrides, but equal overall fluorine content. This is not predicted, however, by Bicerano's method, as shown in Figure 2.6. This may indicate that the 6F group is more effective per fluorine atom than is the side chain in reducing polymer chain packing.

2.3.5. Polyimides containing pentafluorosulfanyl (SF₅)

Recently, St. Clair and St. Clair [19] reported the synthesis of novel fluorinated polyimides containing a pentafluorosulfanyl (SF₅) group. Measured and predicted refractive indices of these polymers are shown in Table 2.5. We found a small deviation between predicted and experimental values. The least deviation occurred in a polyimide containing a bulky isopropylidene group in the dianhydride portion of the chain (IPAN). Likely, the SF₅ group impedes chain packing to some extent, though not as well as the 6F group.

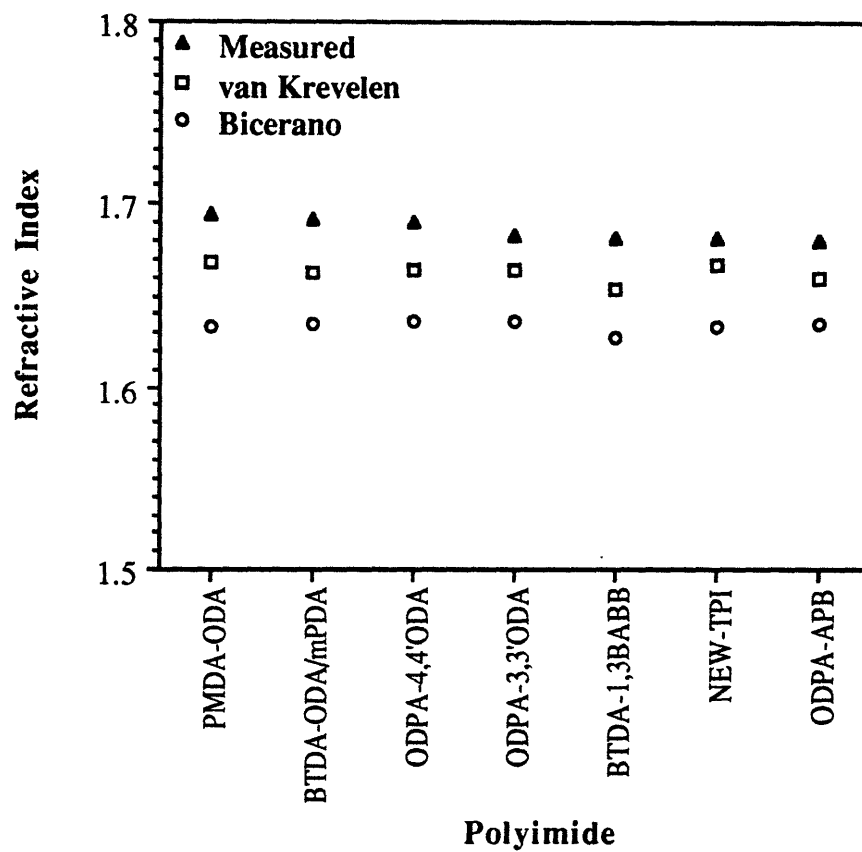


Figure 2.2. Experimental and predicted refractive indices of non-fluorinated polyimides in Table 2.1.

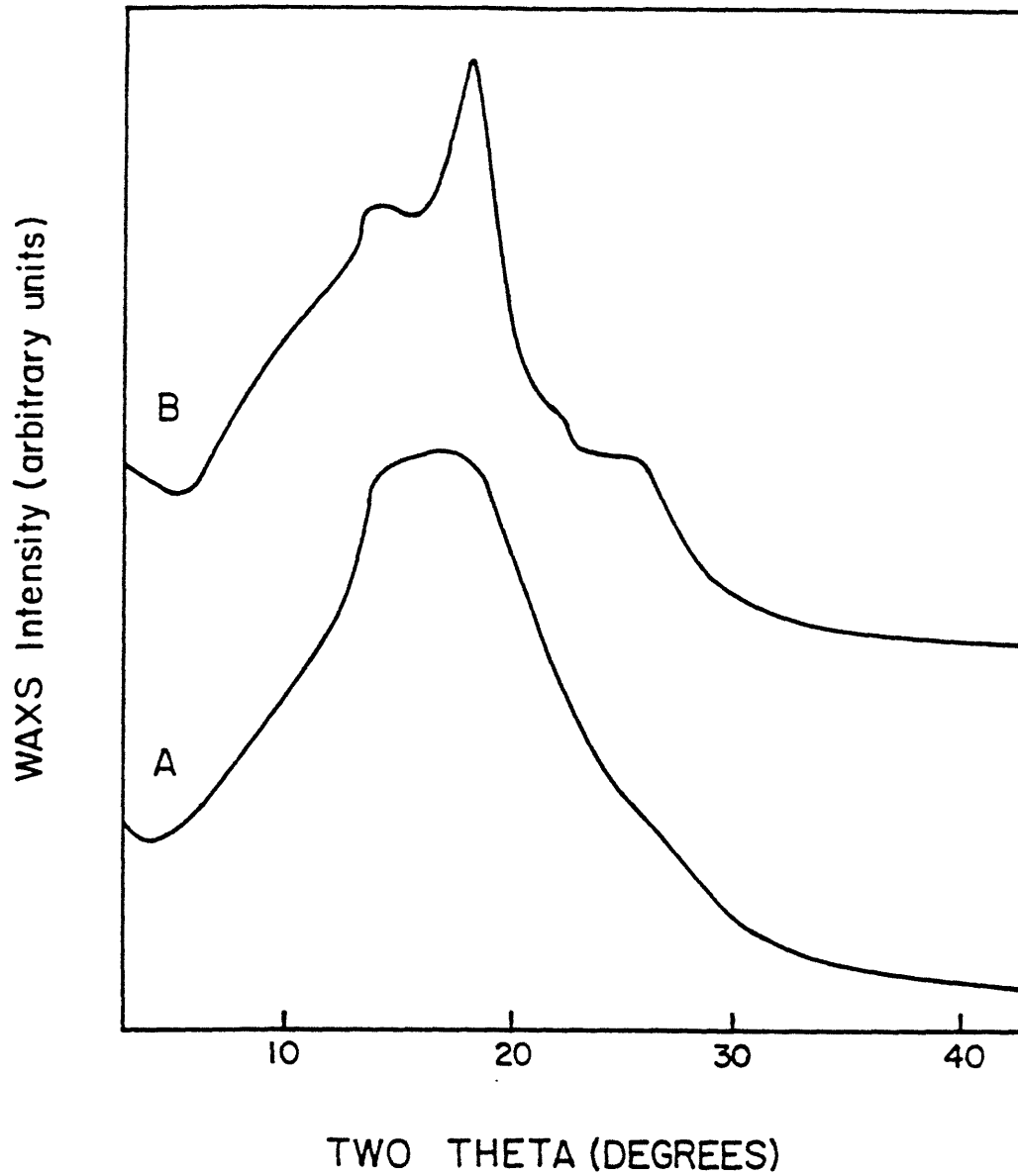
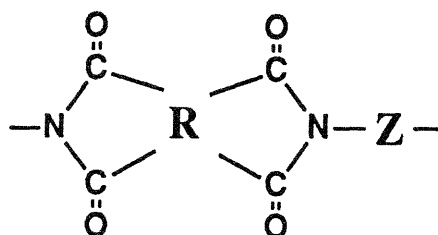


Figure 2.3. Wide angle X-ray scattering (WAXS) of: a.) PMDA-ODA and b.) ODPA-PDA polyimide films. The polymers contain the same exact atoms and bonds, but have very different physical structures, and correspondingly, very different optical properties.

Table 2.1. Dianhydride (R) and diamine (Z) elements of polyimides in Figure 2.2.



Polyimide [ref.]	R	Z
PMDA-ODA [see also 31,32]		
BTDA- ODA/mPDA [33]		
ODPA- 4,4'ODA [2]		
ODPA- 3,3'ODA		
BTDA- 1,3BABB (melted/ quenched)		
NEW-TPI		
ODPA-APB [2]		

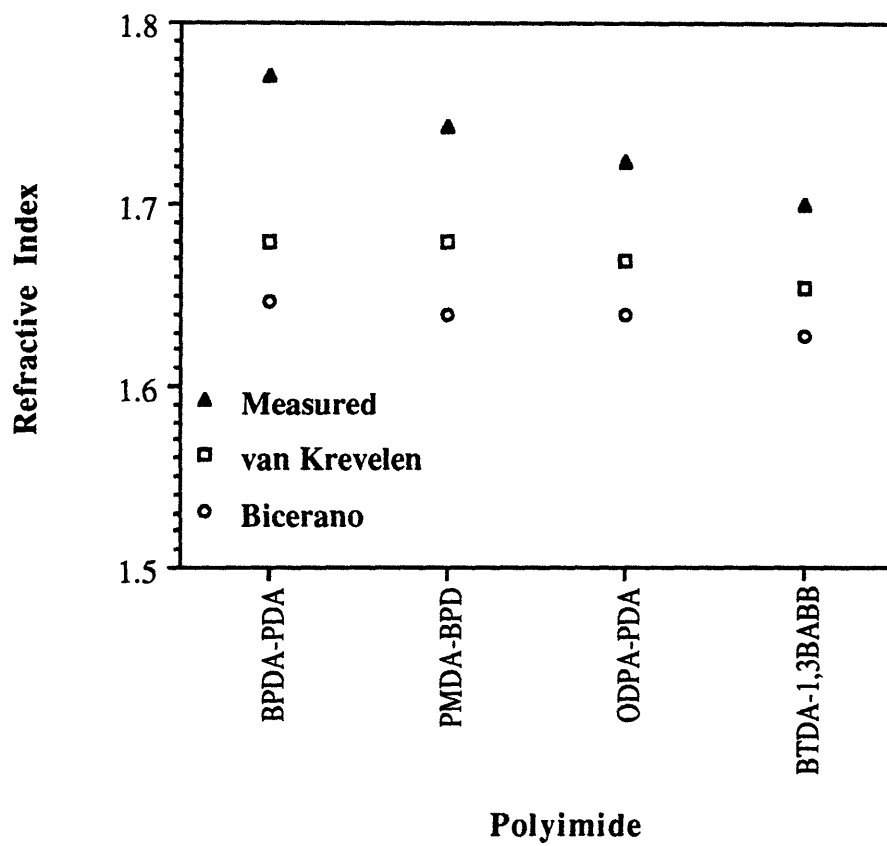
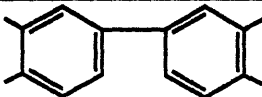

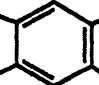
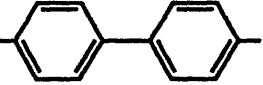
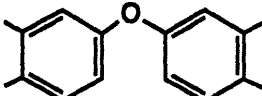

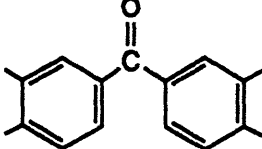
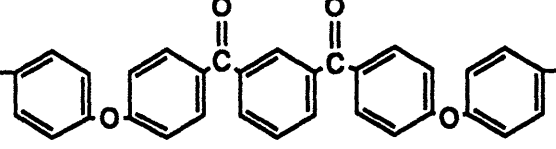


Figure 2.4. Measured and predicted refractive indices of semicrystalline polyimides in Table 2.2.

Table 2.2. Dianhydride (R) and diamine (Z) elements of polyimides in Figure 2.4.

Polyimide [ref.]	R	Z
BPDA-PDA [35]		
PMDA-BPD [34]		
ODPA-PDA		
BTDA- 1,3BABBB		

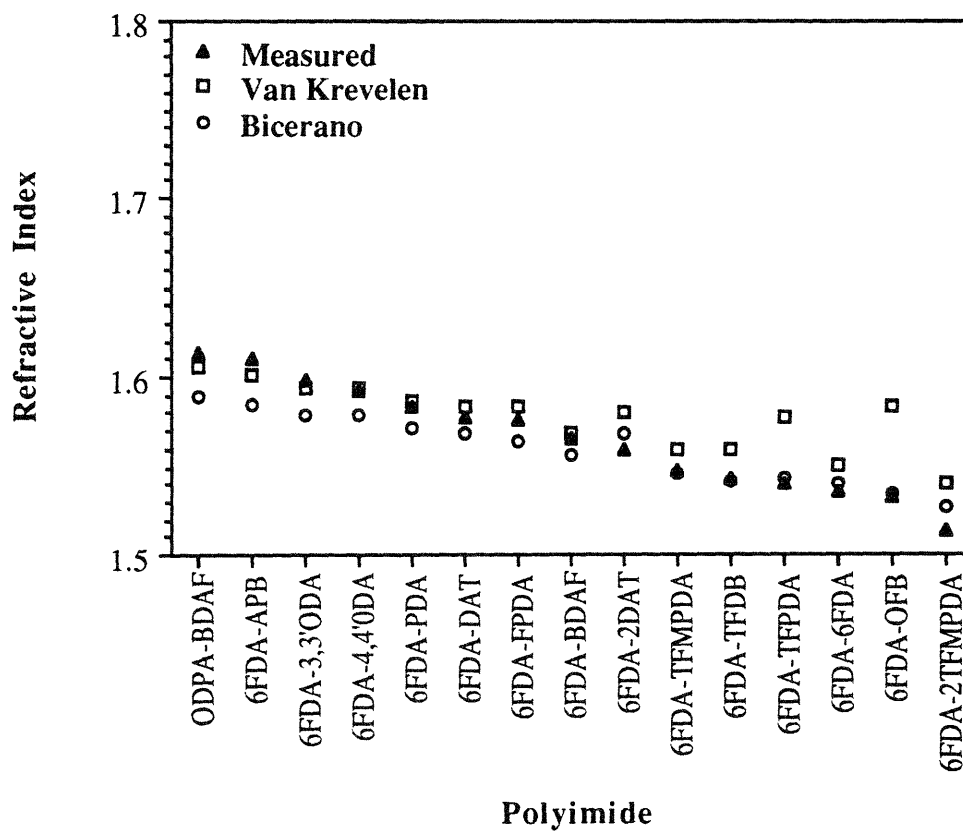
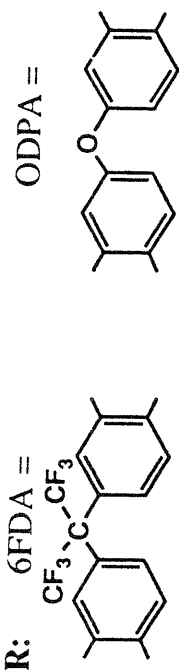


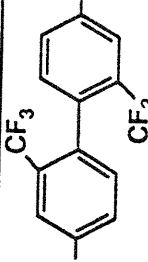
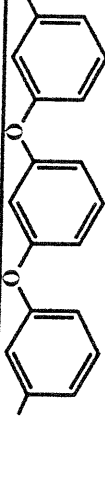
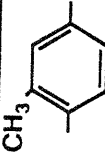
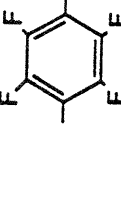
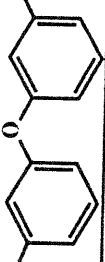
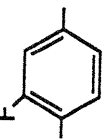
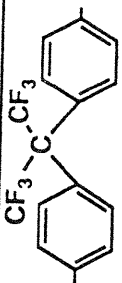
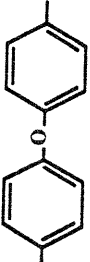
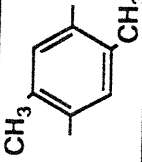
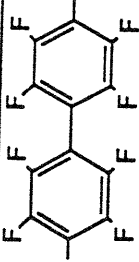
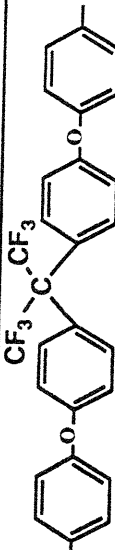
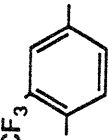
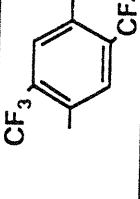


Figure 2.5. Measured and predicted refractive indices of 6F polyimides from Table 2.3.

Table 2.3. Diamine (Z) elements of the 6F polyimides in Figure 2.5.



Polyimide [ref.]	Z	Polyimide [ref.]	Z	Polyimide [ref.]	Z
ODPA-BDAF		6FDA-PDA [5]		6FDA-TFDB [5]	
6FDA-APB [2]		6FDA-DAT [5]		6FDA-TFPDA [5]	
6FDA-3,3'ODA		6FDA-FPDA [5]		6FDA-6FDA [4]	
6FDA-4,4'ODA [4]		6FDA-2DAT [5]		6FDA-OFB [5]	
6FDA-BDAF		6FDA-TFMPDA [5]		6FDA-2TFM PDA [5]	

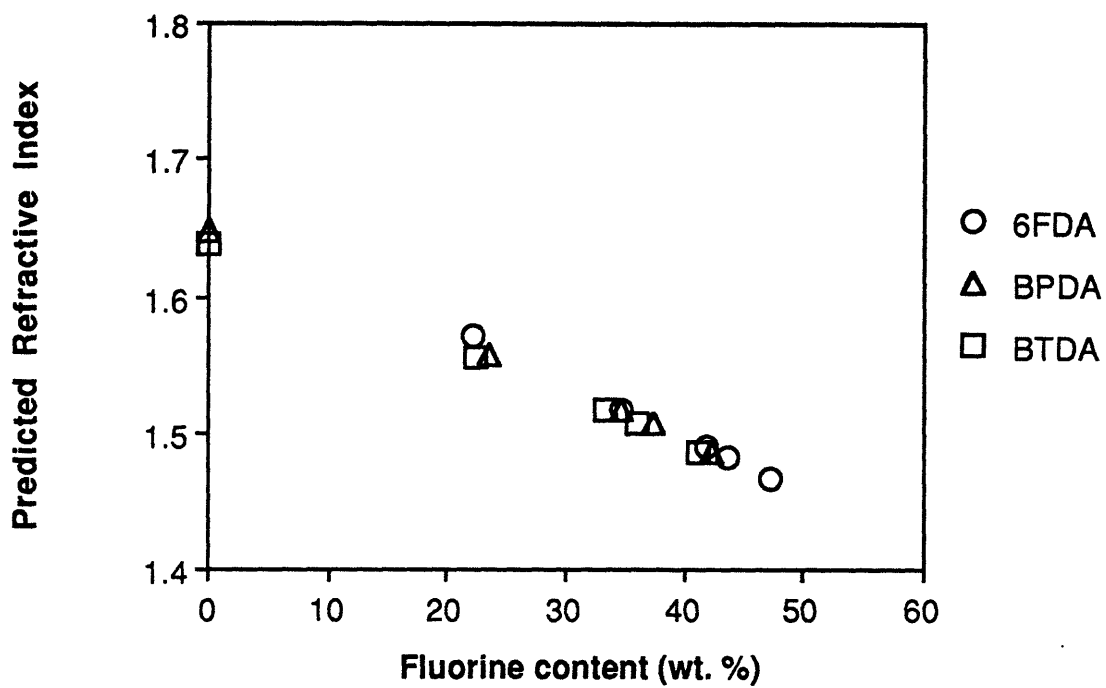


Figure 2.6. Predicted refractive indices (Bicerano's method) of polyimides with fluorinated alkoxy side chains vs. fluorine content. Chemical structures in Table 2.4.

Table 2.4. Dianhydride (R) and diamine (Z) segments of polyimides with fluorinated alkoxy side chains, reported by Inchino *et al.* [3].

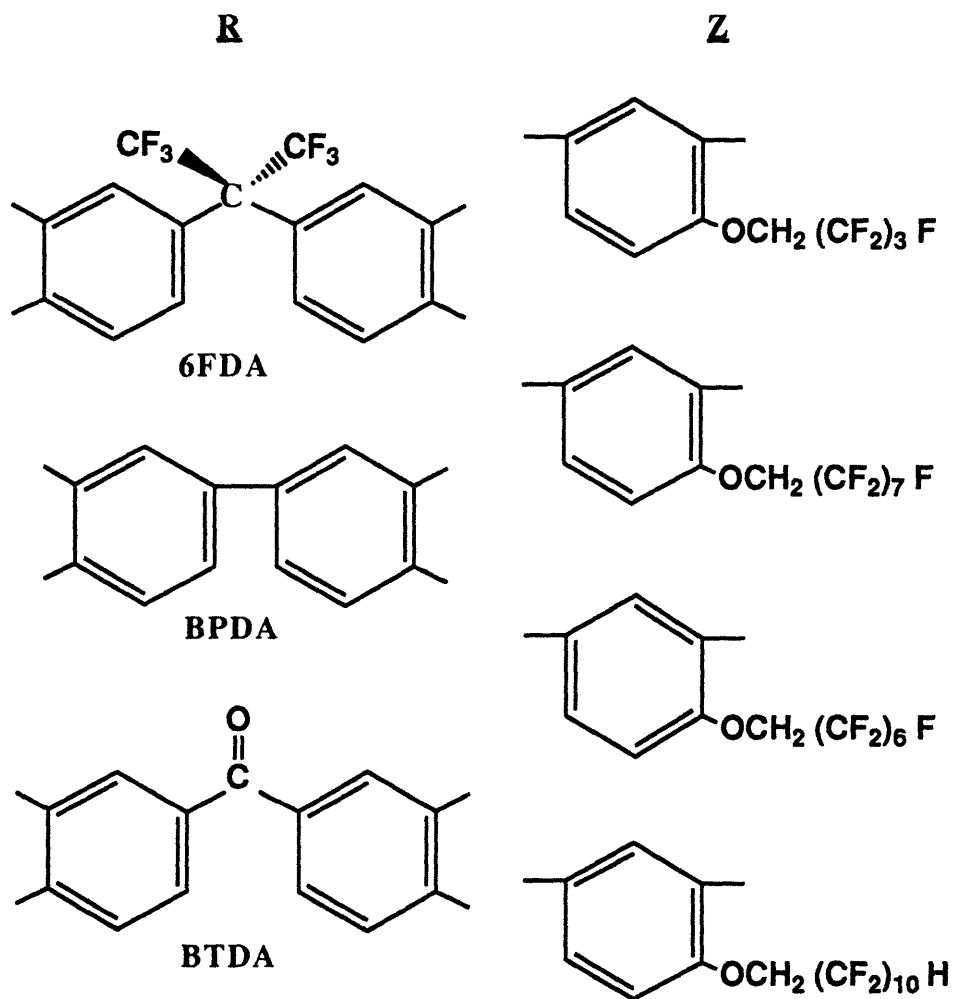
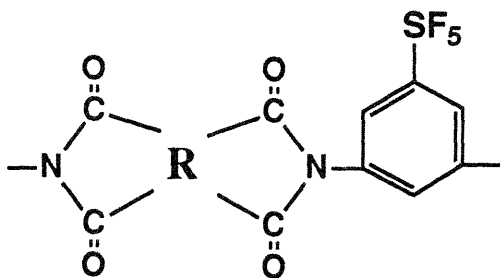


Table 2.5. Measured and predicted refractive indices of SF₅ polyimides.

Polyimide	R	$n_{\text{meas.}}$	$n_{\text{Bic.}}$	n_{vK}
6FDA-DASP		1.541	1.536	1.529
BFDA-DASP		1.576	1.559	1.554
BPDA-DASP		1.640/ 1.635*	1.592	1.582
ODPA-DASP		1.620	1.588	1.576
IPAN-DASP		1.597	1.583	1.570
BTDA-DASP		1.621	1.588	1.577
HQDEA-DASP		1.624	1.594	1.586
BSDA-DASP		1.647	1.616	1.602

* First value represents side 1, the second value, side 2.

2.4. Relationship Between Polyimide Processing and Refractive Index

2.4.1. In-plane birefringence in polyimide films

PMDA-ODA

PMDA-ODA is a polyimide that is widely used commercially. The repeat unit of the polymer is shown below:

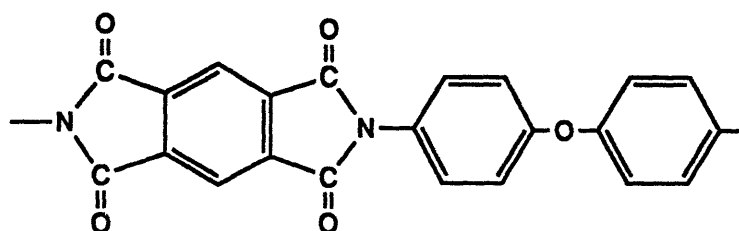


Figure 1.3 shows three types of orientation in polymer films: isotropic orientation, in-plane orientation, and uniaxial orientation. Thin films of PMDA-ODA have been found to have out-of-plane refractive indices, n_{TM} , that are significantly lower than in-plane refractive indices, n_{TE} [31,32]. This is because the main chain (c) axes lie preferentially in the plane of the film as shown in Figure 1.3(b). The average refractive index, $n_{avg} = (2n_{TE} + n_{TM}) / 3$, and birefringence, $\Delta n = n_{TE} - n_{TM}$, of fully annealed spun cast PMDA-ODA films were reported by Russell *et al.*[31]. The authors found $n_{avg} = 1.695$ and $\Delta n = 0.08$. Data for our PMDA-ODA samples are shown in Table 2.6. Solvent cast film received from the NASA Langley Research Center had a birefringence of 0.078, while commercial DuPont Kapton™ H had a birefringence of 0.111. The commercial film, as compared to the NASA Langley film, had a lower out-of-plane refractive index n_{TM} and a higher in-plane refractive index n_{TE} , which suggests that the film has a greater level of in-plane ordering. The average refractive indices, however, of both films were around 1.7.

Table 2.6. Optical Properties of PMDA-ODA.

Material source:	n_{avg}	n_{TE}	n_{TM}	Δn
NASA Langley	1.697	1.723	1.645	0.078
DuPont Kapton™ H	1.702	1.739	1.628	0.111

Optically transparent polyimides

Refractive indices of four optically transparent polyimides synthesized at the NASA Langley Research Center are listed in Table 2.7. Chemical structures can be found in Tables 2.1 and 2.3. Unlike the PMDA-ODA films, very little optical anisotropy is seen in these materials. We conclude that there is little preferential in-plane alignment of the polymer chains in these films, as shown in Figure 1.3(a). This may be a result of either the high thickness of the films or a lack of a tendency of these materials to order in the plane of the film.

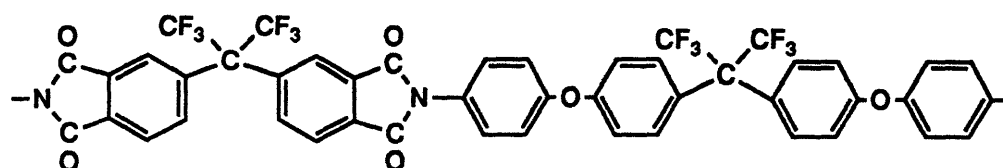
Table 2.7. Refractive indices of optically transparent polyimides.

Name	n_{TM}	n_{TE}	Thickness
ODPA-3,3'-ODA	1.683	1.681	23 μ m
ODPA-4-BDAF	1.615	1.612	28 μ m
6FDA-3,3'-ODA	1.598	1.597	34 μ m
6FDA-4-BDAF	1.566	1.564	34 μ m

2.4.2. Birefringence in zone drawn films

Nakagawa [32] and Smirnova and Bessonov [34] report the optical properties of uniaxially cold drawn PMDA-ODA. They show that the refractive index is highest in the direction of drawing and lowest normal to the direction of orientation. This is because the polarizable groups in the main chain are preferentially oriented along the draw axis, as shown in Figure 1.3(c). Both authors report a maximum birefringence on the order of 0.20. The average refractive index, however, is unaffected by the level of orientation, as it is near 1.7, which is consistent with what was previously mentioned in Section 2.4.1.

The chemical structure of 6FDA+4-BDAF, a fluorinated, low refractive index polyimide, is shown below:



When the material is zone drawn along one axis of the film, significant optical anisotropy is observed. Figure 2.7 shows the refractive index of 6FDA+4-BDAF in three perpendicular directions as a function of draw ratio.

In the direction of the draw in the plane of the film, refractive index increases with draw ratio. Refractive index decreases with draw ratio, however, out of the plane of the film or in the plane of the film perpendicular to the direction of the draw. This is, again, a result of the preferential alignment of the primary polarizable groups along the main chain in the direction of the draw. The average refractive index is not affected by zone drawing. Refractive index is lowest out of the plane of the film. At high draw ratios, it is nearly as low as 1.54, which is about 0.017 less than the average index of the film.

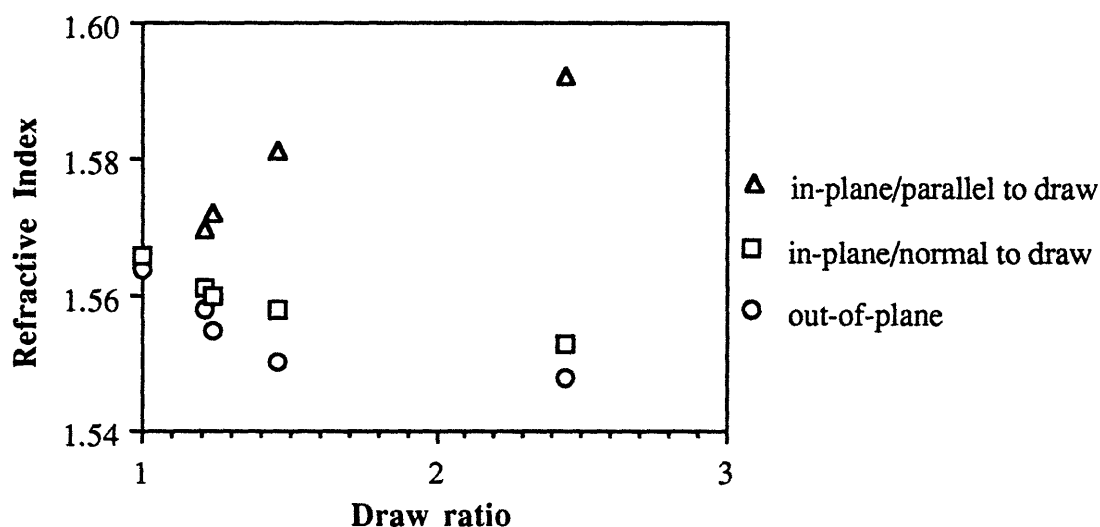


Figure 2.7. Refractive index vs. draw ratio for 6FDA+4-BDAF in the direction of the draw and normal to the draw.

2.4.3. Effect of cure temperature on refractive index

As explained in Chapter 1, polyimides generally begin as polyamic acid precursors, which are thermally converted to polyimides. As the polyimides undergo this reaction, the refractive index of the material increases. This is demonstrated in Figure 2.8, which shows

the average indices of refraction of several polyimides as a function of cure temperature. The films were spin coated from solutions obtained from NASA Langley, and their chemical structures can be found in Tables 2.1-3. Note that, as discussed previously, refractive index decreases with increased fluorine content.

To investigate the reasons for the increase in refractive index with increased cure temperature, the predicted refractive indices of the polyamic acid precursors were calculated using the Bicerano technique. In Figure 2.9(a), these values are compared to the measured refractive indices of the 100°C cured materials. Apparently, the values are in reasonably good agreement, regardless of whether the polyimide contains the 6F group. According to Kan and Kao [50], the imidization reaction does not occur appreciably until about 150°C, but occurs rapidly above 250°C. It is thus reasonable to assume that the 100°C treatment is representative of the unconverted state, while the 300°C is representative of the imidized state.

In Figure 2.9(b), predicted refractive indices of the fully converted polyimide are compared to measured refractive indices after the 300°C cure. As found in the previous sections, the Bicerano underpredicts the refractive indices of the non-fluorinated polyimides, i.e., PMDA-ODA and PMDA-APB, but is in good agreement with the refractive indices of the 6F fluorinated polyimides, i.e., the remaining four polymers.

The good agreement with predicted values for the polyamic acids suggests that there are no unexpected chain packing or charge transfer effects in the precursor materials that go unaccounted for by the Bicerano prediction technique. However, when the materials are converted to polyimide, the non-fluorinated materials undergo a significant unpredicted increase in refractive index. Since this increase in refractive index cannot be accounted for based upon the chemical change alone, this study suggests that the imidization reaction leads to greater chain packing and/or increased interchain interaction in the non-fluorinated polyimides. The 6F materials, on the other hand, remain consistent with predicted values upon imidization, indicating that the 6F group impedes the chain packing.

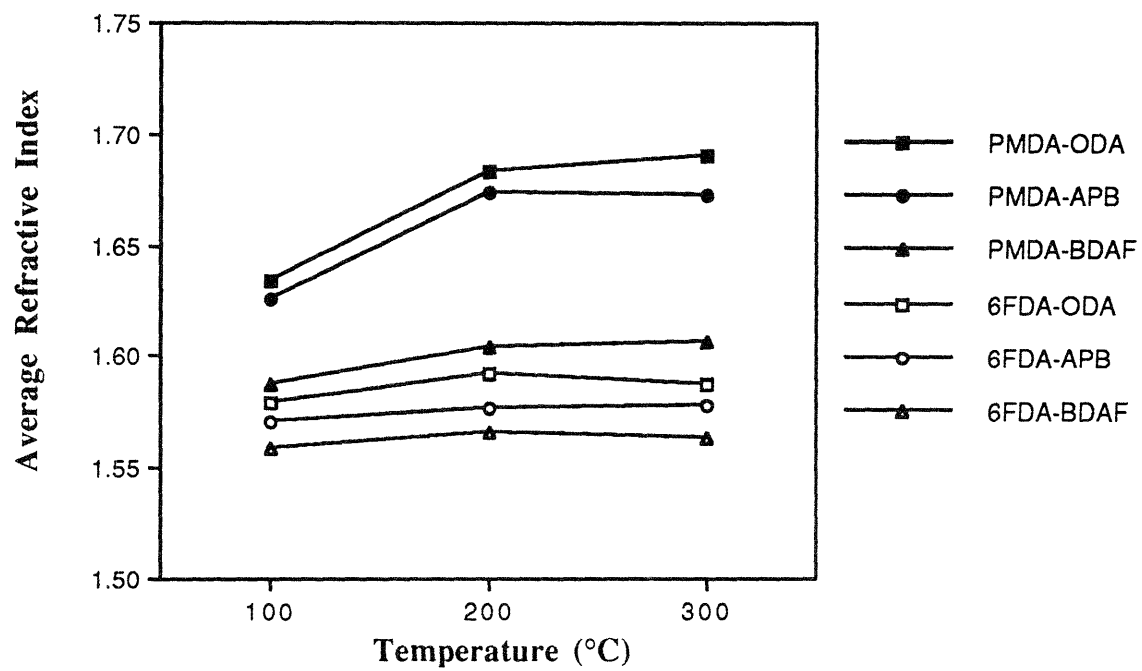


Figure 2.8. Refractive indices of several polyimides as a function of cure temperature.

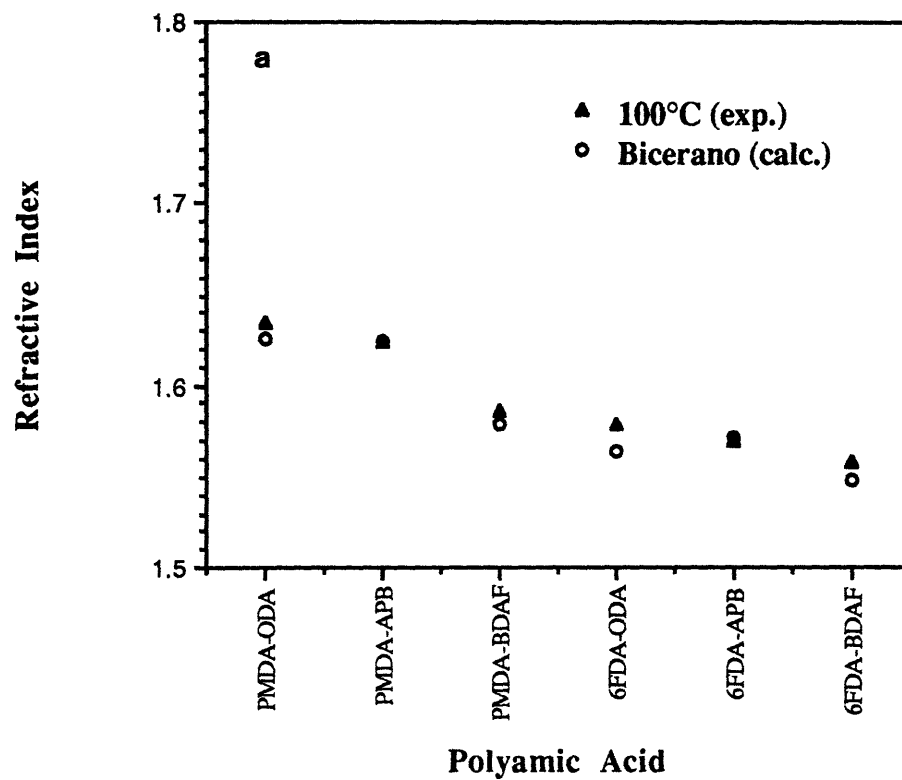


Figure 2.9. Predicted (Bicerano's method) vs. measured refractive indices of several polyimides. a.) Predicted values of the polyamic acid precursors vs. measured values of the films after only 100°C cure.

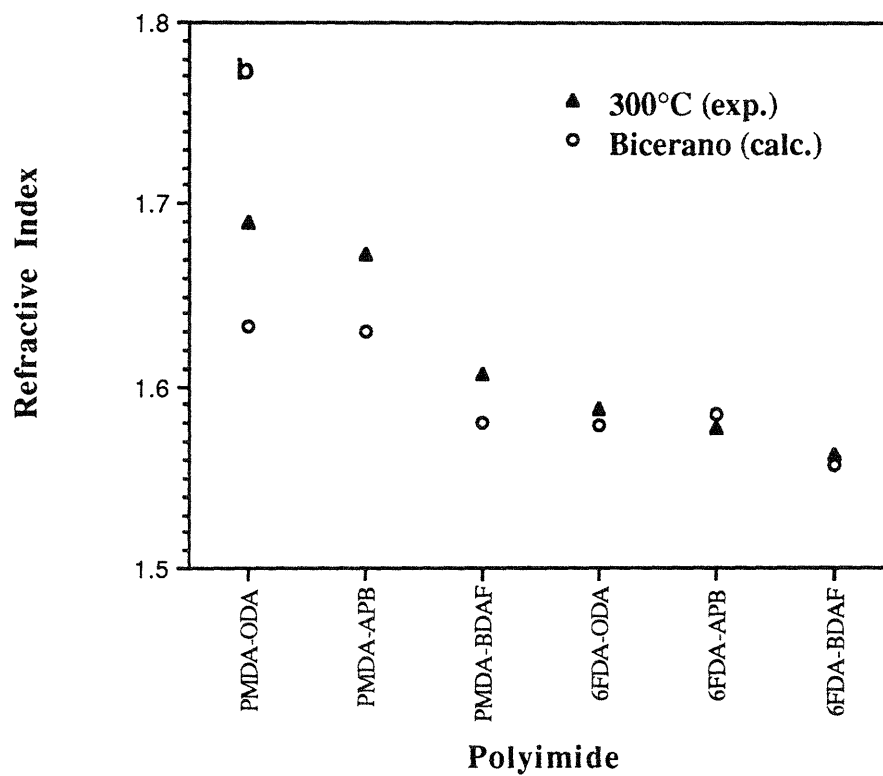


Figure 2.9. continued. b.) Predicted values of the polyimides vs. measured values after the 300°C cure.

2.4.4. Effect of post-cure annealing on NEW-TPI polyimide

Regulus™ NEW TPI [28,29] is a polyimide that is known to crystallize when annealed above its glass transition temperature ($T_g = 250^\circ\text{C}$). Crystallinity, as previously discussed, can increase the index of refraction of a polymer. Several samples of fully cured NEW-TPI were annealed in order to crystallize the material. Films were treated for 10 minutes at various temperatures between 280°C and 320°C , and for various times at 290°C . The annealing process roughened the surface of the films, thus making it more difficult to take accurate data using the Metricon prism coupler. Each refractive index (n_{TE} or n_{TM}) is therefore the average of four measurements.

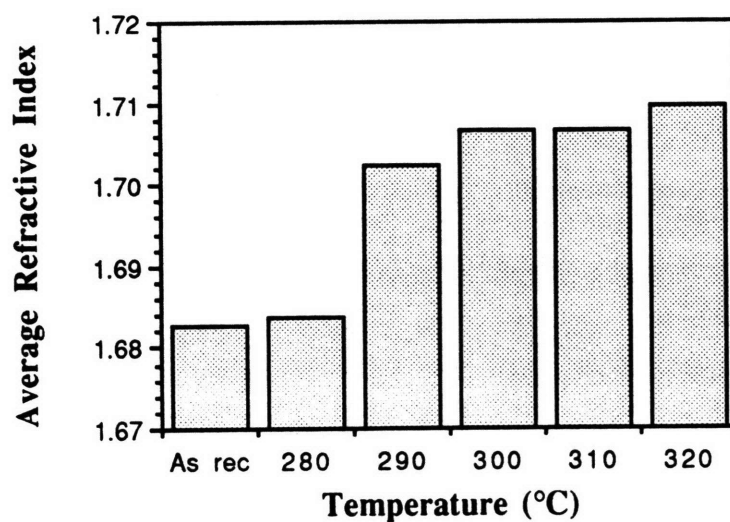
Both the average refractive index and birefringence ($n_{TE} - n_{TM}$) increased with annealing temperature, as shown in Figure 2.10. There is a significant step in average refractive index and birefringence at 290°C , indicating that this could be the onset temperature of rapid crystallization. The increase in bulk birefringence suggests that the crystals may have preferential order in the plane of the film.

The refractive index and birefringence also increase with annealing time at 290°C , as shown in Figure 2.11. Average refractive index appears to begin increasing after about three minutes of annealing, appears to be about half way to its maximum near six minutes, and appears to level after about 10 minutes. Previously reported work [28] for NEW-TPI samples isothermally annealed at 300°C , indicates a crystallization half time ($t_{1/2}$) of about 6.3 minutes and a crystallization completion time (t_c) of about 12 minutes. The general increase in birefringence with annealing time also suggests that the crystals may have in-plane order.

2.5. Conclusions

Significant variations of the refractive index of polyimides have been observed with varying, often subtly varying, chemical structure. Property prediction calculations of refractive indices of polyimides give some insight into the causes of these changes. While charge transfer complexation effects may slightly increase the refractive indices of polyimides, semicrystallinity or short range ordered structure can increase the refractive index substantially. Incorporation of fluorinated groups is an effective means of reducing the refractive index. The observed reduction results from a combination of reduced electronic polarizability and reduced interchain interaction and/or chain packing. Refractive

(a)



(b)

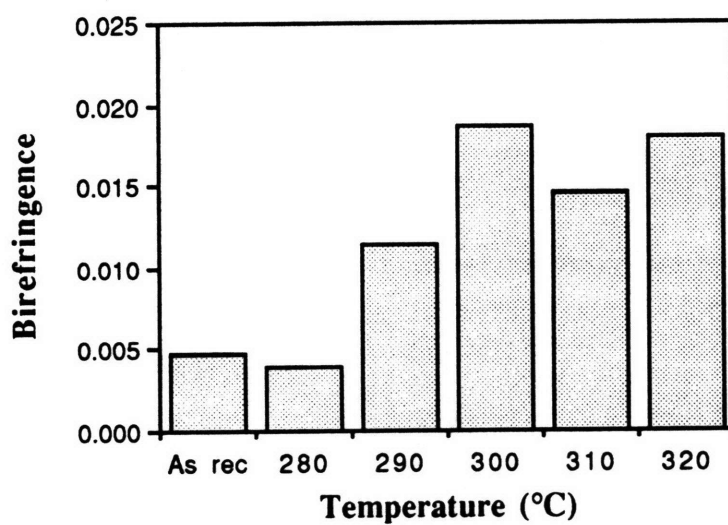
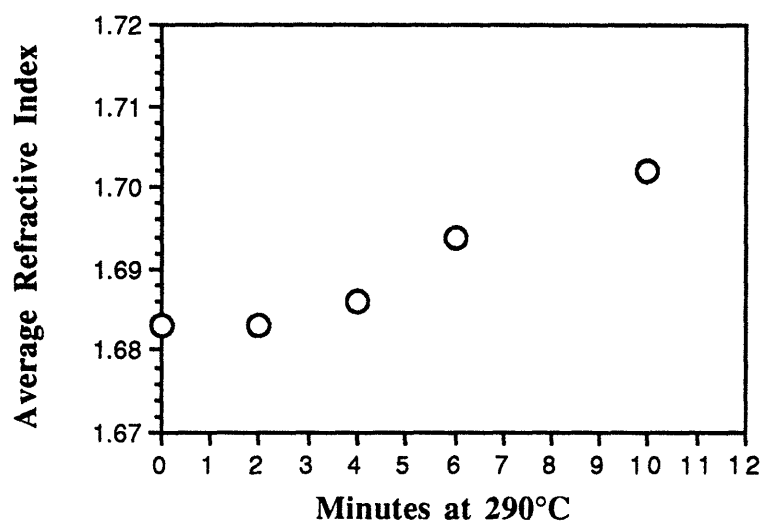


Figure 2.10. a.) Average refractive index of NEW-TPI vs. post-cure annealing temperature. b.) Birefringence vs. post-cure annealing temperature.

(a)



(b)

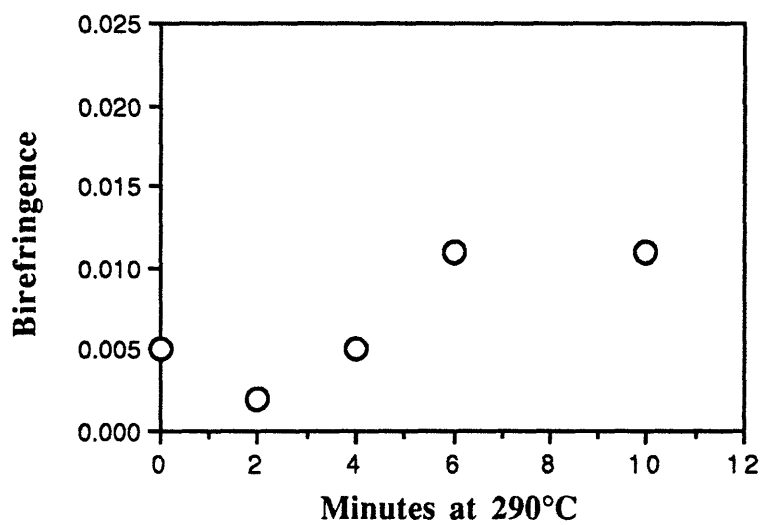


Figure 2.11. a.) Average refractive index vs. post-cure annealing time at 290°C. b.) Birefringence vs. post-cure annealing time

index prediction techniques appear to be highly accurate for polyimides with bulky fluorinated substituents, but underpredict for non-fluorinated polyimides.

In addition to chemical structure, polyimide processing can affect the index of refraction. Oriented materials, for example, will be birefringent. While uniaxially drawing the films will, of course, induce orientation, birefringence can sometimes be induced simply by the casting or annealing process. The overall refractive index can also be dependent upon the annealing conditions, as both amic acid to imide conversion and polymer crystallization increase the refractive index.

2.6. References

1. R. Selvaraj, H.T. Lin, and J.F. McDonald, *J. Lightwave Tech.*, **6(6)**,1034 (1988).
2. A.K. St. Clair and T.L. St. Clair, in *Polymers for High Technology - Electronics and Photonics*, p. 437, M.J. Bowden and S. R. Turner, Eds., ACS, Washington (1987)
3. T. Inchino, S. Sasaki, T. Matsuura, and S. Nishi, *J. Polm. Sci: Polym Chem.*, **28**, 323 (1990).
4. R. Reuter, H. Franke, and C. Feger, *Applied Optics*, **27(21)**, 4565 (1988).
5. G. Hougham; G. Tesoro; A. Viehbeck; J. Chapple-Sokol, *Polym. Prep*, **34(1)**, 371 (1993).
6. S. Sasaki, T. Matsuura, S. Nishi, and S. Ando, in *Materials Science of High Temperature Polymers for Microelectronics*, D.T. Grubb, I. Mita, and D.Y. Yoon, Eds., *Mater. Res. Soc. Proc.*, **227** (1991).
7. J.W. Labadie, M.I. Sanchez, Y.Y. Cheng, and J.L. Hedrick, *ibid.*, p. 43.
8. H. Haider, E. Chenevey, R.H. Vora, W. Cooper, M. Glick, and M. Jaffe, *ibid.*, p. 35.

9. D.M. Stoakley and A.K. St. Clair, in *Optical and Electrical Properties of Polymers*, J.A. Emerson and J.M. Torkelson, Eds., *Mater. Res. Soc. Proc.*, **214** (1990).
10. A.K. St. Clair, T.L. St. Clair, and W.P. Winfree, *Polym. Mat. Sci. Eng.*, **59**, 28 (1988).
11. A.K. St. Clair, T.L. St. Clair, W.S. Slemp, and K.S. Ezzell, "Optically Transparent/Colorless Polyimides", NASA Technical Memorandum 87650 (1985).
12. A.K. St. Clair, T.L. St. Clair, and W.S. Slemp, in *Polyimides: Materials, Chemistry, and Characterization*, p. 16, C. Feger, M.M. Khojasteh, and J.E. McGrath, Eds., Elsevier, Amsterdam (1989).
13. G. Hougham, G. Tesoro, and J. Shaw, *ibid.* p. 465.
14. A. Misra, G. Tesoro, and G. Hougham, *Polymer*, **33**(5), 1078 (1992).
15. T. Matsuura, Y. Hasuada, S. Nishi, and N. Yamada, *Macromol.*, **24**, 5001 (1991).
16. T. Matsuura, M. Ishizawa, Y. Hasuada, and S. Nishi, *Macromol.*, **25**, 3540 (1992). (1990).
17. D.M. Stoakley and A.K. St. Clair, in *Polymeric Materials for Electronic Packaging and Interconnection*, p.87, J.H. Lupinski and R.S. Moore, Eds., ACS, Washington, (1989).
18. D.L. Goff, E.L. Yuan, H. Long, and H.J. Neuhaus, *ibid.*, p. 93.
19. A.K. St. Clair and T.L. St. Clair, *Polym. Prep.*, **34**(1), 385 (1993).
20. M.K. Gerber, J.R. Pratt, and T.L. St. Clair, in *Materials Science of High Temperature Polymers for Microelectronics*, p. 487, D.T. Grubb, I Mita, and D.Y. Yoon, Eds., *Mater. Res. Soc. Proc.*, **227** (1991).

21. P.M. Hergenrother and S.J. Havens, in *Materials Science of High Temperature Polymers for Microelectronics*, p. 453, D.T. Grubb, I Mita, and D.Y. Yoon, Eds., *Mater. Res. Soc. Proc.*, **227** (1991).
22. M. Ree, T.L. Nunes, and D.P. Kirby, *Polym. Prep.*, **33(1)**, 309 (1992).
23. P.M. Hergenrother and S.J. Havens, *J. Polym. Sci. A: Polym. Chem.*, **27**, 1161 (1989).
24. P.M. Hergenrother, N.T. Wakelyn, and S.J. Havens, *J. Polym. Sci. A: Polym. Chem.*, **25**, 1093 (1987).
25. D.C. Rich, P. Huo, C. Liu, and P. Cebe, *ACS Polym. Mat. Sci. Eng.*, **68**, 124 (1993).
26. J. Friler and P. Cebe, *Polym. Eng. Sci.*, **33(10)**, 588 (1993).
27. J. T. Muellerleile, B. G. Risch, D. E. Rodrigues and G. Wilkes. *Polymer*, **34(4)**, 789 (1993).
28. P.P. Huo and P. Cebe, *Polymer*, **34(4)**, 696 (1993).
29. P.P. Huo, J. Friler, and P. Cebe, *Polymer*, **34(21)**, 4387 (1993).
30. W. Groh and A. Zimmermann, *Macromol.*, **24**, 6660 (1991).
31. T.P. Russell, H. Gugger, and J.D. Swallen, *J. Polym. Sci: Polym. Phys.*, **21**, 1745 (1983).
32. K. Nakagawa, *J. Appl. Polym. Sci.*, **41**, 2049 (1990).
33. S. Noe, Ph.D. Thesis, Massachusetts Institute of Technology (1992).

34. V.E. Smirnova and M.I. Bessonov, in *Polyimides: Materials, Chemistry, and Characterization*, edited by C. Feger, M.M. Khojasteh, and J.E. McGrath, Elsevier, Amsterdam, 1989, p. 563.
35. S. Herminghaus, D. Boese, D.Y. Yoon, and B.A. Smith, *Appl. Phys. Lett.*, **59(9)**, 1043 (1991).
36. D. Boese, H. Lee, D.Y. Yoon, J.D. Swallen, and J.F. Rabolt, *J. Polym. Sci.: Polym. Phys.*, **30**, 1321 (1992).
37. T. Kinugi, C. Inchinose, and A. Suzuki, *J. Appl. Polym. Sci.*, **31**, 429 (1986).
38. Y. Aihara and P. Cebe, *Polym. Prepr.*, **33(1)**, 471 (1992).
39. Y. Aihara and P. Cebe, *Polym. Prepr.*, **33(2)**, 633 (1992).
40. J.B. Teverovsky, D.C. Rich, Y. Aihara, and P. Cebe, *J. Appl. Polym. Sci.*, **54**, 497 (1994).
41. D.W. van Krevelen, *Properties of Polymers*, Elsevier, Amsterdam (1990).
42. A. Vogel, W. Cresswell, and I. Leicester, *J. Phys. Chem.*, **58**, 174 (1954).
43. J. Bicerano, *Prediction of Polymer Properties*, Marcel Dekker, New York (1993).
44. R.A. Dine-Hart and W.W. Wright, *Die Makromolek. Chem.*, **143**, 189 (1971).
45. B.V. Kotov, T.A. Gordina, V.S. Voishchev, O.V. Kolinov, and A.N. Pravednikov, *Vysokomol. Soyed.*, **A19(3)**, 614 (1977)
46. J.M. Salley, T. Miwa, and C.W. Frank, in *Materials Science of High Temperature Polymers for Microelectronics*, p. 117, D.T. Grubb, I Mita, and D.Y. Yoon, Eds., *Mater. Res. Soc. Proc.*, **227** (1991).

47. T.L. St. Clair, in *Polyimides*, D. Wilson, H.D. Stenzenberger, and P.M. Hergenrother, Eds., Blackie, Glasgow (1990).
48. YE. P. Krasnov, A.YE. Stepanyan, YU.I. Mitchenko, YU.A. Tolkachev, and N.V. Lukasheva, *Vysokomol. Soyed.*, **A19** (7), 1566 (1977).
49. M. Fryd, in *Polyimides: Synthesis, Characterization, and Applications*, K.L. Mittal, Ed., Plenum Press, New York (1984).
50. L. Kan and K. Kao, *J. Chem. Phys.*, **98**(4), 3445 (1993).

Chapter 3. Curing Study of Probimide[®] 412 Preimidized Photosensitive Polyimide

3.1. Introduction

Over the past decade and a half, there has been substantial interest in photosensitive polyimides (PSPIs) [1]. The photosensitive behavior allows the polyimides, which are widely used in electronics applications, to be patterned photolithographically. The first type of PSPI developed was a photosensitive polyamic ester [2], which crosslinks only in the precursor state. The second type was an intrinsically photosensitive polyimide [3,4] which is both solvent soluble and photosensitive in its fully converted state. It is the latter version of the PSPI with which we are concerned.

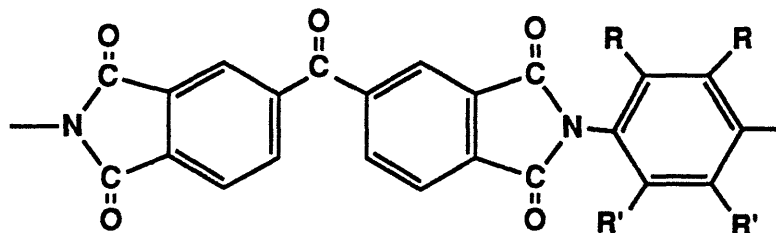
In general, polyimides require high temperature cures for conversion of the precursor polymer and for the removal of solvent. The chemical and physical properties of polyimide systems change substantially as they are cured, and the material is converted from precursor to polyimide. Because the intrinsically photosensitive polyimides are already in their fully converted state, and because they gel upon exposure to ultraviolet light, they show strong potential as high performance materials which can be cured rapidly and at low temperatures. One application in which rapid, low temperature curing is highly desirable is in their use as alignment films for liquid crystal display devices [5,6].

There has been much work published regarding the performance and physical properties of intrinsically PSPI films that have undergone ultraviolet exposure and conventional high temperature thermal cures [7-14]. Ree *et al.* [14] found that chemical crosslinks are formed by both photochemical and thermal curing. In the present work, we show how thermal and ultraviolet curing, which do not involve closure of the imide ring, physically and chemically change the material. We do so by examining a series of films that have undergone step cures from soft bake to hard bake. We report the effects of the atmosphere in which the hard bakes are performed, and the effects of ultraviolet exposure on the films.

3.2. Experimental

3.2.1. Polymer film samples

The polyimide system studied is of the Probimide[®] 400 series produced by OCG Microelectronic Materials, Inc. The polymer contains the following photosensitive structural unit:



where R, R' = alkyl group. The polyimide contains a benzophenone (Ph-CO-Ph) group in the dianhydride portion of the repeat unit. The polyimide is obtained in γ -butyrolactone (GBL) solvent, and the product used in this study, Probimide[®] 412, has a 12.5% original solids content by weight.

Bulk films of Probimide[®] 412 on the order of 100 μm thick were produced. All films were amorphous, and exhibited no Bragg scattering peaks when examined by wide angle X-ray scattering.

The film casting procedure is depicted in Figure 3.1. The polyimide solution was first dropped onto a glass plate and wiped with a metal doctor blade with a 1 mm gap as shown in Figure 3.1(a). The wet films were dried to a tack free state under a dry air current at room temperature overnight as shown in Figure 3.1(b). The parent films were then systematically treated at higher temperatures. Samples were cut from the film after each curing step. The first treatment was 4.5 hours at 100°C in air. The second was 3 hours at 200°C in air. Films were then treated at 300°C for three hours in either air or nitrogen. Material treated at 300°C in nitrogen was then additionally cured at 400°C for one hour in nitrogen. Any Probimide[®] 412 material treated at 400°C in air was essentially destroyed by oxidation. A separate film was treated at 140°C for 3 hours in air after the 4.5 hour bake at 100°C. These thermally cured samples were not exposed to ultraviolet irradiation.

Material that had undergone the 4.5 hour treatment at 100°C was irradiated under a Spectroline model BIB-150B ultraviolet lamp with $\lambda = 364 \text{ nm}$ and an area normalized power of approximately 2.5 mW/cm². The film was exposed to approximately 27 J/cm²

over the course of 3 hours, each side of the film being exposed for 90 minutes. In order to separate the effects of hard bake and UV cures, we did not subsequently hard bake the irradiated film.

Thin films of Probimide[®] 412 were spun cast from the original solution in GBL on glass or KBr at 4000 RPM for 30 seconds. The samples were immediately softbaked at 100°C for fifteen minutes in air. The samples appeared dry after softcuring. The thin films were then progressively cured at 200°C, 300°C, and 400°C, one hour at each temperature. The 200°C cures were performed in air, while the 300°C cures were performed in either air or nitrogen. The 400°C cures were performed in nitrogen only on films previously treated at 300°C in nitrogen. Spin cast films treated at 100°C were irradiated under the UV lamp for various times.

3.2.2. Measurement techniques

A Seiko TG/DTA320 was used for thermogravimetric analysis (TGA) of the bulk films. Samples were scanned from room temperature to 575°C at 10°C/minute in flowing air (300 ml/minute).

Dynamic mechanical analysis (DMA) was performed in tension mode on bulk films using a Seiko DMS200. Samples were scanned under nitrogen at 2°C/minute from room temperature to the temperature above softening at which breakage occurred. Frequencies 1, 2, 5, 10, and 20 Hz were used. Only the 1 Hz data is presented here, as the frequency dependence of the DMA spectra was unnoteworthy.

Index of refraction at $\lambda = 632.8$ nm was measured using a Metricon PC-2000 prism coupler. The prism coupler technique is discussed in Chapter 1. Refractive index was measured by determination of the waveguide propagation modes. Both in-plane (n_{TE}) and out-of-plane (n_{TM}) indices were measured. The average refractive index n_{avg} was calculated as shown below:

$$n_{avg} = (1/3) (2n_{TE} + n_{TM}) \quad (1)$$

Refractive index measurements were taken for the free standing films (by critical angle) and the films spin coated on glass (by waveguide mode determination).

Fourier transform infrared spectroscopy (FTIR) was performed using a Nicolet 510P. FTIR spectra were taken for the Probimide[®] 412 films spin coated on KBr.

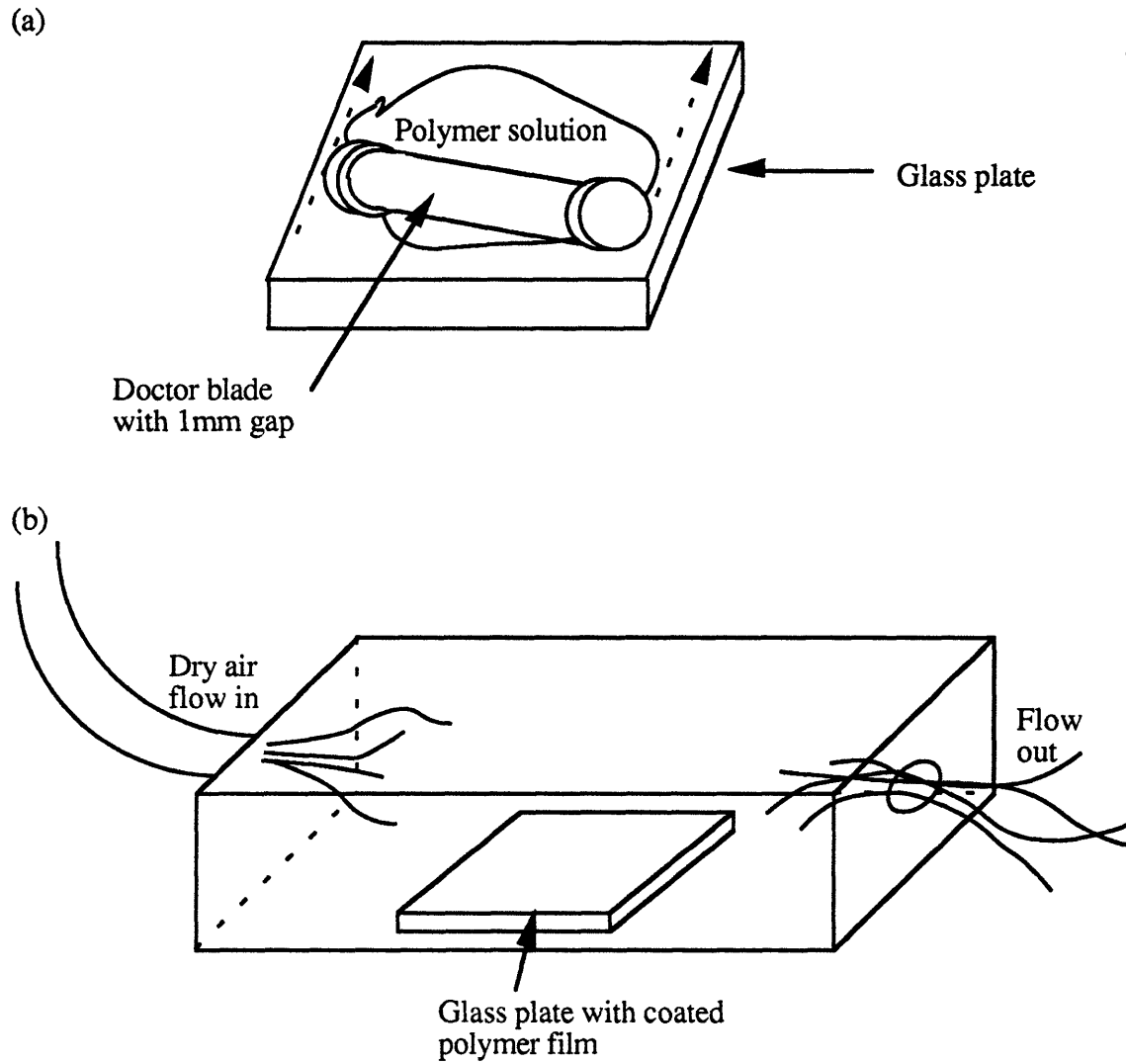


Figure 3.1. Preparation of bulk films. a.) Coating and blading process for optimization of film smoothness and thickness uniformity. b.) Pre-cure air-drying chamber.

3.3. Results And Discussion

3.3.1. Coloration And Brittleness

The changes in coloration and brittleness in Probimide[®] 412 thick films that occur with subsequent cures are summarized in Table 3.1. Probimide[®] 412 is slightly yellow and flexible when cured at 100°C. These characteristics change little upon curing to 200°C. The material becomes dark orange and brittle when cured at 300°C in air, but remains yellow and flexible in nitrogen. However, the polymer turns brown and brittle when treated at 400°C in nitrogen. The dark coloration and brittleness in the films cured at 300°C in air and at 400°C in nitrogen suggest that chemical crosslinking is taking place. Ultraviolet irradiation after thermally curing at 100°C substantially increases the yellowness of the film. The yellowing of the UV irradiated film is indicative of the formation of chemical crosslinks.

Table 3.1. Color and Brittleness in Films Cured at Progressively Higher Temperatures.

Treatment	Environment	Color	Brittleness
100°C	air	light yellow	flexible
200°C	air	light yellow	flexible
300°C	N ₂	light yellow	flexible
300°C	air	dark orange	brittle
400°C	N ₂	brown	brittle
100°C+UV	air	yellow	barely brittle

3.3.2. Thermogravimetric Analysis

Thermogravimetric analysis was used to track the presence of solvent as the bulk films are cured. Thermogravimetric scans in Figures 3.2 and 3.3 also indicate vaporization of absorbed water and, at high temperatures, decomposition of the polymer. All of the films lose about 1% of their original weight below 150°C due to removal of water from the polymer, while the films lose varying amounts of weight, depending upon the cure conditions, between about 150°C and 300°C due to removal of residual solvent. The TGA scans reach a plateau until the temperature exceeds about 400°C, when the films begin to degrade.

In Figure 3.2(a-e), five thermogravimetric scans of Probimide[®] 412 films are compared. Weight loss (left vertical axis) and derivative of weight loss (right vertical axis) are shown as functions of temperature. Each sample has a different highest curing temperature which is indicated by the vertical marker. None of the films in Figure 3.2 has been UV cured. The amount of residual solvent vaporized between 150°C and 300°C decreases substantially as the cure temperature increases. That is, each cure at a higher temperature progressively removes more solvent from the film. There is no residual solvent in the film cured at 300°C, Figure 3.2(e).

The temperature at which the solvent boils off during thermogravimetric analysis also increases with the increased cure temperature. This can be more clearly seen in the plots of the first derivative of weight loss (with respect to scan time) in Figure 3.2. The temperature at which maximum solvent vaporization occurs increases from about 200°C to about 300°C as the cure temperature of the film is increased from room temperature to 200°C.

The observed distribution of solvent removal temperatures, ranging from under 150°C up to about 300°C, is most like the result of polymer-solvent binding. Loosely bound solvent molecules readily evaporate below the boiling point of the solvent, while tightly bound solvent molecules require much higher temperatures in order to evaporate. As the material is cured, loosely bound species vaporize first, and the distribution of removal temperatures of residual solvent moves to higher temperatures.

In Figure. 3.3, thermogravimetric scans of unirradiated and UV irradiated film cured at 100°C are compared. Not only is there less solvent in the UV cured film, but also the volatilization of the residual solvent occurs at higher temperatures after UV exposure. It is thus apparent that the UV curing, by crosslinking the polymer chains, affects the solvent removal dynamics of the thick film.

As Figures 3.2 and 3.3 show, at around 400°C, Probimide[®] 412 begins to decompose. The decomposition temperature is arbitrarily defined as the temperature at which the time derivative of weight loss equals 3% of the polymer per minute (scanning at 10°C/minute). For our Probimide[®] 412 samples, decomposition is around 520°C in flowing air. Other authors [10,11] previously report a decomposition temperature of 527°C in flowing nitrogen.

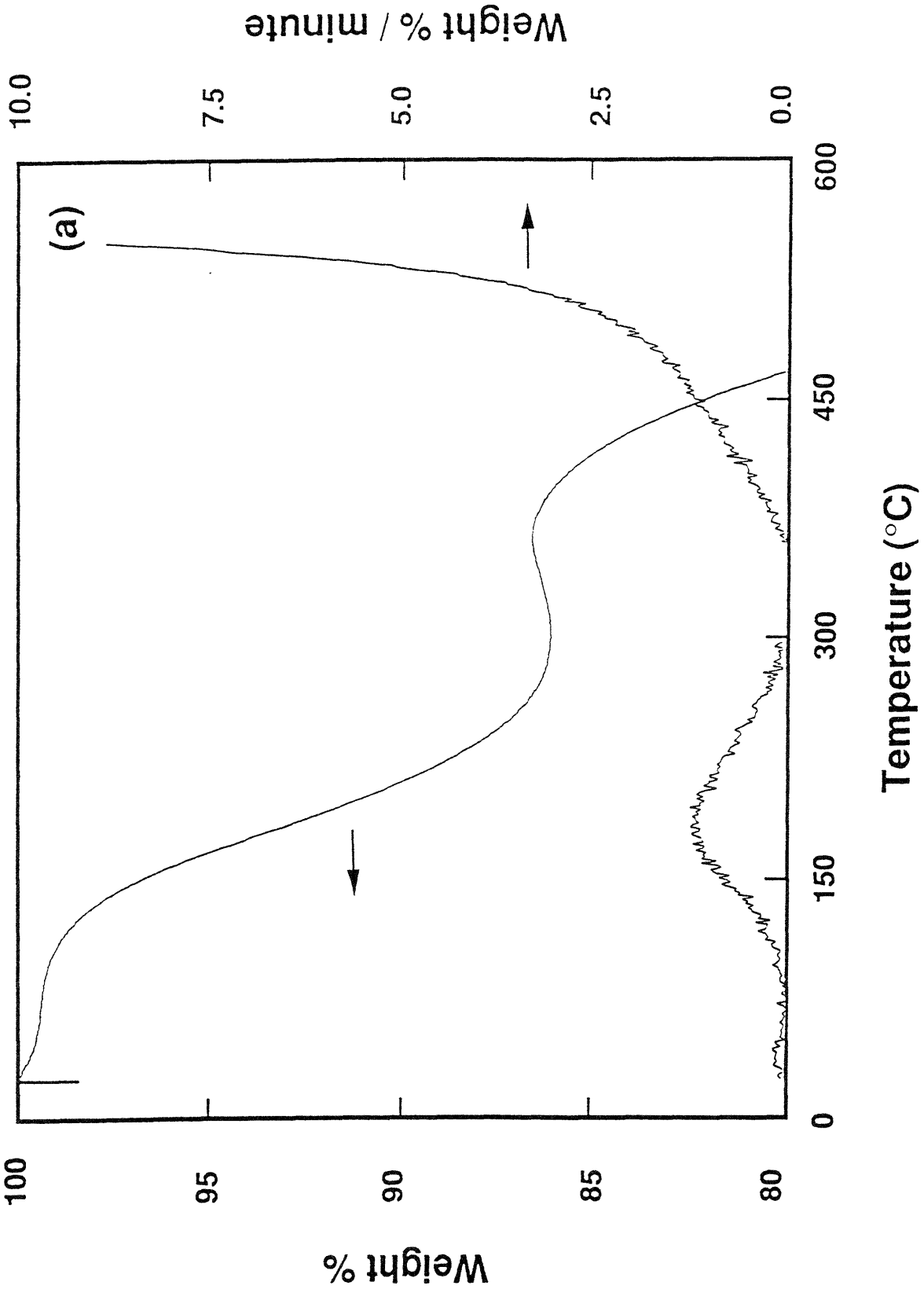


Figure 3.2. Thermogravimetric weight loss and derivative of weight loss vs. temperature for Probimide[®] 412 thick films with highest cure temperature: (a) room temperature,

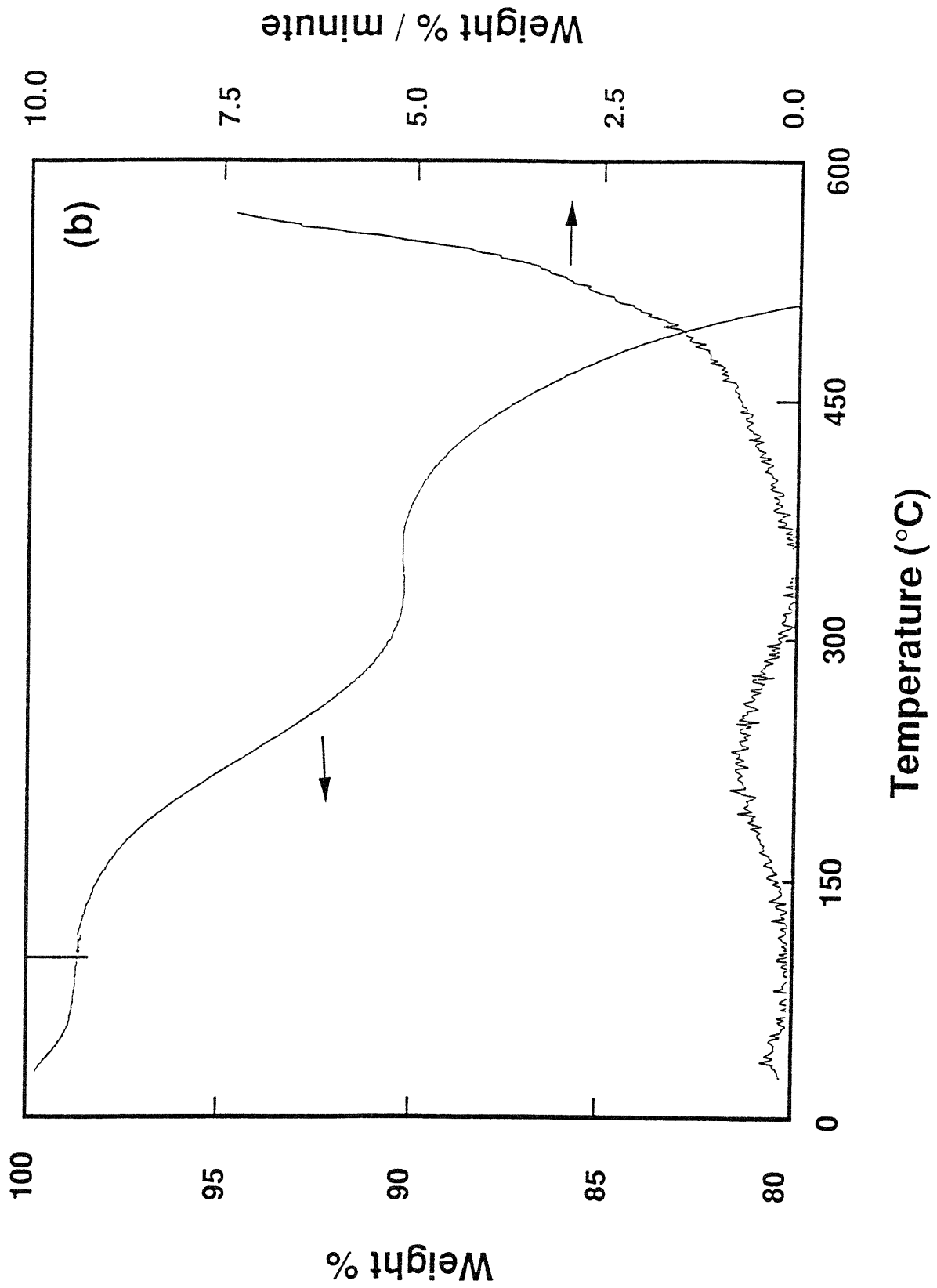


Figure 3.2 continued. (b) 100°C

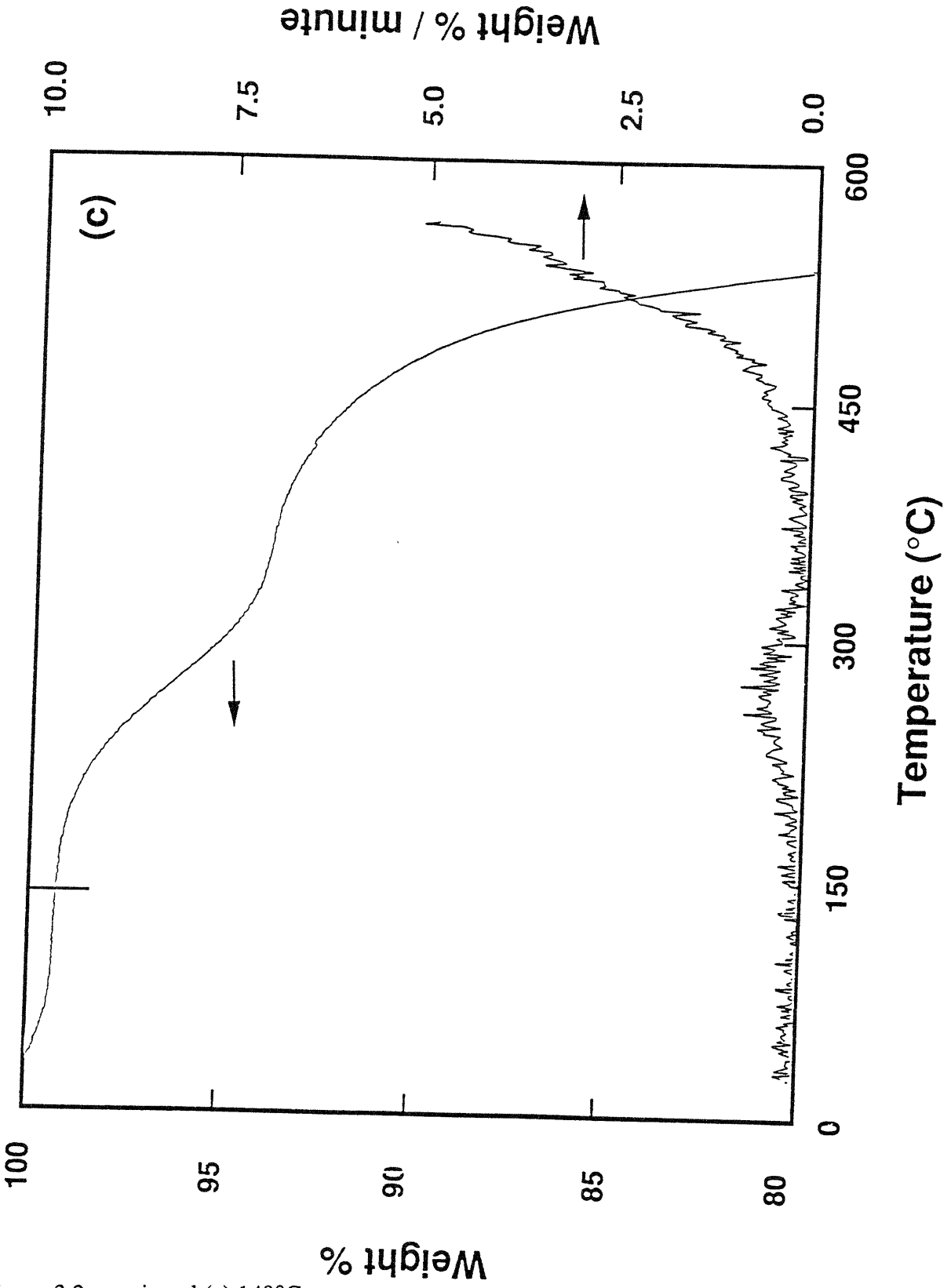


Figure 3.2. continued (c) 140°C

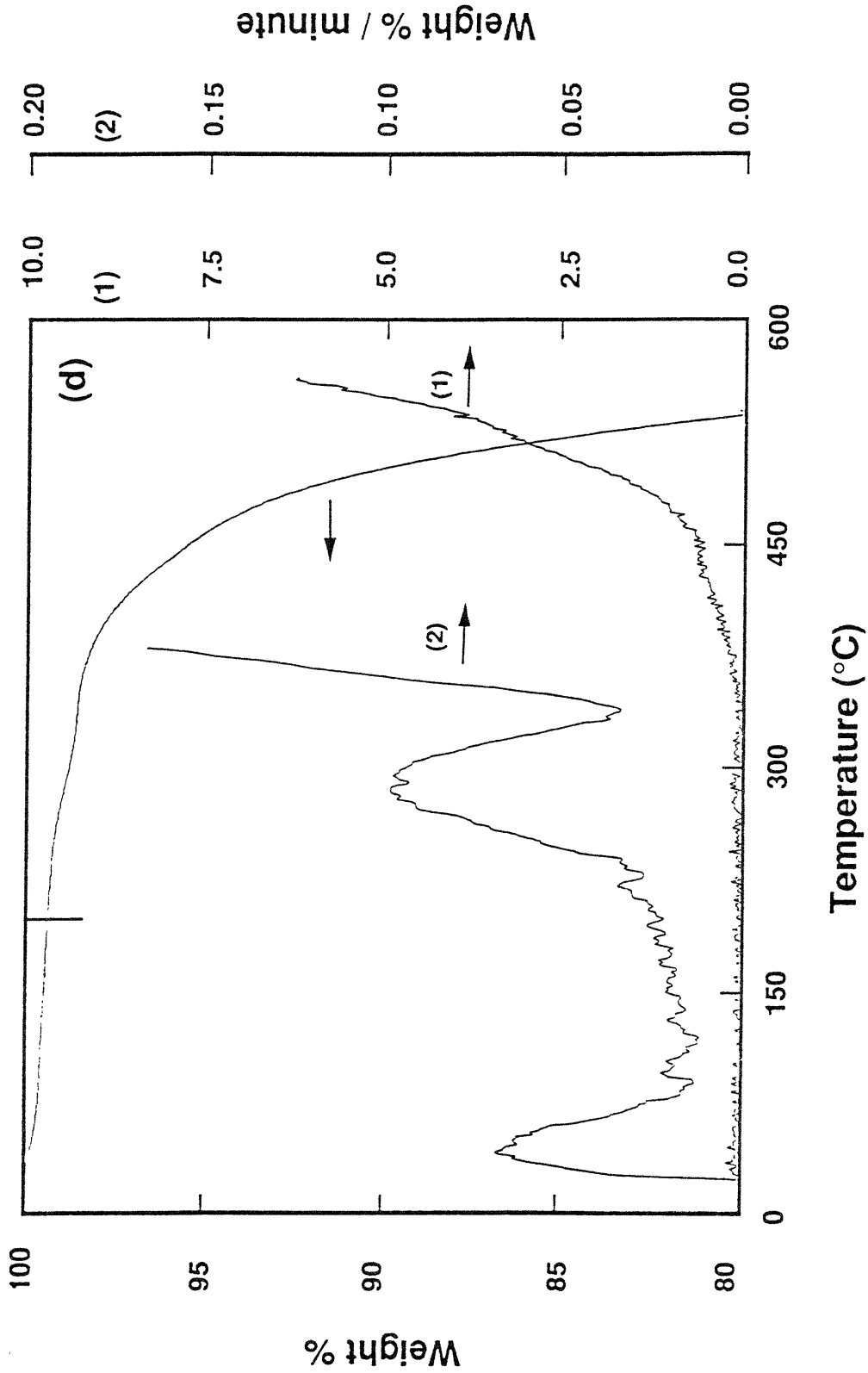


Figure 3.2. continued. (d) 200°C. Derivative curves plotted with two different full scale values, curve (1), 10%/minute, and curve (2), 0.2%/minute.

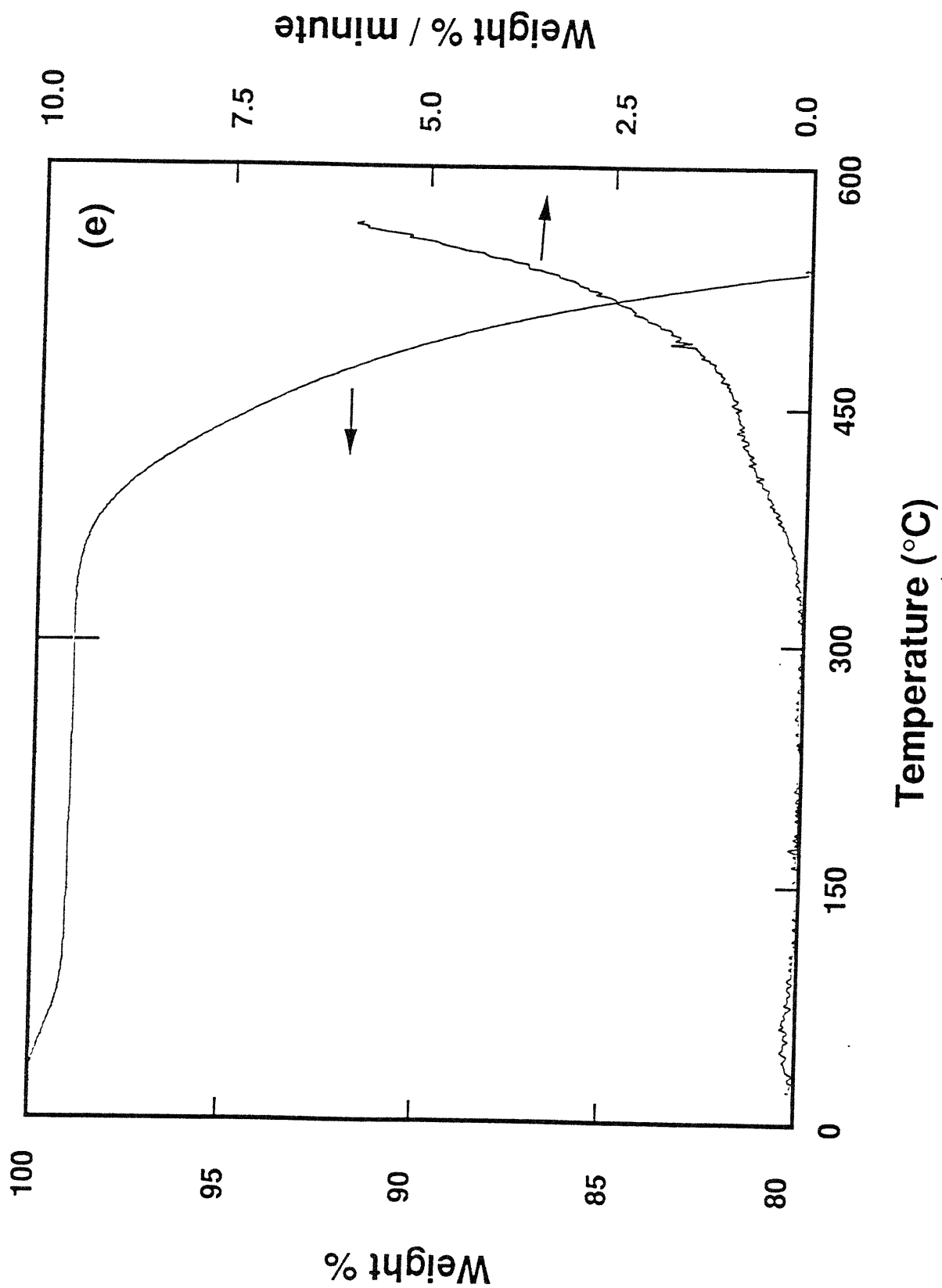


Figure 3.2. continued. (e) 300°C.

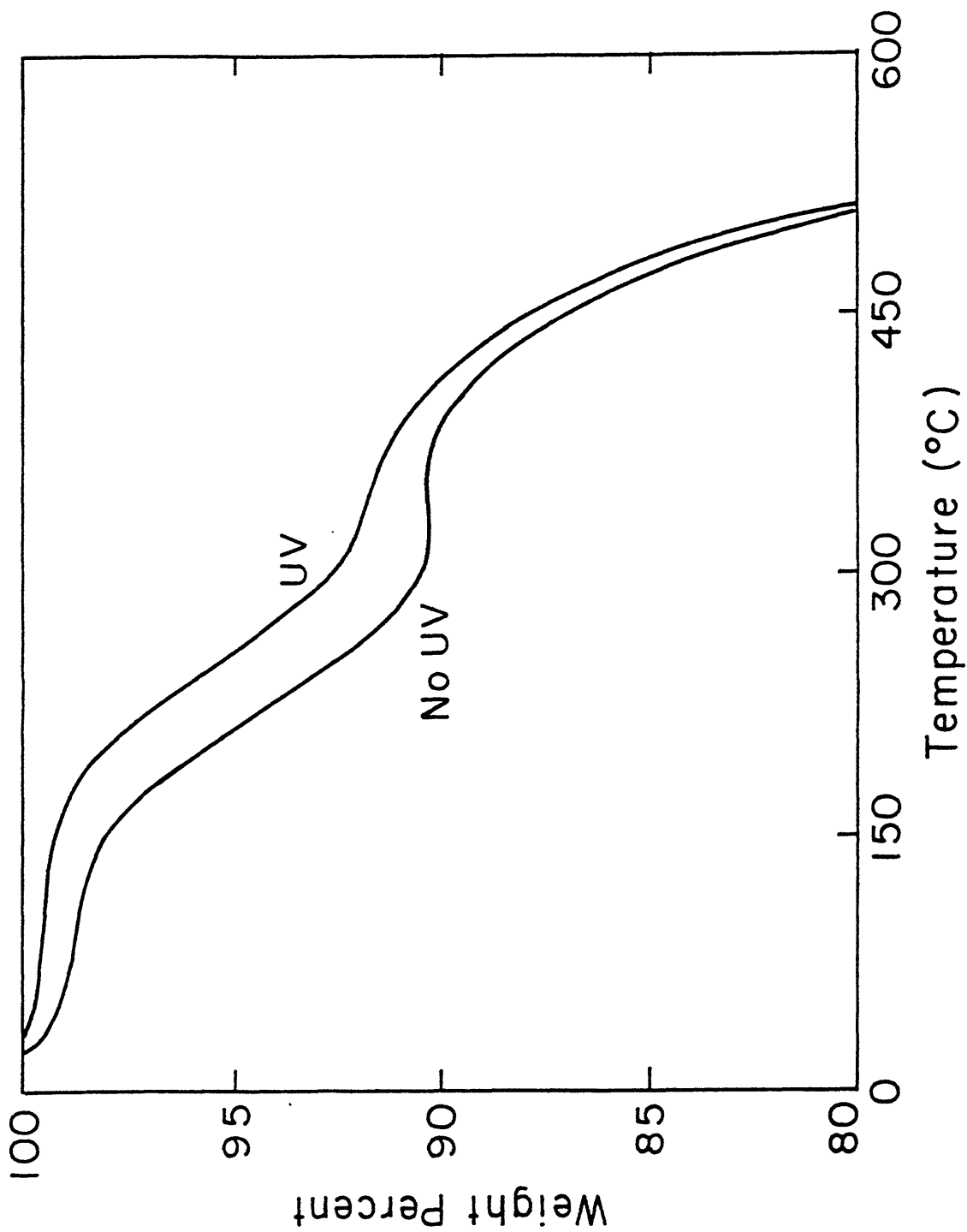


Figure 3.3. Thermogravimetric weight loss vs. temperature for Probimide® 412 thick films baked at 100°C, UV irradiated or unirradiated.

3.3.3. Dynamic Mechanical Analysis

The evolution of mechanical properties during the cure of Probimide[®] 412 bulk films was investigated by dynamic mechanical analysis. The dynamic mechanical spectra at 1 Hz for Probimide[®] 412 samples progressively treated at 100°C, 200°C, 300°C, and 400°C are shown in Figure 3.4(a-d) respectively. Young's modulus and dissipation factor, $\tan\delta$, are shown as functions of temperature. For Figure 3.4, the 300°C and 400°C cures were performed in nitrogen. The DMA scans show both glass transition and secondary transition behavior.

The room temperature Young's modulus does not appear to be dependent upon cure conditions. The glassy moduli of our films are about 2.2-2.5 GPa. Other authors report a modulus of 2.6-2.9 GPa for hard baked Probimide[®] 400 series films [10,13,14].

For the samples cured in air at 100°C, Figure 3.4(a), and at 200°C, Figure 3.4(b), Young's modulus decreases by about an order of magnitude at 375°C. $\tan\delta$ shows a strong maximum at 375°C, which is the glass transition temperature. Several broad and weak maxima occur near 100°C and 250°C.

In the film cured in nitrogen at 300°C, Figure 3.4(c), the glassy modulus decreases slightly at 280°C and sharply at 375°C. Above 425°C, the modulus exhibits an upturn due to the thermal induction of covalent crosslinks. The dissipation factor, $\tan\delta$, shows a strong glass transition at 375°C and a weaker, but distinct, secondary relaxation at 280°C.

In the film cured at 400°C in nitrogen, Figure 3.4(d), above room temperature, the modulus declines with increasing temperature. There is a secondary relaxation at 280°C, and a broad relaxation above the 375°C glass transition temperature seen in the other samples. $\tan\delta$ shows several broad steps. There is no clear glass transition peak seen in this sample.

The glass transition temperatures of all of the samples are near 375°C. However, while the samples treated at 100°C, 200°C, and 300°C have sharp glass transitions at 375°C, the sample treated at 400°C has a broad relaxation shifted to higher temperatures. Ree *et al.* [14] used dynamic mechanical analysis to show that thermal cures from 350°C-400°C induce chemical crosslinks in Probimide 412. Our results confirm that the 400°C treatment in nitrogen causes the polymer to crosslink, reinforcing the rubbery modulus and shifting the softening transition to higher temperatures. We also show that the thermal crosslinking does not occur in the films cured at 300°C and below.

Secondary relaxation also differs among the samples. Ree *et al.* [14] observed broad and weak β relaxation at low temperatures and attributed the phenomenon to the relaxation of phenyl moieties or to absorbed moisture. Our samples cured at 100°C and 200°C have weak and broad secondary relaxations. On the other hand, the samples cured at 300°C and 400°C, which have been shown by TGA to be free of solvent, have well defined relaxations at 280°C.

Ultraviolet irradiation crosslinks the Probimide[®] 412 thick films, affecting its relaxation behavior. In Figure 3.5, unirradiated and UV irradiated samples initially cured at 100°C are compared. The crosslinking causes an elevation of the glass transition temperature by a few degrees, reinforces the rubbery modulus, and broadens the $\tan\delta$ peak. Ree *et al.* [14] observed that UV exposure reinforced the rubbery modulus in samples that had been subsequently hard baked at 350°C in nitrogen. They found, however, that thermally induced crosslinks created by subsequent curing at 400°C dominated over the UV induced crosslinks such that no effect of the UV could be observed.

The polymer also crosslinks when it is cured at 300°C in an oxygen-containing environment. This is demonstrated in Figure 3.6, where the mechanical properties of samples cured at 300°C in air and nitrogen are compared. While the sample baked in nitrogen has a sharp glass transition at 375°C, the sample baked in air has a broad glass transition and a highly reinforced rubbery modulus. It is apparent that the 300°C cure in air has a similar effect on the mechanical properties as does the 400°C cure in nitrogen. A 400°C cure in air, however, severely oxidizes and degrades the specimen.

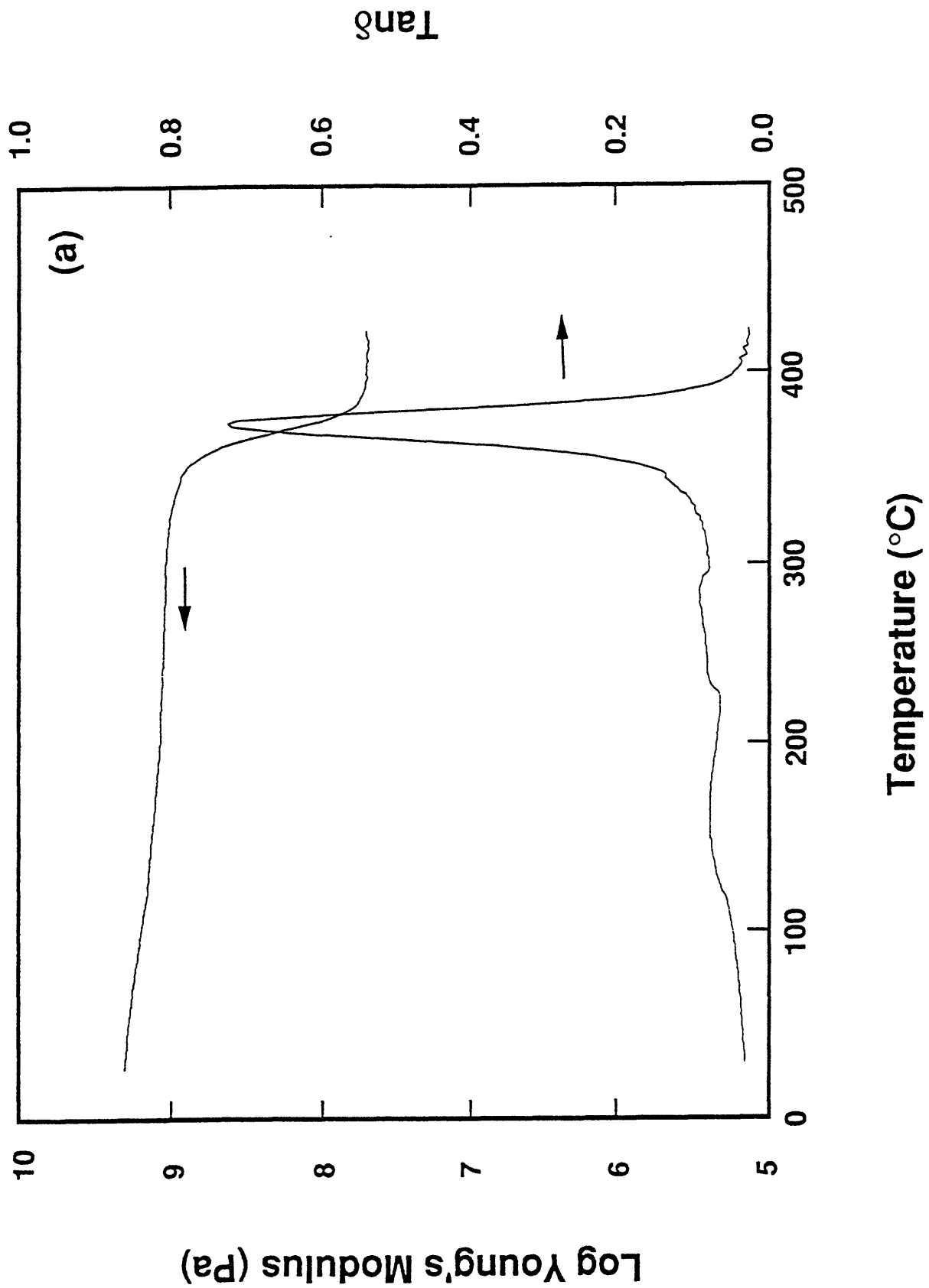
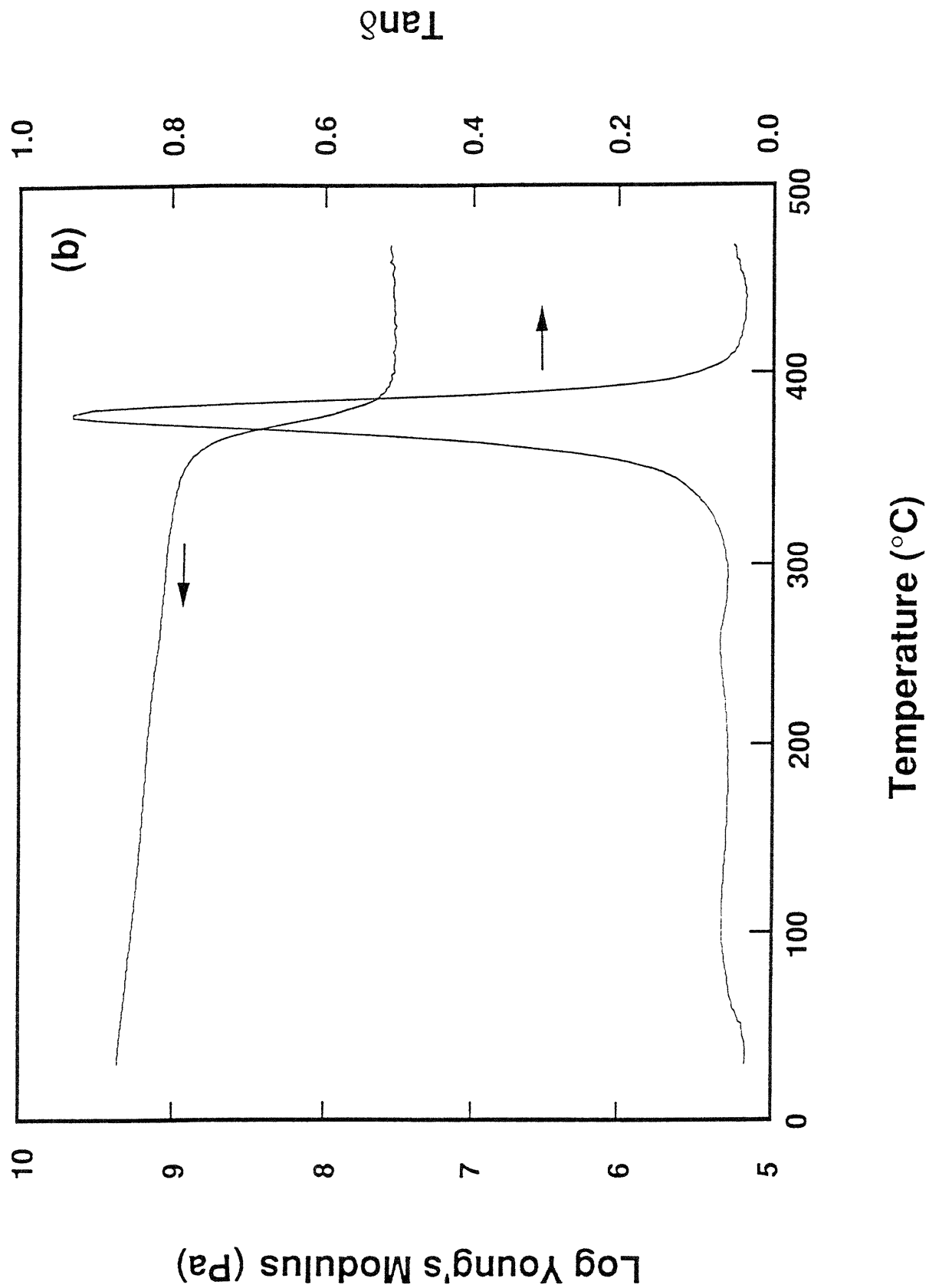


Figure 3.4. 1 Hz dynamic Young's modulus and loss factor, $\tan\delta$, vs. temperature for Probimide[®] 412 thick films with highest cure temperature: (a) 100 $^{\circ}$ C,

Figure 3.4. continued. (b) 200 $^{\circ}\text{C}$,

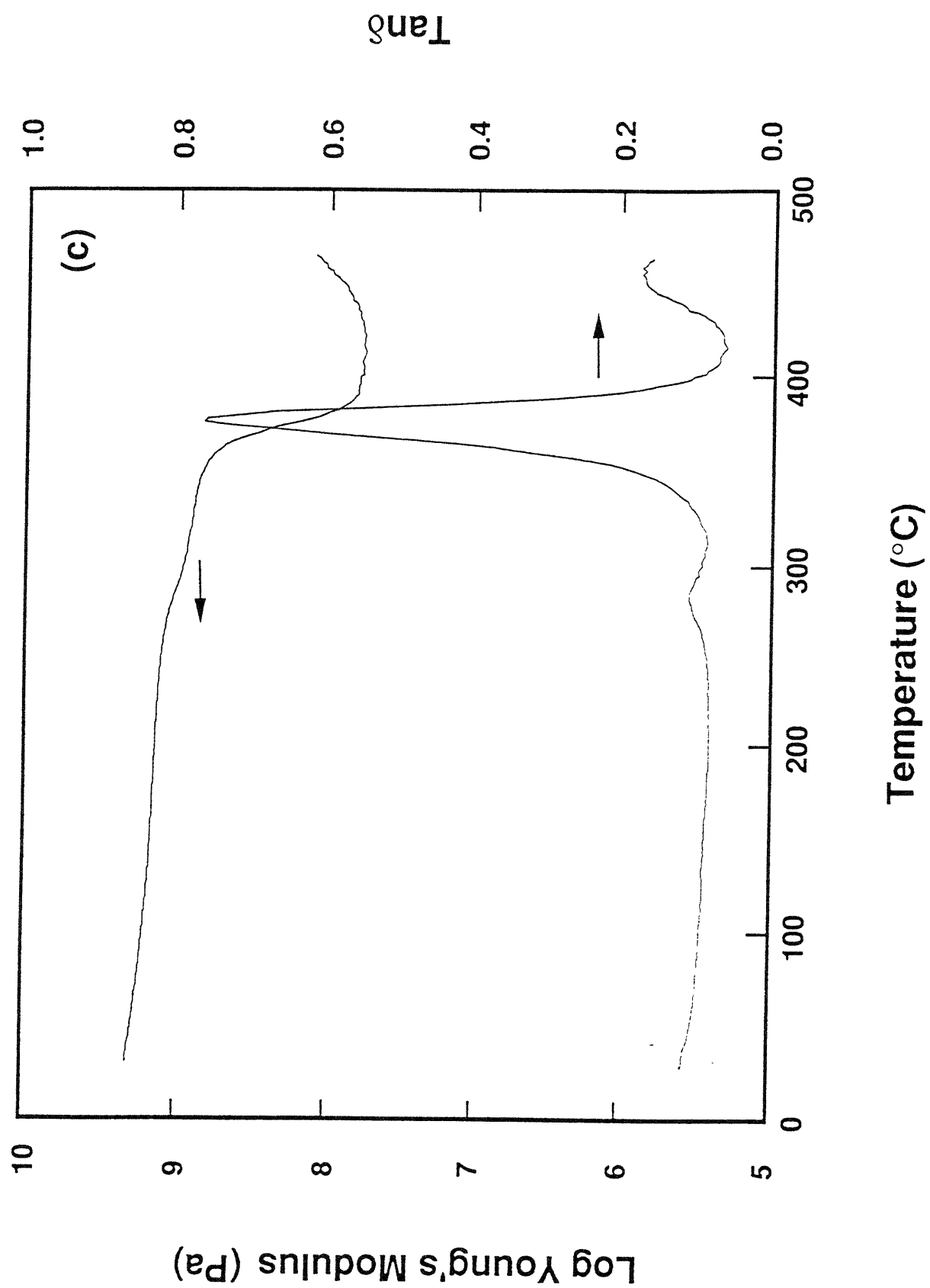


Figure 3.4. continued. (c) 300°C (nitrogen),

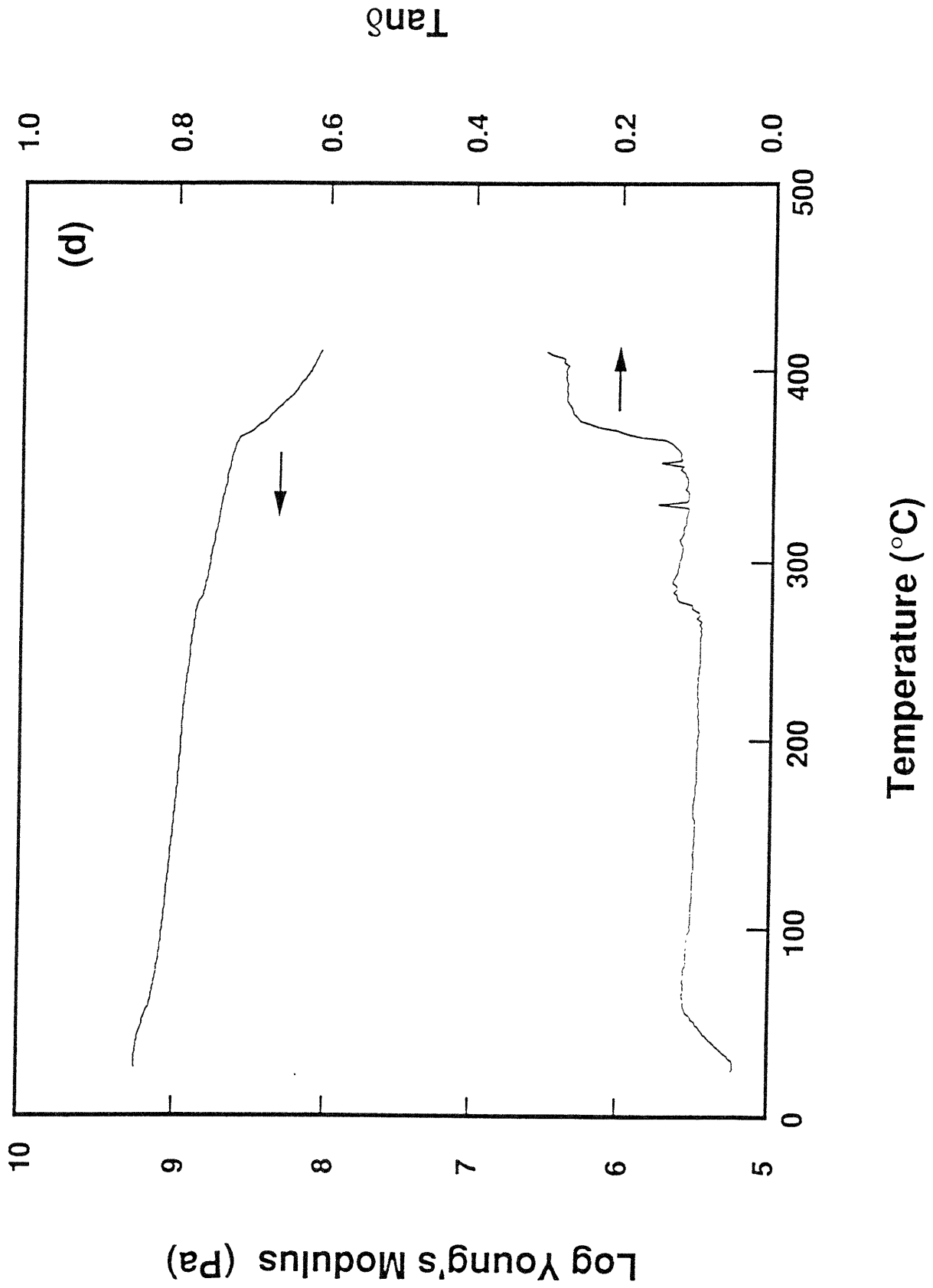


Figure 3.4. continued (d) 400°C (nitrogen).

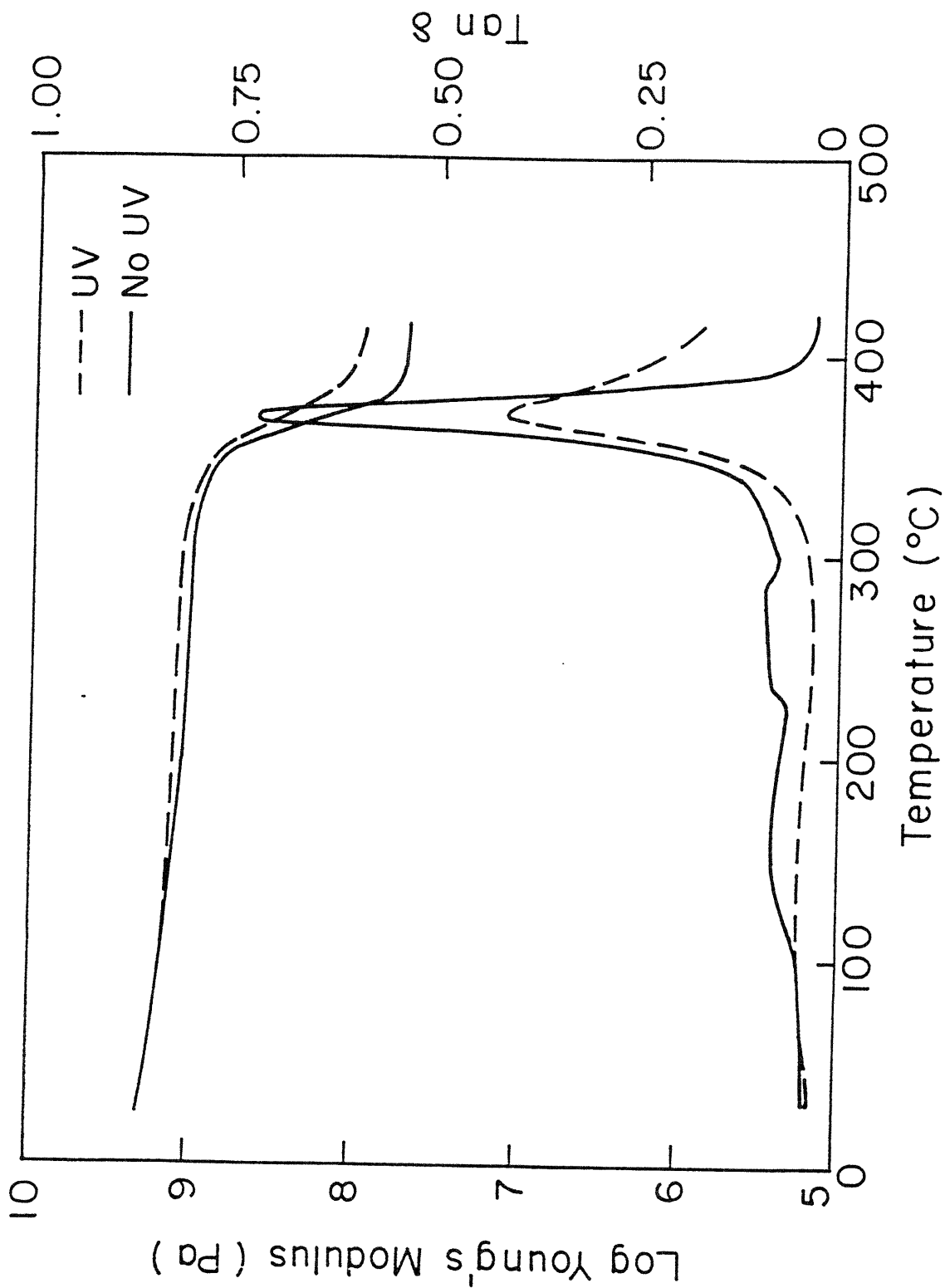


Figure 3.5. 1 Hz dynamic Young's modulus and loss factor, $\tan\delta$, vs. temperature for Probimide[®] 412 thick films cured at 100°C, UV irradiated (dashed line) or unirradiated (solid line).

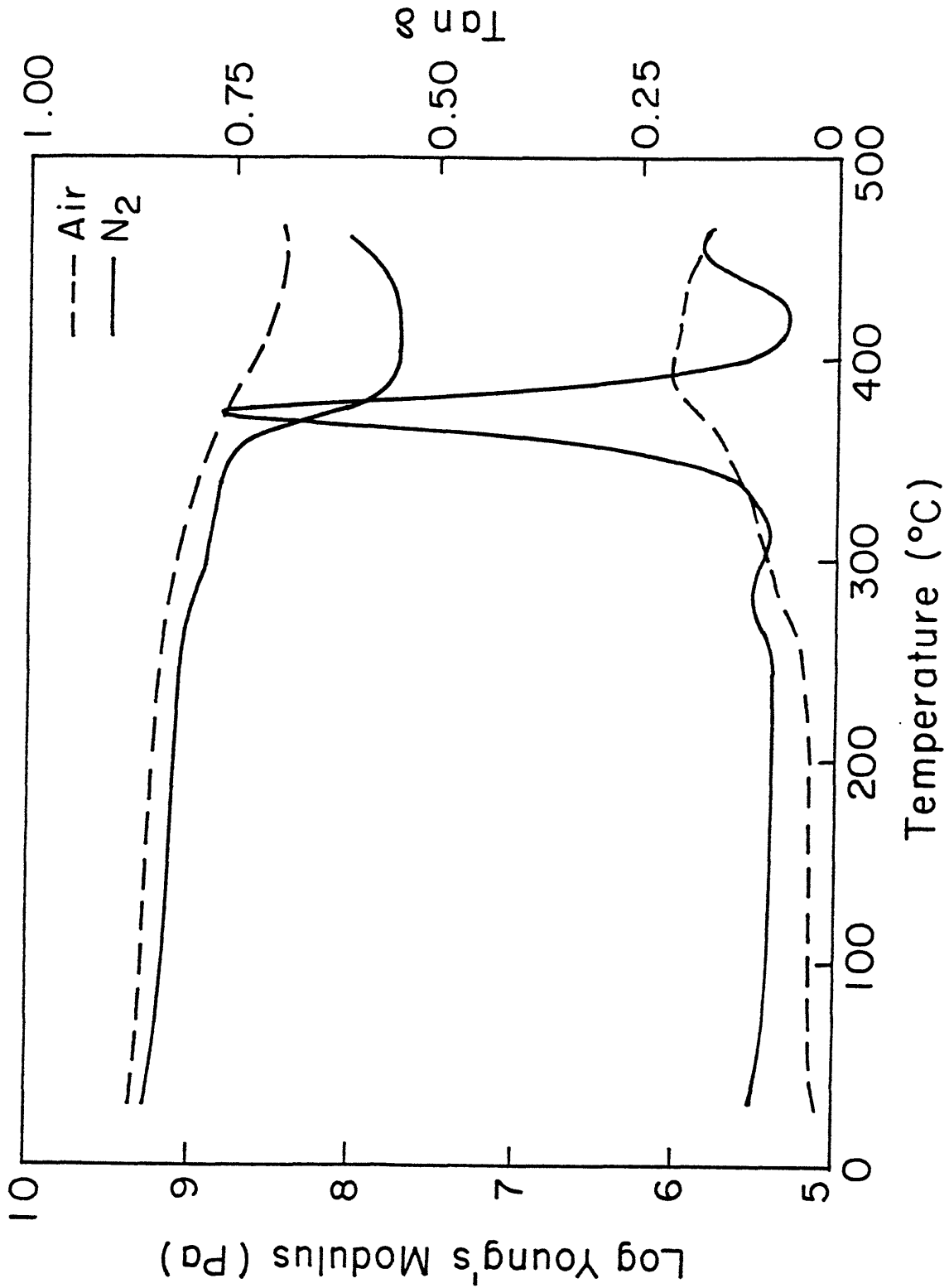


Figure 3.6. 1 Hz dynamic Young's modulus and loss factor, $\tan \delta$, vs. temperature for Probimide[®] 412 thick films cured at 300 $^{\circ}\text{C}$, in air (dashed line) or in nitrogen (solid line).

3.3.4. Index of Refraction

The index of refraction of the polyimide changes as it is cured. Measurements of the refractive indices ($\lambda = 632.8$ nm) of spin coated Probimide[®] 412 films are shown in Figure 3.7. Average indices obtained for bulk films were quite similar to those obtained for the spin coated films, and thus, only the results for the thin films are presented. The average index is about 1.61-1.62 for samples treated at 100°C and 200°C in air, and for the sample treated at 300°C in nitrogen. However, the index of refraction increases after the films are treated at 300°C in air or at 400°C in nitrogen. We attribute the large increase in refractive index to thermally induced crosslinking which takes place at 300°C in air, but at 400°C in nitrogen. These results are consistent with the observed color changes and with changes in the dynamic mechanical relaxation spectra. Previous work [8] reports an in-plane index ($\lambda = 1.06$ μm) for Probimide[®] 400 series films of approximately 1.61, although the authors did not observe an increase in refractive index upon hard curing to 400°C.

Ultraviolet curing also affects the optical properties of the Probimide[®] 412 film. Figure 3.8 shows the index of refraction of 100°C softbaked samples as a function of UV irradiation time. Refractive index increases with UV exposure as a result of crosslinking. Gelation occurs rapidly at first, but slows with larger exposure times.

3.3.5. Fourier Transform Infrared Spectroscopy

We used FTIR spectroscopy to determine how thermal and UV curing changes the chemical structure of the polyimide. Figures 3.9, 3.10, and 3.11 show the effects of curing conditions on the FTIR spectra of Probimide[®] 412. Figure 3.9(a-d) demonstrates the effect of UV exposure, while Figures 3.9 and 3.10 show the effects of thermal cures. Figures 3.9 and 3.11 are scaled to three times the height of the N-C imide peak at 1370 cm^{-1} . Figure 3.10, which shows only the 2000-4000 cm^{-1} region, is scaled to one-third the height of the 1370 cm^{-1} peak. Table 3.2 lists the main absorption bands observed and the bond motion tentatively assigned to the vibrational frequency.

Several IR peak are of particular interest. Polyimides are well known to absorb in the infrared strongly at 1720 cm^{-1} and weakly at 1770 cm^{-1} due to carbonyl absorption [15]. According to Higuchi *et al.* [16] weak absorption can be observed at 1680 cm^{-1} due to benzophenone carbonyl. This was based upon the observation that only benzophenone-containing polyimides absorb at this frequency [17]. The broad absorption regions observed near 3000 cm^{-1} and 3500 cm^{-1} are also of interest. The absorption near 3000

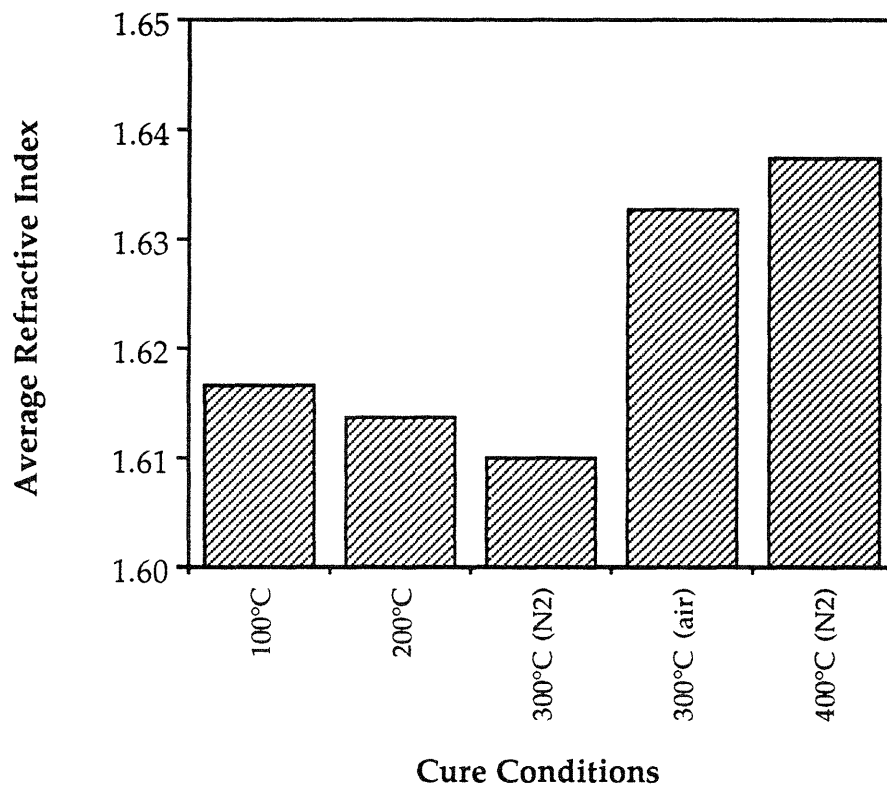


Figure 3.7. Indices of refraction of spin coated Probimide[®] 412 films as a function of highest cure temperature.

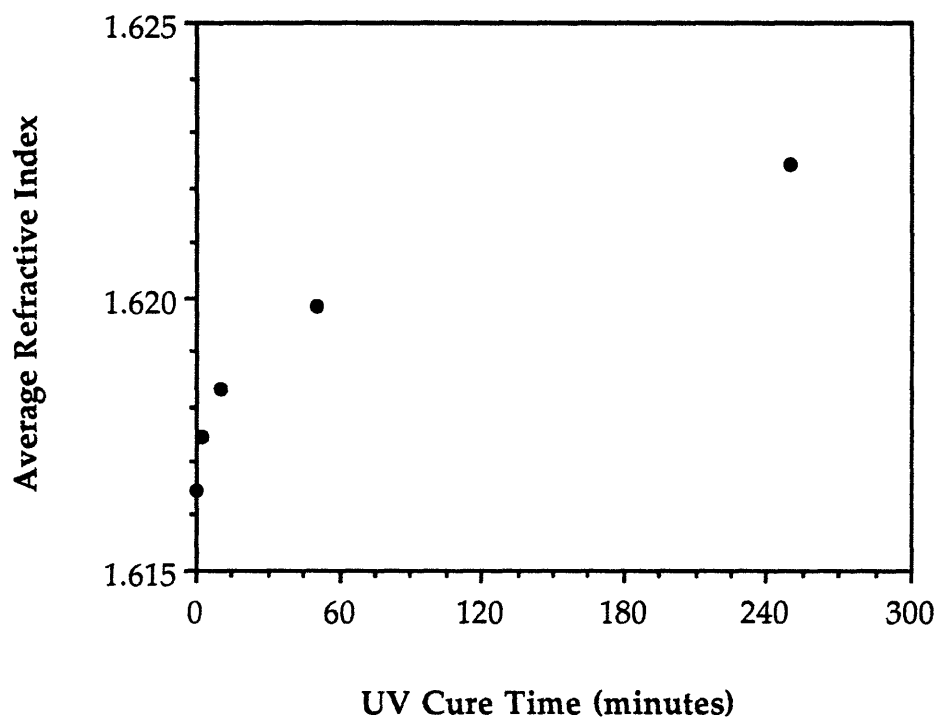
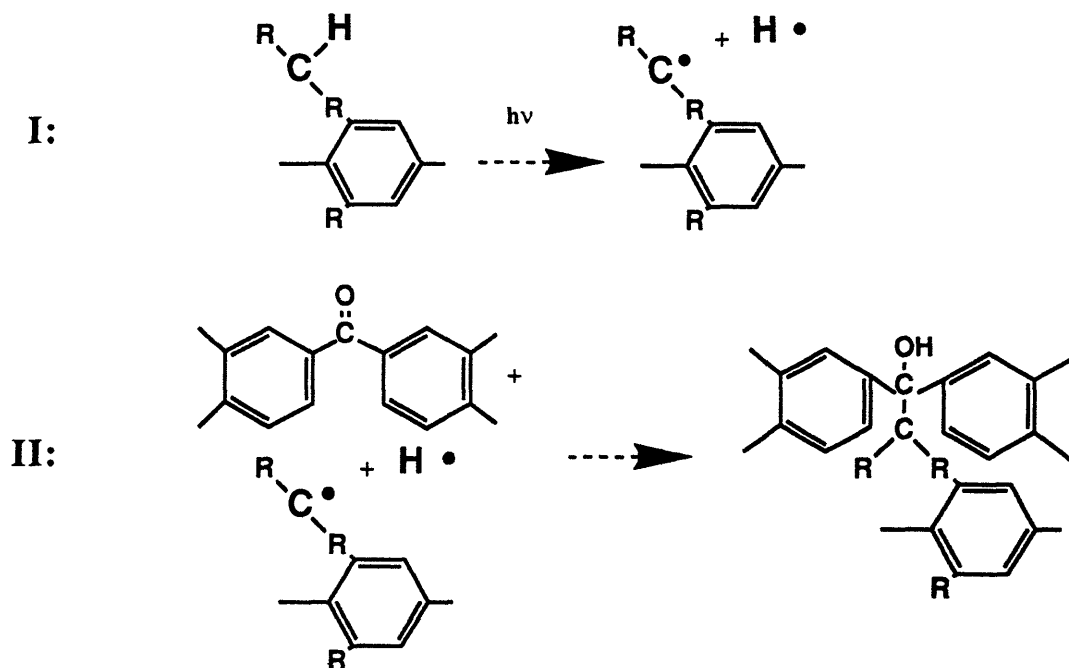


Figure 3.8. Indices of refraction of spin coated Probimide[®] 412 films as a function of UV exposure time.

cm^{-1} is attributed to a series of overlapping hydrocarbon stretching bands [18,19], while the broad absorption near 3500 cm^{-1} is attributed to the stretching of highly hydrogen bonded hydroxyl groups [18,19].

UV Effects

The chemical mechanism of UV crosslinking in inherently photosensitive polyimides has been studied [16,20-22]. UV crosslinking occurs as follows. Hydrogen is first abstracted from an alkyl group (see Scheme I). The resulting free radical attacks the benzophenone carbonyl group (in preference to the imide ring carbonyls), altering the bond to a carbon-hydroxyl group (see Scheme II).



Probimide[®] 412 films spun on KBr were softbaked at 100°C for 15 minutes and cured under ultraviolet. The FTIR spectra at different UV exposure times are shown in Figure 3.9(a-d). Significant absorption band changes that occur with increased UV exposure are observed in Figure 9. First, broad absorption near 3500 cm^{-1} systematically increases with UV exposure, indicative of an increase in hydroxyl groups. Second, the broad absorption near 3000 cm^{-1} declines, indicative of a decrease in hydrocarbon bonds. Third, the peak at 1680 cm^{-1} due to the benzophenone carbonyl group [16] systematically recedes into a shoulder. This is accompanied by a decline in carbonyl absorption at 1720

cm^{-1} . We also note the peak at 1770 cm^{-1} due to the imide ring carbonyl bonds does not seem to be affected.

Thermal Effects

The effects of thermal cures on infrared absorption are shown in Figure 3.10 (2000-4000 cm^{-1} range) and Figure 3.11 (400-2000 cm^{-1} range). Changes in the FTIR spectra occur when the polymer is cured at 300°C in air, Figure 3.10(b,c) and Figure 3.11(b,c), or at 400°C in nitrogen, Figure 3.10(d) and Figure 3.11(d). Under these conditions, the IR spectra from 2000 to 4000 cm^{-1} in Figure 3.10 show a decrease in absorbance from C-H bonds (near 3000 cm^{-1}) and an increase in absorbance from O-H groups (near 3500 cm^{-1}). This suggests that the mechanism of thermally induced crosslinking may be similar to that of the UV induced crosslinking. The IR absorption spectra from 400 to 2000 cm^{-1} in Figure 3.11 indicate that, as in the UV exposed samples, the carbonyl peak at 1720 cm^{-1} declines and the benzophenone carbonyl peak at 1680 cm^{-1} becomes slightly flatter. We also notice that there is general broadening of all peaks across the finger print region of the spectra in the thermally crosslinked samples. Virtually all of the peaks appear wider and less resolved under conditions of thermal crosslinking. Thus, there are probably many random, nonspecific degradation and crosslinking reactions simultaneously taking place during the thermal cure. The aliphatic-group attack upon carbonyl may be one of many reactions.

3.4. Conclusions

Cures above 200°C are required to remove solvent from thick films of Probimide[®] 412. However, ultraviolet curing also drives out solvent. Regardless of cure treatment, however, the films contain about 1% absorbed water. Thermogravimetric analysis reveals a decomposition temperature around 520°C .

Probimide[®] 412 undergoes glass transition softening at about 375°C and a secondary relaxation at about 280°C . Although residual solvent does not appear to affect the primary glass transition, it may induce secondary relaxation at lower temperatures.

Ultraviolet curing at $\lambda = 364 \text{ nm}$ crosslinks the polymer. The crosslinks reinforce the rubbery modulus and broaden the distribution of relaxation times. The UV exposure yellows the polymer and increases its refractive index. The crosslinking mechanism is

Table 3.2. IR absorption regions of Probimide[®] 412.

Wavenumber (cm ⁻¹)	Tentative Assignment [†]	Strength [*]
3600-3400	O-H	w
3000-2800	C-H	w
1770	C=O (imide)	m
1720	C=O (imide and benzophenone)	s
1680	C=O (benzophenone)	w
1610	C-C (phenyl)	w
1600	C-C (phenyl)	w
1490	C-C (phenyl)	m
1420	C-C (phenyl)	m
1370	N-C (imide)	s
1300	C-C-C (benzophenone)	m
1240	C-F	m
1100	N-C (imide)	m
850	phenyl substitution	w
710	phenyl substitution	m

† see references 15-19

* s = strong, m = medium, w = weak

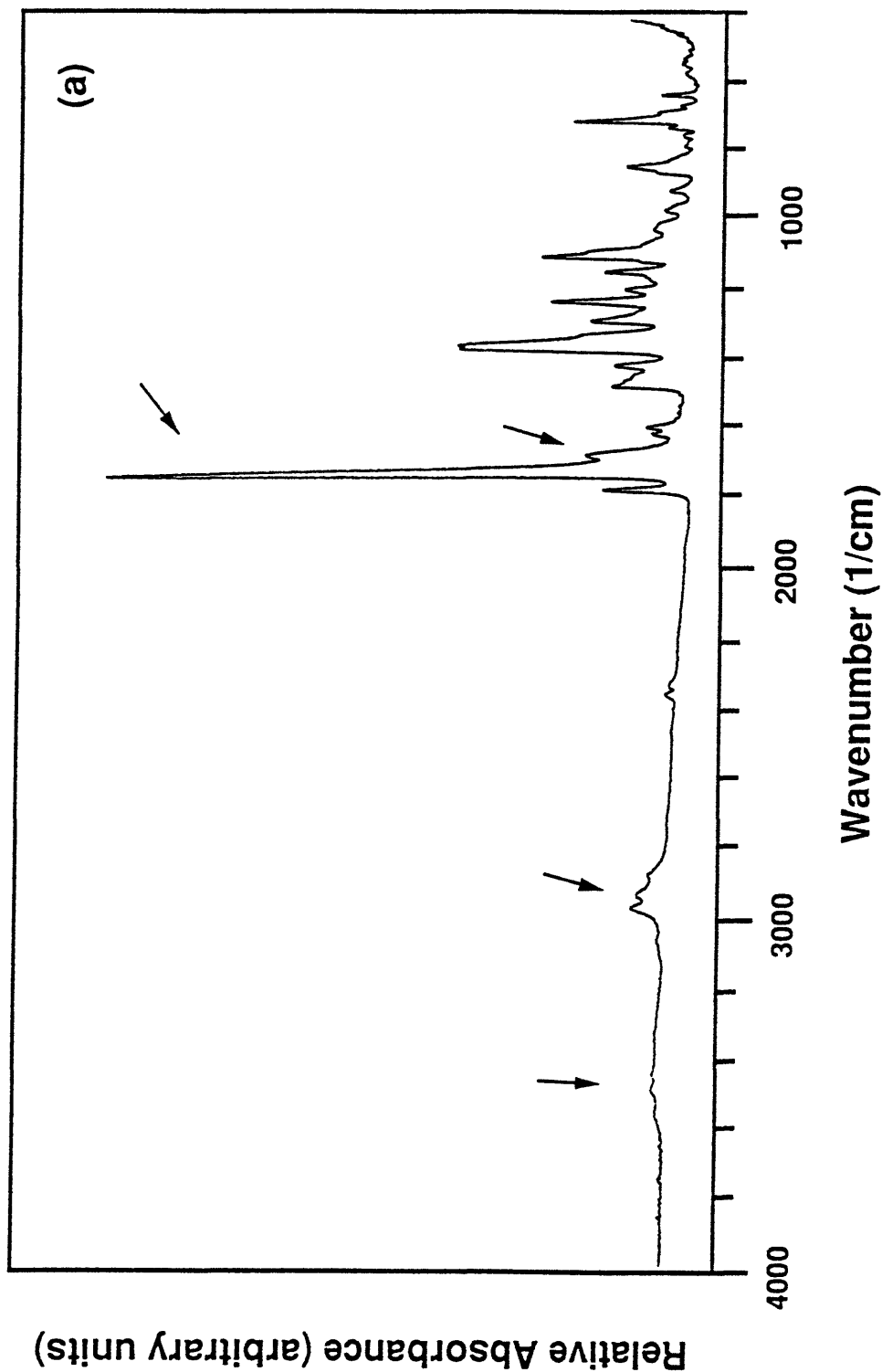


Figure 3.9. Relative IR absorbance vs. wavenumber for spin coated Probimide[®] 412 films softbaked 15 minutes at 100°C and exposed to UV. Arrows point to carbonyl (1680, 1720 cm^{-1}), hydrocarbon (2800-3000 cm^{-1}) and hydroxyl (3400-3600 cm^{-1}) bands. (a) 0 minutes (no irradiation).

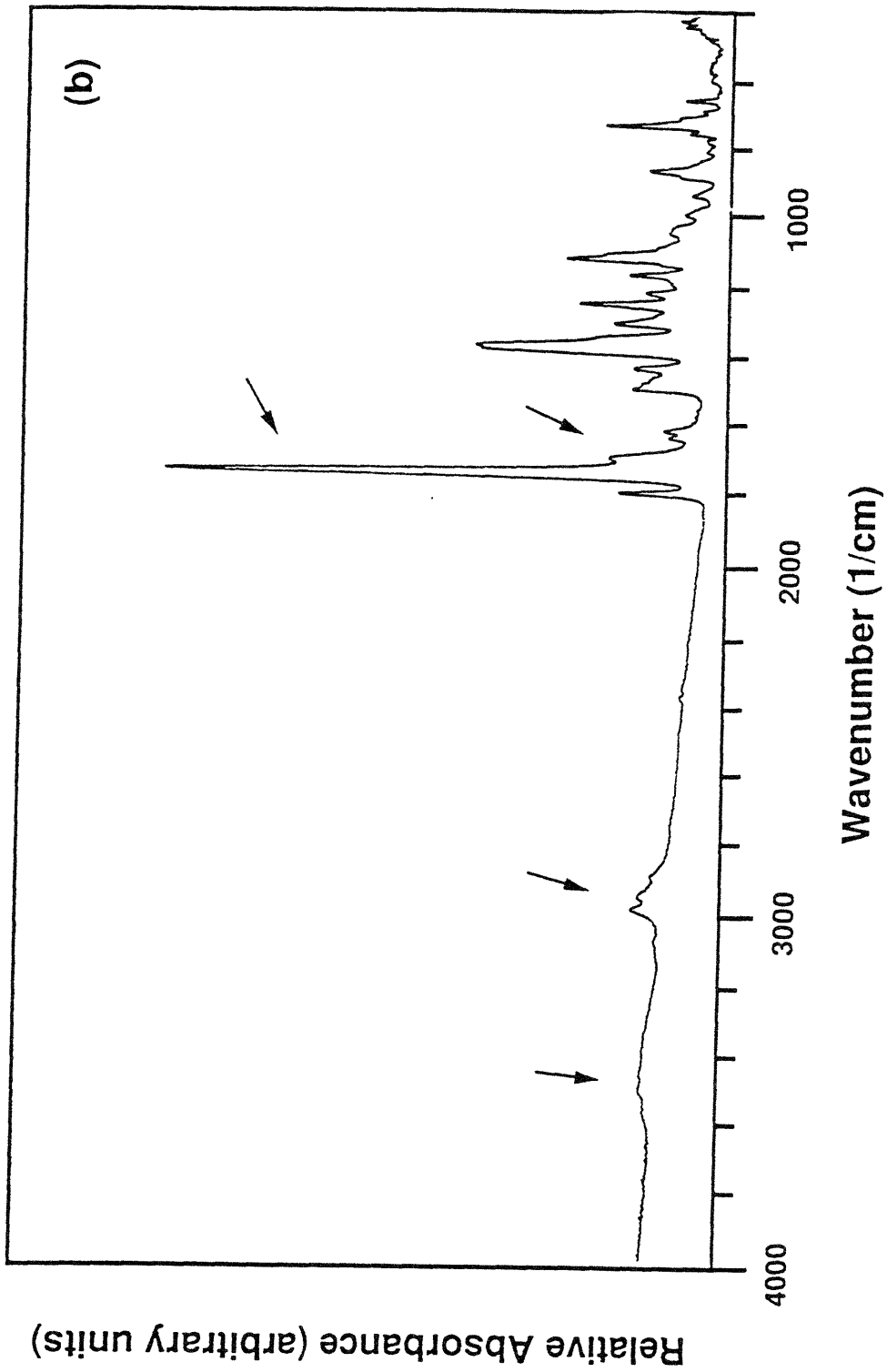


Figure 3.9 continued. (b) 2 minutes,

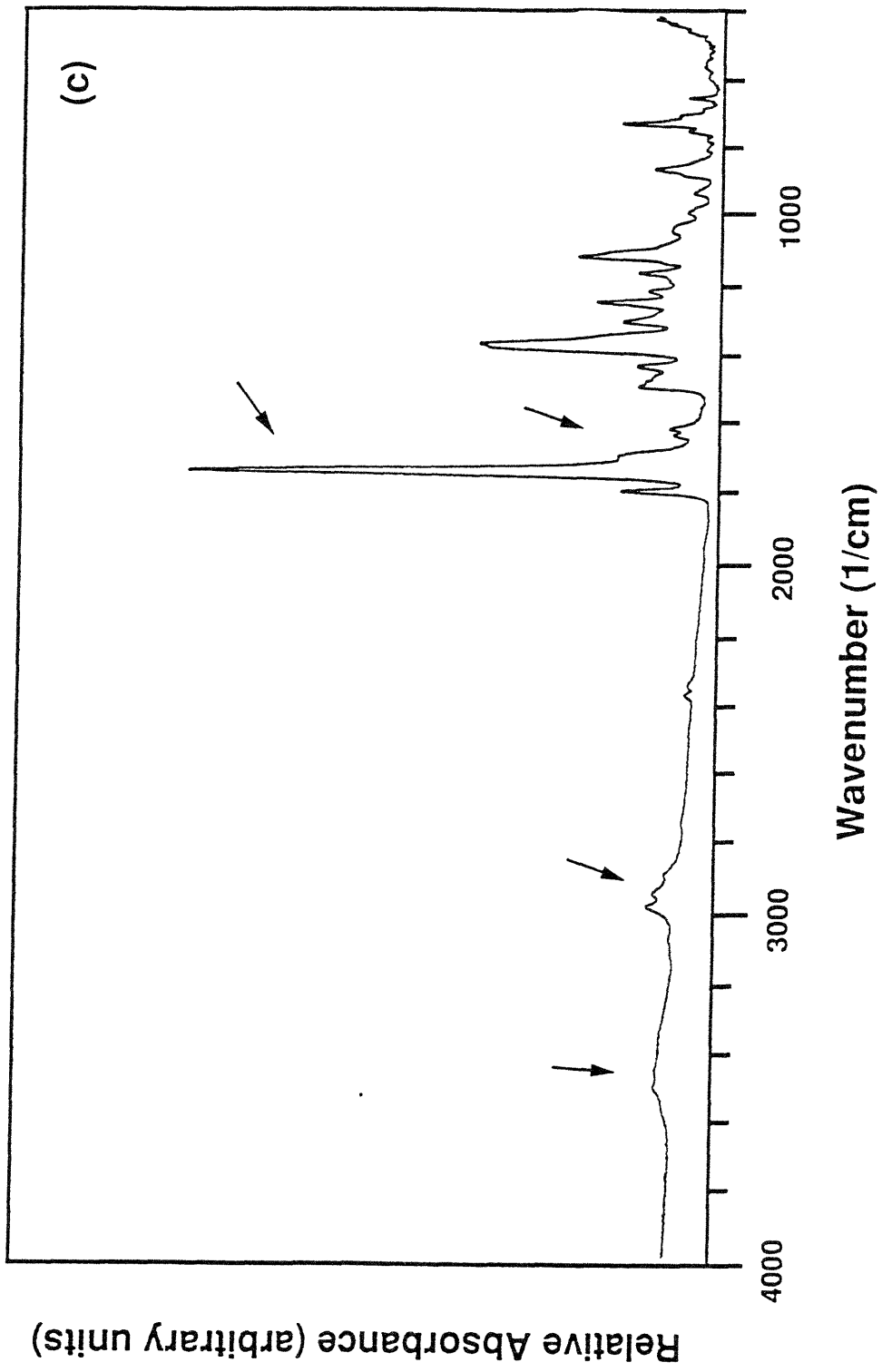


Figure 3.9 continued. (c) 10 minutes,

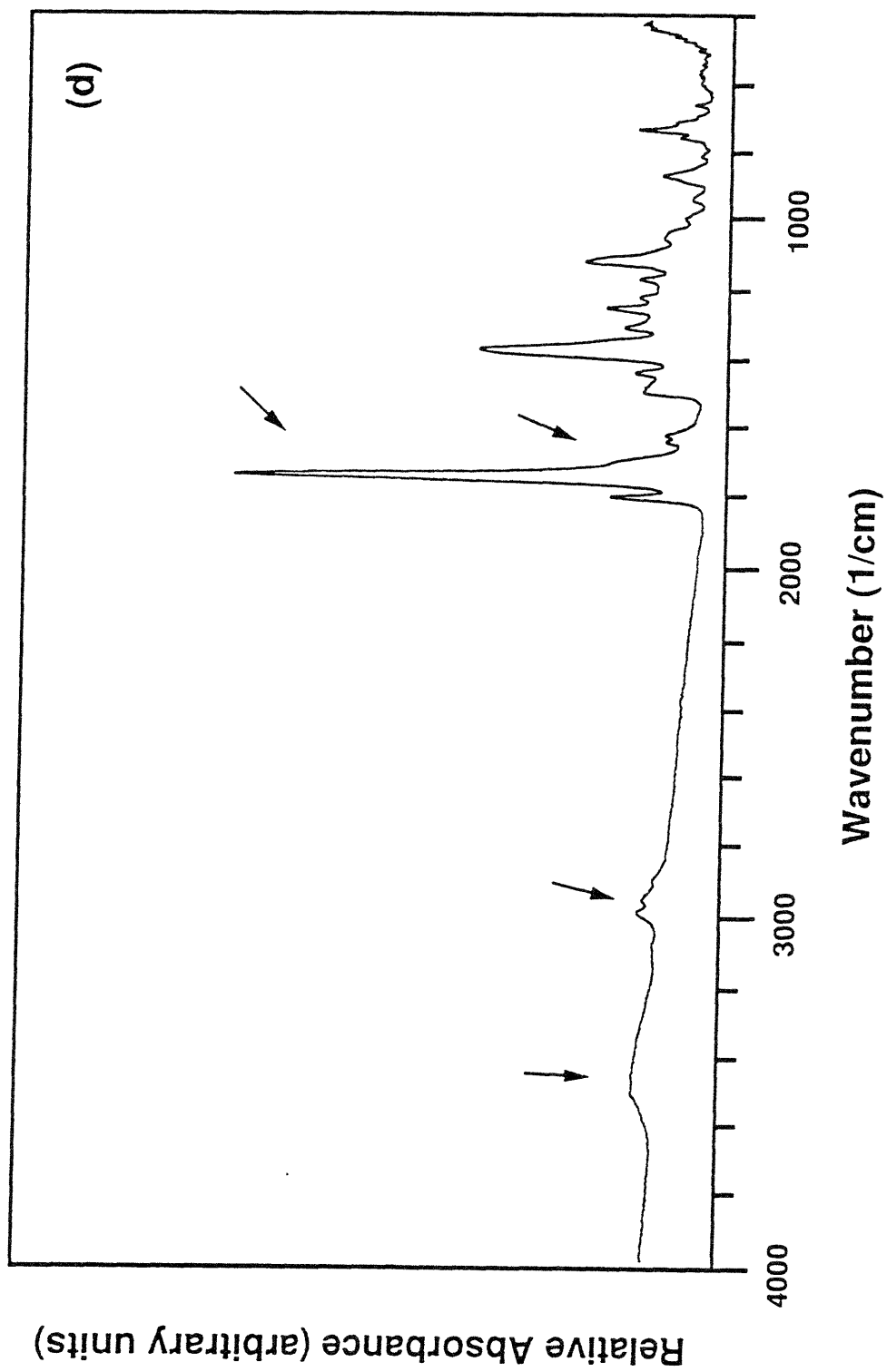


Figure 3.9 continued. (d) 50 minutes.

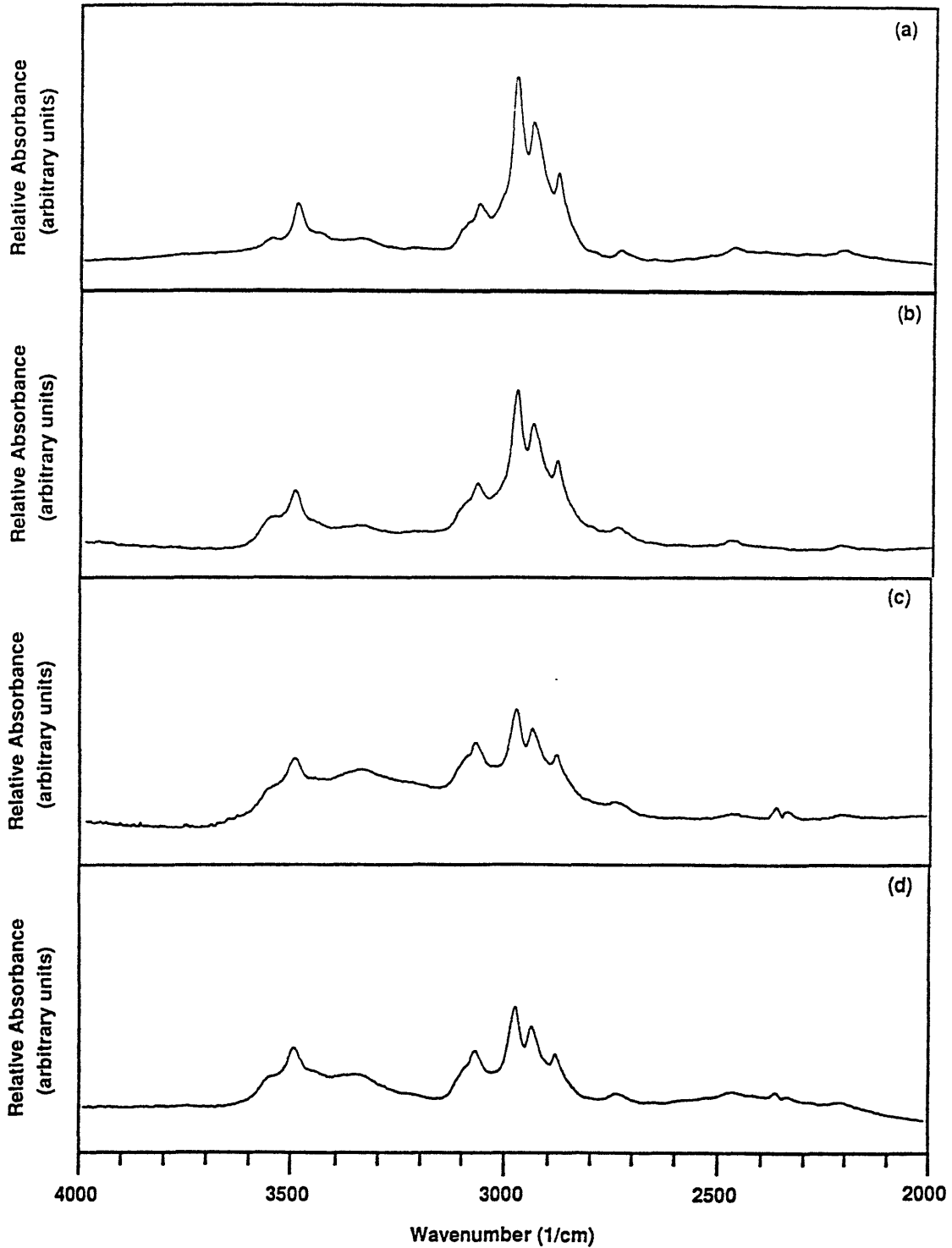


Figure 3.10. Relative IR absorbance vs. wavenumber (2000-4000 cm^{-1} range) for spin coated Probimide[®] 412 films with highest cure temperature treatment: (a) 300°C (3 hours in nitrogen), (b) 300°C (1 hour in air), (c) 300°C (3 hours in air), (d) 400°C (1 hour in nitrogen).

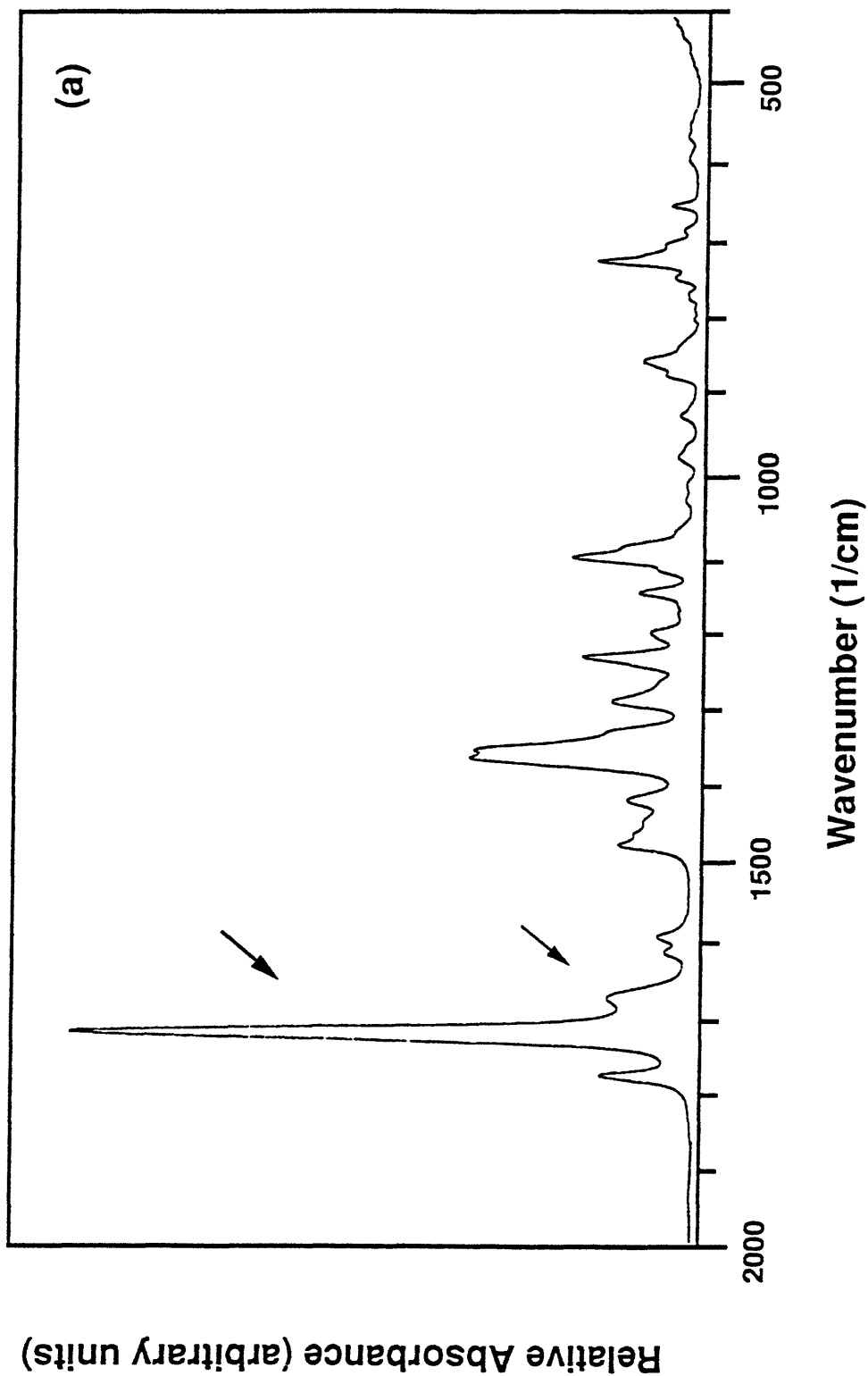


Figure 3.11. Relative IR absorbance vs. wavenumber ($400\text{-}2000\text{ cm}^{-1}$ range) for spin coated Probimide[®] 412 films with highest cure temperature treatment: (a) 300°C (3 hours in nitrogen), {arrows point to carbonyl bands at 1680 cm^{-1} and 1720 cm^{-1} }

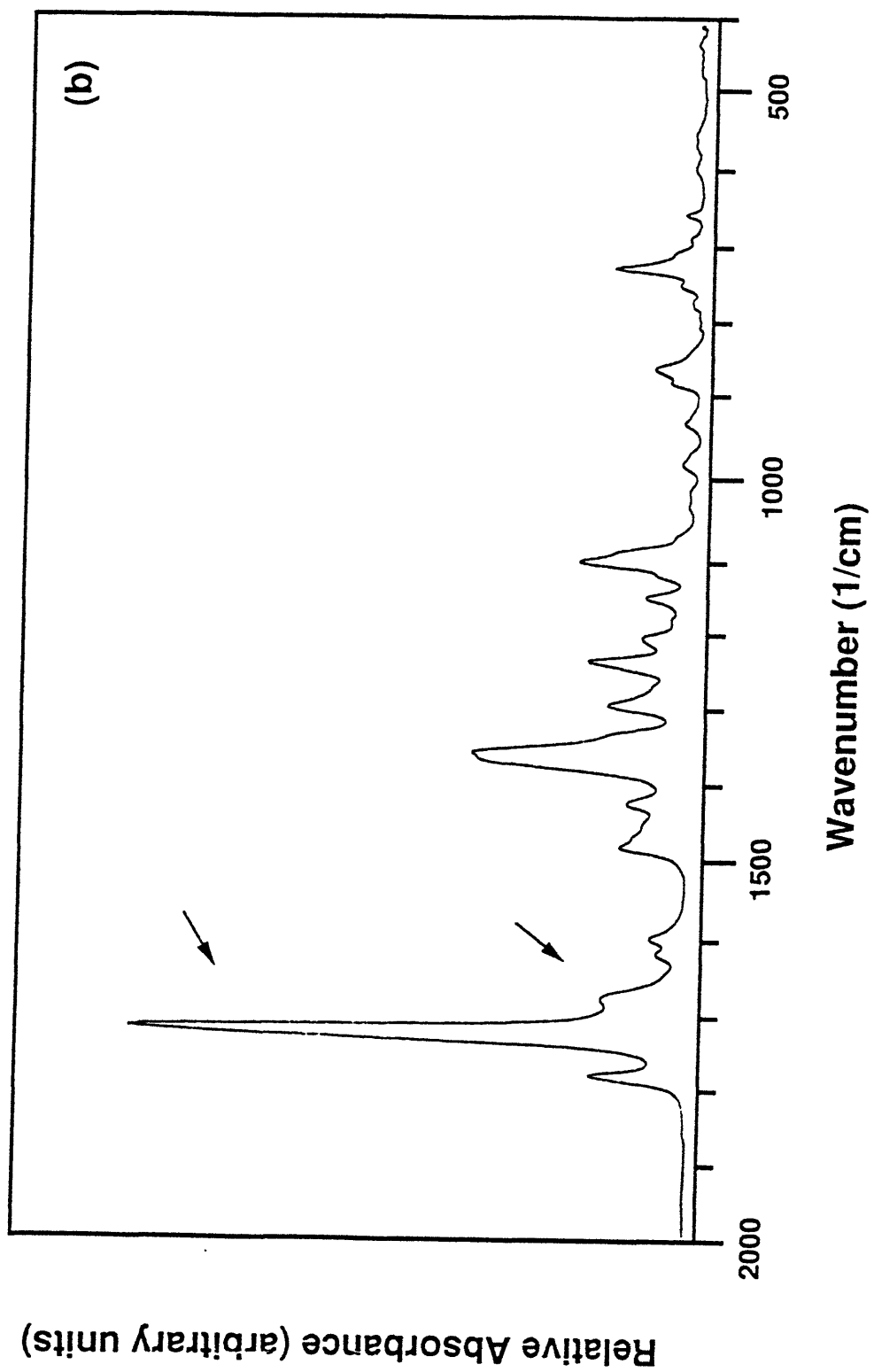


Figure 3.11. continued. (b) 300°C (1 hour in air),

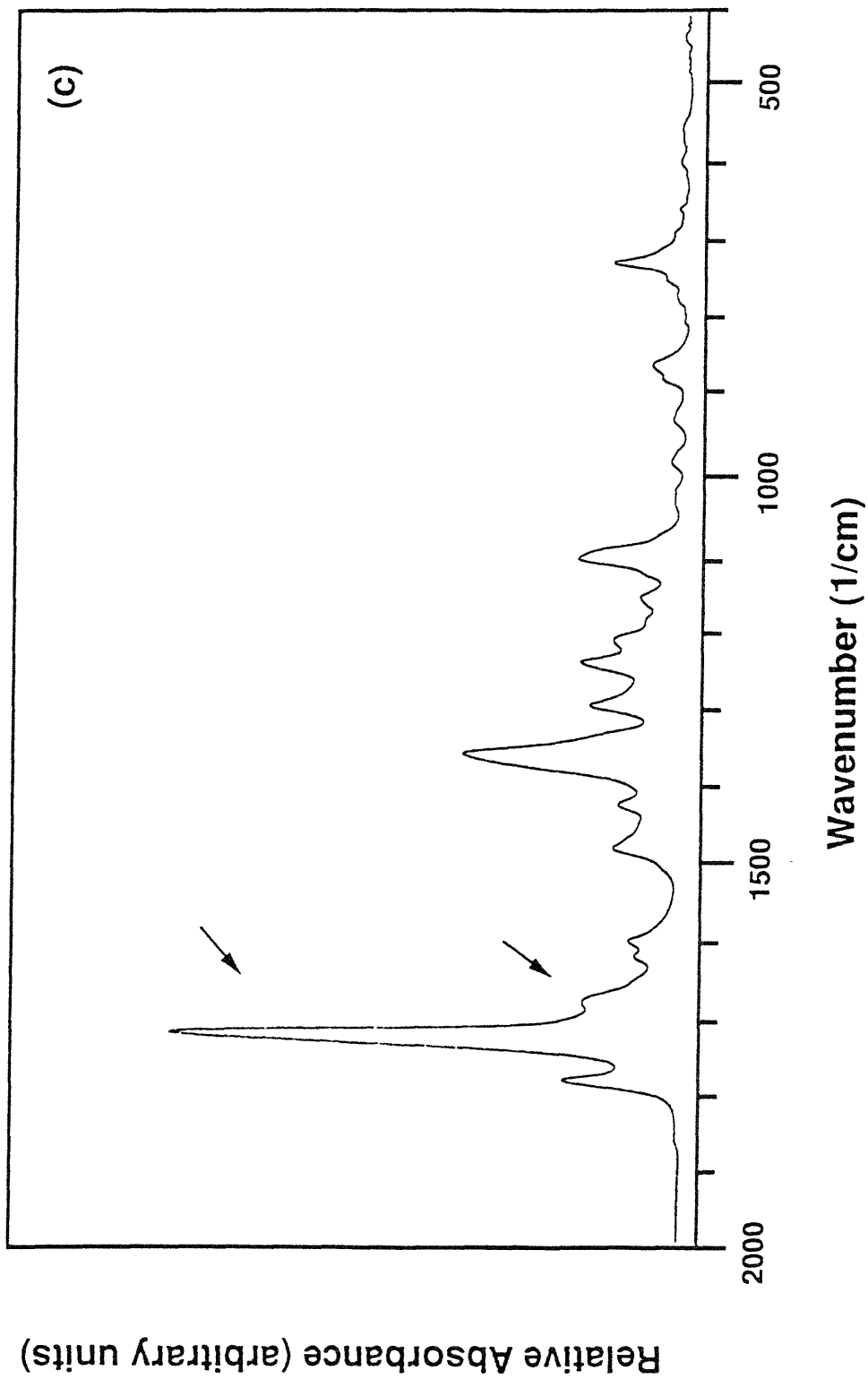


Figure 3.11. continued. (c) 300°C (3 hours in air)

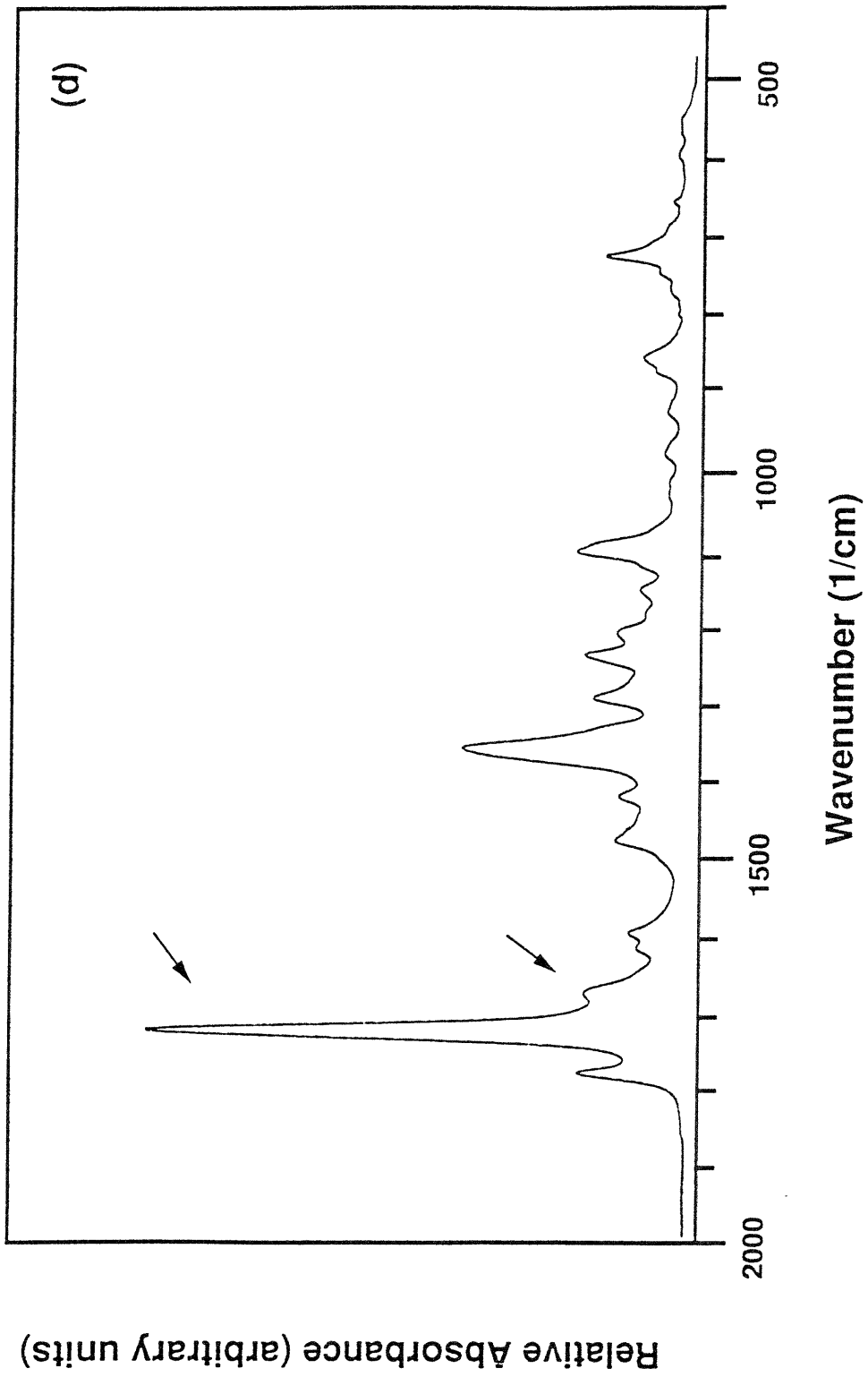


Figure 3.11. continued. (d) 400°C (1 hour in nitrogen).

highly specific and occurs by hydrogen abstraction and attack of the free radical at the benzophenone carbonyl.

The material also undergoes substantial thermally induced crosslinking which is especially favored in an oxygen containing environment. We found extensive crosslinking to occur when films are baked at 400°C in nitrogen or at 300°C in air. A nitrogen environment appears to inhibit crosslinking at 300°C. The thermal crosslinking process makes the polymer more brittle, reinforces its rubbery modulus, and broadens its distribution of relaxation times. Also, it gives the material a deep yellow to brown color and increases the index of refraction by approximately 20%. Although one possible crosslinking mechanism may be similar to that of the UV process, the thermally induced crosslinking is probably not limited to one mechanism.

3.5. References

1. H. Hiramoto, *Mat. Res. Soc. Symp. Proc.*, **167**, 87 (1990).
2. R. Rubner, H. Ahne, E. Kuhn, and G. Kolodziej, *Photo. Sci. Eng.*, **23(5)**, 303 (1979).
3. J. Pfeifer and O. Rhode, in *Recent Advances in Polyimide Science and Technology*, W.D. Weber and M.R. Gupta, Eds., Society of Plastic Engineers, New York, 1987, p. 336.
4. O. Rhode, P. Smolka, P. Falcigno, and J. Pfeifer, *Polym. Eng. Sci.*, **32(21)**, 1623 (1992).
5. Japanese patent #5034699, A (1993).
6. J. Cognard, *Mol. Cryst. Liq. Cryst. Suppl. Ser.*, Suppl. 1 (1982).
7. K.K. Chakravorty and C.P. Chien, *SPIE Int. Conf. on Adv. in Intercon. and Packaging*, **1389**, 559 (1990).
8. C.P. Chien and K.K. Chakravorty, *SPIE Optical. Thin Films III: New Developments*, **1323**, 338 (1990).

9. R. Mo, T. Maw, A. Roza, K. Stefanisko, and R. Hopla, *Proc. 7th Int. IEEE VLSI Multilevel Intercon. Conf.*, 390 (1990).
10. T. Maw and R. Hopla, *MRS Symp. Proc.*, **203**, 71 (1991).
11. T. Maw and R. Hopla, *MRS Symp. Proc.*, **227**, 205 (1991).
12. T. Maw, M. Masola, and R. Hopla, *Polym. Mat. Sci. Eng.*, **66**, 247 (1992).
13. M. Ree and K. Chen, *Polym. Prep.*, **31(2)**, 594 (1990).
14. M. Ree, K. Chen, and G. Czornyj, *Polym. Eng. Sci.*, **32(14)**, 924 (1992).
15. H. Ishida, S. Wellinghoff, E. Baer, and J. Koenig, *Macromol.*, **13**, 826 (1980).
16. H. Higuchi, T. Yamashita, K. Horie, and I. Mita, *Chem. Mater.*, **3**, 188 (1991).
17. R. Dine-Hart and W. Wright, *Die Makromolekulare Chemie*, **143**, 189 (1971).
18. R. Silverstein and G. Bassler, *Spectrometric Identification of Organic Compounds*, John Wiley & Sons, New York, 1967.
19. C. Pouchert, *The Aldrich Library of Infrared Spectra Edition III*, Aldrich Chemical Company, Milwaukee, WI 1981.
20. J. Scaiano, A. Becknell, and R. Small, *J. of Photochem. Photobio. A*, **44**, 99 (1988).
21. A. Lin, V. Sastri, G. Tesoro, A. Reiser, and R. Eachus, *Macromol.*, **21(4)**, 1165 (1988).
22. J. Scaiano, J. Netto-Ferreira, A. Becknell, and R. Small, *Polym. Eng. Sci*, **29(14)**, 942 (1989).

Chapter 4. Effect of Cure Conditions on Probimide® 32 Polyamide-imide

4.1. Introduction

Polyimides, as discussed in the previous chapters, are important members of the class of high temperature heterocyclic polymer materials [1-3]. They are well known for their outstanding thermal stability, mechanical and electrical properties, and chemical resistance. Polyimides are used in electronic, display, and aerospace applications.

Polyamide-imides [4] are related polymers whose repeat units contain both an imide ring linkage and an amide linkage. Polyamide-imides are less expensive than polyimides, readily processed from solutions, and still have outstanding properties. There is expanding interest in polyamide-imides as engineering plastics [4], as materials for molecular composites [5,6], and as liquid crystal display (LCD) alignment films [7].

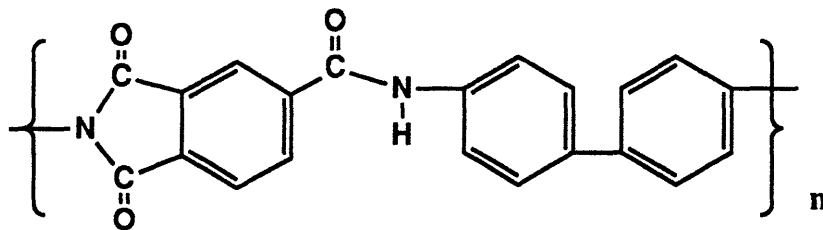
In Chapter 1, it is explained that polyimides generally require high temperature treatments which are necessary both for ring closure of the polyamic acid precursor, and for the removal of high boiling point solvents. Studies show [8-16] that the chemical and physical properties of polyamic acid precursor systems change substantially as they are cured, primarily because of the chemical conversion from polyamic acid to polyimide. Unlike most polyimides, polyamide-imides are available in solutions of their fully converted (i.e., fully imidized) form. The fully imidized polyamide-imides systems do not require post-processing heat treatment to effect closure of the imide ring.

It is important that the outstanding features, as well as the limitations, of polyamide-imides be well understood. It is furthermore crucial to understand these materials from a processing-structure-properties perspective. Since reducing the cure temperature of polyimides may reduce processing cost and time, as well as allow their compatibility with inexpensive low temperature materials, it is interesting to learn how these systems respond to differing thermal treatments. Thus, this work explores the effects of cure temperature and environment on the properties and structure of a preimidized polyamide-imide system. Our goal is to learn how the pre-converted polymer changes physically and chemically during its cure treatment. We report here the processing-structure-property relationships in Probimide® 32 polyamide-imide as a part of an ongoing evaluation of the material for liquid crystal alignment applications.

4.2. Experimental Section

4.2.1. Polymer film processing

We studied the material Probimide[®] 32, a fully imidized polyamide-imide resin produced by OCG Microelectronic Materials, Inc. The polymer is provided in an NMP/xylene solution with 21% solids content by weight. The material has the following chemical repeat unit:



Bulk films were formed by the technique described in Section 3.2.1 and depicted in Figure 3.1. The Probimide[®] 32 solution was dropped onto a glass plate and wiped with a metal doctor blade with a 1 mm gap. The wet films were dried to a tack free condition under a dry air current at room temperature overnight. The films were then progressively cured at 100°C for six hours, then 200°C for three hours, and then 300°C for three hours. Thermal cures of 100°C and 200°C were performed in air with the polymer on glass, while the 300°C cures (which we will call “hard cures”) were performed on free-standing film in either air or nitrogen environments. Film thicknesses were on the order of 100µm. All films were amorphous, as the samples exhibited no Bragg scattering peaks when examined by wide angle X-ray scattering.

Thin films were formed by spin casting the undiluted Probimide[®] 32 solution on glass or KBr at 4000 RPM for 30 seconds. The samples were immediately softbaked at 100°C for fifteen minutes in air. The samples appeared to be dry after softcuring. The samples then progressively underwent one hour cures at 200°C and then 300°C. The 200°C cures were performed in air, while the 300°C cures were performed either in air or nitrogen.

4.2.2. Measurement techniques

A Seiko TG/DTA320 was used for thermogravimetric analysis of the bulk films. Samples were scanned from room temperature to 575°C at 10°C/minute in flowing air (300ml/minute).

Dynamic mechanical analysis was performed in tension mode on bulk films using a Seiko DMS200. Samples were scanned under nitrogen at 2°C/minute from room temperature to the temperature above T_g at which breakage occurred. Frequencies 1, 2, 5, 10, and 20 Hz were used.

Index of refraction at $\lambda = 632.8$ nm was measured using a Metricon PC-2000 prism coupler. Refractive index was measured by determination of the critical angle. Both in-plane n_{TE} and out-of-plane n_{TM} indices were measured. Average refractive index n_{avg} was calculated as:

$$n_{avg} = (1/3) (2n_{TE} + n_{TM}). \quad (1)$$

Refractive index measurements were taken for the free standing films and the thin films spin coated on glass slides.

Fourier transform infrared spectroscopy was performed using a Nicolet 510P. FTIR spectra were taken for the Probimide[®] 32 thin films spin coated on KBr.

Differential scanning calorimetry (DSC) measurements were made for bulk films using a Perkin Elmer DSC-7 calibrated to zinc and indium standards. The scan rate was 20°C per minute.

4.3. Results and Discussion

4.3.1. Coloration and Brittleness

The changes in coloration and brittleness in Probimide 32 thick films that occur with subsequent cures are summarized in Table 4.1. The films were considered “brittle” if they were easily broken upon flexing. Probimide[®] 32 becomes progressively darker as it is cured to higher temperatures, and it is darkest when cured at 300°C in air. The polymer is brittle after it is cured at only 100°C. However, the brittleness recedes when it is cured to 200°C. The film then becomes brittle if cured at 300°C in air, but does not become brittle if cured at 300°C in nitrogen. The brittleness and dark coloration of the air cured, hard baked film suggests that abundant chemical crosslinks have formed.

Table 1. Color and Brittleness in Films Cured at Progressively Higher Temperatures.

Temperature	Environment	Color	Brittleness
100°C	air	yellow	very brittle
200°C	air	brown	flexible
300°C	air	dark, reddish brown	brittle
300°C	N ₂	brown	flexible

4.3.2. Thermogravimetric Analysis

Thermogravimetric spectra of Probimide[®] 32 bulk films chart the removal of solvent and water from the films, as well as indicate decomposition of the polymer. Our primary goal is to observe solvent content as a function of cure conditions. We demonstrate here how solvent is progressively removed from the bulk polymer films as they are cured at 100°C, 200°C, and 300°C.

Polyimide Solvents

Polyimide solvents typically have very high boiling points. N-methylpyrrolidone boils at 202°C, while xylene boils at 138°C-144°C. However, while solvents unbound to polymer typically evaporate at temperatures below their boiling points, solvents bound to polymer may require higher temperatures in order to vaporize. In the 10°C/minute thermogravimetric scan of Fisher Scientific N-methylpyrrolidone in Figure 4.1, all solvent has evaporated by about 190°C.

Probimide 32

In Figure 4.2(a-d), thermogravimetric and derivative scans of Probimide[®] 32 treated at room temperature, 100°C, 200°C, and 300°C, respectively, are compared. The scans depict the loss of water at 80°C, loss of residual solvent at about 200°C, and decomposition of the polymer above 350°C. The films lose about 3% of their initial weight below 150°C due to water removal. All samples treated at or below 200°C have a large loss in weight in the 150°C to 350°C region due to vaporization of residual solvent. For the derivative curves, the higher the cure temperature, the higher the temperature at which maximum rate of weight loss of solvent occurs. While the rate of weight loss is maximal at

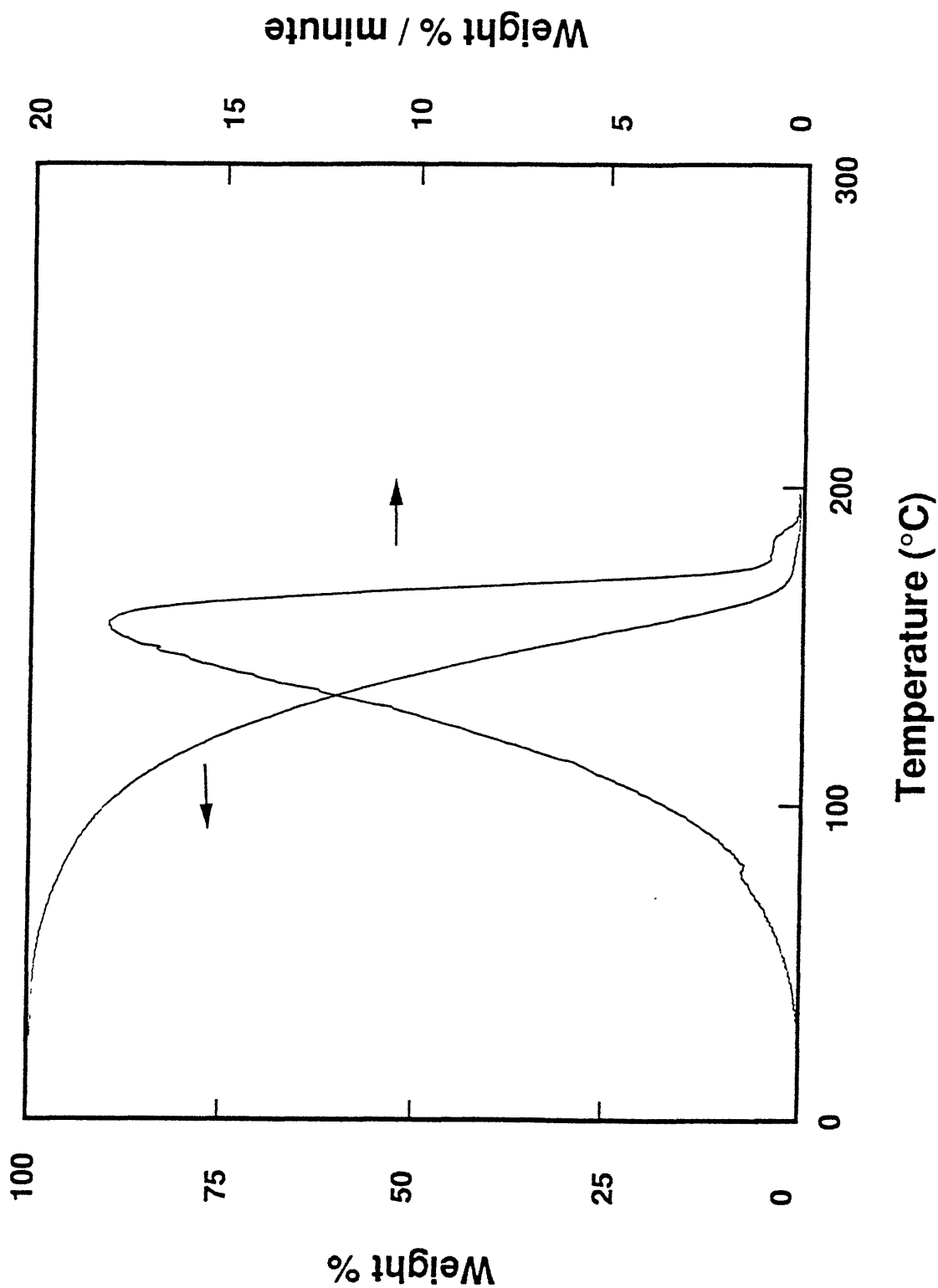


Figure 4.1. Weight loss and derivative of weight loss vs. temperature for N-methyl pyrrolidone (NMP).

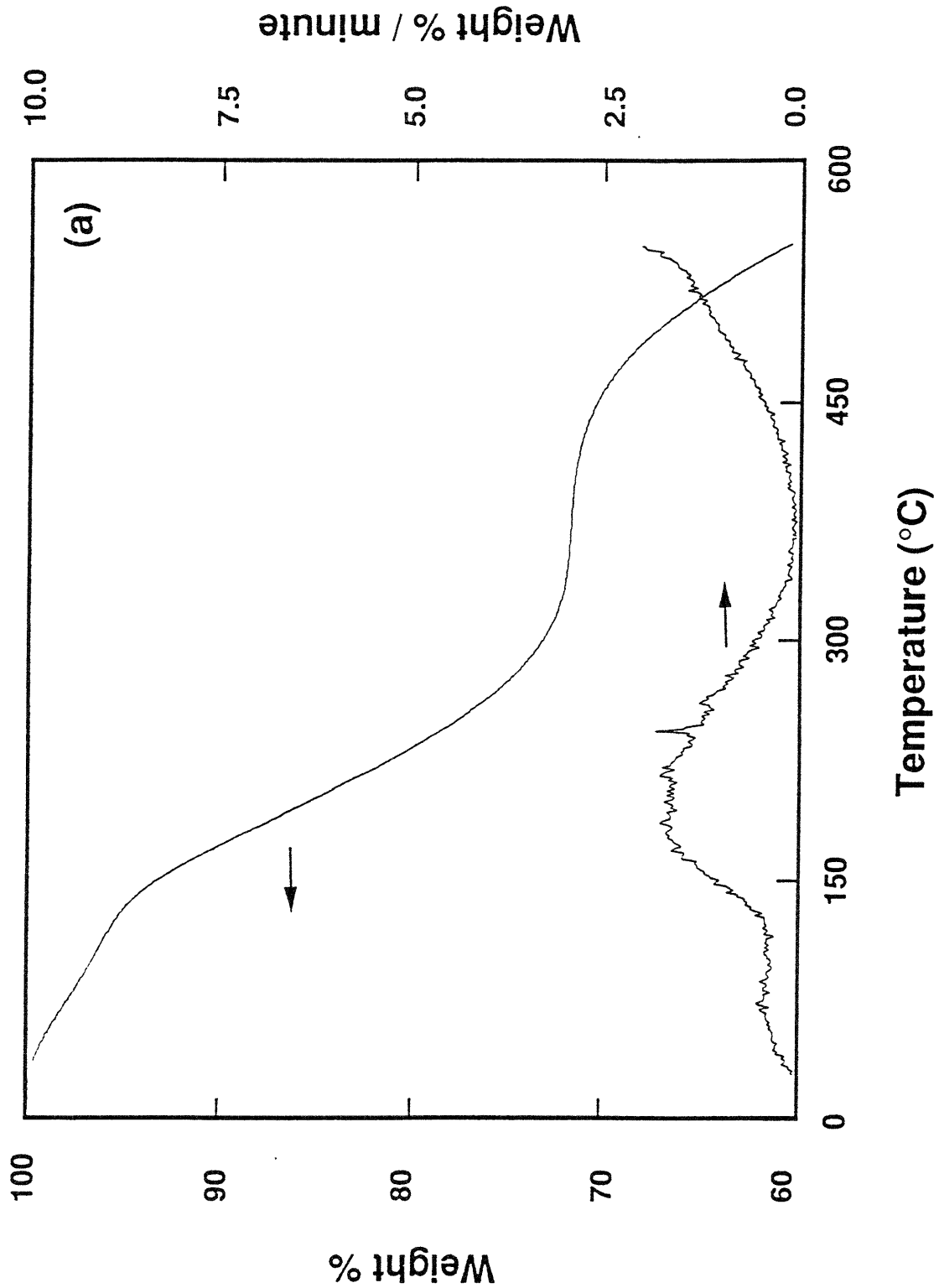


Figure 4.2. Weight loss and derivative of weight loss vs. temperature for Probimide[®] 32 thick films: a.) dried under an air current at room temperature,

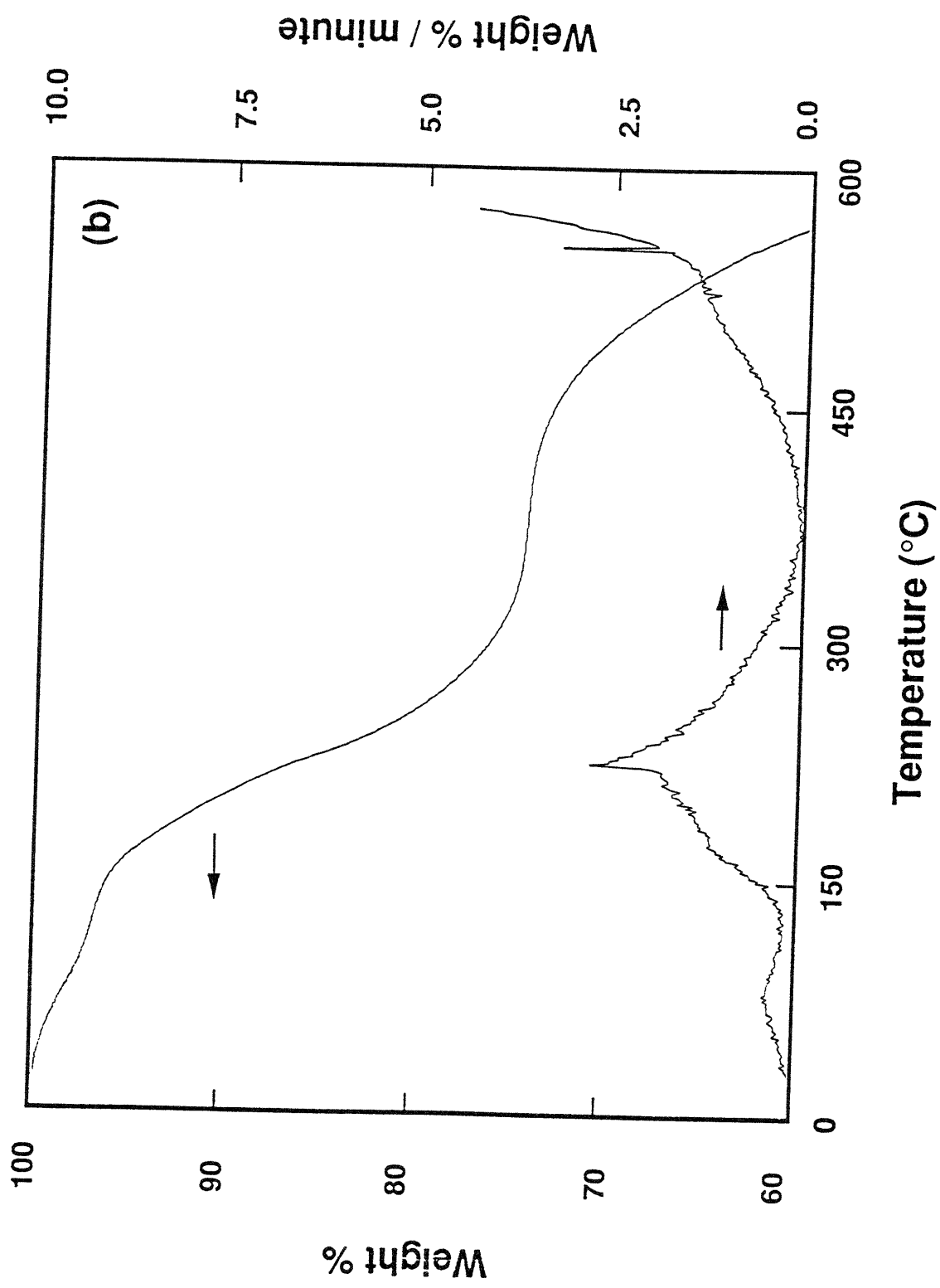


Figure 4.2. continued. b.) then baked 6 hours at 100°C ,

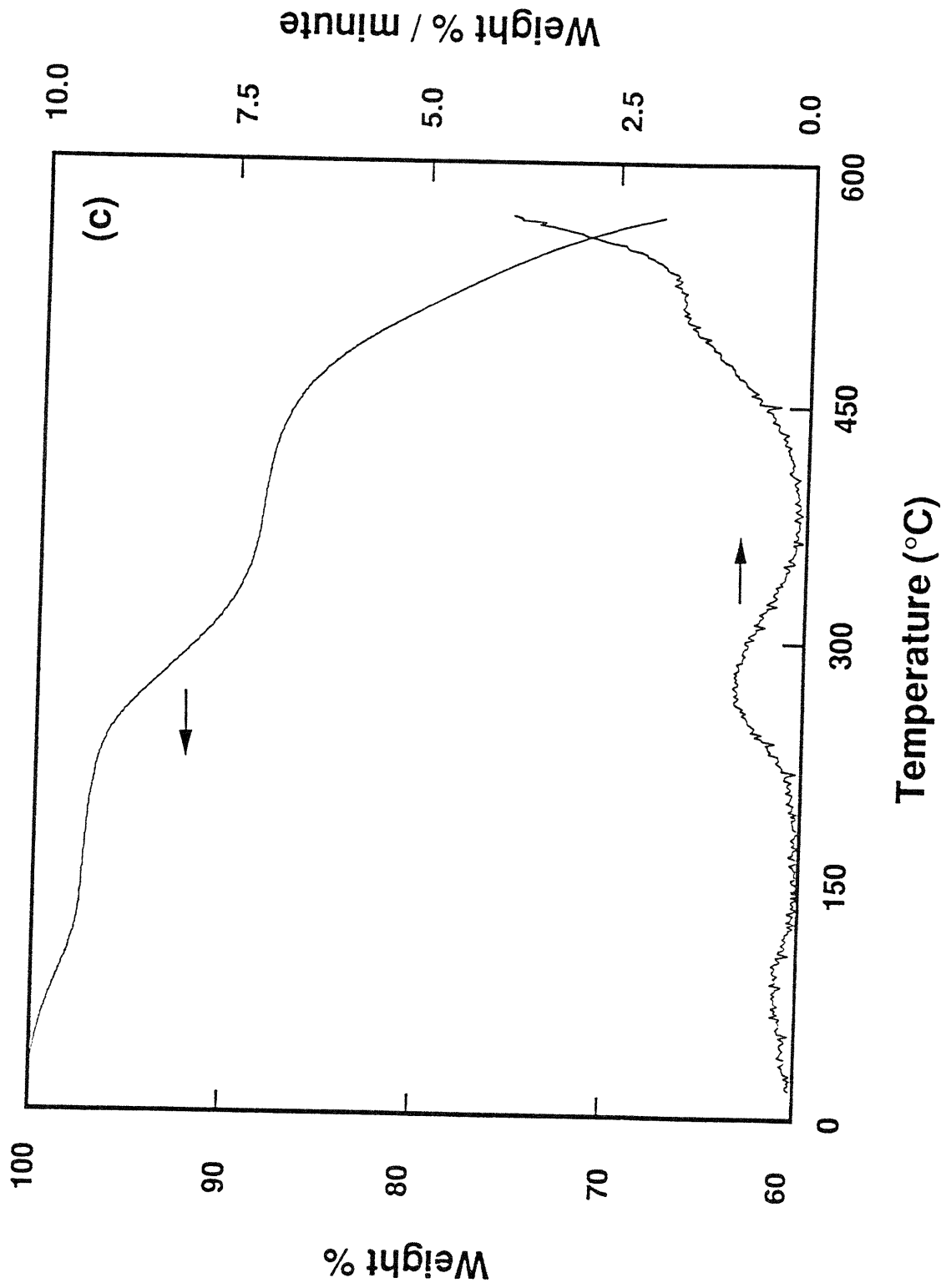


Figure 4.2. continued. c.) then 3 hours at 200°C,

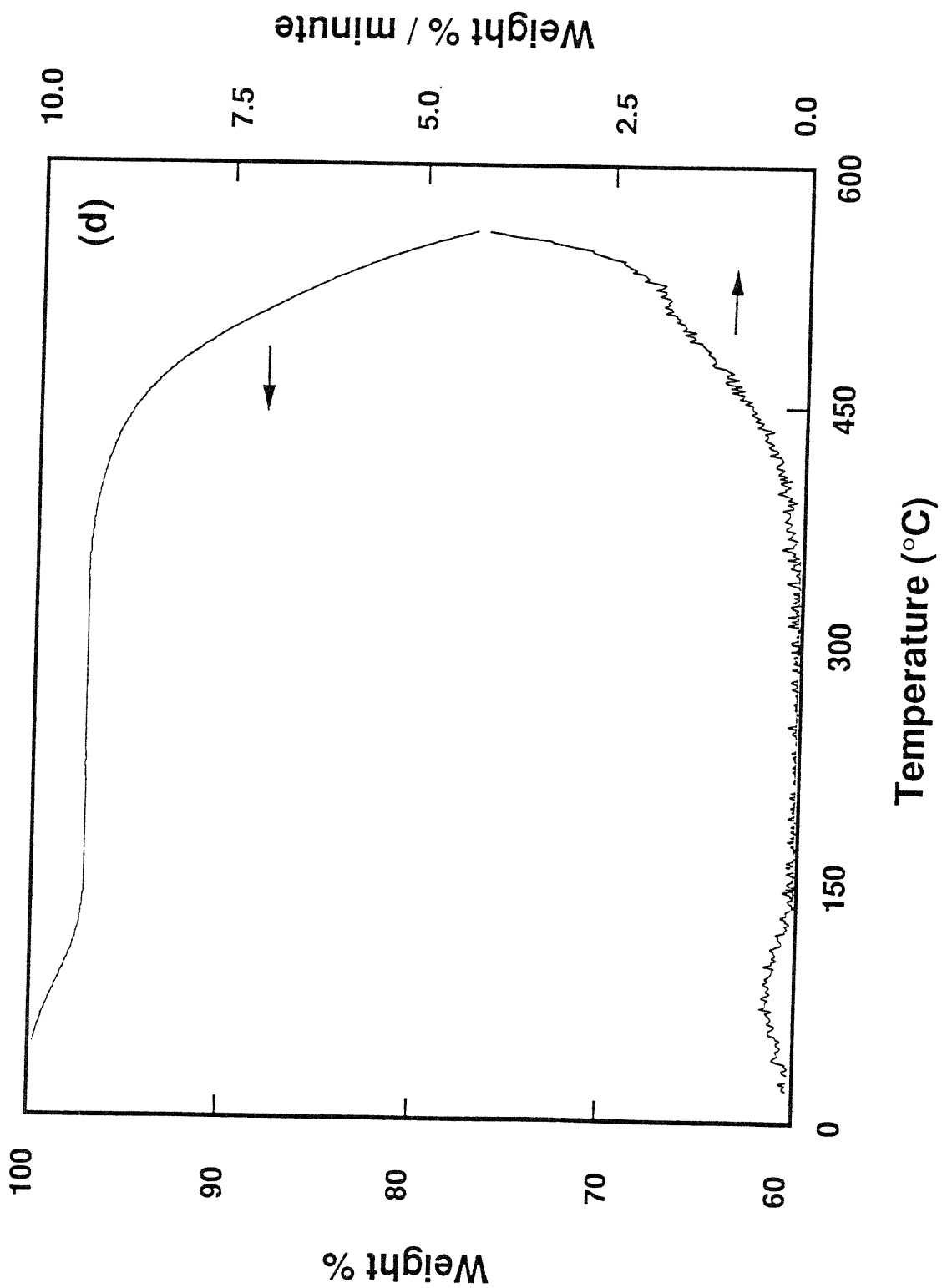


Figure 4.2. continued. d.) then 3 hours at 300°C.

around 200°C in the room temperature cured sample, the rate of weight loss is maximal at almost 300°C in the 200°C cured sample. The peak height decreases as the cure temperature increases. In the 150°C to 350°C region, the room temperature cured sample (Figure 4.2(a)) has the largest weight loss, the 100°C cured sample less (Figure 4.2(b)), and the 200°C cured sample even less (Figure 4.2(c)). Thus, each cure at a progressively higher temperature removes more solvent from the film. There is apparently no residual solvent remaining in the 300°C cured film (Figure 4.2(d)). The weight loss curves shows a plateau until the temperature exceeds 400°C, at which point film degradation begins.

As also shown in the previous study of Probimide[®] 412, there is a distribution of solvent removal temperatures ranging from below 150°C to above 350°C. The 32 films, however, contained more solvent than the 412 films of Chapter 3. The distribution, hence, is even more apparent. Solvent molecules removed at or below the boiling point of the solvent represent loosely bound species that readily vaporize, while molecules that are removed at temperatures far above the boiling point represent species that are physically bound to the polymer. Thus, as the material is cured, low boiling species are removed, and the distribution of removal temperatures of residual solvent species is pushed to higher temperatures.

Cure time also affects the residual solvent in the polymer film. Figure 4.3 depicts thermogravimetric scans of Probimide[®] 32 treated for 1, 6, and 24 hours at 100°C. As cure time increases, the amount of residual solvent decreases. There is also a small shift in the distribution of solvent removal temperatures between 1 and 6 hours and a larger shift after 24 hours of cure.

As Figures 4.2 and 4.3 show, at around 450°C, decomposition of the polymer begins, as indicated by a large loss in weight. If we arbitrarily define the decomposition temperature as the temperature above 350°C at which the time derivative of weight loss equals 3% per minute (scanning at 10°C/minute), the decomposition temperature of Probimide[®] 32 is about 550°C in flowing air. The manufacturer reports a decomposition temperature of 494°C [17] though they do not report the scan conditions.

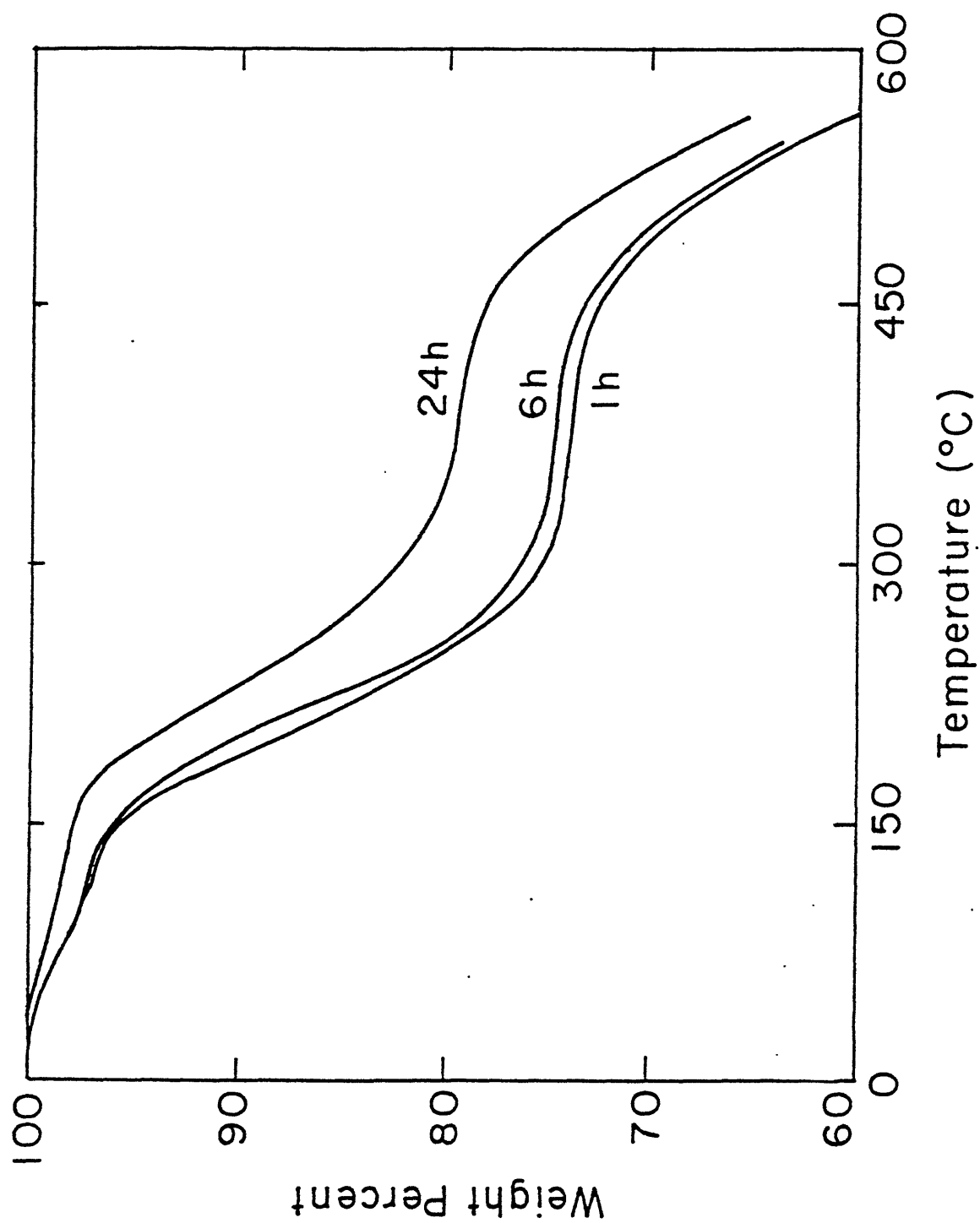


Figure 4.3. Weight loss and derivative of weight loss vs. temperature for Probimide[®] 32 thick films baked at 100°C for 1, 6, and 24 hours.

4.3.3. Dynamic Mechanical Analysis

The dynamic mechanical relaxation of Probimide[®] 32 films provides a wealth of property and structure information. DMA data demonstrate how the glassy regions, the relaxation regions, and the rubbery regions are affected during the cure and how they are dependent upon cure environment. The changing dynamic mechanical spectra can be attributed to changing solvent content and to changing degrees of crosslinking.

The DMA spectra for Probimide[®] 32 are shown in Figure 4.4(a-d) for samples cured at 100°C, 200°C, 300°C in air, and 300°C in nitrogen, respectively. Young's modulus E' and loss factor $\tan\delta$ are shown as functions of temperature. For brevity, only measurements at 1Hz are shown.

The glassy Young's modulus at 25°C is affected by the cure conditions of the polymer film. The glassy modulus of film treated at 100°C and 200°C (Figure 4.4(a,b)) is 1.9-2.0 GPa. The glassy modulus of Probimide[®] 32 film treated at 300°C in nitrogen (Figure 4.4(d)) is somewhat higher, 2.7 GPa, which agrees with reported values of the modulus [17]. It appears that residual solvent in the films cured at 100°C and 200°C plasticizes the films, lowering the glassy modulus. The measured glassy modulus of film treated at 300°C in air (Figure 4.4(c)) is fairly low, 1.3 GPa. This is either because of oxidative damage inflicted upon the polymer during the cure, or because of an inability to make an accurate measurement due to the brittleness of the film.

In Figures 4.4(a,b), Young's modulus for samples cured at 100°C and 200°C drops by about two orders of magnitude as a result of polymer relaxation. In the $\tan\delta$ curves, two relaxations are seen in these samples. The first relaxation in each scan occurs at about the curing temperature, while the second relaxation occurs just below 300°C. The material is highly plasticized by residual solvent, giving the material a low softening temperature. Once the solvent is driven out, the material again relaxes at the glass transition temperature of the unplasticized polymer.

In Figures 4.4(c,d), the samples treated at 300°C, in air or in nitrogen, have only a single relaxation. The glass transition relaxation is centered above 300°C in the air-treated sample. The $\tan\delta$ peak is shallow, suggesting the sample is highly crosslinked by the 300°C cure in air. The sample treated under nitrogen at 300°C, on the other hand, has a well defined glass transition relaxation at 300°C. It is thus apparent that the degree of crosslinking in Probimide[®] 32 is substantially greater when hard cured in air than when hard cured under flowing nitrogen.

The rubbery modulus region is also very different in the Probimide[®] 32 films. The films cured at 100°C and 200°C have extremely low rubbery moduli, the 200°C cured film

having a slightly greater rubbery modulus than the 100°C treated film. In the 300°C nitrogen-treated material, the rubbery Young's modulus reaches a minimum value of 0.16 GPa shortly after relaxation. This rubbery modulus is about ten times greater than that observed in the 100°C and 200°C treated films. Apparently, the 300°C cure in nitrogen not only increases the glass transition temperature, but also provides reinforcement to the rubbery state, probably as a result of backbone crosslinks that form during the hard cure. The rubbery modulus of the film cured 300°C in nitrogen slowly increases with temperature as the high temperatures induce more non-oxidative crosslinks in the polymer. In the film cured at 300°C in air, no rubbery region is clearly observed because gel network has already formed before the polymer relaxes. Instead, the modulus slowly declines and does not appear to flatten entirely before the sample breaks.

In a polyimide that is not preconverted, the modulus and glass transition temperature increase as the polymer is cured. This is not surprising, as the conversion of polyamic acid to polyimide increases the stiffness of the chemical backbone. This study shows, however, that even in a fully converted system, residual solvent can also have a marked effect on the mechanical properties of the material. The study also demonstrates that the extent of interchain covalent bonding strongly impacts the mechanical behavior of the polyamide-imide.

4.3.4. Index of Refraction

The optical properties of Probimide[®] 32 are also cure-dependent. They change with cure temperature and cure environment. The indices of refraction of thin films of Probimide[®] 32 spin coated on glass are presented in Figure 4.5(a,b). The average indices of refraction of the bulk films were identical to those of the thin films.

Average indices of refraction of spin coated films are plotted against highest cure temperature in air in Figure 4.5(a). There is a general increase in refractive index with increasing cure temperature. These changes coincide with the observed changes in coloration described in Table 1. The increase in index is associated with increased density and/or electronic polarizability due to a combination of several factors: loss of solvent, crosslinking, and increased interchain interaction.

Average indices of films cured at 300°C are shown in Figure 4.5(b) as a function of 300°C cure conditions. The films hard baked under nitrogen have slightly lower average refractive indices than do those treated in air. This suggests that the crosslinking reaction at 300°C is faster in air than in nitrogen.

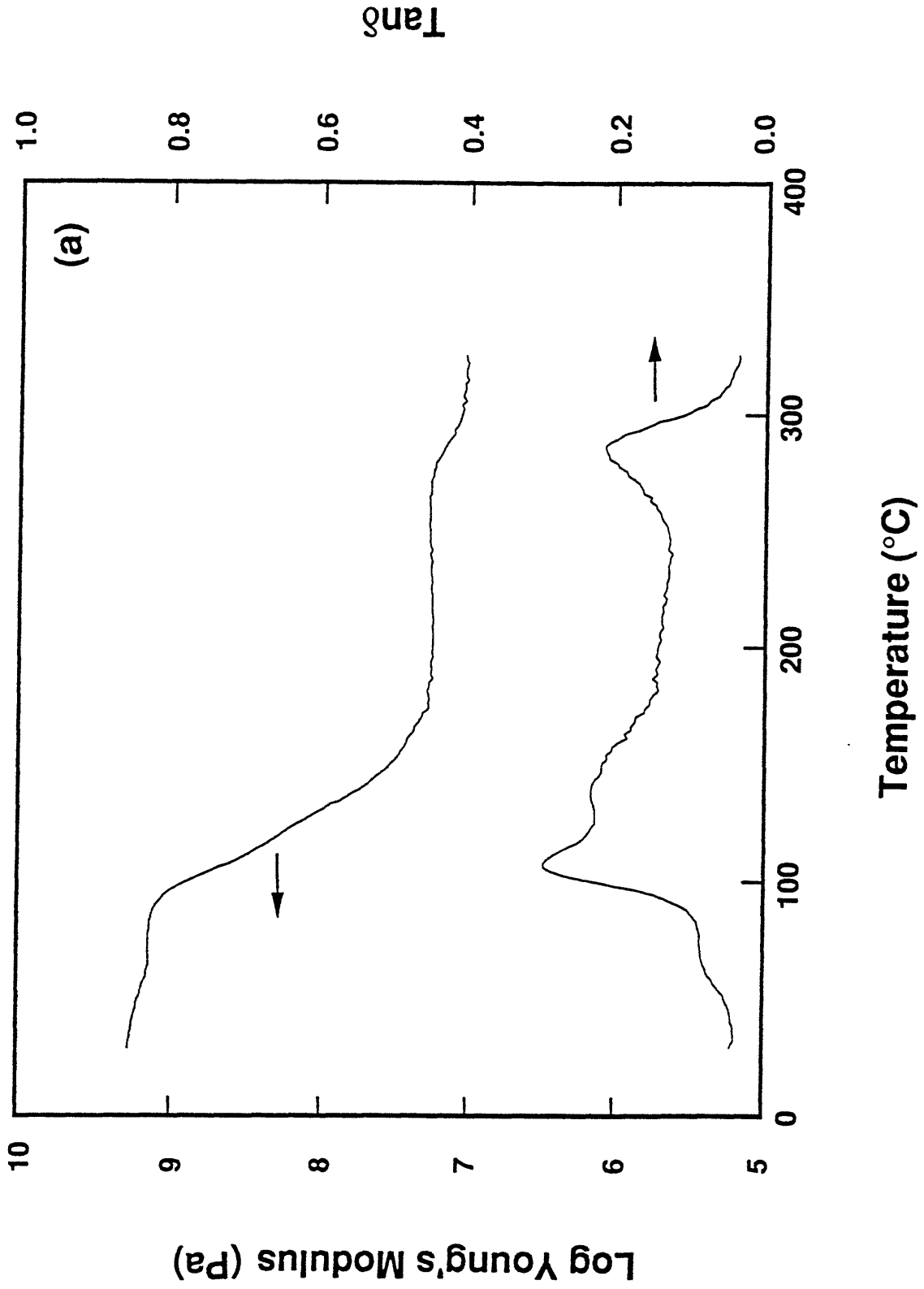


Figure 4.4. Young's modulus and dissipation factor, $\tan\delta$, for Probimide[®] 32 thick films:
 a.) cured 6 hours at 100°C,

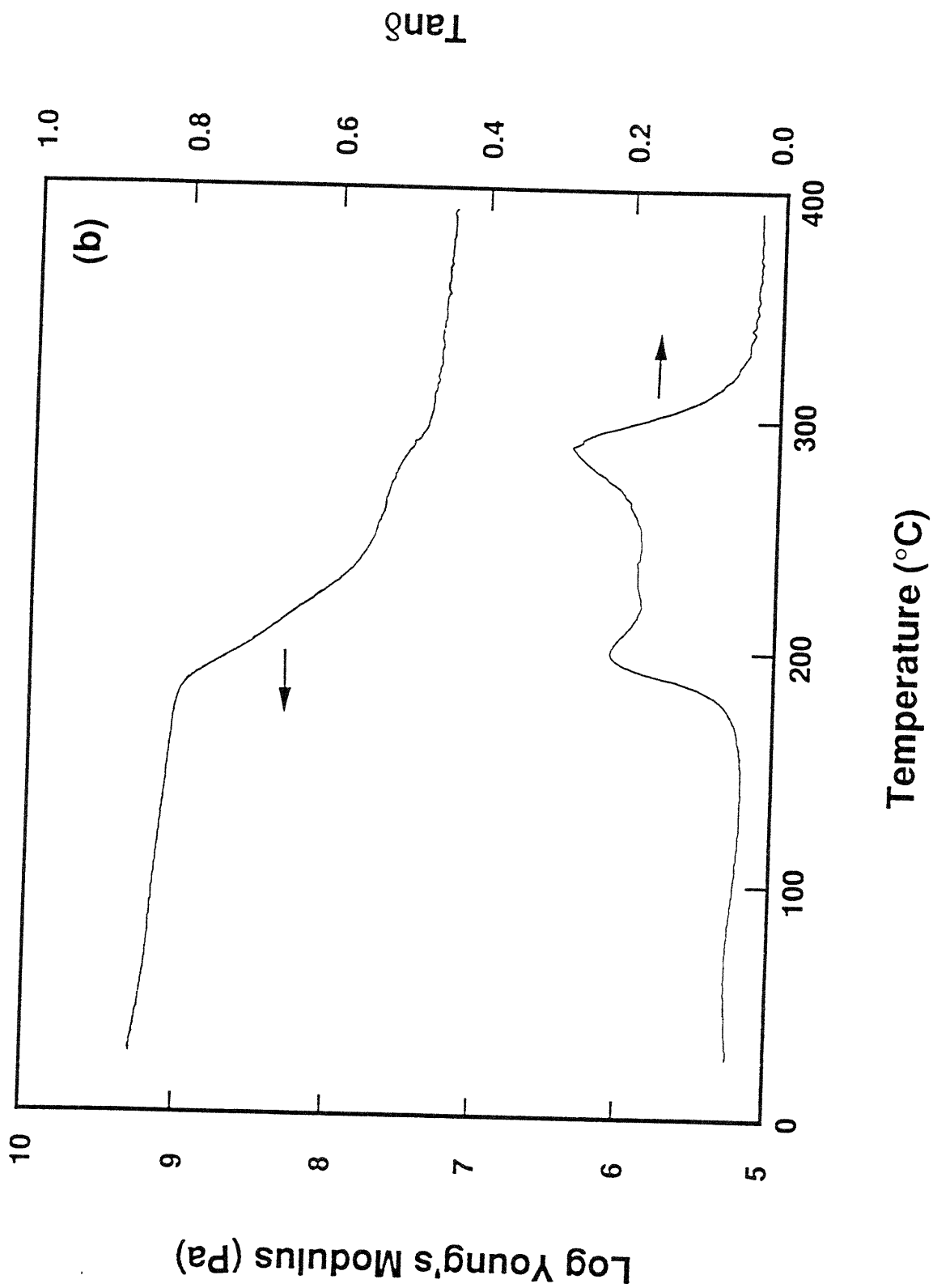


Figure 4.4. continued. b.) then 3 hours at 200°C,

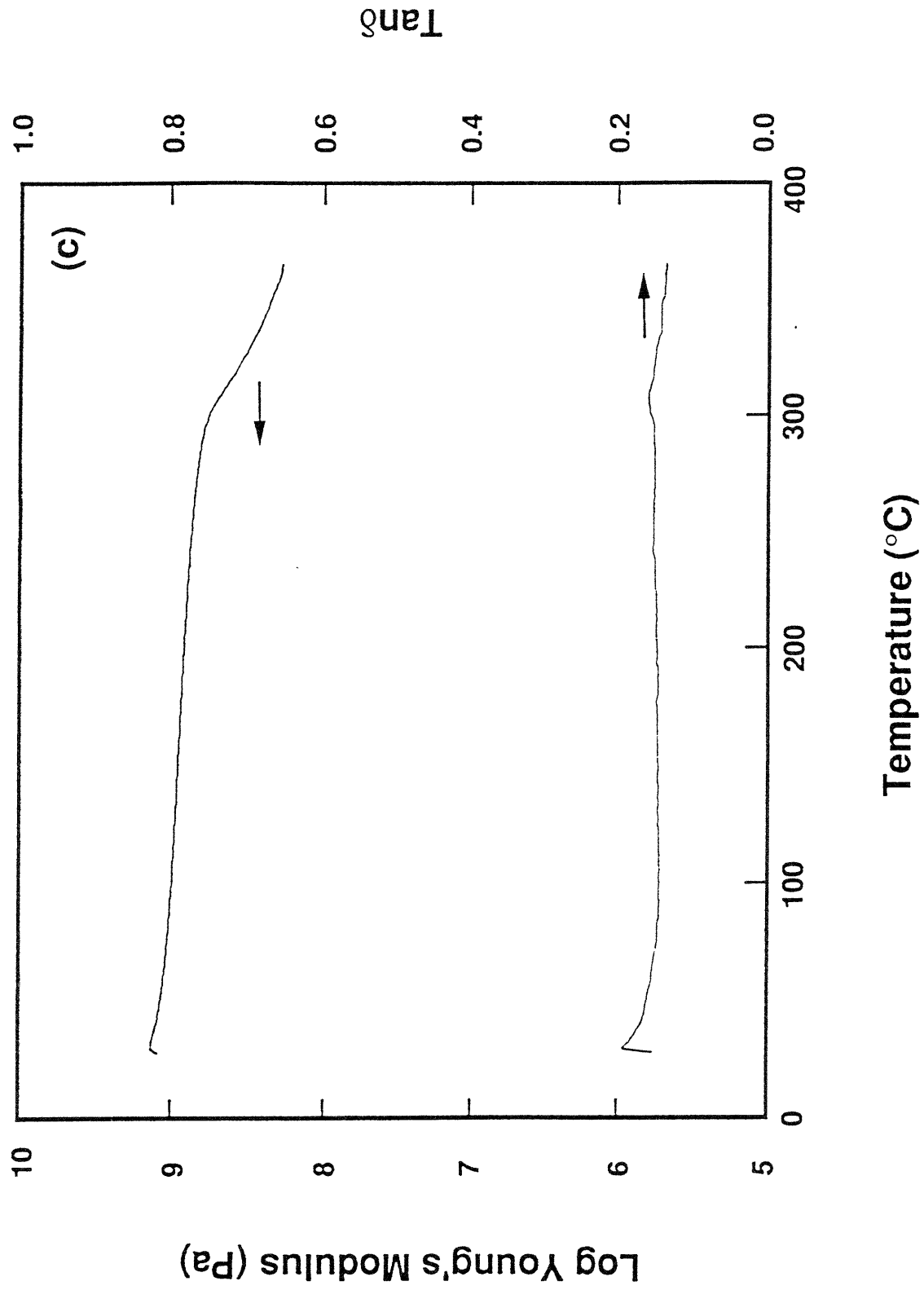


Figure 4.4. continued. c.) then 3 hours at 300°C in either air or,

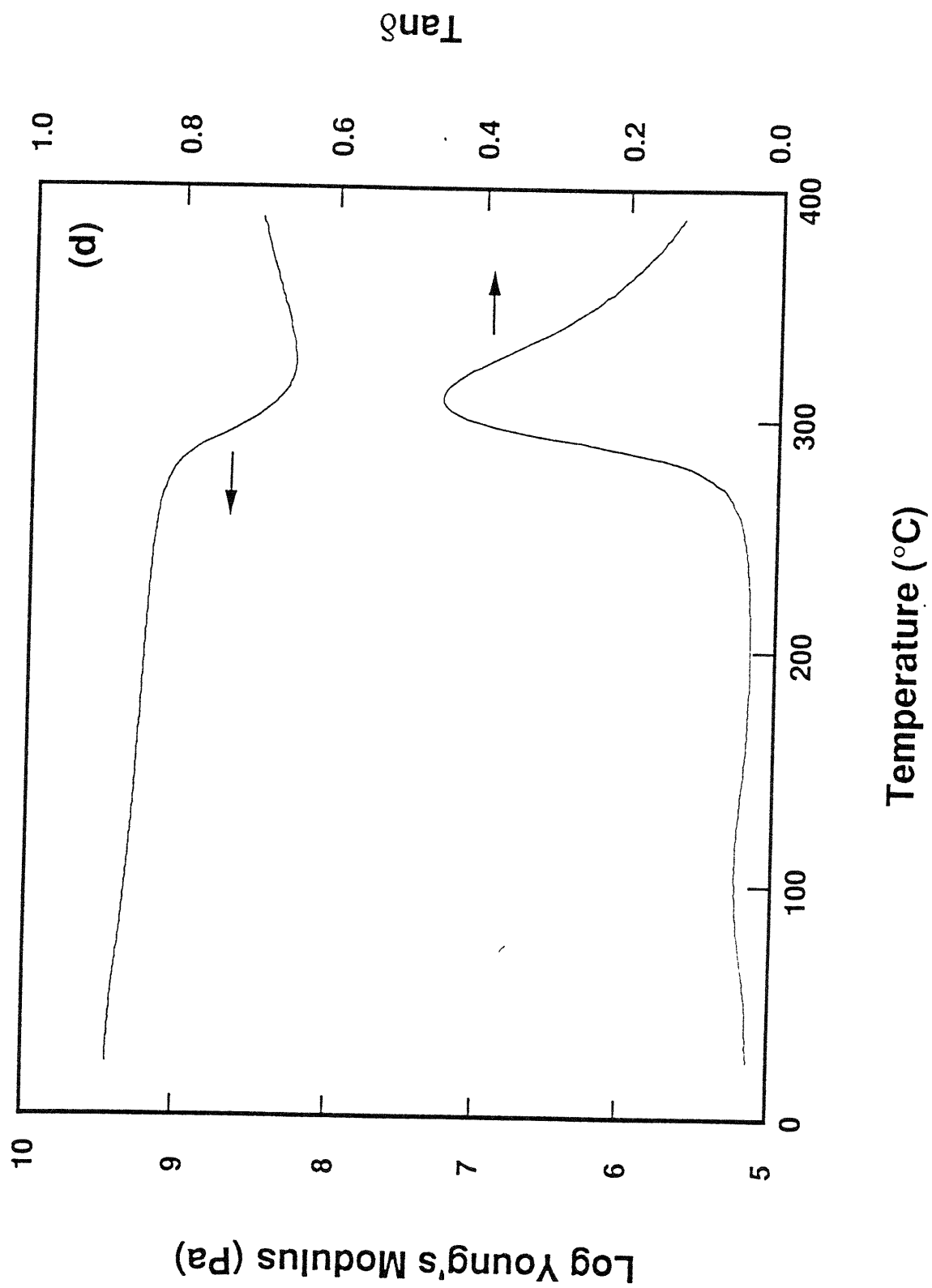


Figure 4.4. continued. d.) nitrogen.

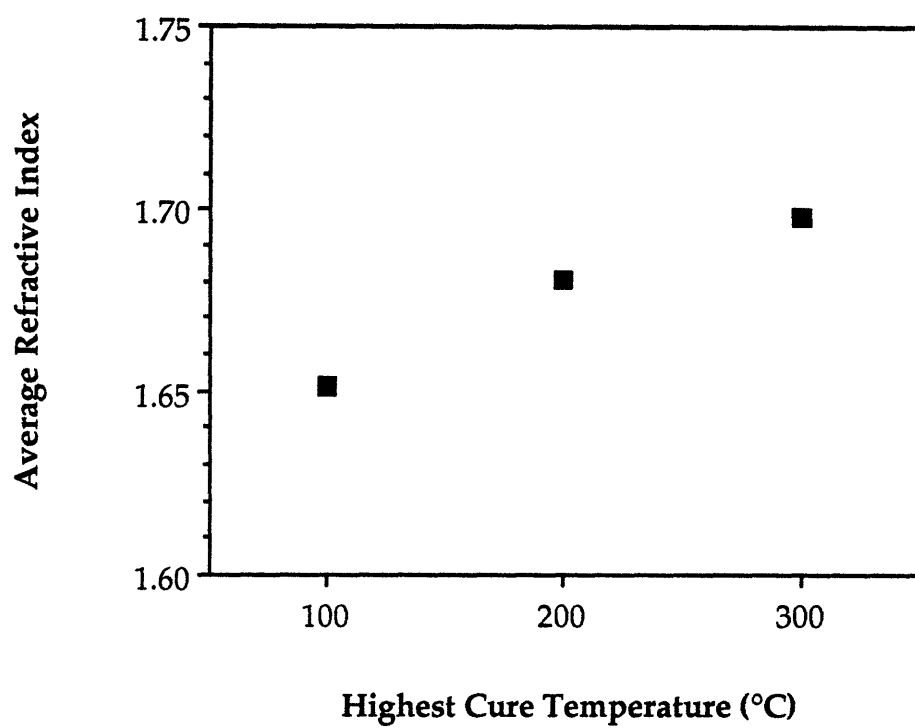
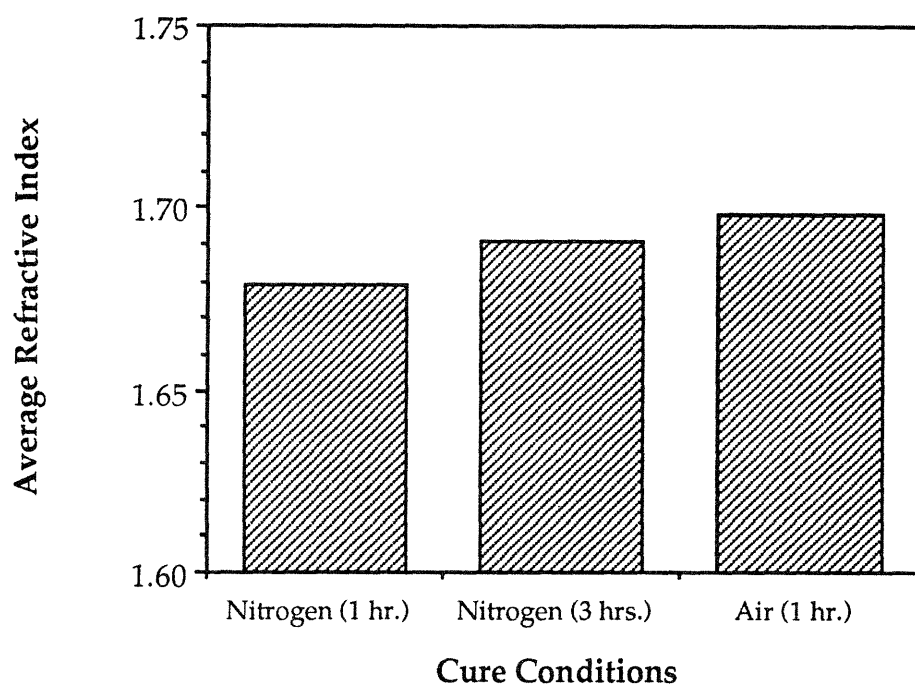


Figure 4.5. a.) Indices of refraction of spin coated Probimide[®] 32 films vs. highest cure temperature in air. Cure cycle was 15 minutes at 100°C, 1 hour at 200°C, 1 hour at 300°C.



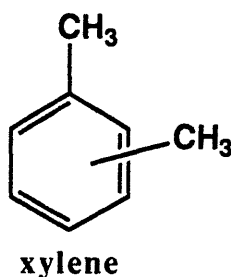
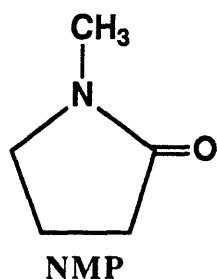
b.) Refractive indices for different cure conditions at 300°C.

4.3.5. Fourier Transform Infrared Spectroscopy

Fourier transform infrared spectroscopy is a powerful method of examining the progress of a polyimide cure. This is especially true in polyamic acid precursor materials, which undergo significant changes in their infrared spectra as they are converted to polyimides. Our fully preconverted polyamide-imide, on the other hand, gives us an interesting opportunity to observe the effects of solvent removal and oxidative crosslinking in the absence of the amic acid to imide conversion. We demonstrate here how the FTIR spectrum of Probimide[®] 32 evolves during curing. The study below suggests a technique for monitoring the cure in fully converted polyimide and related systems.

Solvent Spectra

N-methylpyrrolidone (NMP) and xylene are the two solvents used in the Probimide[®] 32 system. Their chemical structures are shown below:



FTIR spectra of these compounds can be found in most infrared spectra atlases [18]. The main IR absorption regions and our peak assignments are shown in Table 4.2.

The three chemicals in the Probimide[®] 32 system, the polyamide-imide polymer, NMP, and xylene have a number of chemical units in common. For example, both the polyamide-imide and NMP contain an amide unit, the polymer a secondary amide, and the NMP a tertiary amide. The carbonyl bond of the amide group in both molecules contributes an extremely strong infrared absorption band at about 1680 cm^{-1} . Also, the xylene and the polyamide-imide contain aromatic bonds, which have a number of IR absorption bands, which are listed in Table 4.2. One key spectral peak, due to carbon-carbon skeletal stretching of the aromatic ring, appears at around 1500 cm^{-1} . There can be multiple bands in this region at slightly different absorption frequencies depending upon the ring substituents. In addition, all three substances have carbon-hydrogen bonds. These bonds typically have broad absorption in the locality of 3000 cm^{-1} .

Table 4.2. IR absorption regions of NMP and xylene.

Compound	Peak Location or Approx. Region (cm ⁻¹)	Tentative Assignment [†]	Peak Strength*
NMP	2800-3000	v(C - H)	s
	1680	v(C = O)	s
	1380-1500	δ(C - H), δ(N-CH ₃)	s
	1300	v(C-N)	s
	1110	v(C - N)	m
	980	β(ring)	m
xylene	2900-3100	v(C - H)	s
	1380-1650	v(C = C)	s
	1000-1050	aryl δ(C - H)	m
	790, 760, 740, 690	δ ring substitution bands	s

[†] see references 18,19

* s = strong, m = medium, w = weak

Probimide 32 Spectra

Fourier transform infrared spectroscopy of spin coated thin films of Probimide[®] 32 on KBr, shown in Figures 4.6-4.9, revealed two processes that take place in the system upon curing. The first process is the systematic removal of solvent. The second is crosslinking and degradation at 300°C in air. Assignments of the main absorbance bands [18,19] in the polyamide-imide polymer are shown in Table 4.3.

The presence and removal of residual solvent is apparent in the “finger print” region of the FTIR scans. Figure 4.6(a-f) shows the 400-2000 cm^{-1} region of Probimide[®] 32 samples treated for 10 minutes at 20°C intervals between 100°C and 200°C. As the sample is cured from 100°C to 200°C (Figure 4.6(a-f)), a number of peaks decline or disappear. These changes are consistent with removal of solvent. The most important peak is associated with the amide carbonyl bond, which is present in both the polyamide-imide and the NMP solvent. The tertiary amide in the NMP and the secondary amide in the polyamide-imide both absorb at about 1680 cm^{-1} . This strong absorption peak gradually declines in Figure 4.6 as NMP is removed from the polymer by treating it to progressively higher temperatures.

Observation of the strong reflection at 1510 cm^{-1} due to aromatic skeletal stretching also proves quite interesting. As the polymer is treated to higher temperatures, an overlapping side peak systematically recedes. The best explanation for this occurrence is that NMP or xylene, either of which could contribute to this side peak, is systematically removed. When the solvent is eliminated, a shoulder to the peak at 1510 cm^{-1} remains, reflecting the fact that there are two differing aromatic substitution environments in the polyamide-imide.

As the polymer is cured, we also observe the gradual disappearance of a shoulder peak near 1300 cm^{-1} , decline of a peak at around 1110 cm^{-1} , and disappearance of a small peak at about 980 cm^{-1} . All three of these changes are consistent with the gradual removal of NMP from the system.

We also see an increase in the band 1770 cm^{-1} associated with in-phase stretching of the imide ring carbonyl. However, there is no obvious explanation for this.

The 2000-4000 cm^{-1} region is shown in Figure 4.7. Two marked changes are observed. First, there is decline in absorption in a broad range around 3000 cm^{-1} . This indicates a decrease hydrocarbon bonds, and thus, is consistent with the removal of solvent. Second, there is gradual shifting of the N-H amide peak from about 3300 cm^{-1} to almost 3400 cm^{-1} . It is typical for the location of this band in amide compounds to exist at

Table 4.3. Partial list of IR absorbance bands in Probimide[®] 32 polyamide-imide.

Peak Location or Approx. Region (cm ⁻¹)	Tentative Assignment [†]	Peak Strength*
3100-3400 (broad)	v(N-H)	w
3000-3100 (broad)	v(C-H)	w
1770	v(C=O) (imide)	m
1720	v(C=O) (imide)	s
1680	v(C=O) (amide)	s-m
1600	v(C=C) (phenyl)	m
1510	v(C=C) (phenyl)	s
1410	v(C=C) (phenyl)	m
1380	v(N-C) (imide)	s
1320	v(N-C) (amide)	m
720	δ phenyl substitution	m

[†] see references 18,19

* s = strong, m = medium, w = weak

a lower wavenumber in the solid state than in the solution state as a result of increased hydrogen bonding [19]. A shift to a higher wavenumber as solvent is removed suggests that the polymer forms stronger hydrogen bonds with the NMP than it does with itself.

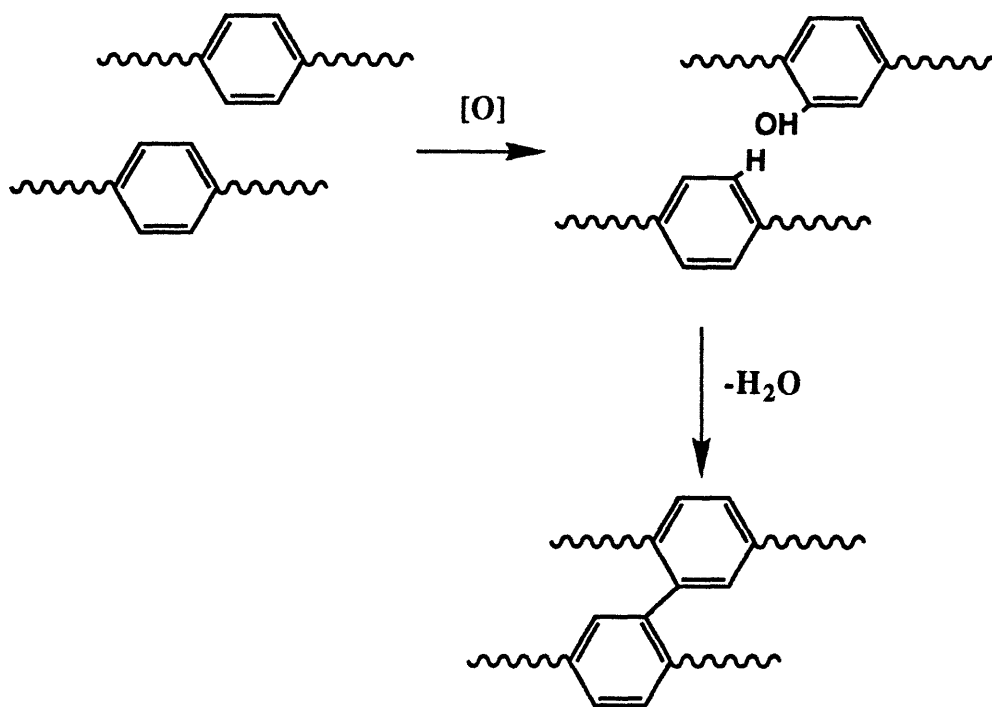
In Figure 4.8(a-d), 400-2000 cm^{-1} FTIR scans region of Probimide[®] 32 treated at 100°C, 200°C, and 300°C in air, and 300°C in nitrogen, respectively, are shown. The effects of solvent removal described above are clearly seen in these scans as the films are treated above 100°C. Also, we note that the peak at 1770 cm^{-1} corresponding to in-phase stretching of the imide carbonyl increases as the polymer is heated from 100°C to 200°C, but returns to its original height after treating at 300°C in either air or nitrogen. Again, there does not seem to be an obvious explanation for this.

The 2000-4000 cm^{-1} region is shown in Figure 4.9. Reduced absorption near 3000 cm^{-1} , as well as shifting of the N-H peak from 3300 to 3400 cm^{-1} , both a result of solvent removal, are again apparent as the material is treated above the softbake temperature.

Previously, we showed that a 300°C treatment in air initiated substantial chain crosslinking, while the same thermal treatment in nitrogen did not. There are noticeable differences the FTIR spectra of Probimide 32 films treated at 300°C in air, Figures 4.8(c) and 4.9(c), and at 300°C in nitrogen, Figures 4.8(d) and 4.9(d). These changes suggest possible mechanisms for the oxidative crosslinking reaction. The most apparent difference is a reduction in the air-treated sample in C=C phenyl stretching near 1510 cm^{-1} . This is accompanied by a drop in C-H stretching near 3000 cm^{-1} . In fact, two distinct hydrocarbon peaks near 2900 cm^{-1} are nearly eliminated. The amide C=O peak at 1680 cm^{-1} appears to become nearly a shoulder of the imide C=O peak at 1720 cm^{-1} . Also, there is an increase in the C=C phenyl vibration at 1600 cm^{-1} .

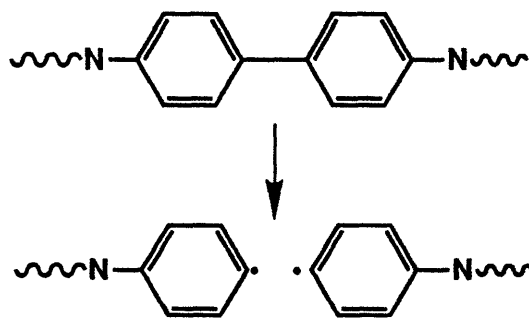
Kuroda and Mita [20] also observed a large drop in the 1510 cm^{-1} phenyl vibration, accompanied by an increase in the 1600 cm^{-1} phenyl vibration, in their studies of thermo-oxidative degradation of a polyimide. They interpreted the decline in the 1510 cm^{-1} peak as the cleavage of $\phi\text{-CH}_2$ bonds. The authors speculate that the increase in the vibration at 1600 cm^{-1} might be associated with the formation of diphenyl crosslinks, as suggested by Dine-Hart *et al.* [21,22], though Kuroda and Mita [20] do not suggest this to be a primary path of crosslinking in their material.

Dine-Hart *et al.* [21,22], in their investigations of the oxidative curing of PMDA-ODA polyimide, concluded that the main crosslinking reaction appeared to be the intermolecular coupling of phenyl rings in the diamine segments of the main chains. This occurred by the formation of phenolic groups which subsequently react. The phenolic bonds were formed either by direct dehydrogenation of the phenyl rings, as shown in Scheme I, or by scissioning of aryl-ether bonds.



Scheme I

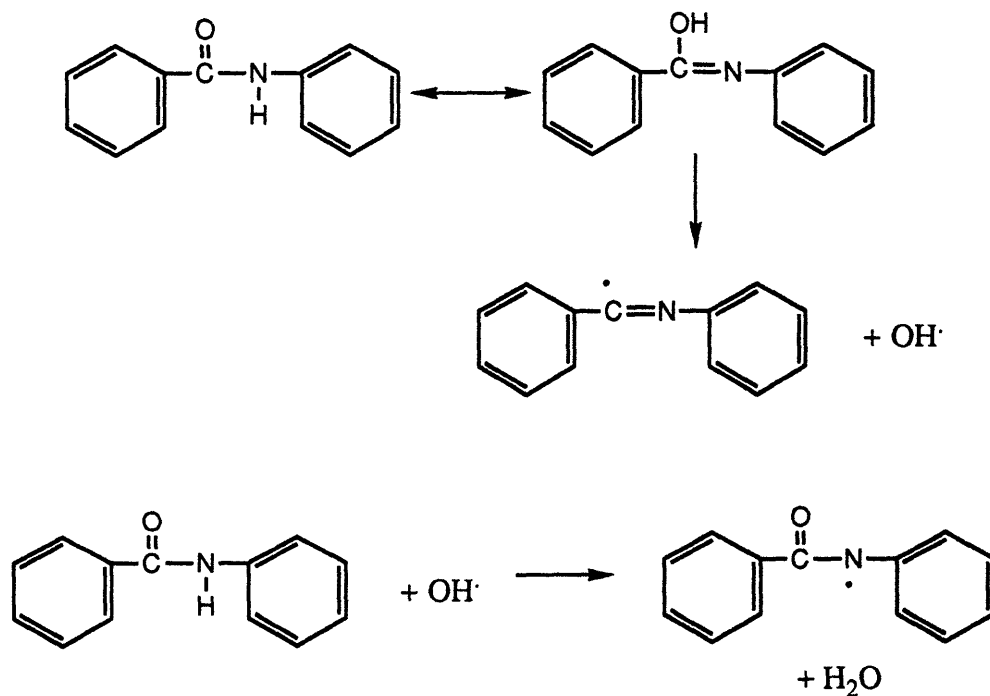
The reduction in the 1510 cm^{-1} phenyl vibration, increase in the 1600 cm^{-1} phenyl vibration, and reduction in C-H stretching near 3000 cm^{-1} in the Probimide 32 polyamide-imide might be associated with the formation of the crosslinks shown in Scheme I. The diphenyl crosslinks must occur in the diamine portion of the polyamide-imide repeat unit, as the 1510 cm^{-1} vibration is associated with 1,4- C_6H_4 groups [23], while the 1600 cm^{-1} band can be attributed to more highly substituted phenyl groups [23]. The inter-chain crosslinks in Scheme I might occur in the conjunction with the intra-chain breakage of 1,4-phenyl-phenyl bonds in the diamine, as shown in Scheme II. The radicals in Scheme II may subsequently produce random bond reformations.



Scheme II

Broadbelt *et al.* [24] reviews the various reactions that may occur on the amide linkage of an aromatic amide model compound as the substance undergoes elevated temperature treatments. A reaction mechanism that would be consistent with an increase in molecular weight would be a [1,3] sigmatropic shift (see Scheme III) followed by random radical recombination reactions. It is also likely that many of the other reactions could simultaneously take place, including various bond homolyses of the amide bond followed by random radical recombinations which do not result in a net increase in molecular weight.

If the sigmatropic shift and random crosslinking at the amide bond were to occur in the polyamide-imide during its 300°C treatment in air, we would expect to see decreases in amide C=O stretching at 1680 cm⁻¹ and in N-H stretching in the 3100-3400 cm⁻¹ region. These changes appear to have occurred in the FTIR spectra for the 300°C air treatment in Figures 4.8(c) and 4.9(c)).



Scheme III

The above data suggest that cure can be monitored in the polyamide-imide system by FTIR. This could be an especially valuable tool if, for example, a new processing scheme and cure cycle were to be tested for solvent removal effectiveness. The most apparent change in the FTIR spectrum as solvent is eliminated is the decline of the amide carbonyl peak at 1680 cm⁻¹. In Figure 4.10, the peak height at 1680 cm⁻¹ relative to that at 1370 cm⁻¹ is plotted against highest cure temperature for FTIR data shown in Figures 4.6

and 4.8. The ratio declines steadily with increasing cure temperature. Because the spin coated films are thin, we expect the films to be nearly free of solvent after the one hour cure at 200°C. The drop in peak height after the 300°C cure could be due to either further removal of high boiling point solvent species or to non-oxidative crosslinking at the amide carbonyl. The films appear to be solvent free when the relative absorption ratio is about 0.6-0.7.

4.3.6. Differential Scanning Calorimetry

The calorimetric relaxation response of Probimide[®] 32 was studied as a function of cure temperature and environment in order to gain further insight into the processes that take place during curing. DSC scans of Probimide[®] 32 bulk films treated at 100°C, 200°C, and 300°C (air and nitrogen) are shown in Figure 4.11(a-d), respectively. Several physical phenomena can be observed in these scans: the vaporization of water, the vaporization of solvent, and transition from the glassy to rubbery state.

Vaporization of water contained by the polymer, also observed in the TGA scans in Figures 4.2 and 4.3, is seen in all DSC scans in Figure 4.11. It appears as a broad endothermic response near 100°C.

Vaporization of residual solvent is observed in the 100°C treated sample, Figure 4.10(a), as indicated by the large endothermic response seen in the scan between 150°C and 300°C. It is possible that the spikes observed are a consequence of instrument noise caused by the violent vaporization occurring in the encapsulated sample. Any glass transitions that might have occurred in the 100°C treated sample are hidden by the strong vaporization response. Solvent vaporization is not clearly indicated in any other sample.

In the 200°C treated sample, Figure 4.11(b), a glass transition is seen at about 200°C, as indicated by the step increase in heat capacity. A weak response at about 300°C is also seen. These data are in good agreement with the DMA results shown in Figure 4(b).

In both the 300°C air-cured and nitrogen-cured samples, glass transitions are seen at 300°C. The transition in the air-treated sample, Figure 4.11(c), is broader and slightly shifted to a higher temperature, as compared to the transition in the nitrogen-treated film, Figure 4.11(d). This is consistent with the DMA scans shown in Figure 4.4(c,d). However, in the DSC scans, a weak step in the heat capacity is seen at about 330°C, where no comparable change in mechanical modulus was observed in the DMA data.

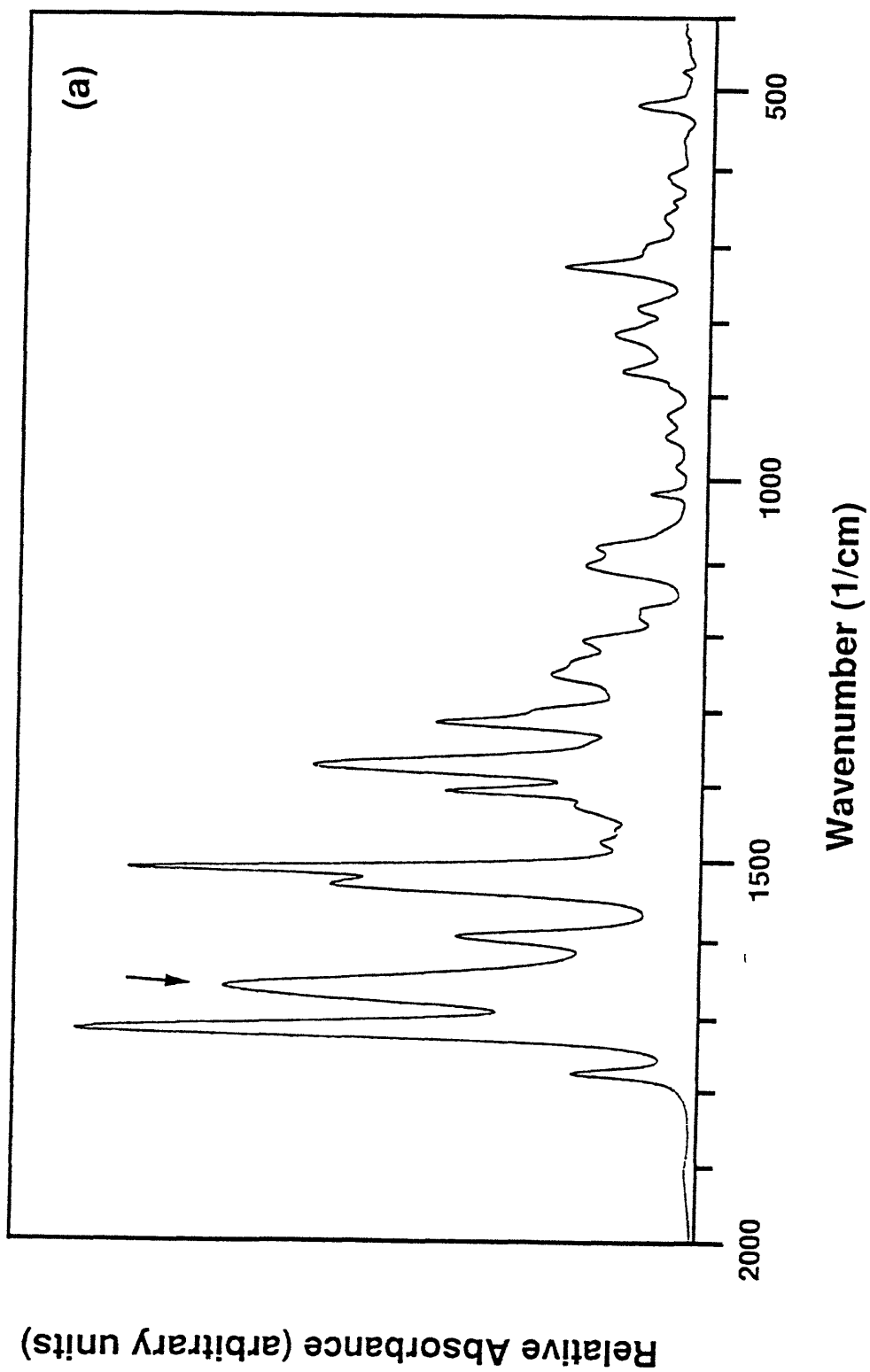


Figure 4.6. Relative absorbance vs. wavenumber ($400\text{-}2000\text{ cm}^{-1}$) for spin coated Probimide[®] 32 films. Arrow points to 1680 cm^{-1} carbonyl peak: a.) 10 minutes at 100°C ,

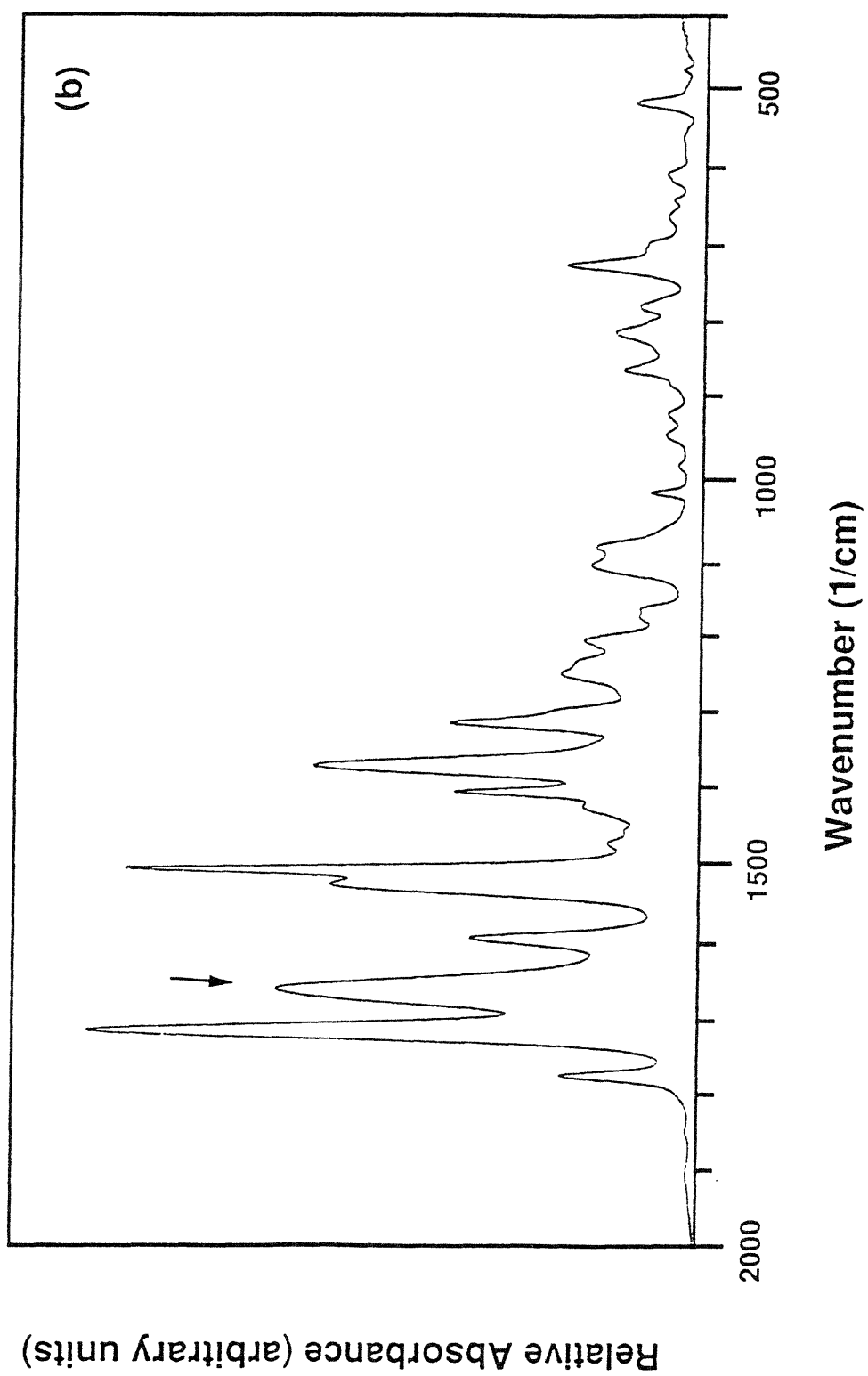


Figure 4.6. continued. b.) then 10 minutes at 120°C,

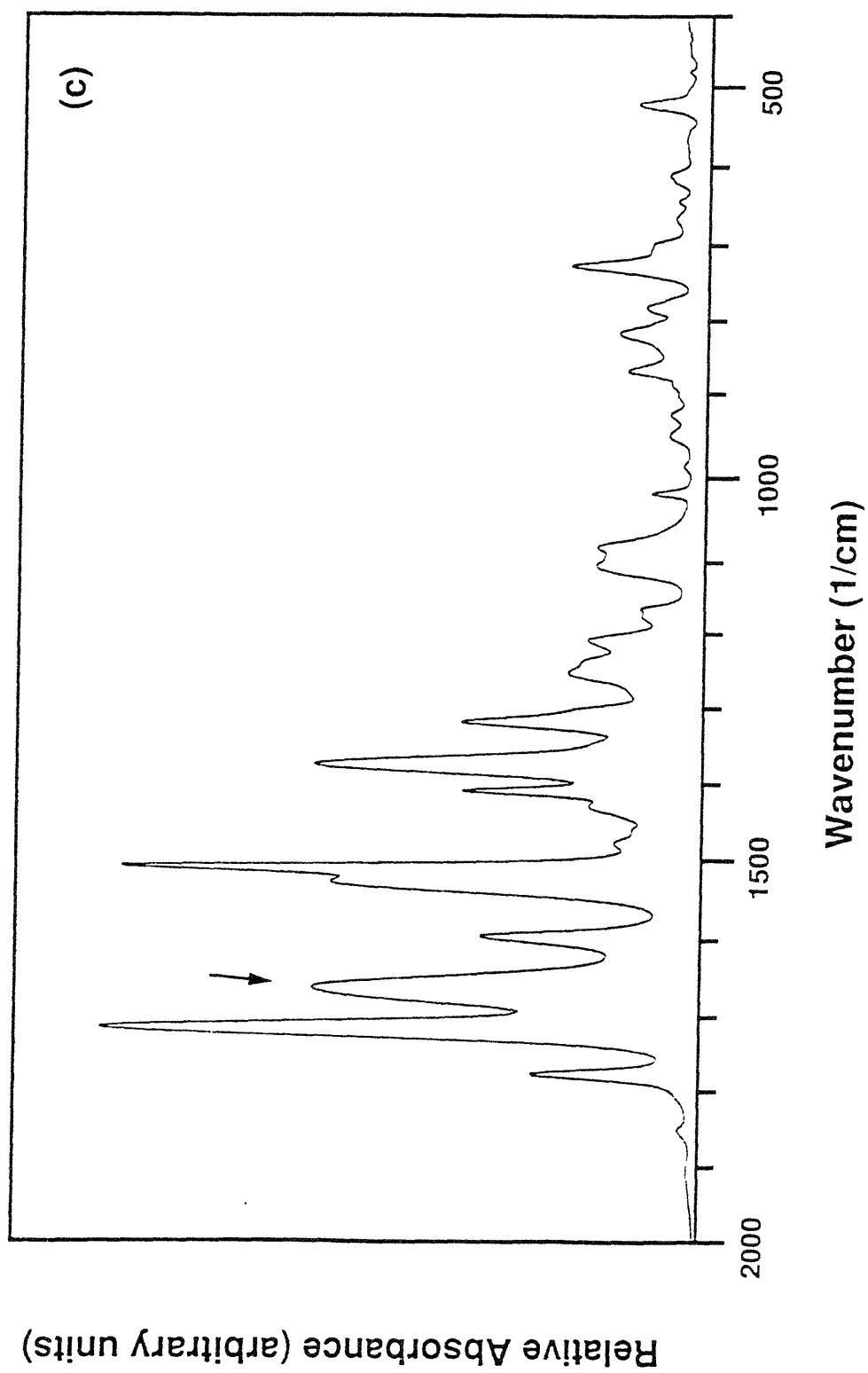


Figure 4.6. continued. c.) then 10 minutes at 140°C,

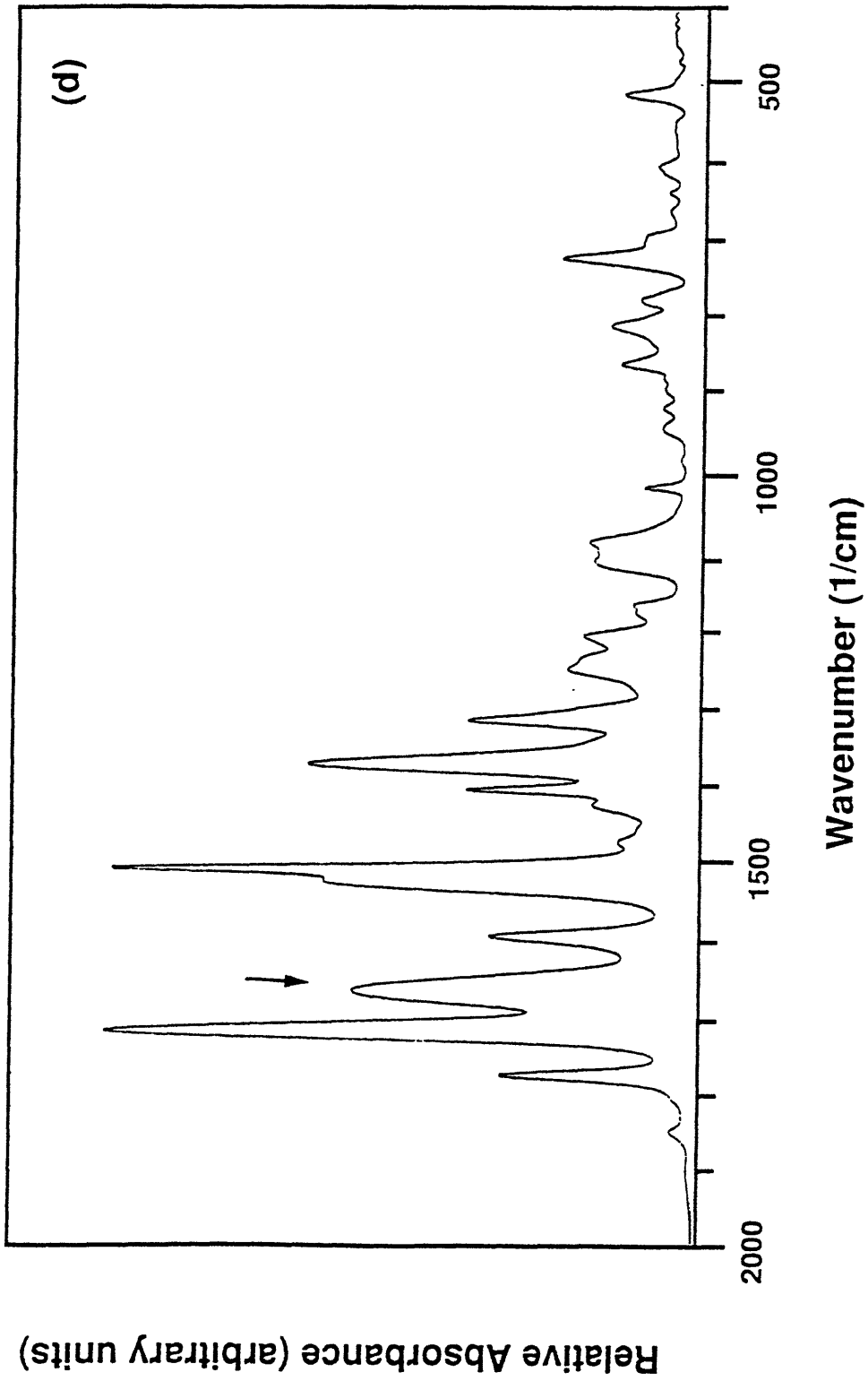


Figure 4.6. continued. d.) then 10 minutes at 160°C,

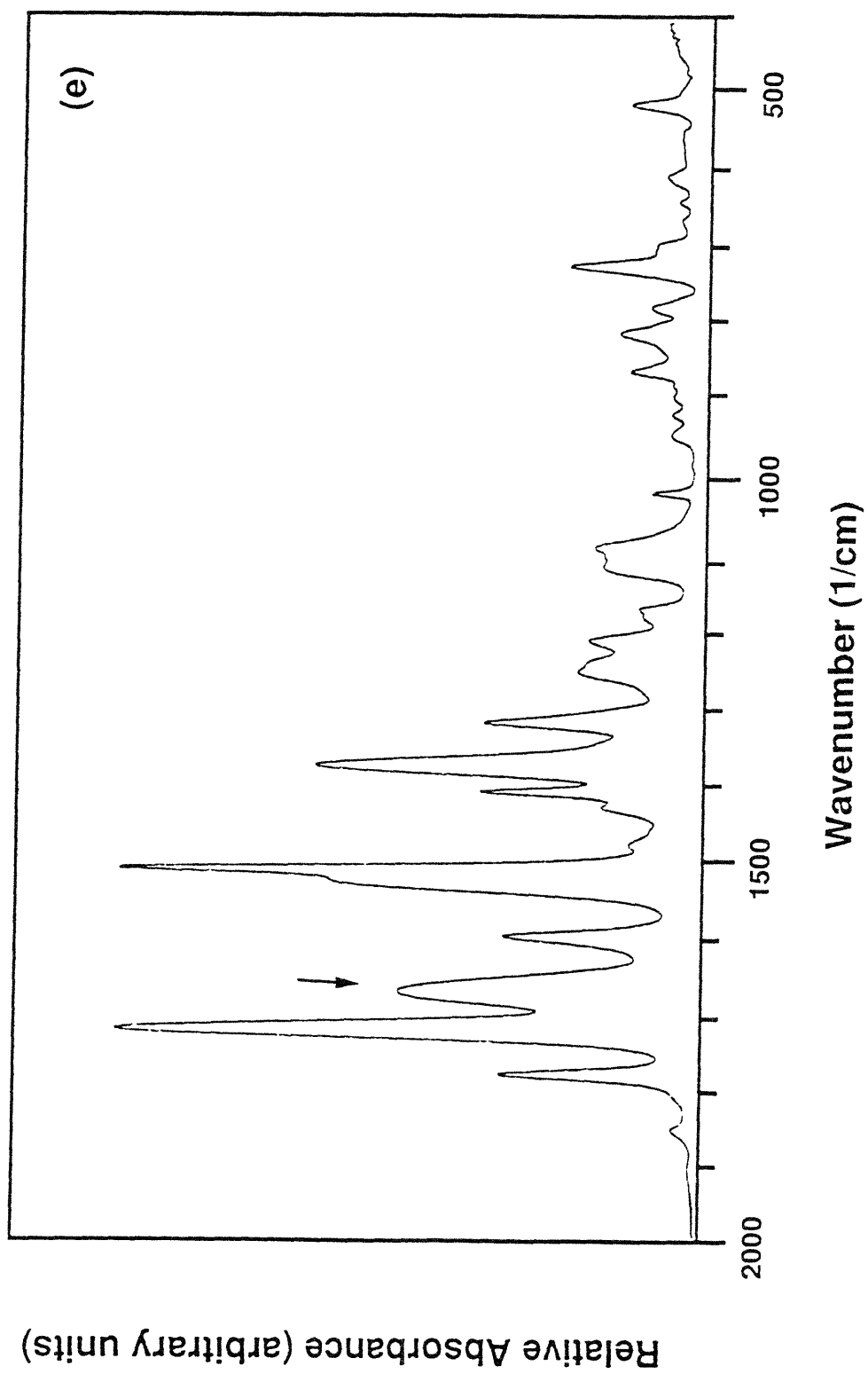


Figure 4.6. continued. e.) then 10 minutes at 180°C,

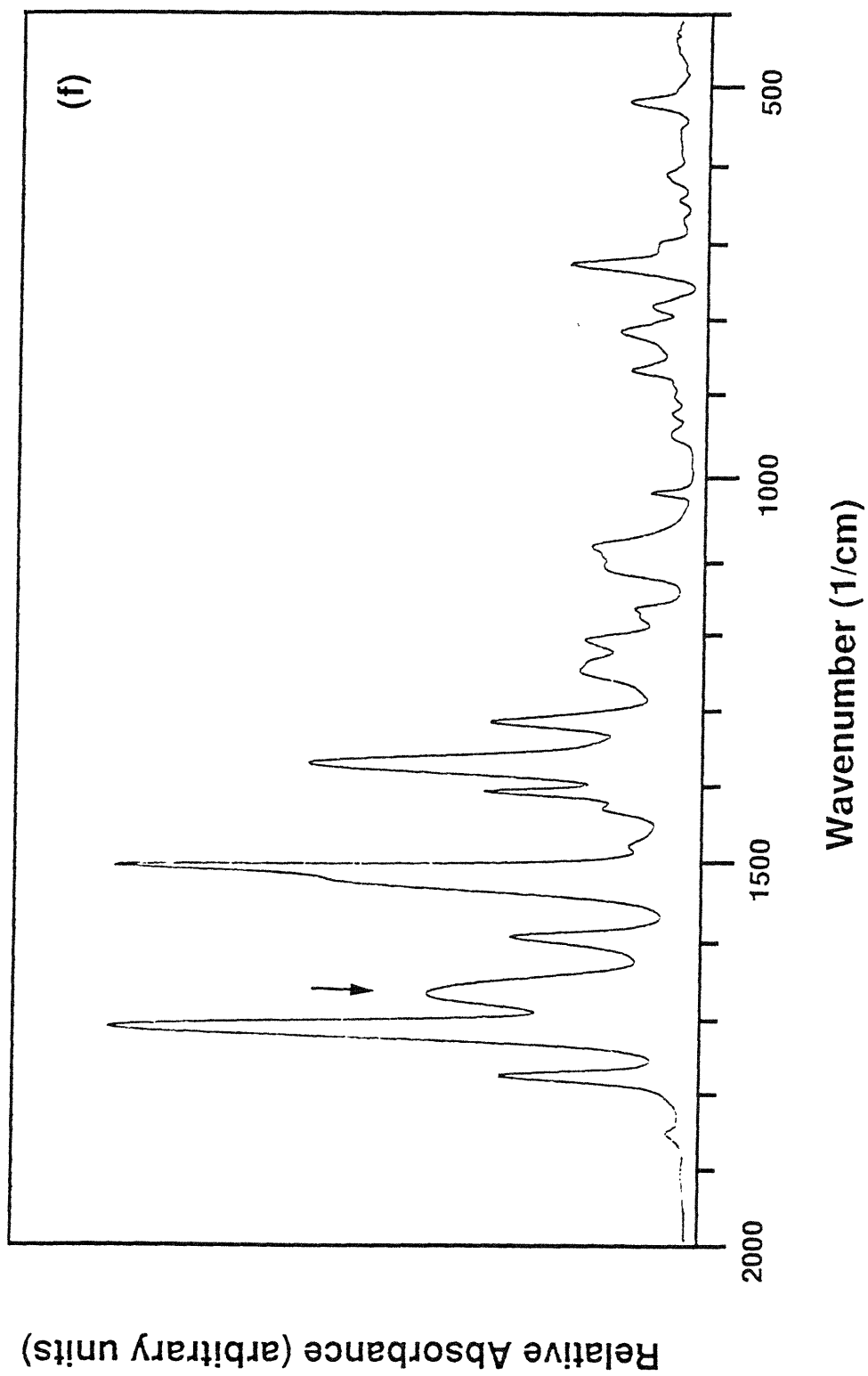


Figure 4.6. continued. f.) then 10 minutes at 200°C.

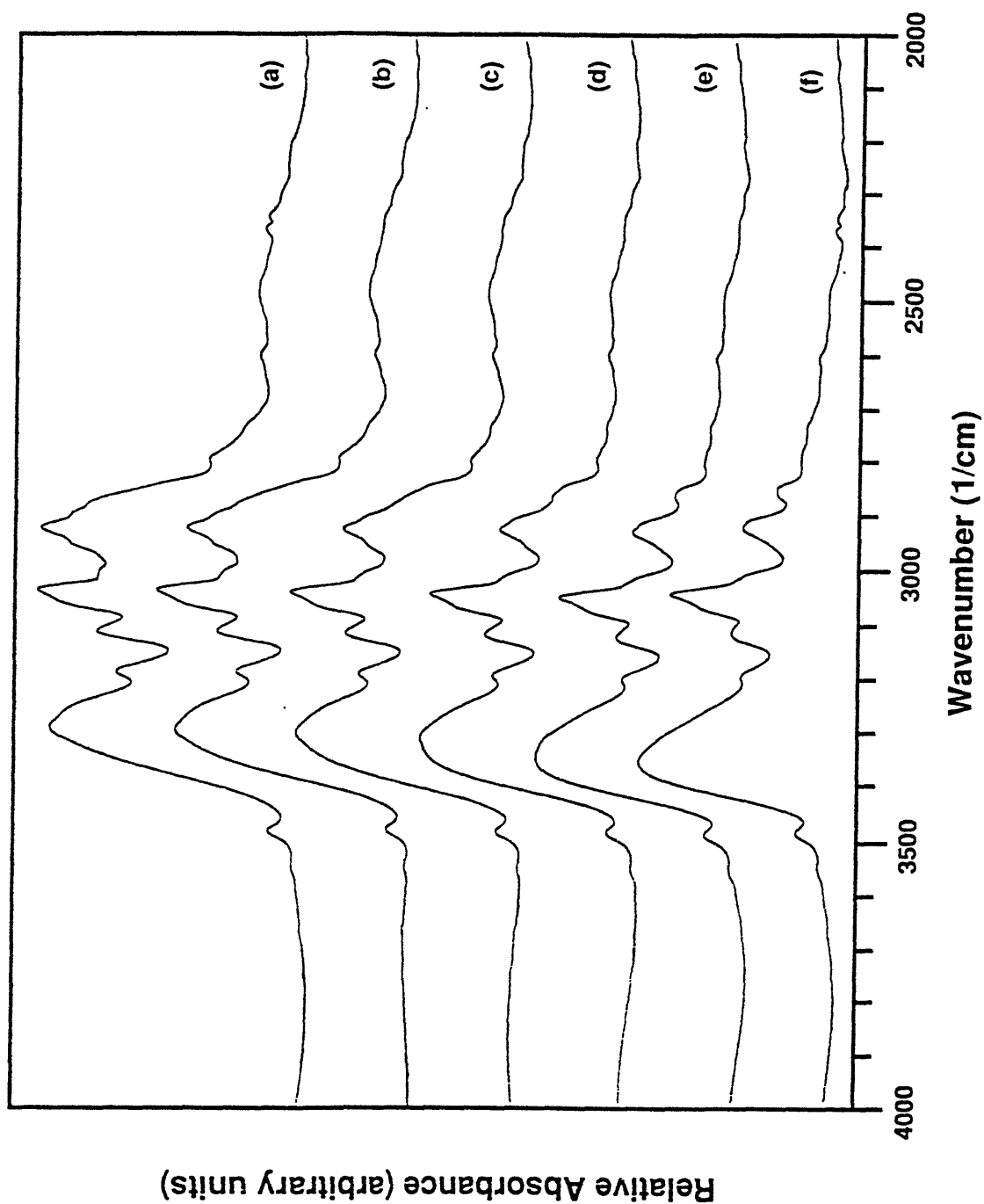


Figure 4.7. Relative absorbance vs. wavenumber ($2000\text{-}4000\text{ cm}^{-1}$) for spin coated Probimide[®] 32 films: a.) baked 10 minutes at 100°C , b.) then 10 minutes at 120°C , c.) then 10 minutes at 140°C , d.) then 10 minutes at 160°C , e.) then 10 minutes at 180°C , f.) then 10 minutes at 200°C .

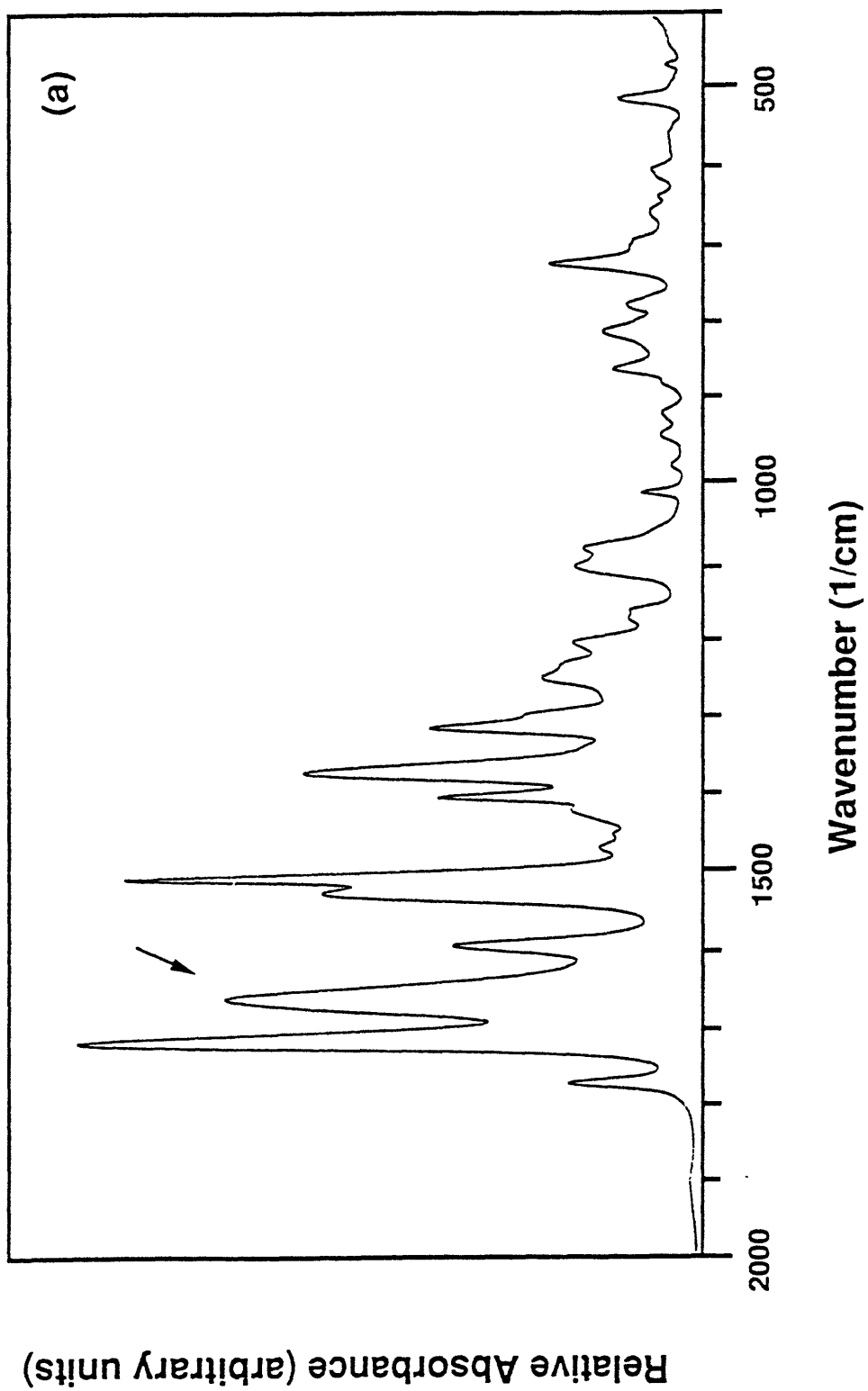


Figure 4.8. Relative absorbance vs. wavenumber ($400\text{-}2000\text{ cm}^{-1}$) for spin coated Probimide[®] 32 films: a.) 15 minutes at 100°C (arrow points to 1680 cm^{-1} carbonyl peak),

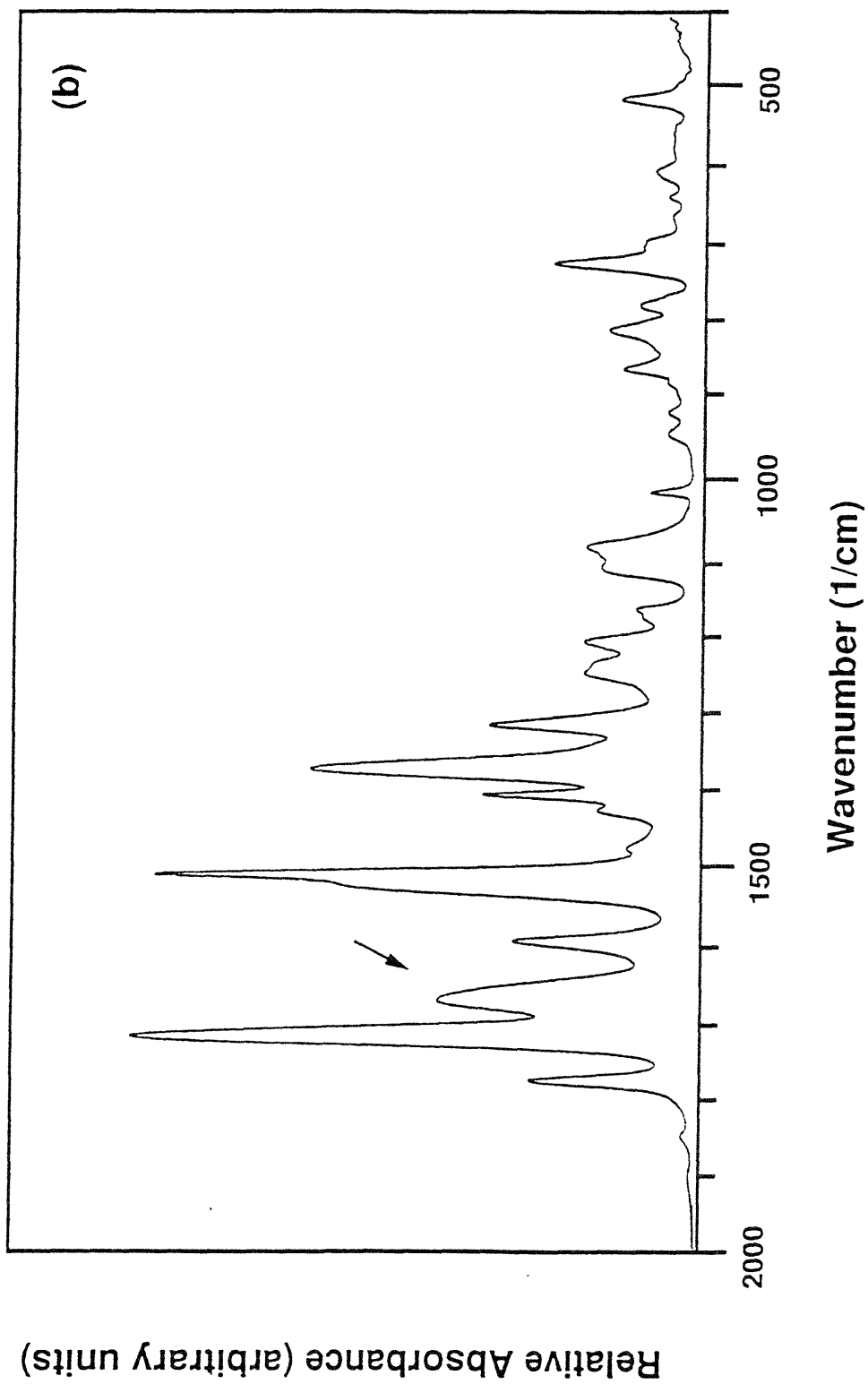


Figure 4.8. continued. b.) then 1 hour at 200°C (arrow points to 1680 cm^{-1} carbonyl peak),

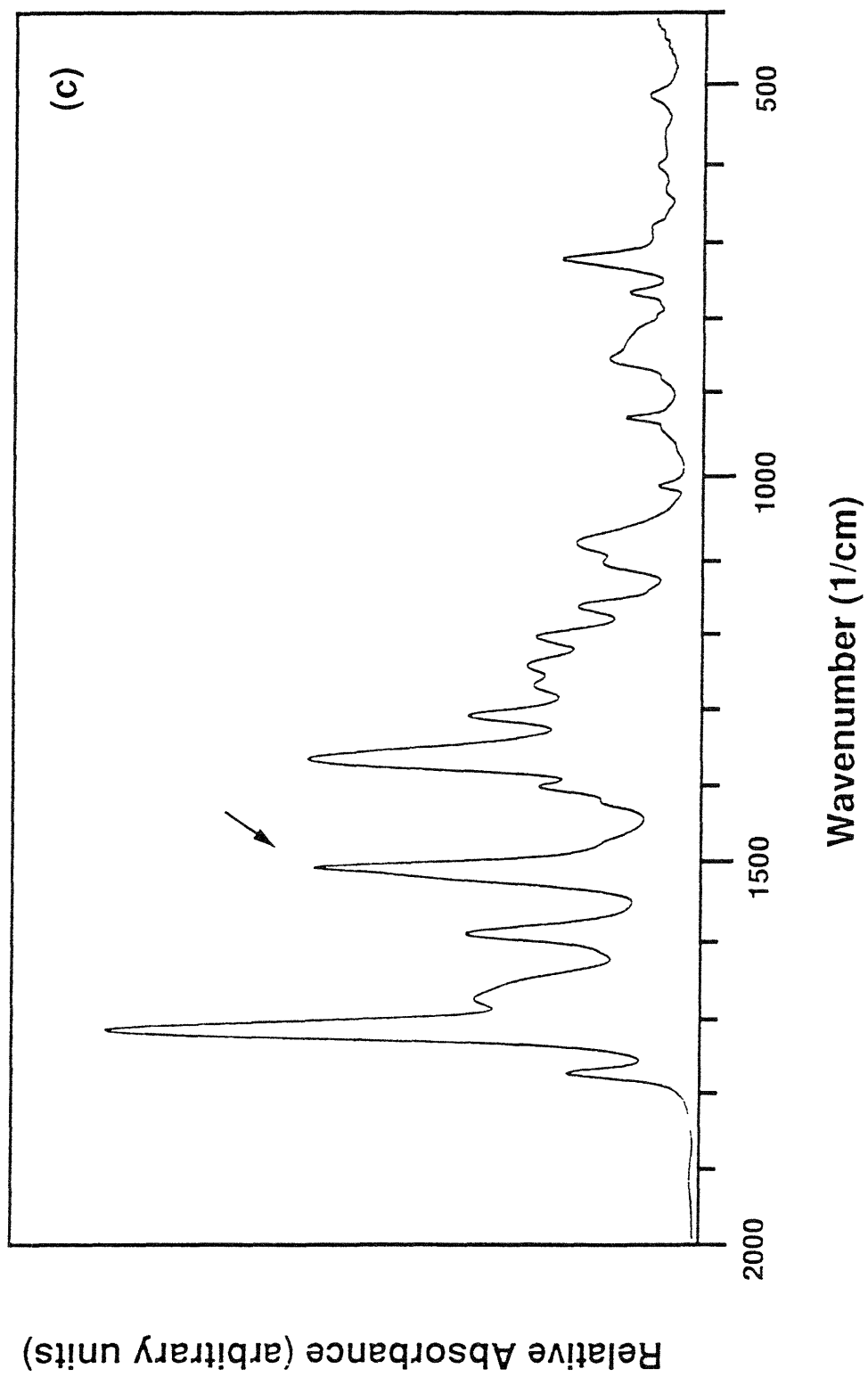


Figure 4.8. continued. c.) then 1 hour at 300°C in either air or (arrow points to 1510 cm^{-1} C=C peak),

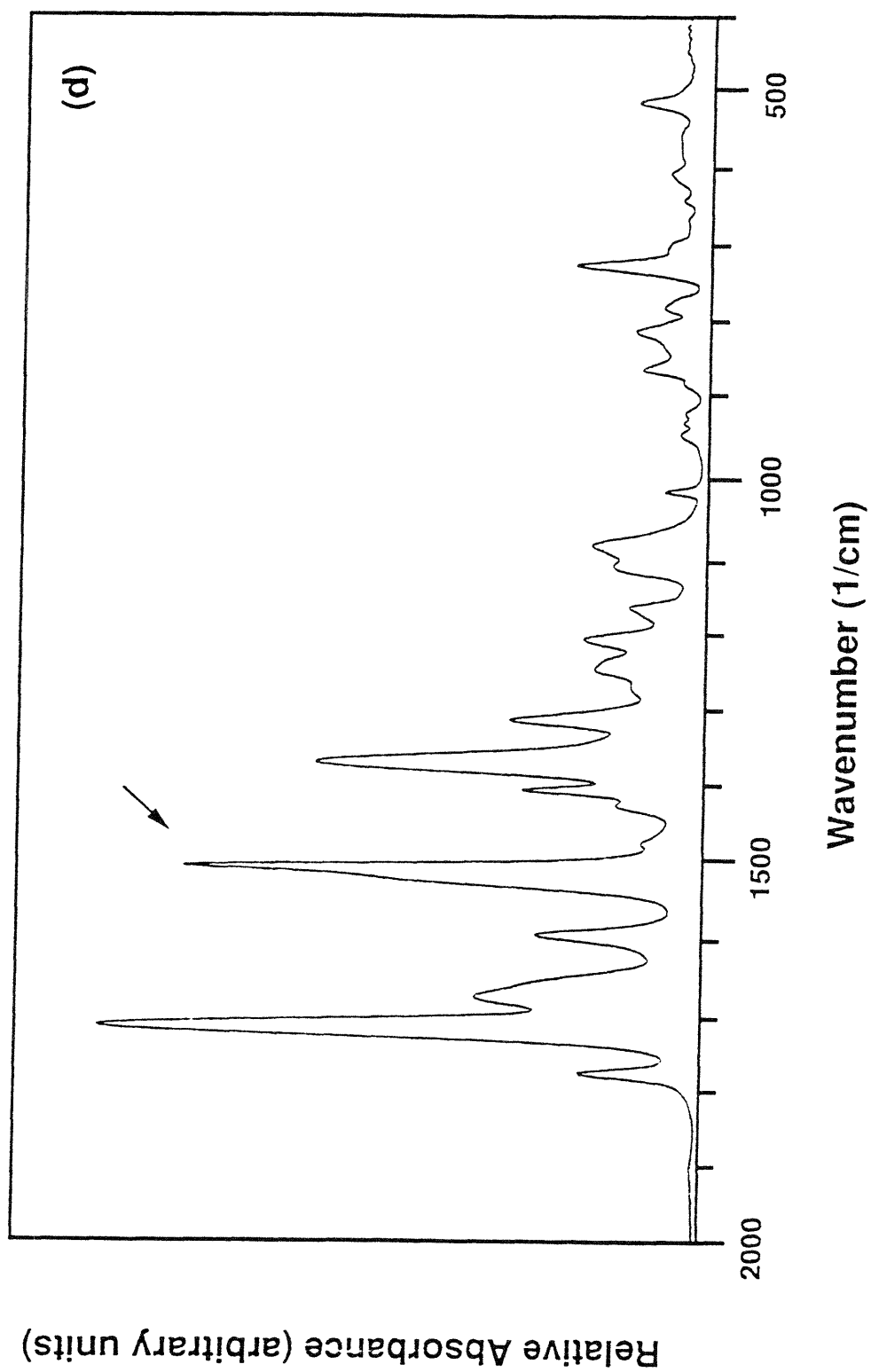


Figure 4.8. continued. d.) nitrogen (arrow points to 1510 cm^{-1} C=C peak),

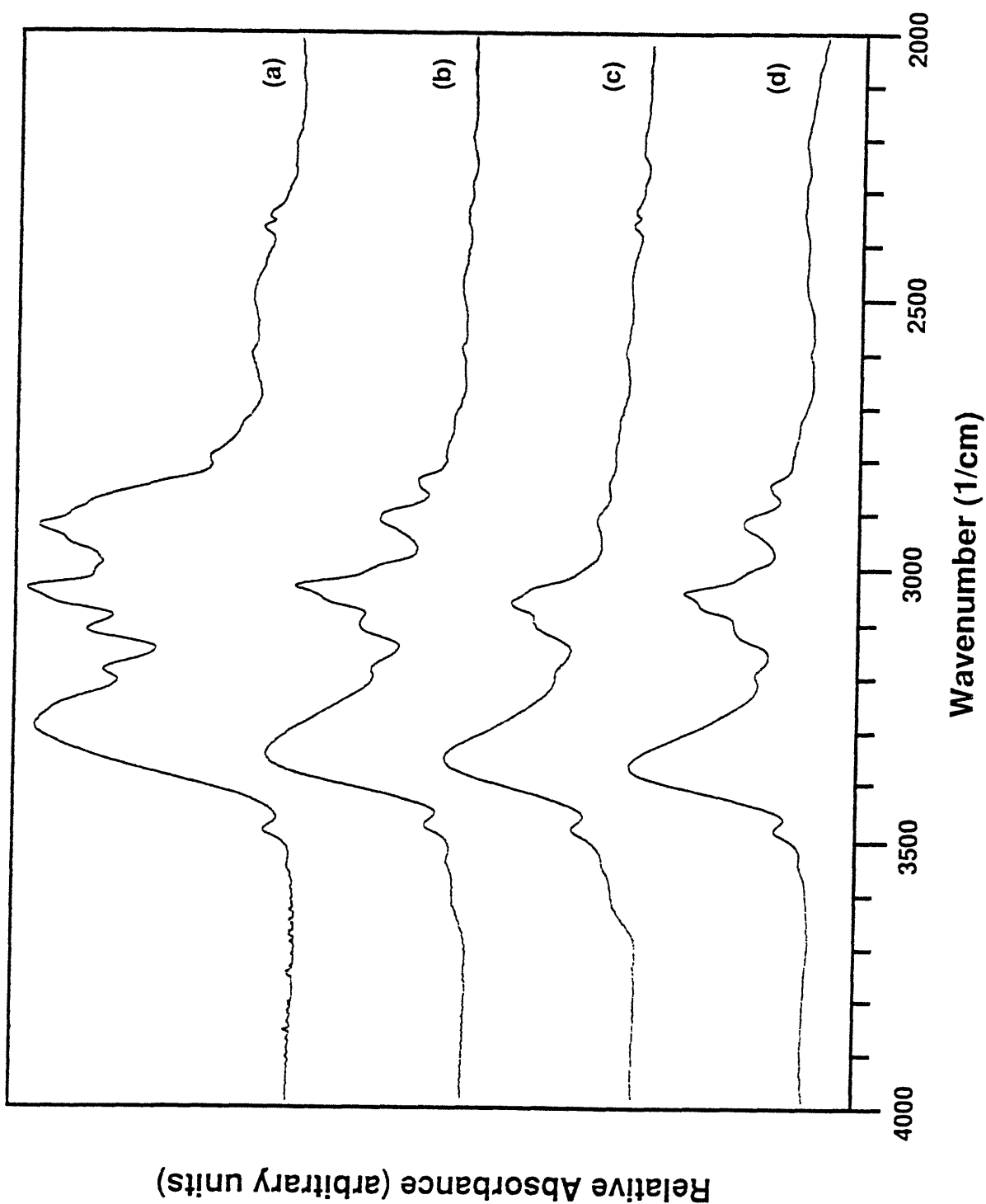


Figure 4.9. Relative absorbance vs. wavenumber ($2000\text{-}4000\text{ cm}^{-1}$) for spin coated Probimide[®] 32 films: a.) baked 15 minutes at 100°C , b.) then 1 hour at 200°C , c.) then 1 hour at 300°C in either air or, d.) nitrogen.

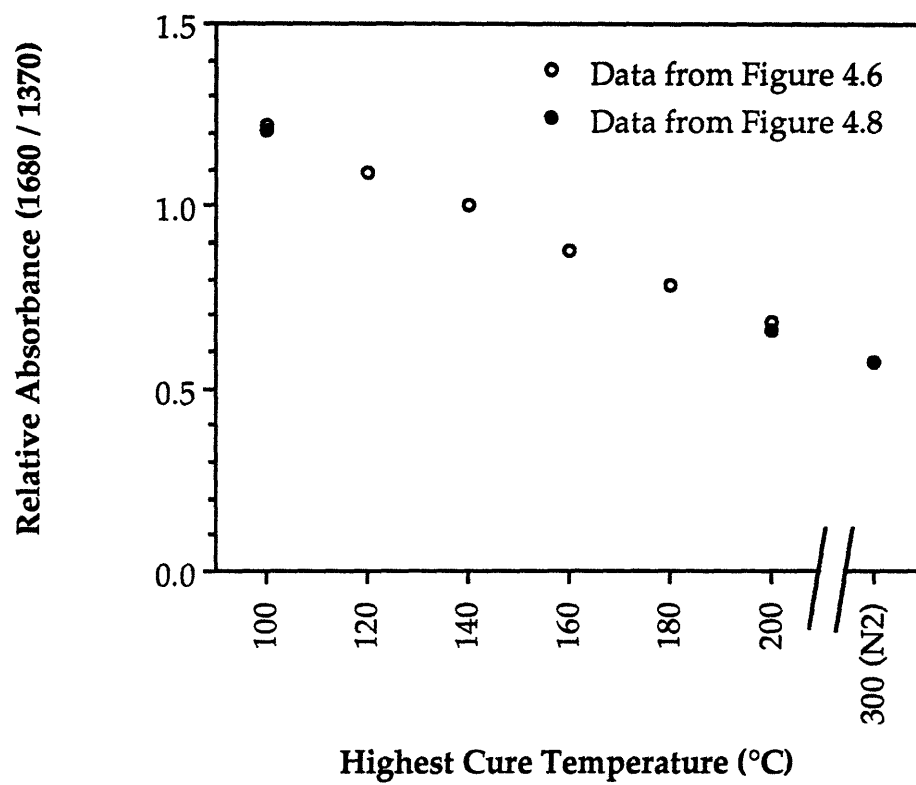


Figure 4.10. Ratio of relative absorbance of peak at 1680 cm^{-1} to that of the 1370 cm^{-1} vs. highest cure temperature.

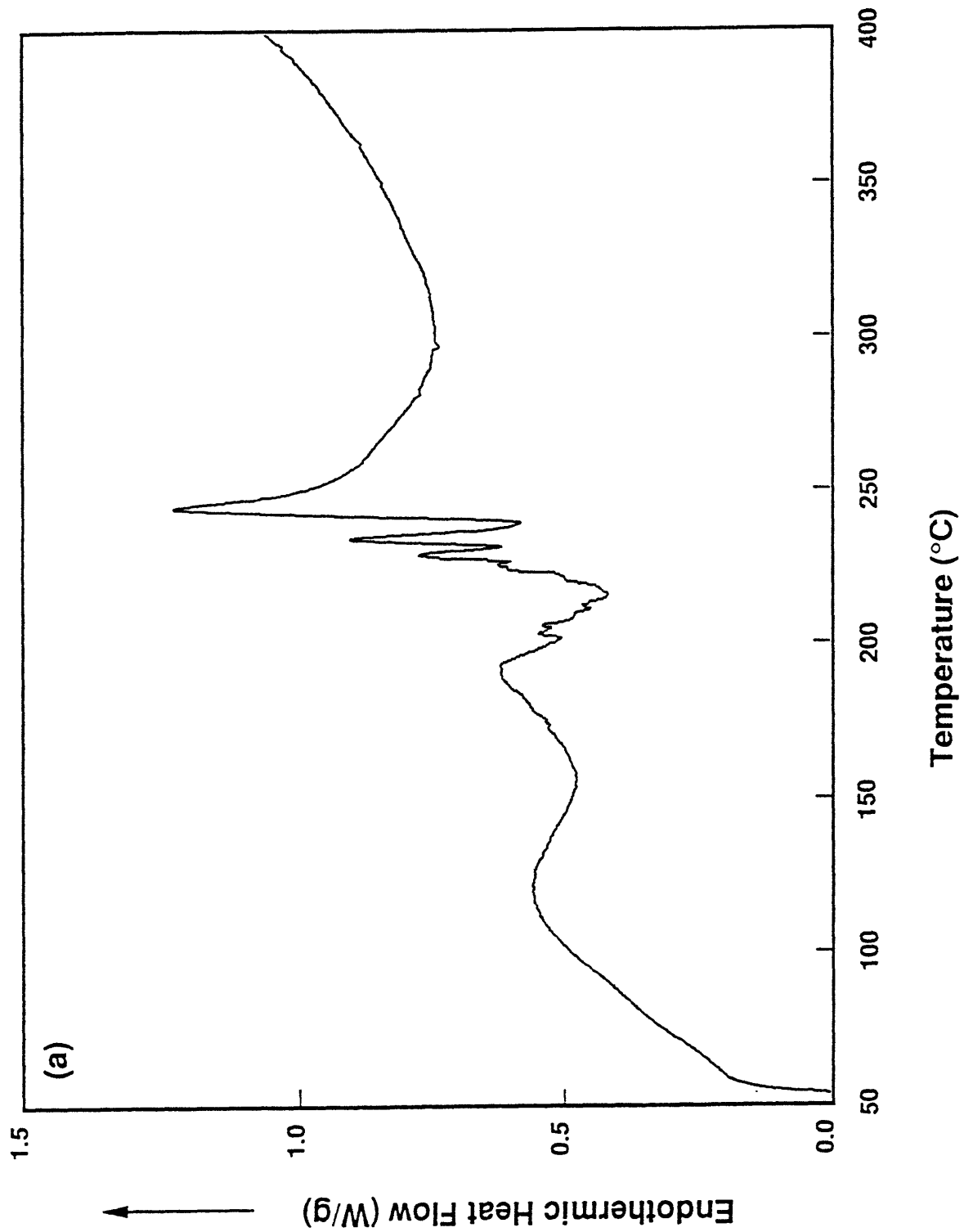


Figure 4.11. Endothermic heat flow vs. temperature for Probimide[®] 32 thick films: a.) baked 6 hours at 100°C,

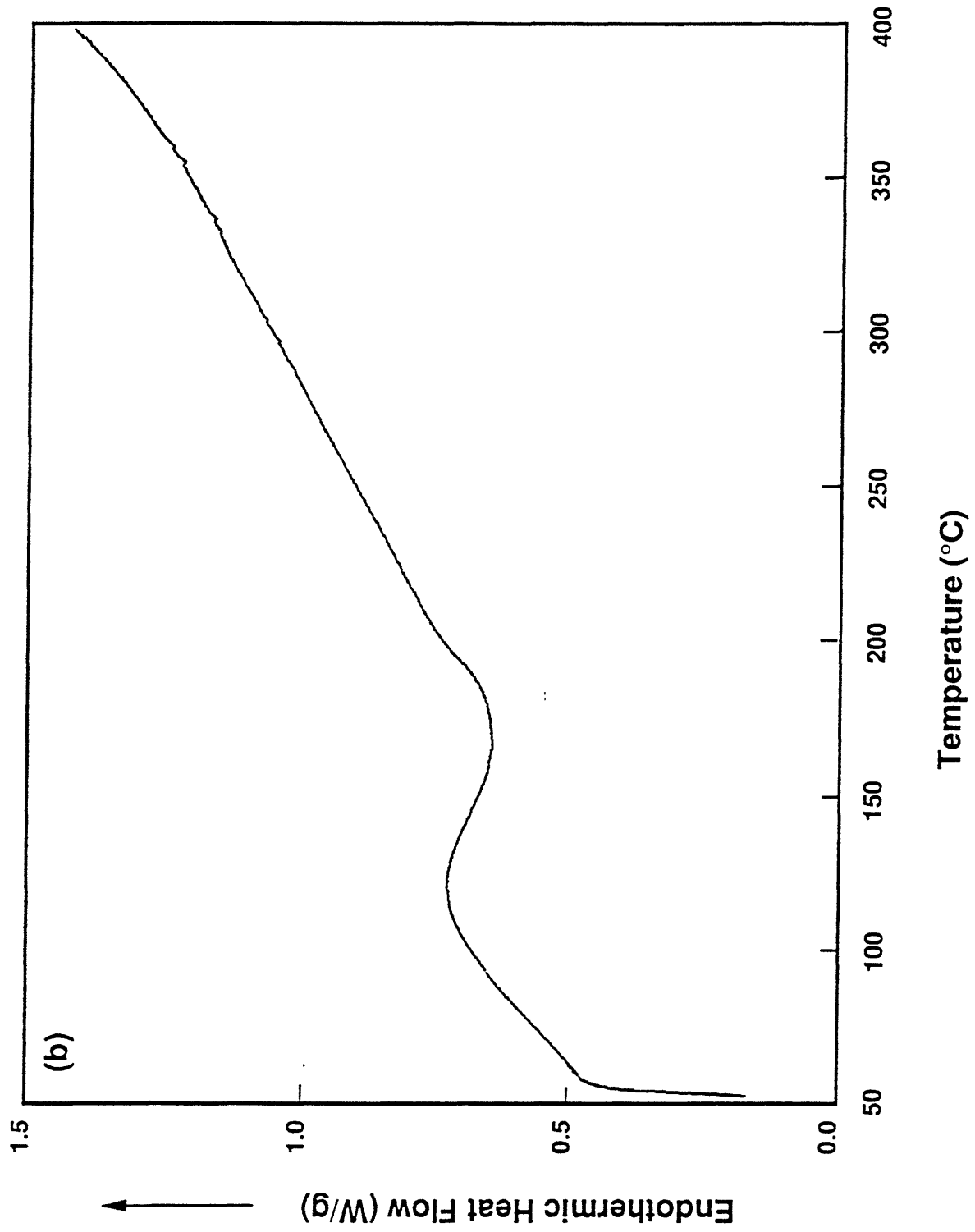


Figure 4.11. continued. b.) then 3 hours at 200°C,

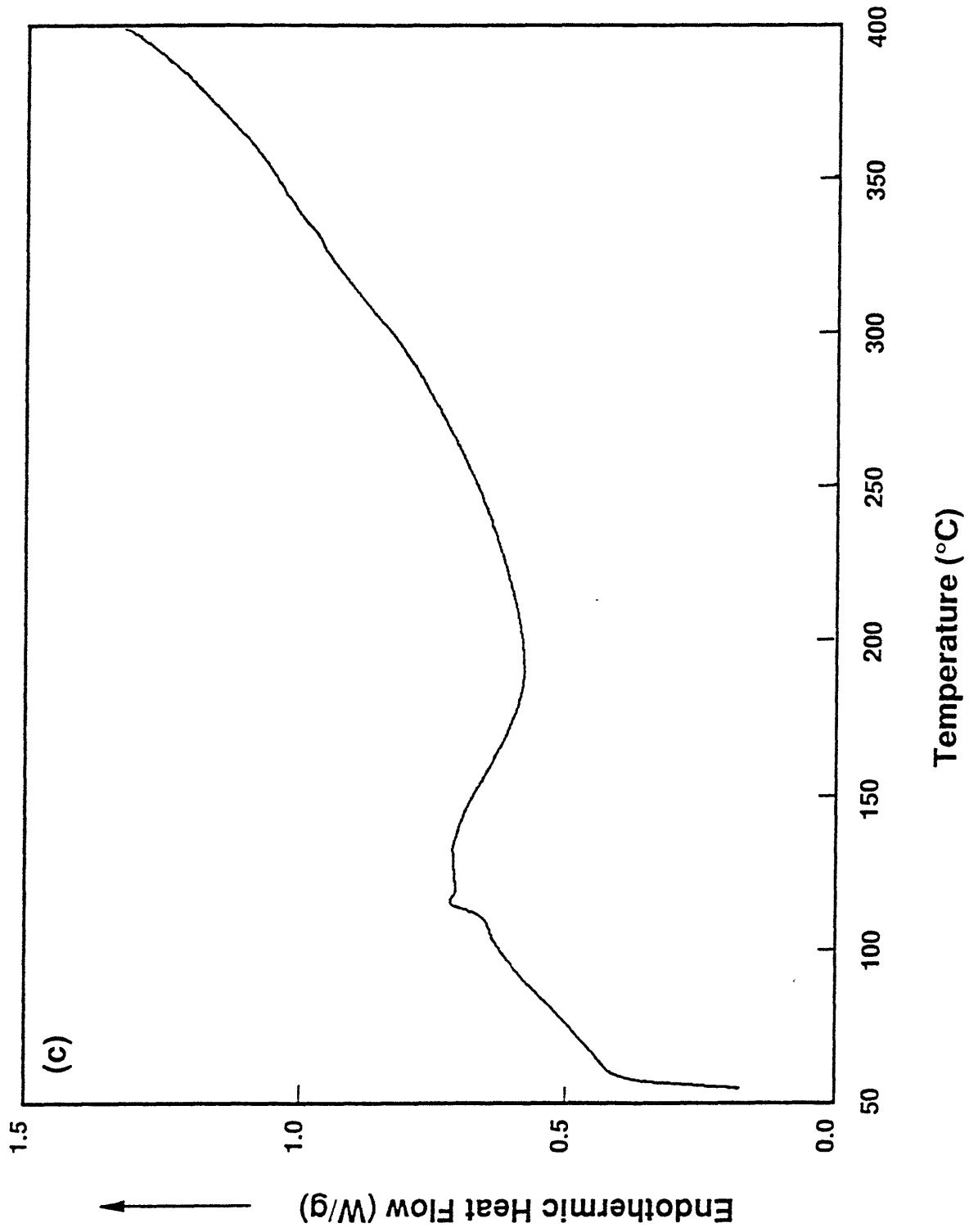


Figure 4.11. continued. c.) then 3 hours at 300°C in either air or,

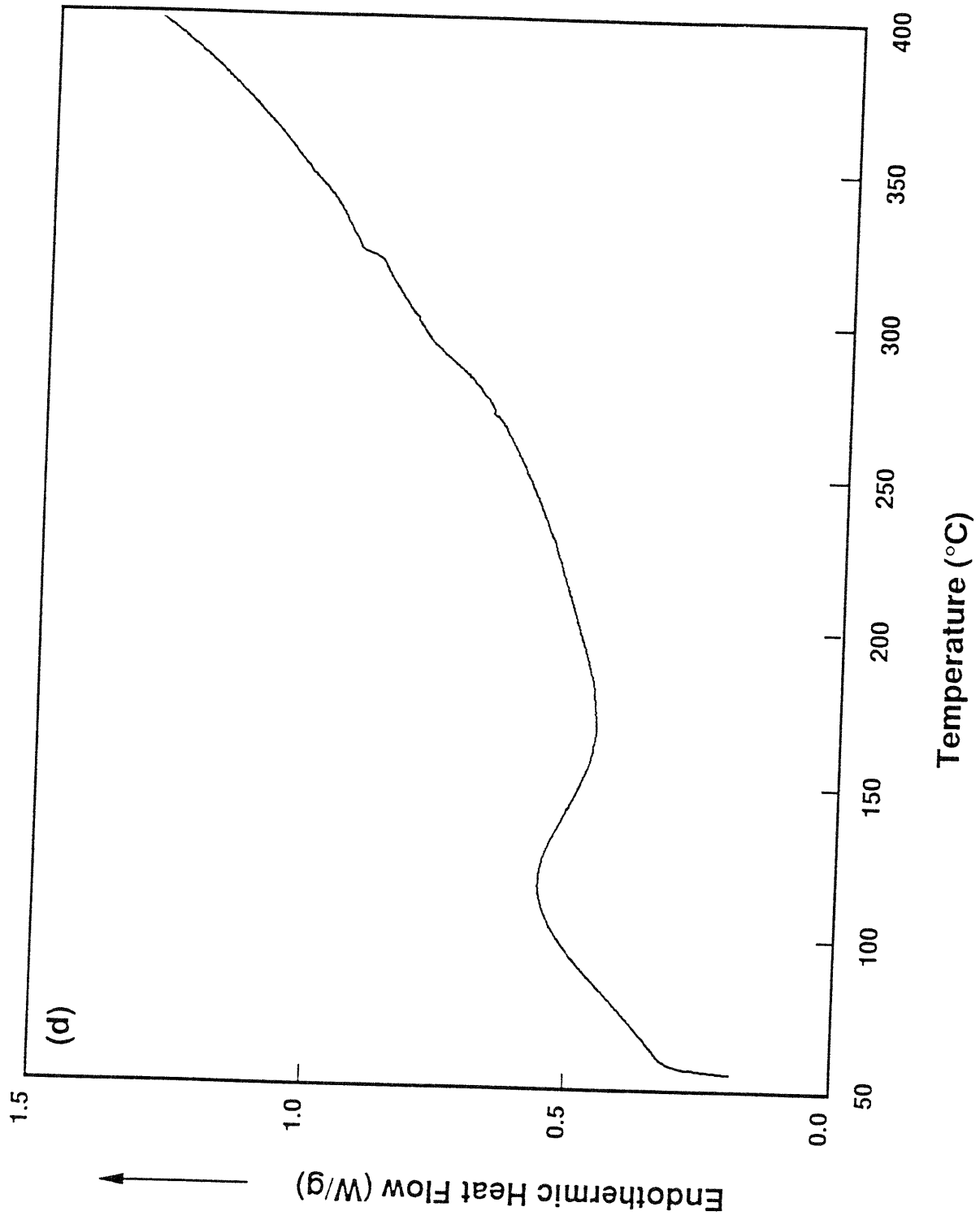


Figure 4.11. continued. d.) nitrogen.

4.4. Conclusions

Although the polyamide-imide Probimide[®] 32 undergoes no thermal imidization reaction during curing, the structure and properties of the polymer system are dependent upon its curing conditions. The effects of progressive cure conditions on the properties and physiochemistry of the polymer have been studied by several characterization methods. When bulk films of Probimide[®] 32 are treated at only 100°C, a great deal of solvent remains. The residual solvent affects the properties and deteriorates the thermal stability of the material. The volume of residual solvent is reduced and the properties and thermal stability improved when the polymer is cured to 200°C. Samples treated at 300°C were solvent free and were highly thermally stable. However, substantial oxidative crosslinking occurs if the polymer is cured at 300°C in air rather than in an inert environment such as nitrogen.

4.5. References

1. C.E. Sroog, *Macromolecular Reviews, Vol. II, J. Polym. Sci.* (1976).
2. S.D. Senturia, in *Polymers for High Technology - Electronics and Photonics*, M.J. Bowden and S.R. Turner, Eds., American Chemical Society, Washington, D.C., 1987, p. 428.
3. J.W. Verbicky, Jr., "Polyimides" in *Encyclopedia of Polymer Science and Engineering*, J.I. Kroschwitz, Ed., John Wiley and Sons, Inc., New York, 1987.
4. H.R. Slater, *Advanced Materials and Processes*, **1**, 19 (1995).
5. R.J. Karcha and R.S. Porter, *Polymer*, **33(22)**, 4866 (1992).
6. S. Palsule and J.M.G. Cowie, *Polym. Bull.*, **33(2)**, 241 (1994).
7. D.C. Rich, E.K. Sichel, and P. Cebe, MRS Fall Meeting 1995, *in press*.
8. M.H. Kailani, C.S.P. Sung, and S.J. Huang, *Macromol.*, **25**, 3751 (1992).

9. P.R. Dickinson and C.S.P. Sung, *Macromol.*, **25**, 3758 (1992).
10. E. Pyun, R.J. Mathisen, and C.S.P. Sung, *Macromol.*, **22**, 1174 (1989).
11. J.R. Ojeda, J. Mobley, and D.C. Martin, *J. Polym. Sci. B*, **32**, 559 (1995).
12. J. Jou and P. Huang, *Macromol.*, **24**, 3796 (1991).
13. C.A. Pryde, *SPE ANTEC '90*, 439 (1990).
14. M.-J. Brekner and C. Feger, *J. Polym. Sci. A*, **25**, 2005 (1987).
15. E.D. Wachsman and C.W. Frank, *Polymer*, **29**, 1191 (1988).
16. R.W. Snyder, B. Thomson, B. Bartges, D. Czerniawski, and P.C. Painter, *Macromol.*, **22**, 4166 (1989).
17. OCG Microelectronic Materials, Inc., Probimide 32 product bulletin.
18. E.g., C.J. Pouchert, *The Aldrich Library of Infrared Spectra Edition III*, Aldrich Chemical Company, Inc., Milwaukee, WI (1981).
19. R. Silverstein and G. Bassler, *Spectrometric Identification of Organic Compounds*, John Wiley & Sons, New York (1967).
20. S. Kuroda and I. Mita, *Eur. Polym. J.*, **25(6)**, 611 (1989).
21. R. Dine-Hart, D. Parker, and W. Wright, *Br. Polym. J.*, **3**, 222 (1971).
22. R. Dine-Hart, D. Parker, and W. Wright, *Br. Polym. J.*, **3**, 226 (1971).
23. H. Ishida, S. Wellinghoff, E. Baer, and J. Koenig, *Macromol.*, **13**, 826 (1980).
24. L. Broadbelt, S. Dziennnik, and M. Klein, *Polym. Degr. Stab.*, **44**, 137 (1994).

Chapter 5. Alignment of Liquid Crystals on Brushed Polymer Layers.

5.1. Introduction

Despite the tremendous industrial importance of, and scientific interest in, the surface alignment of liquid crystals on polymer films, it is still a poorly understood phenomenon. Berreman and others [1-3] have argued that the liquid crystals align along microgrooves created by the rubbing. The irregularity in size and location of these scratches [4-8] in buffed polymer films, however, might cast some doubt upon this theory. On the other hand, researchers have shown that the non-rub formation of microgroove patterns can in fact produce alignment of nematic liquid crystals [9,10]. For example, Kawata *et al.* [10] have shown that liquid crystal alignment can be achieved using fine microgroove surface patterns with pitches less than $2\mu\text{m}$ produced by photolithography.

More recently, authors have suggested that molecular orientation of the main chains produced by the brushing is responsible for alignment [8,11-19]. For example, Aoyama *et al.* [11] have shown that liquid crystals can be aligned on polymer films that have been stretched but not scratched. In addition, authors have observed that the direction of alignment is not always identical to the direction of the scratches. For example, while the grooves in rubbed polystyrene films run parallel to the brushing, the liquid crystal alignment is perpendicular to the brush direction [6-8]. This suggests that orientation of the phenyl side groups, which are approximately perpendicular to the main chain, might be responsible for alignment in these films. It seems reasonable that if the physical groove pattern were the *only* factor responsible for alignment, then nearly any grooved polymer film should be able to align liquid crystals and the alignment should always occur in the same direction.

Geary *et al.* [13] have suggested that high crystallinity in polymer films is associated with the polymer's ability to align liquid crystals. Russell [18] reports, using a surface-sensitive X-ray reflectivity technique, that brushed polyimide films develop an oriented crystalline structure at the surface. On the other hand, polyimides, though widely used for liquid crystal alignment, are not widely known for being crystalline. The BPDA-PDA polyimide studied by Russell [19] is one that is known to develop high degrees of crystallinity [20], which is an unusual characteristic for polyimides. Though polyimides are typically amorphous, it is possible that crystalline structures could form at the polymer

surfaces. Factor *et al.* [21], for example, report crystalline structure on the top 90Å of PMDA-ODA polyimide films.

Polyimides with long alkyl side groups and bulky fluorinated groups are frequently used for liquid crystal alignment. These alignment materials are known to generate large pretilt bias angles in the liquid crystal layer [22-27]. In addition photocrosslinkable polyimides are commercially available for liquid crystal alignment applications [28]. These polymers allow the alignment films to be patterned by photolithography. It is unlikely that any of these polyimides could crystallize due to the bulky side groups or to the photocrosslinked main chains. Hence, this casts substantial doubt that crystallinity could be a necessary feature for liquid crystal alignment.

In conclusion, the surface alignment of liquid crystals on polymer layers is not well understood despite the significant amount of work that has been done. Conventional thin film and surface evaluation techniques do not seem to be generating highly insightful information regarding the phenomenon. In this chapter, the alignment of liquid crystals on Probimide 32 polyamide-imide and other polymer layers is demonstrated and discussed. A optical transmission technique for quantitatively evaluating parallel alignment is presented. A highly novel technique for investigating thermophysical transitions in surface layers is then demonstrated.

5.2. Experimental Section

The following section describes the experimental techniques used for producing and evaluating liquid crystal alignment cells. It was necessary to use laboratory techniques that optimally reflected the goals of, and were realistic to, the resources available. Thus, extensive consultations with LCD researchers at the 3M Corporation [29] were helpful in developing the experimental approach described in this section. The goals of these experiments were to:

1. Obtain data that are physical meaningful and have real scientific merit.
2. Present proof of new concept research on the laboratory scale.
3. Focus on the materials science of the liquid crystal surface alignment phenomenon, rather than on LCD device technology in general.

Many decisions were made during the course of this project in order to serve and focus upon the above goals. For example, it was decided to build cells in a university laboratory rather than in an industrial clean room. A hand brushing technique was used rather than a commercial buffing wheel for the induction of alignment. Merck E7 liquid crystal mixture, which is mainly used in research rather than in commercial displays, was selected as the nematic material. Parallel nematic alignment was chosen as the geometry for the evaluation of alignment. The techniques described below are optimal methods with respect to the purposes of this research.

5.2.1. Construction of liquid crystal alignment cells

Preparation of substrates

The following procedure was adopted for preparing glass substrates for spin coating. The purpose of the following cleaning procedure was to remove grease, dirt, and dust particles from the glass. This was desired so that the substrate coverage and smoothness of the polymer coating could be optimized. Poor substrate preparation resulted in poor polymer coatings.

1. Glass microscope slides (25 x 75 x 1 mm) were cut approximately in half by mechanically etching the slide down the middle along its width. The etched slides were then gently broken in half.
2. The slides were blown clean of particles and dust with an air jet stream.
3. The slides were soaked for 15-20 minutes in isopropyl rubbing alcohol for removal of organic contaminants.
4. The slides were rinsed of the alcohol by soaking for 15-20 minutes in distilled or deionized water.
5. The slides were cleaned in an ultrasonic bath with detergent for 20 minutes.
6. The slides were rinsed in distilled or deionized water for 15-20 minutes.

7. The slides were rinsed again in an ultrasonic bath of distilled or deionized water. It was found that this dual rinse procedure was necessary for thorough removal of the detergent. Residual detergent was found to have a significant adverse affect on coating quality.
8. The wet slides were blown dry with an air jet stream.
9. The slides were stored in a PTFE, low-dust sample holder which held twenty glass slides.

Spin coating procedure

The following general procedure was adopted for applying polymer alignment films to the cleaned glass substrates. I specifically thank Prof. Anne Mayes for use of the Headway Research spin coater.

1. A dilute solution of the polymer was prepared. The primary polymer of interest, Probimide 32 polyamide-imide, was obtained from OCG Microelectronic Materials, Inc., as 21 wt% solids and was diluted to approximately 3 wt% solids with N-methyl pyrrolidone (NMP). For example, to 2.5 mL of Probimide 32 original solution, 15 mL NMP were added.
2. The glass substrates were blown clean of dust with an air jet just prior to spin coating.
3. The glass substrates were prewet with solvent, which was spin coated at 4000 RPM for 30 seconds. For Probimide 32 coatings, the substrates were prewet with NMP.
4. The polymer solution was spin coated onto the prewet glass substrates at 4000 RPM for 30 seconds.
5. The films were softbaked about 15-20 minutes at approximately 110°C at atmospheric pressure on a hot plate or on a temperature-controlled metal block in a National Appliance Oven. The films appeared dry after the softbake. The resulting Probimide 32 polyamide-imide films were approximately 450Å thick, as measured by a Dektak 8000 profilometer.

Alignment layer buffing procedure

The following technique was used to brush the polymer films for liquid crystal alignment. The procedure is depicted in Figure 5.1. The substrates were temporarily adhered with two-sided tape in a locked position to a glass plate, which was in turn, securely taped to a horizontal bench top. A rayon cloth was wrapped around a cylindrical bar which weighed approximately 1 lb. The bar was dragged across the polymer film by hand exactly 25 times such that the vertical force on the film was equal to that of the weight of the bar. Although this technique is not as controllable as a commercial brushing wheel, researchers at 3M Corporation believe this technique to be highly adequate in producing reasonably consistent alignment films [28].

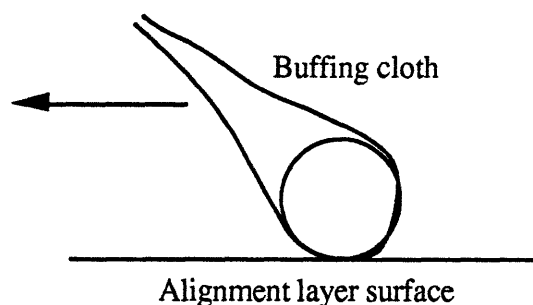


Figure 5.1. Alignment film brushing technique.

Liquid crystal alignment cell building procedure

Liquid crystal cells were constructed by the following procedure, which is depicted in Figure 5.2.

1. Two alignment films on glass were prepared and brushed as described above.
2. PF-70 7 μ m diameter microrod spacers obtained from Nippon Electric Glass were mixed into a globule of Norland Optical Adhesive 61 UV-curable epoxy (Norland

Products, Inc., New Brunswick, NJ 08902). The mixture was mixed fresh prior to cell building. A tiny clump of the spacer rods, approximately 0.03 mg, was added to around 3 drops of the epoxy. This was enough mixture to make about 4 cells.

3. The epoxy/microrod mixture was placed near the edges of one substrate parallel to the brush direction.
4. The two slides were pressed firmly together with the alignment films on the inside of the cell and the brushing directions parallel.
5. The epoxy was exposed through the top glass substrate to i-line ($\lambda = 365$ nm) ultraviolet light under a Spectroline BIB-150B black light UV lamp (average area normalized energy delivered to glass approximately 2.5 mW/cm^2) for about 3.5 minutes. The cell was about 10" from the bulb. The energy required to cure the UV sensitive epoxy was many orders of magnitude less than what might affect the polymer films.
6. The cell gaps were filled by capillary action with Merck E7 liquid crystals. The E7 liquid crystals are low-cost monomeric nematic liquid crystals used primarily in laboratory research. The chemical composition of the liquid crystals is proprietary, though Cognard [30] reports from chromatographic analysis the materials to be the mixture of molecules shown in Table 5.1. The physical properties [31] of the E7 liquid crystals are listed in Table 5.2. The liquid crystals were filled parallel to the direction of alignment, a technique which appeared to minimize the cell defects.
7. The cells were maintained at about 80°C on a temperature-controlled metal block in a National Appliance oven for approximately one-half hour and then cooled. This treatment was sufficient to clear the liquid crystals and minimize defects.
8. The cells were sealed with Devcon 5 Minute epoxy so that the liquid crystals could not seep out of the cells.

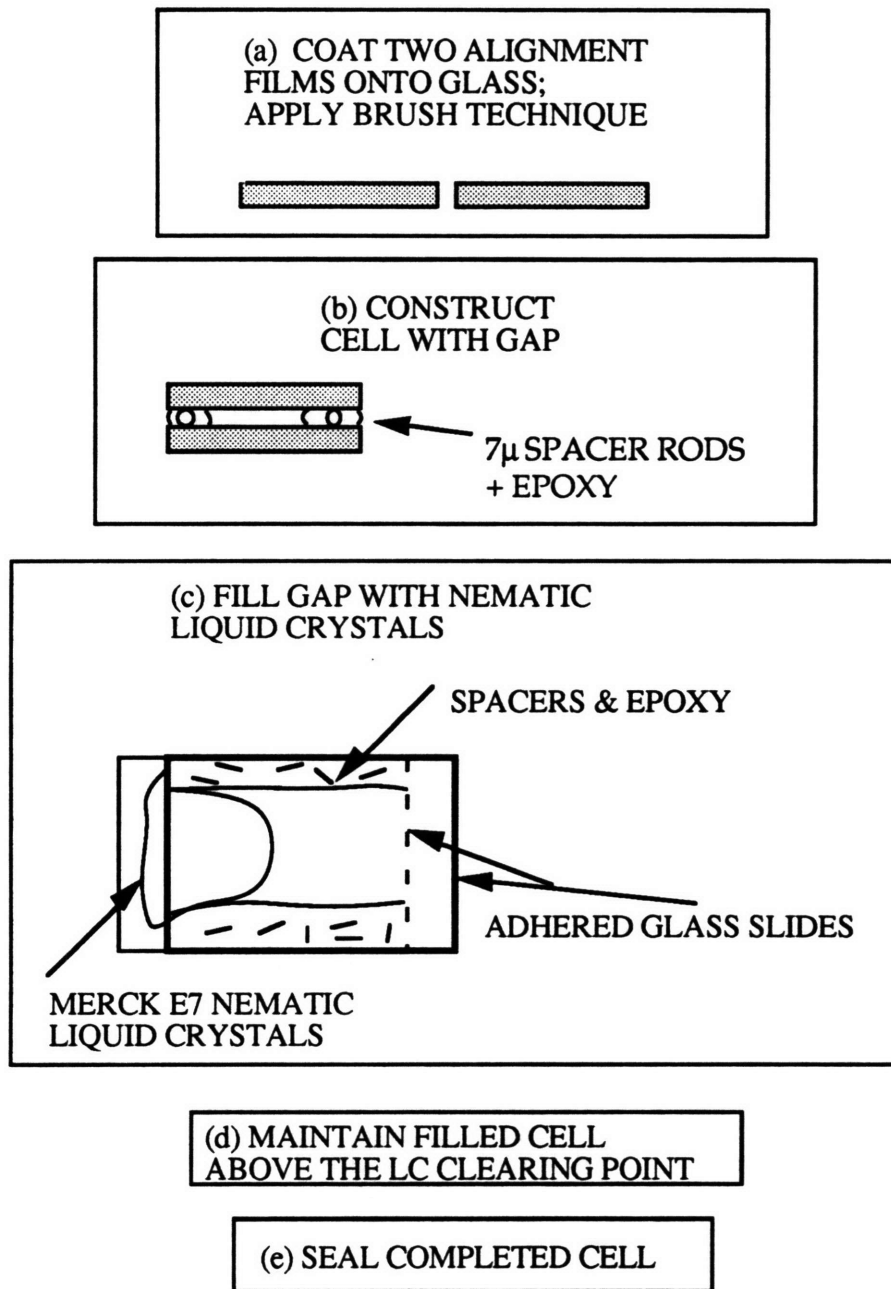


Figure 5.2. Cell construction procedure. (a) Alignment film formation, (b) Empty cell construction, (c) Cell filling, (d) Cell annealing, and (e) Cell sealing.

Table 5.1. Composition of Merck E7 nematic liquid crystals from chromatographic analysis [30].

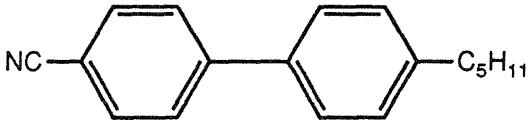
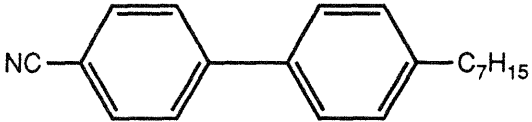
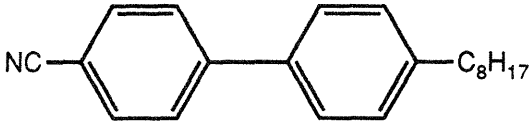
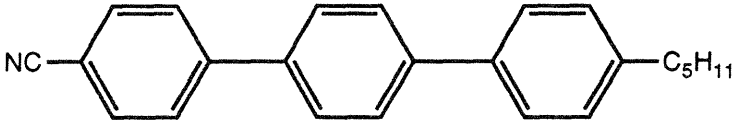
51%	
25%	
16%	
8%	

Table 5.2. Physical properties of Merck E7 nematic liquid crystals [31].

Melting Point	-10°C
Liquid Crystal Clearing Point	60.5°C
Extraordinary Refractive Index at 589 nm	1.746
Ordinary Refractive Index at 589 nm	1.522
Birefringence	0.224
Viscosity (20°C)	39 mm ² /s

5.2.2. Evaluation of alignment cells

Qualitative evaluation of alignment

The liquid crystal alignment in the cells was judged qualitatively by illuminating and rotating the cells between two crossed polarizers. The observations made for aligned and unaligned cells are summarized in Figure 5.3. This technique is an excellent first order test of an alignment film's ability to orient the liquid crystals macroscopically.

Aligned cells exhibited macroscopic optical birefringence, with four extinctions occurring 90° apart upon rotation when the alignment direction is parallel to either polarizer axis (Figure 5.3(a)). Light is transmitted when the cell is rotated off one of these orientations. The maximum transmitted light intensity occurs when the nematic director is 45° to the polarizers' axes (Figure 5.3(b)).

In contrast, unaligned liquid crystal cells were bright (i.e., they evidenced no extinction of light) for all rotations of the cell between crossed polars (Figure 5.3(c)). This is because the unaligned liquid crystals form arbitrary nematic phases with randomly varying nematic directors. The birefringence is microscopic but not macroscopic.

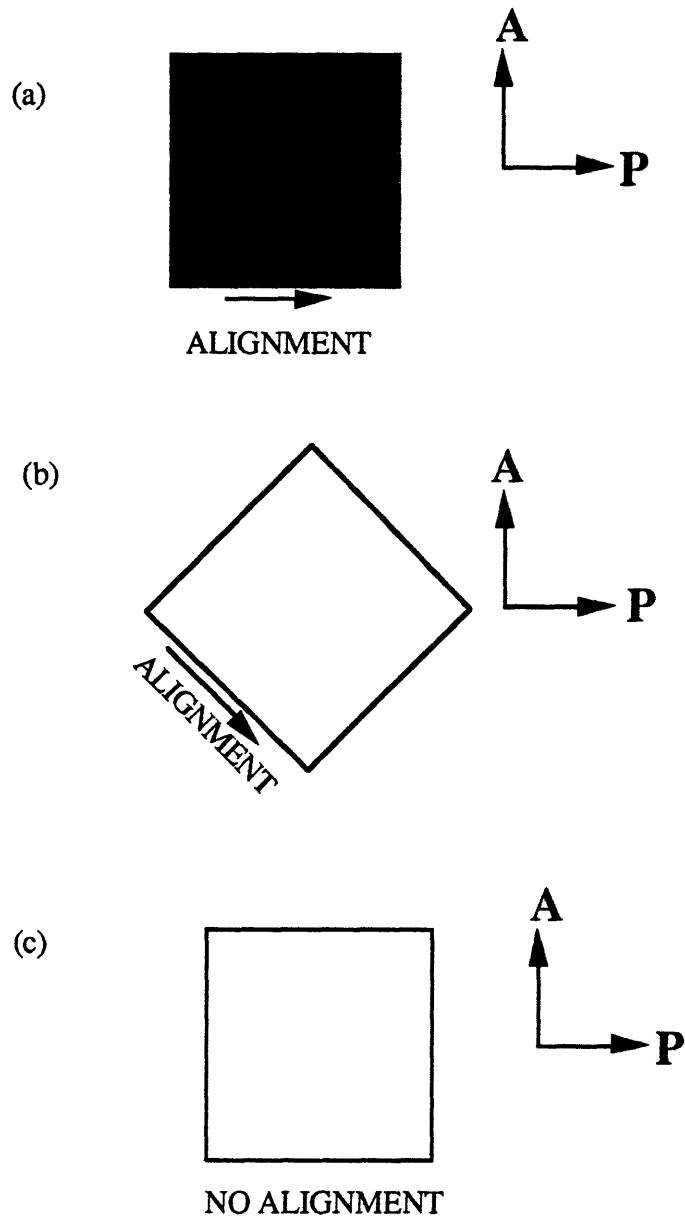


Figure 5.3. Qualitative observations of liquid crystal alignment cells between crossed polarizers. For aligned cells, a.) the light is extinguished when the alignment director is parallel to either polarizer, and b.) maximum intensity is transmitted when the alignment director is 45° with respect to the polarizers. For unaligned cells, c.) the cell appears bright for all rotations.

Measurement of optical transmission

The optical transmission of the liquid crystal cells between a crossed polarizer (P) and analyzer (A) was measured using the configuration shown in Figure 5.4. The laser is a Spectra-Physics Model 159 He-Ne laser ($\lambda = 6328\text{\AA}$). Phase sensitive detection was achieved by use of a Stanford Research Systems SR540 chopper and EG&G Model 5209 lock-in amplifier. A diagram of the connections is shown in Figure 5.5, and the settings for the lock-in amplifier are listed in Table 5.3. A Newport 818-SL detector with 883-SL attenuator and Model 835 power meter were used to detect transmitted intensity. The time constant for intensity measurements was 1 second. A chopping speed of 100 Hz was used. The polarizers had an extinction ratio (intensity $A//P$ / intensity $A\perp P$) of about 10^5 . The intensity transmitted by the crossed polarizers was negligible compared to the lowest cell transmission measurement.

Measured voltage was linear with light intensity for the range studied. This is proven in Figures 5.6 and 5.7. First, a series of calibrated neutral density filters were placed in front of the detector with no other components in the optical train. The measured relative intensity is plotted in Figure 5.6 against expected relative intensity, which was calculated according the extent of calibrated neutral density filtration. Figure 5.6 indicates a linear relationship between real and measured intensity. The data is plotted on a linear scale in Figure 5.6(a) and on a log-log scale in Figure 5.6(b) so that both data approaching one and data approaching zero can be seen.

Next, a polarizer and analyzer were placed in the beam. The transmitted intensity was measured as the analyzer was rotated with respect to polarizer. Expected relative intensity was calculated according to the theoretical relationship:

$$I/E^2 = \cos^2 \chi \quad (1)$$

where I/E^2 is relative intensity and χ is the angle between the polarizer and analyzer. Measured relative intensity is plotted against expected relative intensity in Figure 5.7. The data are plotted on a linear scale in Figure 5.7(a) and on a log-log scale in Figure 5.7(b) so that both data approaching one and data approaching zero can be seen.

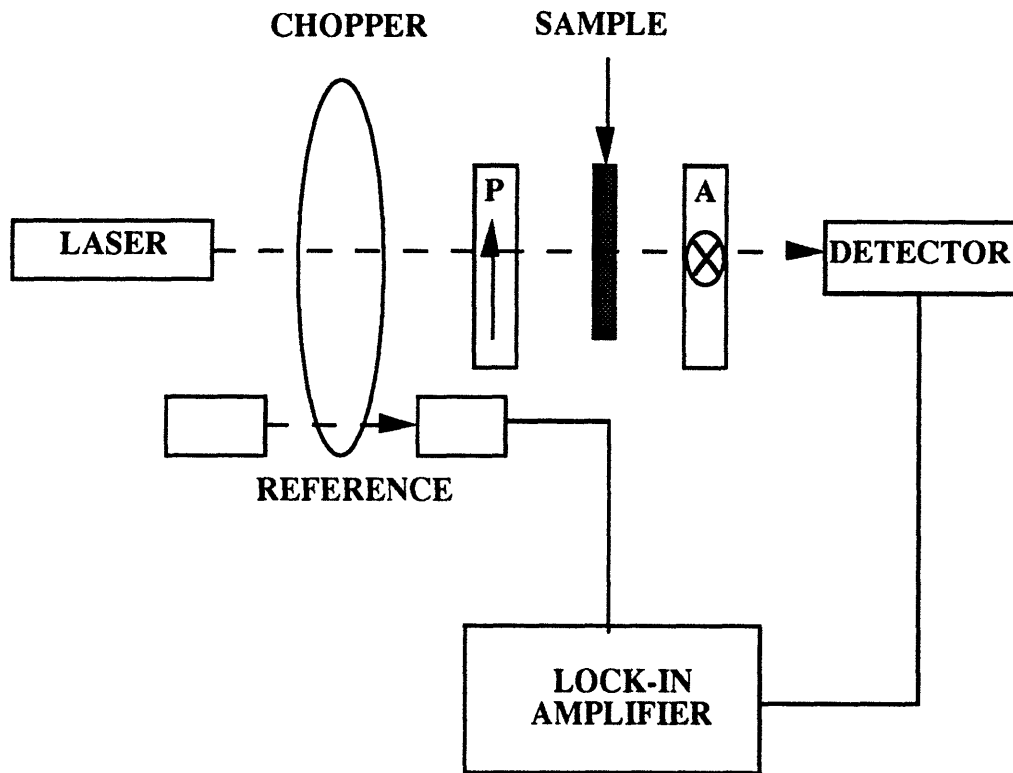


Figure 5.4. Optical transmission apparatus with phase sensitive detection.

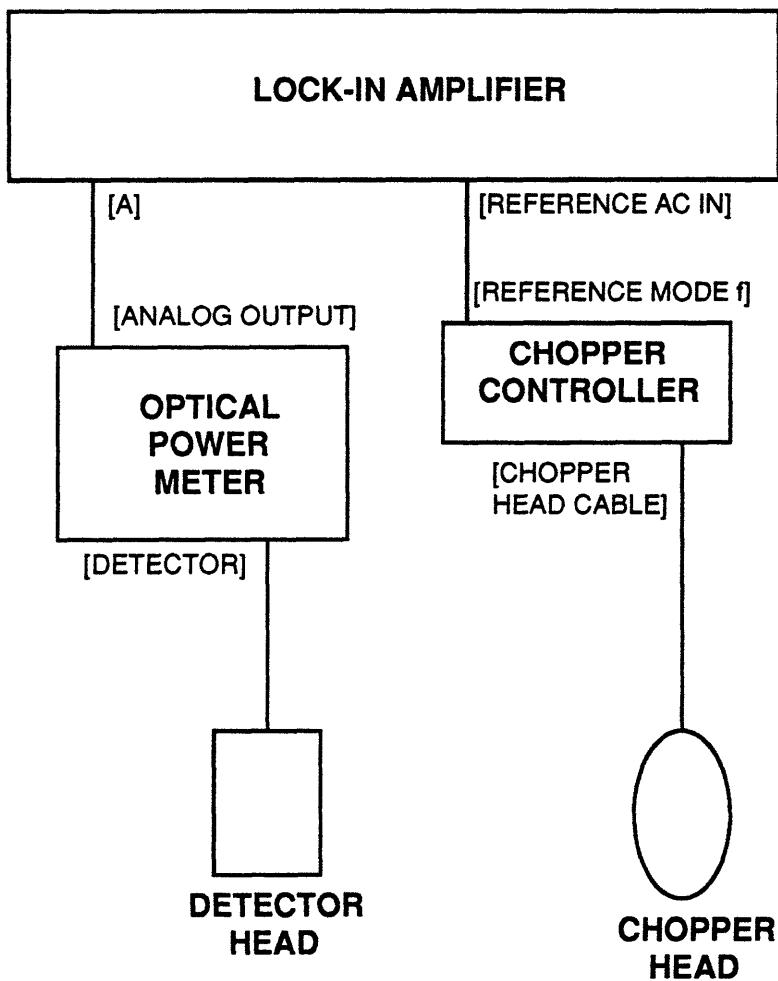


Figure 5.5. Instrument connections for phase sensitive detection. Port labels are stated in brackets where appropriate.

Table 5.3. Settings for the EG&G 5909 lock-in amplifier used for phase sensitive detection of chopped light.

SENSITIVITY

Input from voltage source (i.e. power meter) at A port and press A key
Adjust sensitivity scale with up and down keys as appropriate

FILTERS

Use Bandpass BP filter mode.
Use TRACK to track the reference chopping frequency.
Set LINE REJECT such that neither F nor 2F filters are lit.

TUNING

Hit red AUTO key, then AUTO PHASE key, and wait for red AUTO light to turn off.
This procedure automatically determines the phase adjustment for maximum output signal.
The adjustment is necessary because the external electronics are not necessarily in phase.
Use +90° to shift the phase adjustment by 90°, twice to shift by 180°

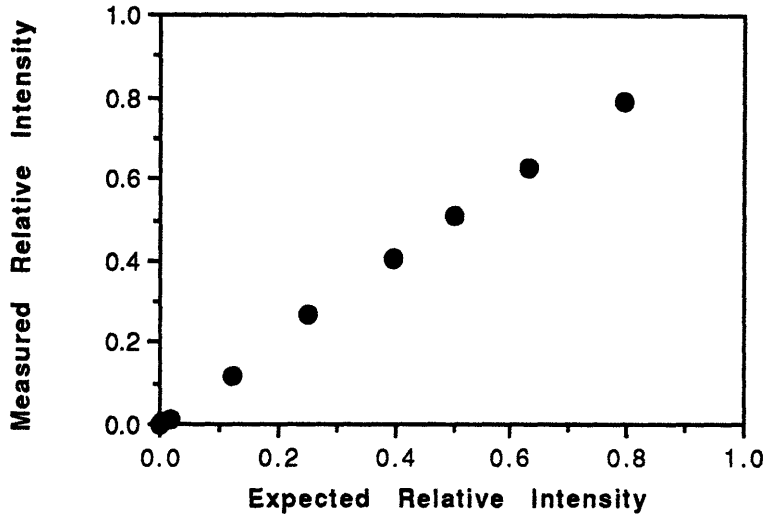
REFERENCE

Connect chopper signal at AC IN port
INT (internal reference) should not be lit, since an external reference is being used
2F should not be lit, as this would double the reference frequency

OUTPUT

Adjust TIME CONSTANT as desired
The higher the time constant, the less the noise, but the longer it takes to produce data
10 sec is a good time constant to begin with
Use SLOPE 6dB, though this is not crucial in most cases
DYN RES - NORM
DISPLAY - %FS.SIGNAL (% of full scale sensitivity setting of output signal)
OFFSET & EXPAND - keep unlit

(a)



(b)

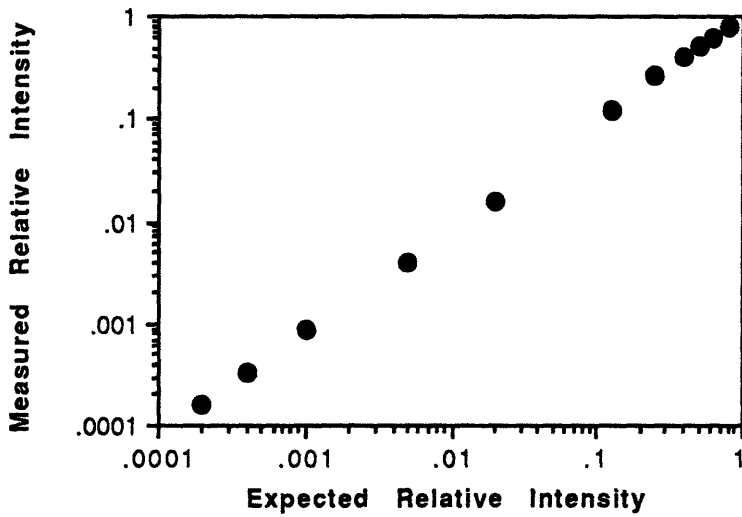
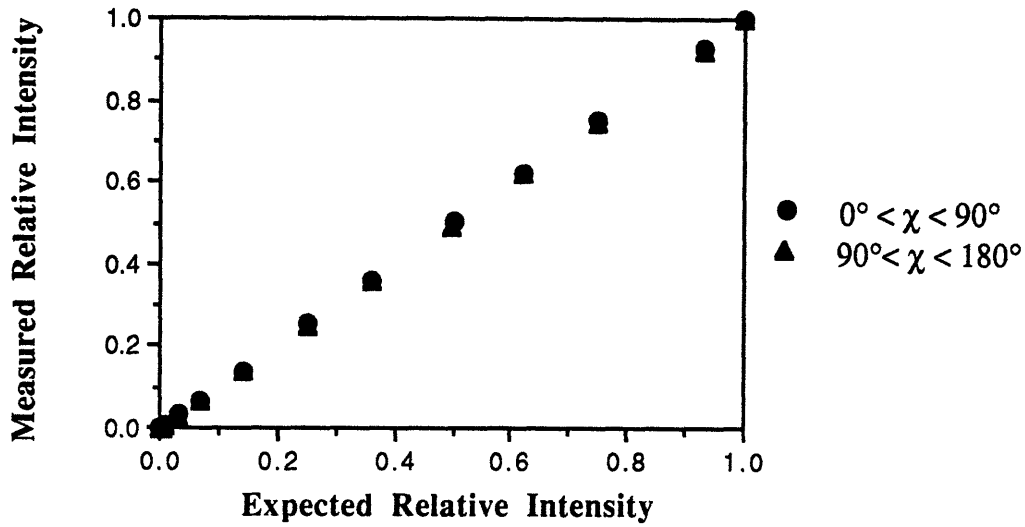


Figure 5.6. Measured relative intensity vs. expected relative intensity for phase-sensitive detection of neutral density filtered light. Expected relative intensity is calculated from the extent of calibrated neutral density filtration. a.) linear scale, and b.) log-log scale.

(a)



(b)

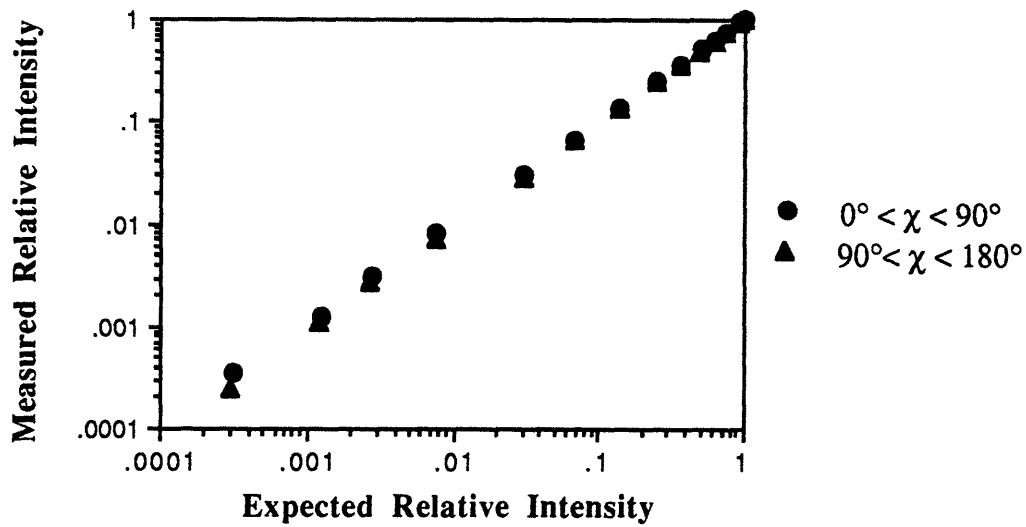


Figure 5.7. Measured relative intensity vs. expected relative intensity for phase-sensitive detection of light diminished by two consecutive polarizers with their polarizing axes lying at an angle χ . Expected relative intensity is given by $\cos^2\chi$. a.) linear scale, and b.) log-log scale.

The optical transmission intensities of the liquid crystal alignment cells were measured between the crossed polarizer and analyzer. To calculate the alignment parameter $A=I(0^\circ)/I(45^\circ)$ discussed in Chapter 1, both the intensities $I(0^\circ)$, brushing axis parallel to the polarizer, and $I(45^\circ)$, brushing axis 45° to the polarizer were measured. Approximately 12 measurements were taken for each orientation, i.e., 0° or 45° , of each sample cell. The measurements were taken for sample spots distributed throughout the cell. Highest and lowest values of the data sets were discarded and average values were calculated from the remaining measurements. The experimental error is discussed in Section 5.4.

The optical transmission of the liquid crystal cells was measured while adjusting for very small (up to 3°) Maguin twist distortions [32] in the cells that appear to have been introduced during cell construction. Such distortions rotate the axis of polarization of the light, but do not represent defects in the surface alignment of the liquid crystals. The analyzer and cells were adjusted such that for the 0° state, the polarizer was parallel to the first LC surface director and the analyzer was perpendicular to the second LC surface director. This is shown in Figure 5.8. The adjustment should counteract the affect of the twist distortion. Failing to adjusting for twist distortions in the 0° extinction position can have a serious affect on the accuracy of the data. The small twist distortions should not have a significant affect on the intensity at the 45° orientation, as can be shown by equation (25) of Chapter 1, and it does not matter therefore whether an adjustment is made for this position.

Twist distortions can also introduce ellipticity in the light passing through even if the components are adjusted as shown in Figure 5.8. However, one can show that for small twist angles $<3^\circ$, by making this adjustment, the ellipticity of the transmitted light due to twisting is very small, and that cell can be reasonably approximated as a parallel-aligned layer. According to Gooch and Tarry [33], after making the adjustment shown in Figure 5.8, the relative transmission (T) due to elliptically polarized light is given by:

$$T = [\sin^2 (\theta (1+u^2)^{1/2}) / [1+u^2]] \quad (2)$$

where θ is the twist angle and u is given by:

$$u = \pi h \Delta n / \theta \lambda \quad (3)$$

where h is the liquid crystal layer thickness, Δn is the birefringence, and λ is the

wavelength of light in free space. If we assume $h=7\mu\text{m}$, $\Delta n=0.224$, $\lambda=6328\text{\AA}$, and for the worst case scenario, $\theta=3^\circ$, the calculated value for T is approximately 4.5×10^{-5} , which is more than two orders of magnitude below the lowest measured value of cell transmission. Hence, it is reasonable to conclude that ellipticity due to twist distortion is not significant.

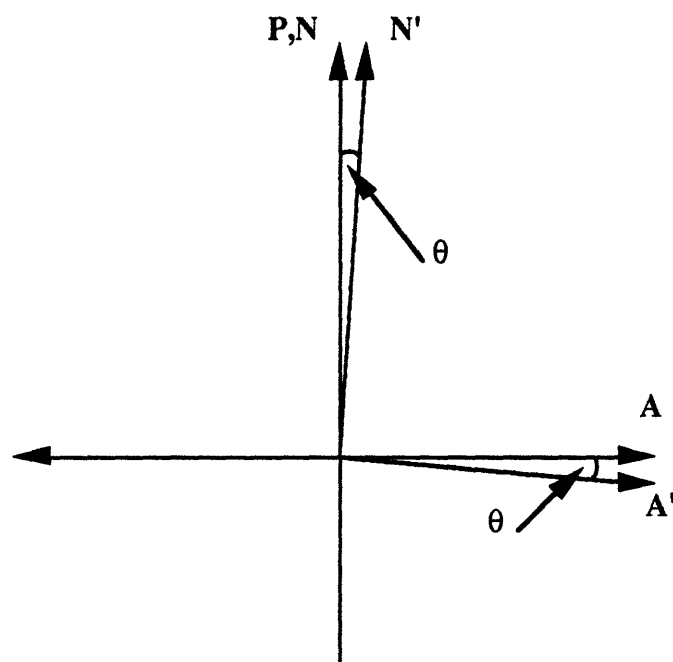


Figure 5.8. Adjustment made for a cell with small degree of twist distortion θ . The first liquid crystal surface director N is oriented parallel to polarizer P . The second surface director is N' . The analyzer is adjusted by θ from A to A' such that A' is perpendicular to N' .

5.3. Results and Discussion

5.3.1. Brushing induced alignment in Probimide 32 polyamide-imide

The processing, structure, and properties of Probimide 32 polyamide-imide were previously discussed in Chapter 4. In this section, it is shown that this polymer can be used as an alignment layer for nematic liquid crystal. Alignment films of Probimide 32 and liquid crystal parallel alignment cells were produced by the techniques described in Section 5.2. The brushing method was used to induce the liquid crystal aligning properties in the polyamide-imide. Qualitatively, it was apparent that the liquid crystal cells produced by this method were strongly aligned along the brushing axis.

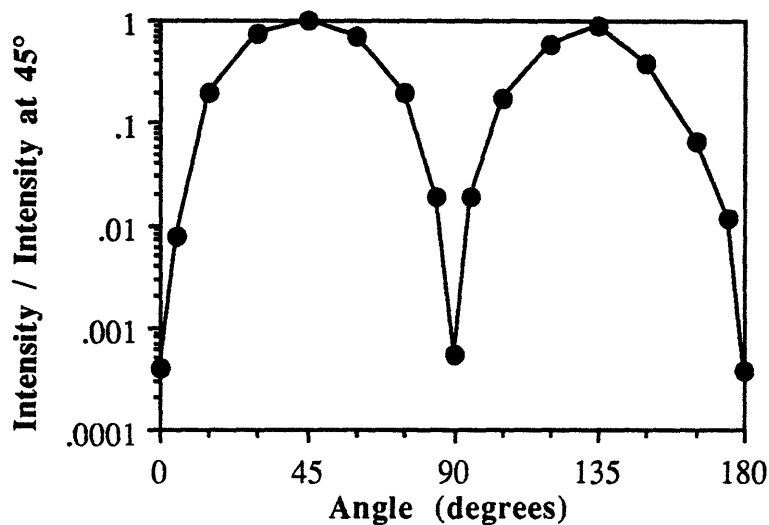
The alignment of the liquid crystal cells was evaluated by use of the laser optics method described in Section 5.2. A brush-aligned cell was placed between the crossed polarizer and analyzer. The azimuthal angle of the alignment director with respect to the polarizer was varied. The transmitted intensity is plotted in Figure 5.9(a) as a function of the azimuthal angle of the alignment director. The intensity axis is normalized by the transmitted intensity measured with the alignment director at 45° with respect to the polarizer. For ideal alignment, we expect the transmitted intensity to follow the expression:

$$I(\phi)/I(45^\circ) = \sin^2(2\phi) \quad (4)$$

where ϕ is the angle of the alignment axis with respect to the polarizer and $I(\phi)/I(45^\circ)$ is the transmitted intensity normalized by that at $\phi=45^\circ$. The theoretical relationship is plotted in Figure 1.13 in Chapter 1. It is apparent that the measured relationship shown in Figure 5.9(a) closely approximates the theoretical relationship in Figure 1.13. Thus, it is clear that there is a strong degree of alignment in the brush aligned cell. On the other hand, the intensity at 0° , 90° , and 180° is not zero as theoretically predicted, indicating that the alignment of the liquid crystals is not perfect. The ratio of minimum to maximum intensity is on the order of 10^{-3} .

The optical transmission of a liquid crystal control cell in which there was no brushing treatment to the alignment film is shown in Figure 5.9(b). Qualitatively, no alignment was observed in this cell. The cell was placed between the crossed polarizer and analyzer of the laser optical transmission apparatus. The length axis of the cell (which would have been the brush axis had the alignment films been brushed) was selected as the axis of reference. The cell was rotated through 180° and relative intensity was plotted

(a)



(b)

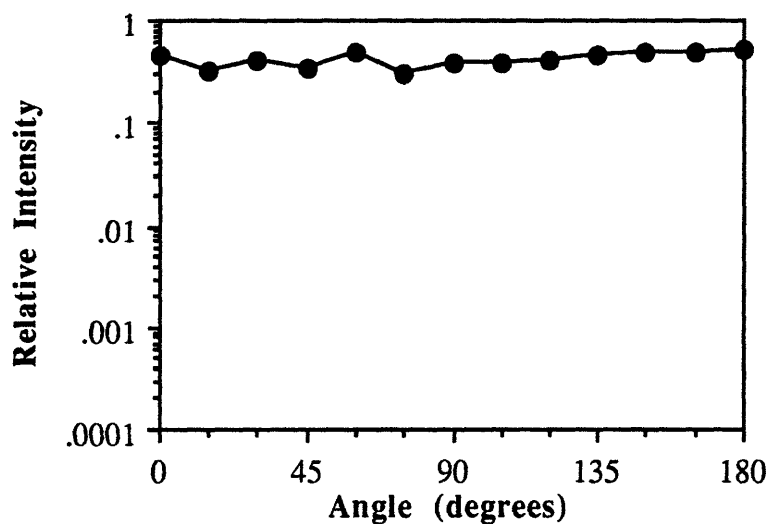


Figure 5.9. a.) Intensity / intensity at 45° vs. rotation angle for a nematic liquid crystal cell aligned with brushed Probimide 32 polyamide-imide layers. The x-axis is the azimuth of the alignment director with respect to the polarizer. b.) Relative intensity vs. rotation angle for nematic liquid crystal cell with untreated Probimide 32 polyamide-imide layers. The x-axis represents the azimuth of an arbitrary reference axis with respect to the polarizer.

against the angle between the polarizer axis and the reference axis. It is apparent that, unlike the aligned cell, there is no systematic change in the transmitted intensity as the sample is rotated. This indicates that there is no macroscopic alignment in this sample.

For all aligned liquid crystal cells produced with brushed polyamide-imide layers, the average ratio of intensity at 0° to intensity at 45° is approximately 1.04×10^{-3} with a standard deviation of 2.8×10^{-4} (27%). This ratio, which is referred to as the *A* parameter in Chapter 1, is three orders of magnitude lower than unity, the value of the *A* parameter which should occur in the case of no macroscopic alignment. Hence, it is clear that there is very strong and significant alignment in these specimens. The effective angle of misalignment Φ , defined by:

$$A \equiv \sin^2 (2\Phi) \quad (5)$$

is approximately 0.92° for the brushed polyamide-imide aligned cells. Since $\Phi=0^\circ$ for an ideally aligned specimen and $\Phi=45^\circ$ for an unaligned specimen, it is quite apparent that the misalignment of the liquid crystals with respect to the alignment director is very small.

5.3.2. Brushing-induced alignment in other polymers

During the course of these investigations, it was desired to find other polymers which effectively align the E7 nematic liquid crystals by the rubbing technique. A brief discussion of the results of this search is worthwhile. In Table 5.4, polymers which were used as alignment films are listed. Their success in parallel-aligning the liquid crystals in the brush direction is stated in the second column of Table 5.4. Some characteristics of the polymeric materials are listed in the remaining columns. The polymers in Table 5.4 were said to have a "rigid backbone" if the repeat unit contained ring structures or bulky side groups. The polymers were said to have "strong intermolecular forces" if the repeat unit contained highly dipolar moieties, such as those involved in hydrogen bonding or charge transfer complexation. Calculated effective angles of misalignment for cells produced with various polymer layers are shown in Figure 5.10.

Two characteristics which appeared not to be necessary for aligning the E7 liquid crystals were backbone rigidity and aromatic content. Since aromatic polyimides have both these characteristics, one might have speculated that these characteristics may be necessary for, or associated with, liquid crystal aligning properties. However, this does not appear to be the case. For example, poly(vinyl alcohol), a non-aromatic vinyl polymer, was an effective alignment layer material, while polycarbonate, a rigid aromatic polymer, was not.

The polymers with strong intermolecular forces, on the other hand, appear to be strong aligners of the E7 liquid crystals. Polyimides are, for example, known to exhibit strong intermolecular charge transfer interactions. The polyamic acid, though weaker in charge transfer, contains both carboxylic acid and amide groups, which are strongly hydrogen bonding moieties. The polyamide-imide is a hybrid of the polyimide and the polyamide and should also exhibit strong intermolecular forces. Poly(vinyl alcohol) contains strongly hydrogen bonding hydroxyl groups. The poly(phenylene ether sulfone) molecule contains highly electron withdrawing sulfone groups, which should engender strong permanent dipoles in the main chain. All of these polymers have a yellowish appearance in the solid film state, which might suggest a helpful rule of thumb in selecting a good alignment polymer.

Table 5.4. List of polymers which were examined as liquid crystal aligning agents and some of their characteristics.

Polymer	Aligns E7 LCs?	Rigid Backbone?	Aromatic Groups?	Strong Intermolecular Forces?	Color
Probimide 32 polyamide-imide (PAI)	yes	yes	yes	yes	yellow
PMDA-APB polyamic acid (PAA)	yes	yes	yes	yes	yellow
PMDA-APB polyimide (PI)	yes	yes	yes	yes	yellow
poly(vinyl alcohol) (PVA)	yes	no	no	yes	yellow
poly(methyl methacrylate) (PMMA)	no	no	no	no	none
polycarbonate (PC)	no	yes	yes	no	none
poly(phenylene ether sulfone) (PPES)	yes	yes	yes	yes	yellow

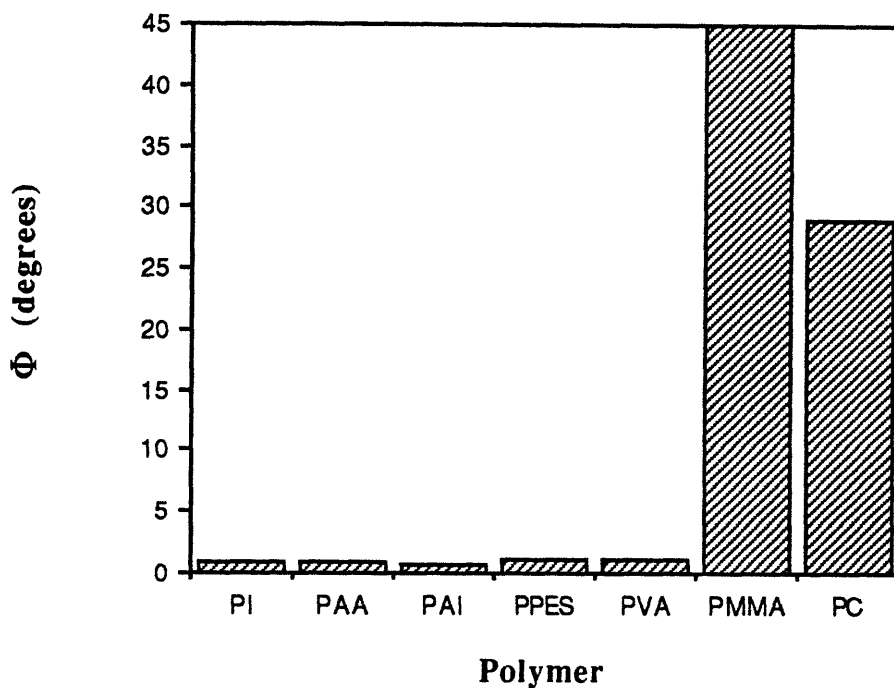


Figure 5.10. Values of Φ , the effective angle of misalignment, for liquid crystal cells produced with alignment films of brushed PMDA-APB polyimide (PI), PMDA-APB poly(amic acid) (PAA), polyamide-imide (PAI), poly(phenylene ether sulfone) (PPES), poly(vinyl alcohol) (PVA), poly(methyl methacrylate) (PMMA), and polycarbonate (PC). All cells but those produced with PMMA and PC appear to have very strong macroscopic alignment.

5.3.3. FTIR Spectra of Probimide 32 polyamide-imide alignment films

FTIR spectra of Probimide 32 films are displayed and discussed in Chapter 4. The films in Chapter 4, however, were spin coated from 21wt% solids and were approximately 4 μ m thick. The polyamide-imide films used in this chapter for liquid crystal alignment cells, on the other hand, were coated from 3wt% solids and are approximately two orders of magnitude thinner.

The FTIR study in Chapter 4 showed that solvent was systematically removed from the 4 μ m films as the material was heated from 100°C to 200°C. This was primarily evidenced by the significant change in peak height of the 1680 cm^{-1} amide carbonyl vibration relative to the 1370 cm^{-1} imide N-C vibration. The 1680 cm^{-1} peak declined as

NMP solvent was driven from the film. The ratio of the 1680 cm^{-1} band to the 1370 cm^{-1} settled near 0.6-0.7 at point of full solvent removal.

The solvent dynamics are significantly different, however, in the thin alignment layer films. Figure 5.11 shows the FTIR spectrum of a thin Probimide 32 alignment layer film on KBr which was cured by only the 110°C soft bake treatment. The 1680 cm^{-1} vibration appears to be mitigated as compared to the solvent-containing films in Chapter 4. The ratio of the peak height of the 1680 cm^{-1} band to that of the 1370 cm^{-1} is about 0.63, which is consistent with a solvent free film. Thus, this study indicates that the solvent in the Probimide 32 preimidized polyamide-imide resin can be removed rapidly at low temperatures in very thin films (approximately 450\AA).

Brushing the polyamide-imide film induces orientation of the polymer chains in the direction of the brushing. This is consistent with what other researchers [8,11-19] have found in brushed alignment films of other polymeric materials. The orientation is clearly indicated by the dichroic FTIR spectra of brushed films in Figure 5.12(a,b). The polyamide-imide films have been brushed, then scanned in the FTIR after placing a gold wire grid IR polarizer in the path of the beam. For Figure 5.12(a), the IR is parallel to the direction of brushing, and for Figure 5.12(b), the IR is perpendicular to the direction of brushing. It is important here to notice the relative ratios of the 1370 cm^{-1} imide N-C peak to that of the 1720 cm^{-1} imide C=O peak. These values are listed in Table 5.5. The 1370 cm^{-1} band represents vibration parallel to the main chain, while the 1720 cm^{-1} represent vibration approximately perpendicular to the main chain. The ratio of the heights of these peaks increases approximately 37% from 0.63 to 0.86 as the brushed polymer film is rotated from the perpendicular to the parallel position with respect to the IR polarization axis.

5.3.4. Atomic Force Microscopy of brushed polamide-imide films

Atomic force microscopy (AFM) images are shown in Figure 5.13 for brushed and unbrushed Probimide 32 polyamide-imide alignment layer films. For the brushed material, Figure 5.13(a), there appear to be grooves running through the film parallel to the brush direction. These grooves are not present in the unbrushed sample, Figure 5.13(b). These relatively large scratches observed in the brushed material appear consistent with what other researchers [4-8] have observed in brushed polymer layers. Seo *et al.* [5,7], however, observed grooves structures in rubbed polystyrene and alkyl-branched polyimides, but not in a brushed straight chain polyimides, which they observed to have only a rough, bumpy surface.

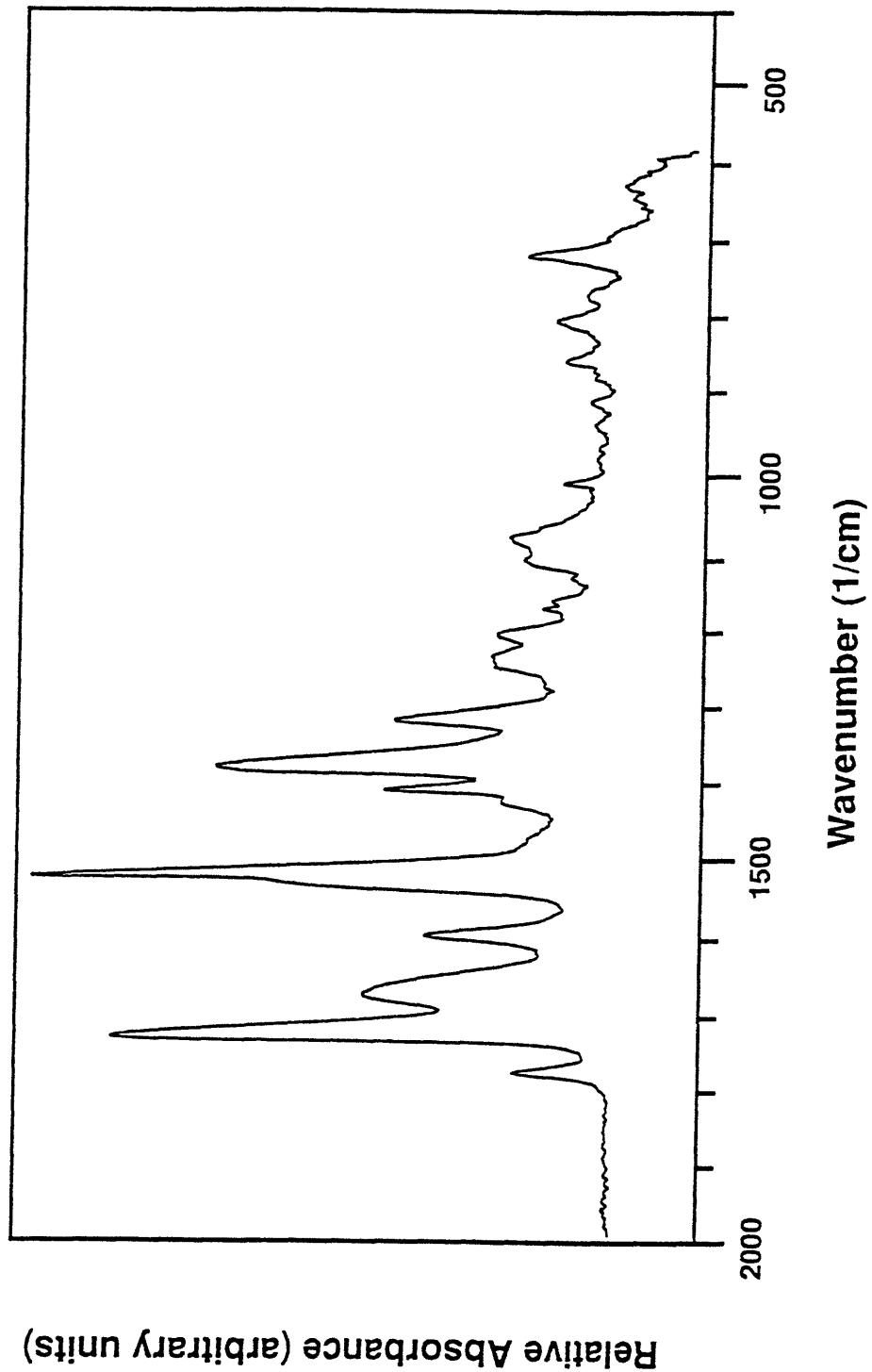


Figure 5.11. Relative absorbance vs. wavenumber for Probimide 32 polyamide-imide coated from 3wt% solids content and softbaked at 110°C, with final film thickness approximately 450Å.

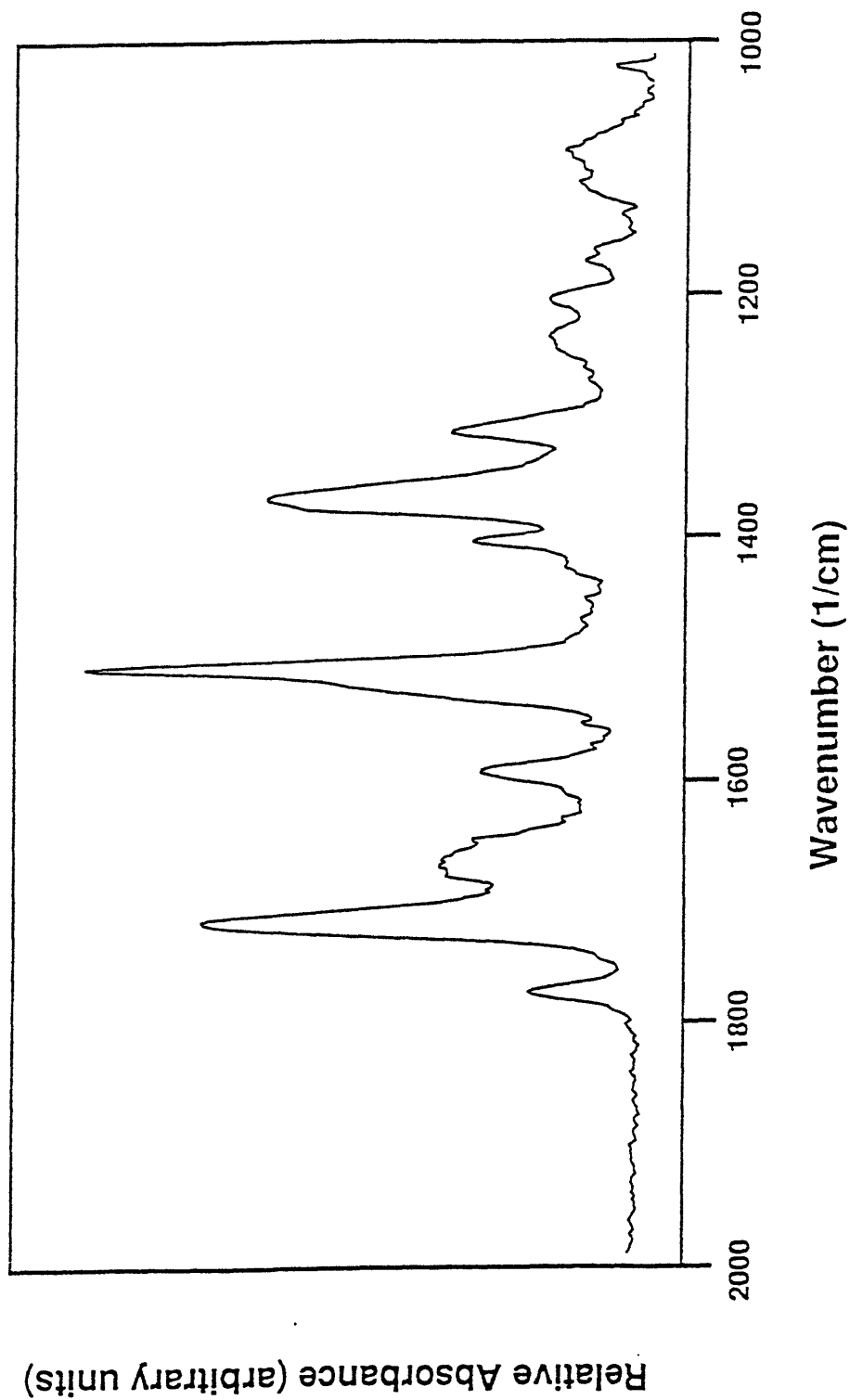


Figure 5.12. Relative absorbance vs. wavenumber for a brushed Probimide 32 polyamide-imide thin film. a.) Incident infrared electric field polarized parallel to the brushing direction.

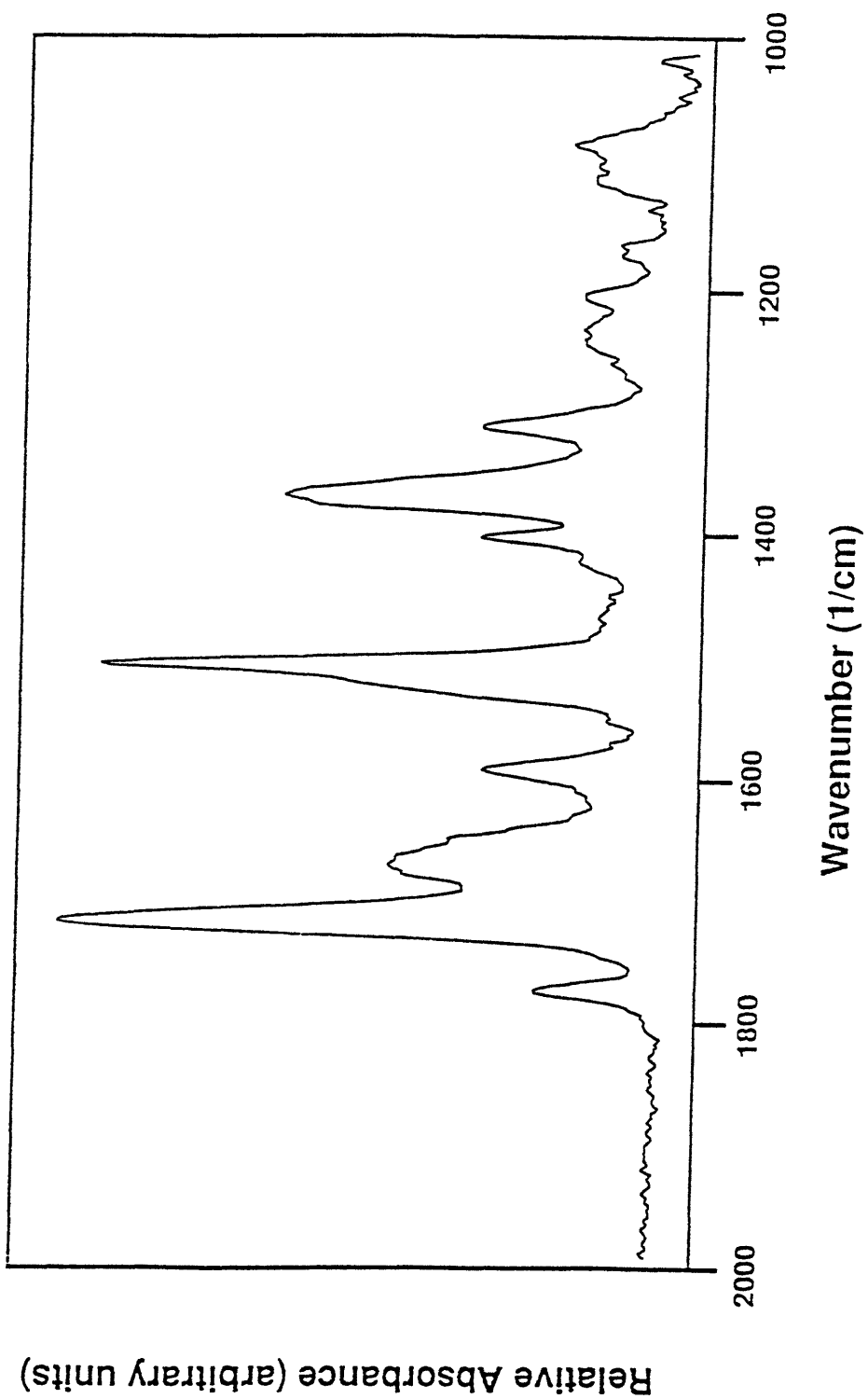


Figure 5.12. continued. b.) Incident infrared electric field polarized perpendicular to the brushing direction.

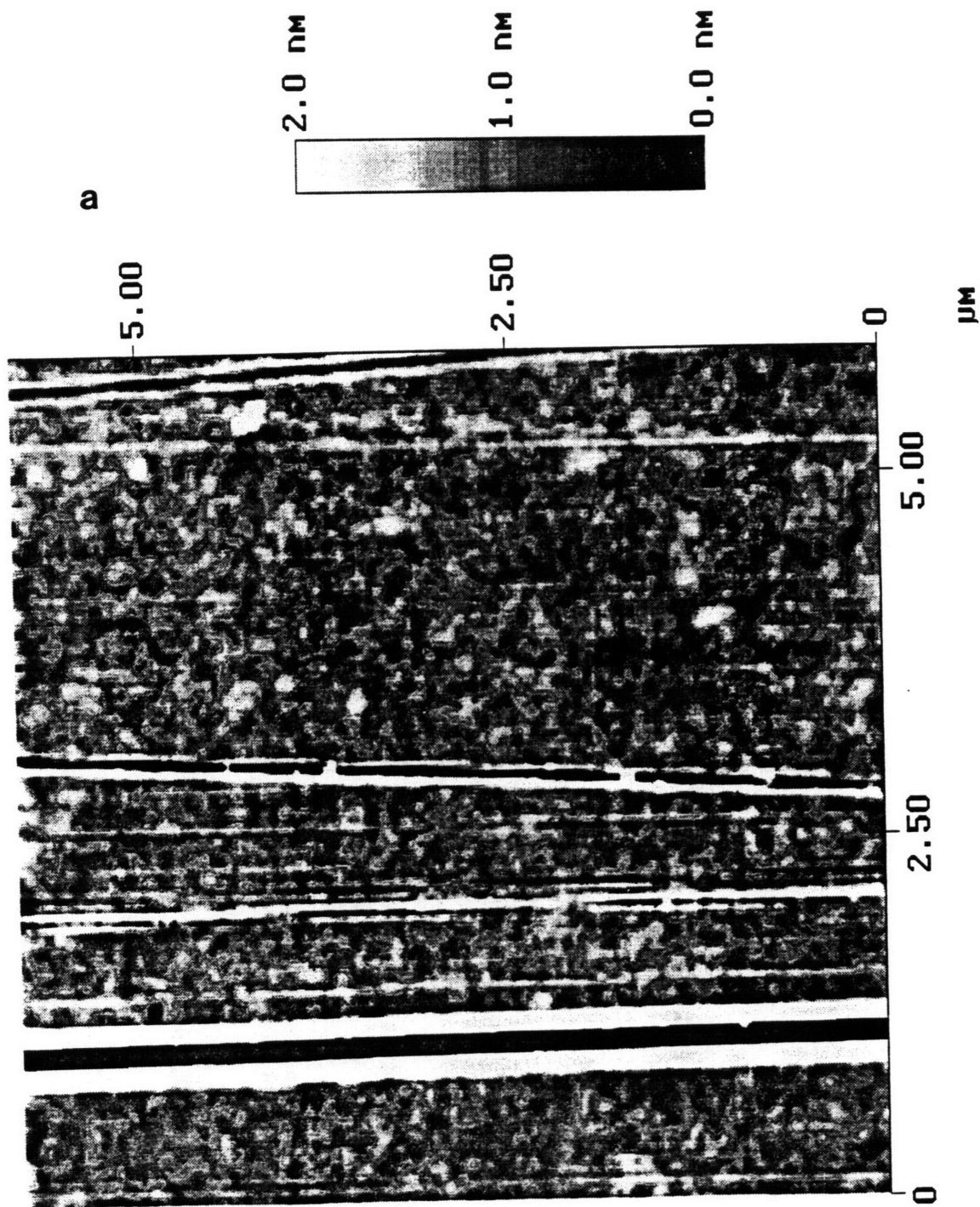


Figure 5.13. Atomic force microscopy (AFM) images of polyamide-imide films. a.) brushed.

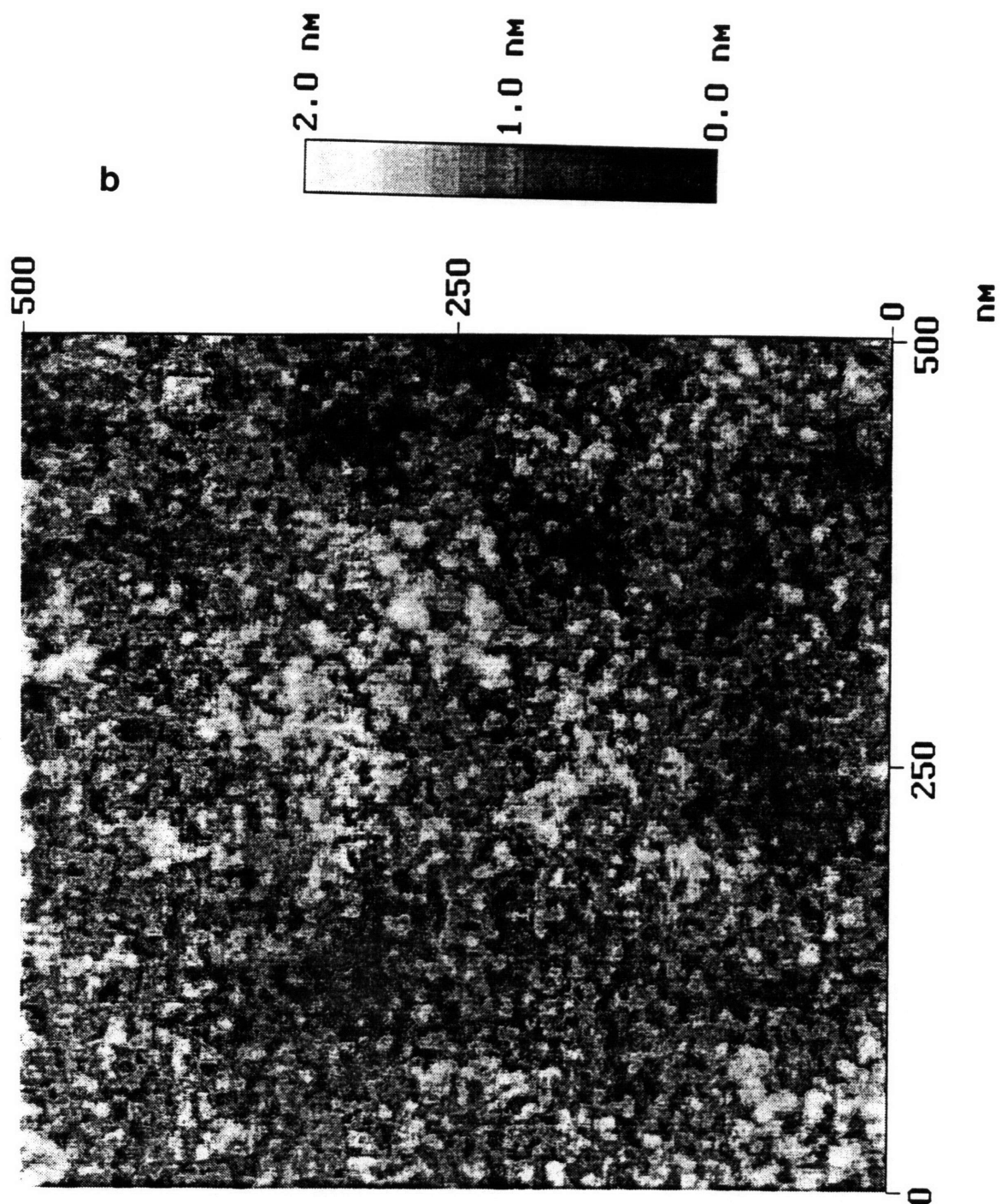


Figure 5.13. continued. b.) unbrushed

Table 5.5. Relative ratios of the heights of the imide N-C (1370 cm^{-1}) peaks to the imide C=O (1720 cm^{-1}) peaks for brushed Probimide 32 layers.

Scan conditions	Absorbance Ratio ($1370 / 1720\text{ cm}^{-1}$)
No brush, unpolarized IR	0.76
IR // Brushing	0.63
IR \perp Brushing	0.86

5.3.5. *In situ* thermal stability of liquid crystal alignment on brushed Probimide 32 polyamide-imide layers.

The surface alignment of the E7 liquid crystals on brushed Probimide 32 alignment layers was stable to very high temperatures. A completely constructed cell was annealed for half an hour at progressively higher temperatures in 20°C intervals from 80°C to 180°C . The cell was cooled after each annealing and the alignment parameter $A = I(0^\circ)/I(45^\circ)$ was measured. Treatment above 180°C damaged the epoxy, thus ruining the cell. The quality of alignment is plotted against annealing temperature in Figure 5.14. The data indicate that the liquid crystals remain strongly aligned throughout the cure cycle.

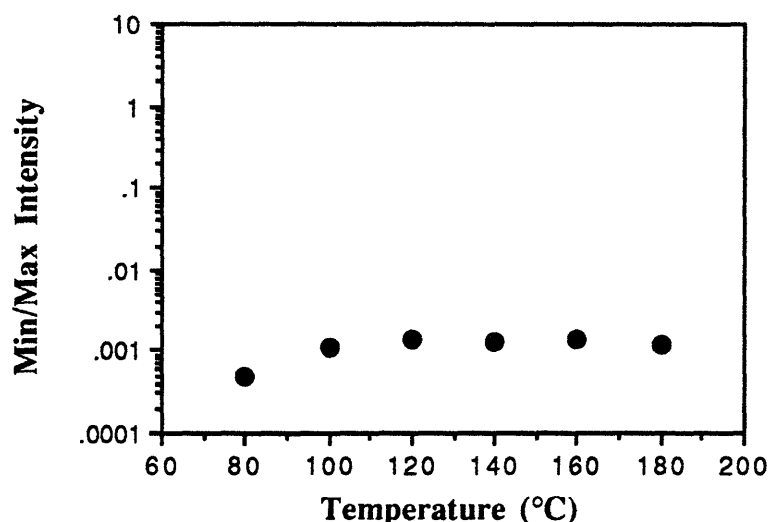


Figure 5.14. $I(0^\circ)/I(45^\circ)$ vs. temperature for a polyamide-imide aligned liquid crystal cell undergoing an annealing cycle of systematically increasing temperature treatments.

5.3.6. “Liquid crystal alignment relaxation” - a new technique for measuring thermal transition temperatures in surface layers.

The technique in the previous section for measuring the *in situ* thermal stability is disadvantageous in that it is limited by the chemical thermal stability of the cell epoxy and the liquid crystals themselves. The following technique was employed to measure the thermal stability of only the polymer alignment films:

1. Coat and cure many polymer alignment layers.
2. Apply brushing treatment.
3. Cure the brushed alignment films at an array of temperatures (with at least two films per treatment temperature). Hold each alignment film at a single temperature for 30 minutes, then cool.
4. Build liquid crystal cells from the post-brush cured alignment films.
5. Measure alignment strength $A = I(0^\circ)/I(45^\circ)$.
6. Plot alignment strength $I(0^\circ)/I(45^\circ)$ vs. post-brush cure temperature.

Probimide 32 polyamide-imide

For cells constructed with Probimide 32 polyamide-imide alignment films, the alignment strength is plotted against post-brush annealing temperature in Figure 5.15. There is a sharp break in the alignment near 270°C as $I(0^\circ)/I(45^\circ)$ changes from approximately 10^{-3} to approximately 10^0 . For post-brush temperatures 300°C and above, $I(0^\circ)/I(45^\circ)$ remains around one, indicating that the alignment is completely destroyed.

The 300°C “alignment relaxation temperature” correlates with the glass transition temperature for solvent-free Probimide 32 found in Chapter 4. The change that occurs in the polymer surface layer can be visualized as shown in Figure 5.16. The original coated surface begins as an isotropic random coil in the plane of the film. The brushing process orients the polymer chains in the direction of brushing. This orientation process is associated with the layer’s ability to align liquid crystals in the brushing direction. When the material is treated above its glass transition temperature, however, the oriented structure

relaxes and the surface's ability to align liquid crystals is irreversibly lost. The alignment with this polymer layer, thus, appears to be associated with the *frozen-in ordering of amorphous chains which relax at T_g* .

The relaxation of the aligning ability of the polymer layer suggests a new technique for measuring the thermophysical transitions in polymer surfaces. It also suggests a way in which processing / structure / property studies of liquid crystal alignment surface layers can be performed. For example, it was observed in Chapter 4 that residual solvent in Probimide 32 bulk films substantially reduced the mechanical softening temperature. The single glass transition temperature observed for the polyamide-imide alignment films near 300°C suggests, in agreement with FTIR results in Section 5.3.3, that the 110°C treated alignment films are essentially free of solvent.

This technique is not a direct measure of the bulk T_g such as that obtained by DSC or DMA. This technique measures the ability of the surface to perform a function, i.e., align nematic liquid crystals. Hence, the relaxation technique measures only the thermophysical properties of the material responsible for aligning the liquid crystals. Authors [18] have suggested that only the first 10-60 nm is responsible for the alignment. It is therefore unclear at this point whether this functional T_g is that of the surface monolayer or of the first several nanometers.

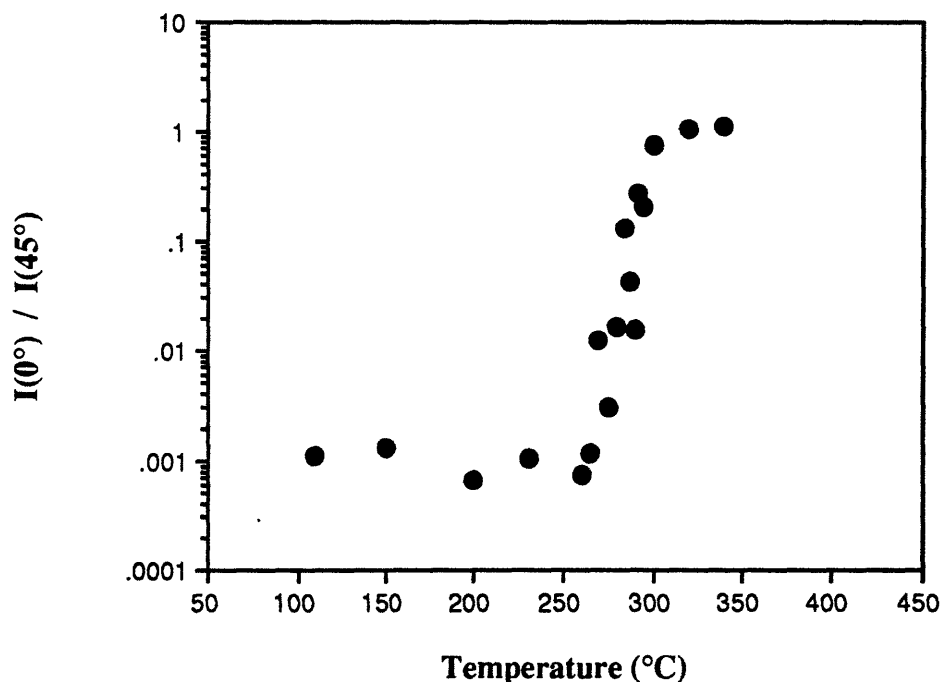


Figure 5.15. $I(0^\circ)/I(45^\circ)$ vs. post-brush cure temperature for liquid crystal alignment cells produced with Probimide 32 polyamide-imide alignment films.

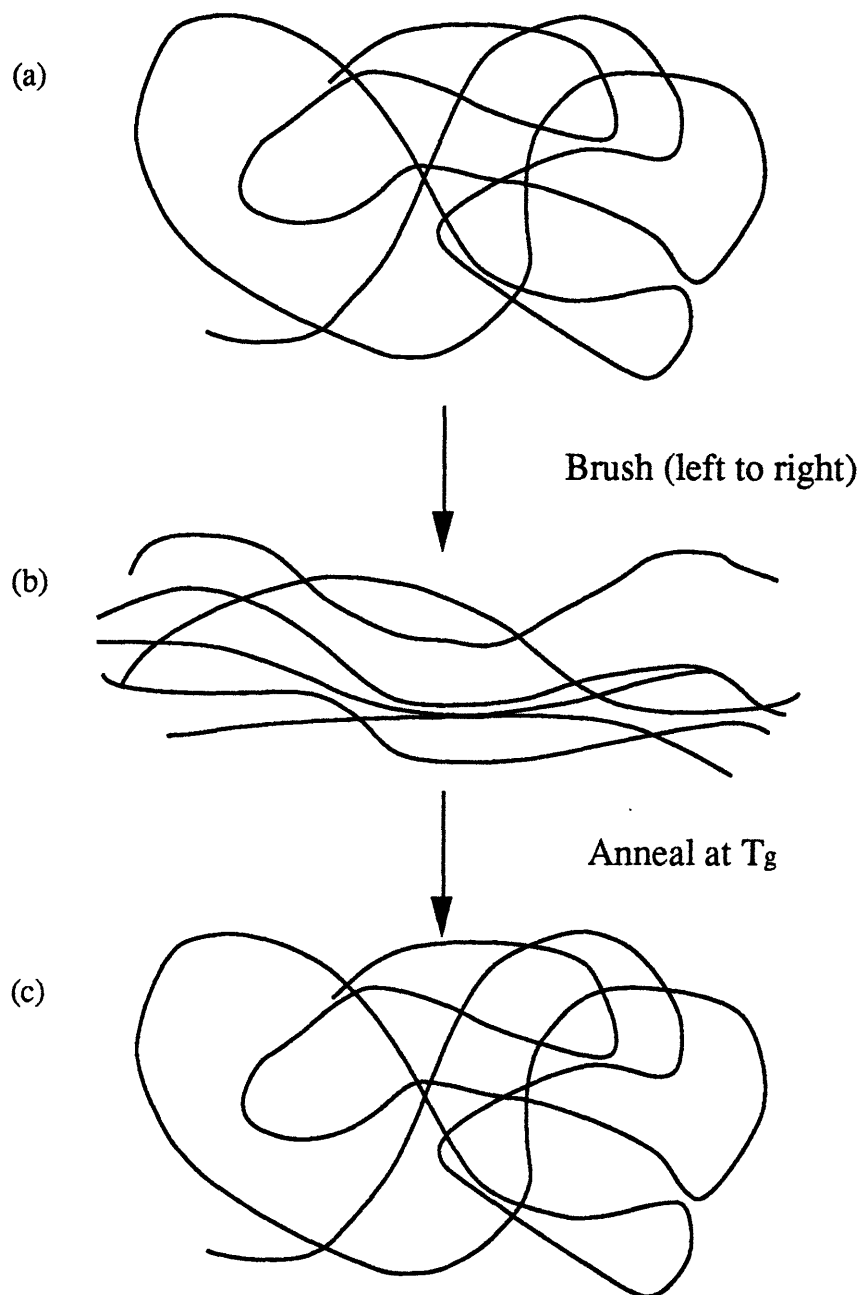


Figure 5.16. Depiction of the structure of the alignment layer films during alignment relaxation process of the polyamide-imide. The amorphous chains begin randomly coiled in the plane of the film (a). They are oriented by the brushing process (b). The orientation is reversed by annealing above T_g (c).

In Chapter 4, it was found that a 300°C curing treatment in air crosslinked the polyamide-imide bulk films, increasing the glass transition temperature. To determine whether this effect can be observed in surface alignment layers, the alignment relaxation methodology was employed. Polyamide-imide alignment films were baked at 300°C in air for 30 minutes. This treatment was expected to induce chemical crosslinks in the material and increase its thermal stability. The films were then brushed to produce liquid crystal alignment. Before building the alignment cells, the films were treated at an array of post-brush curing temperatures in order to see what temperature treatment destroyed the alignment.

The alignment parameter $I(0^\circ)/I(45^\circ)$ is plotted against post-brush curing temperature in Figure 5.17. The data in Figure 5.17 are compared to the data obtained with no pre-brush 300°C air treatment, i.e., the data in Figure 5.15. Clearly, the 300°C air treatment has increased the thermal stability of the films. The alignment material can withstand higher temperature treatments before its aligning capacity is destroyed because the material is chemically crosslinked prior to brushing.

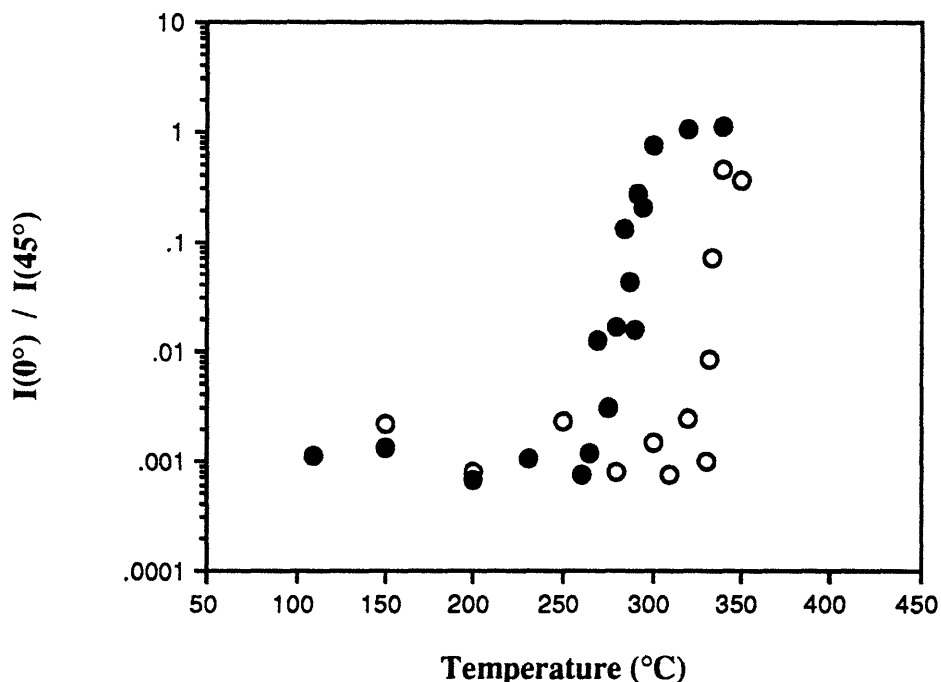
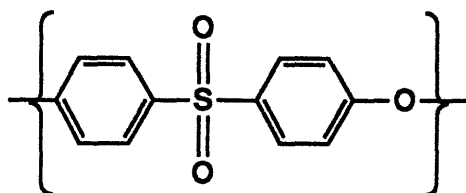


Figure 5.17. $I(0^\circ)/I(45^\circ)$ vs. post-brush cure temperature for liquid crystal alignment cells produced with brushed polyamide-imide that were either softbaked (filled circles) or cured at 300°C in air (open circles) prior to brushing.

Poly(phenylene ether sulfone)

Poly(phenylene ether sulfone) was found to have strong liquid crystal aligning properties. It was selected as a candidate for alignment based on its highly polar backbone and its yellowish color. The chemical repeat unit of this polymer is shown below:



The bulk glass transition temperature is 226°C [34]. The material was obtained as pellets from Scientific Polymer Products and was dissolved to 3wt% solids in N-methyl pyrrolidone. The material was spin coated to form films for liquid crystal alignment cells.

The alignment relaxation technique was employed for the poly(phenylene ether sulfone) films. The relaxation “scan” obtained is shown in Figure 5.18. Destruction of the alignment begins near 210°C and is complete near 230°C, as frozen-in, oriented amorphous chains are relaxed above T_g .

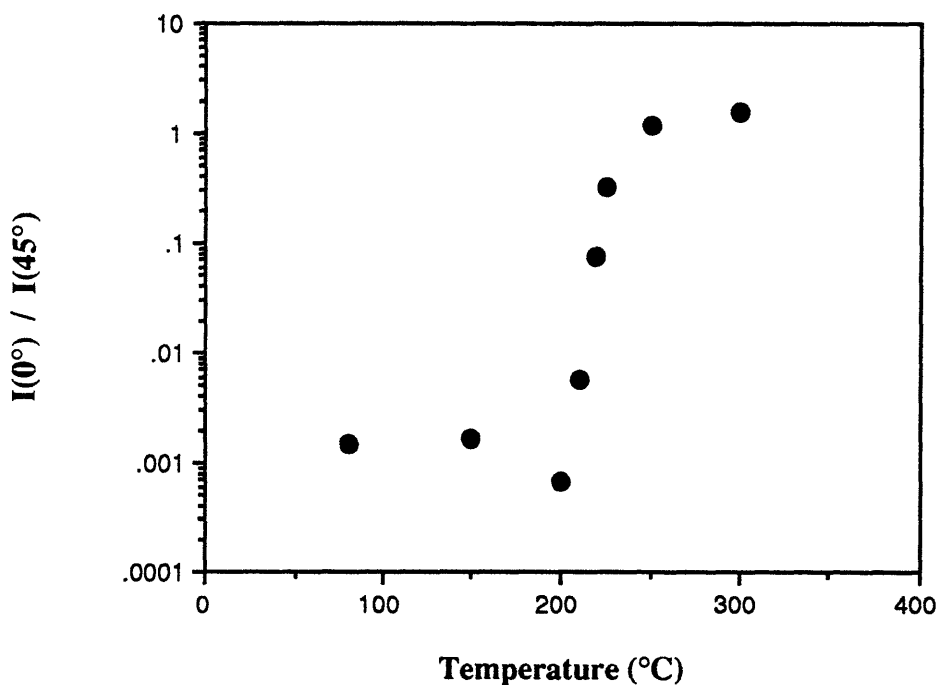
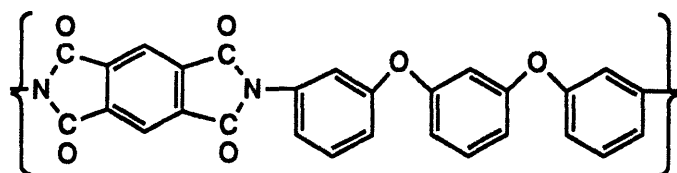


Figure 5.18. $I(0^\circ)/I(45^\circ)$ vs. post-brush cure temperature for liquid crystal alignment cells produced with brushed poly(phenylene ether sulfone) alignment films.

PMDA-APB Polyimide and the Effect of Imidization

The alignment relaxation of PMDA-APB polyimide films was investigated. The polyamic acid precursor solution was obtained from the NASA Langley Research Center as 15wt% solids in dimethylacetamide (DMAc). The polymer solution was diluted in DMAc to 5wt% solids and spin coated onto glass slides for liquid crystal cell construction. The alignment film thicknesses were about 1500Å as measured by a Dektak 8000 profilometer. The chemical repeat unit of the fully imidized polyimide is shown below. St. Clair [35] previously reports a 221°C glass transition temperature for this polymer.



The alignment relaxation technique was employed for the softbaked films and for films baked at 275°C for 1 hour prior to brushing. The $I(0^\circ)/I(45^\circ)$ alignment parameter is plotted against post-brush cure temperature in Figure 5.19. The relaxation temperature is apparently quite low, approximately 170°C, in the softbaked films, Figure 5.19(a), because the material has not yet been converted from polyamic acid to polyimide. The glass transition temperature is much higher in the 275°C pre-brush treated material, Figure 5.19(b). T_g is around 250°C, which is only slightly higher than the previously reported 221°C [35]. Clearly, the imidization reaction has increased the thermal stability of the aligning properties of the material.

A series of PMDA-APB films were also pre-brush cured at 221°C for 30 minutes. The alignment relaxation scan is shown in Figure 5.19(c). The thermal stability limit appears to be below 250°C. However, there appears to be a reversal of the alignment destruction slightly above this temperature. This reversal might be associated with the completion of imidization of the material.

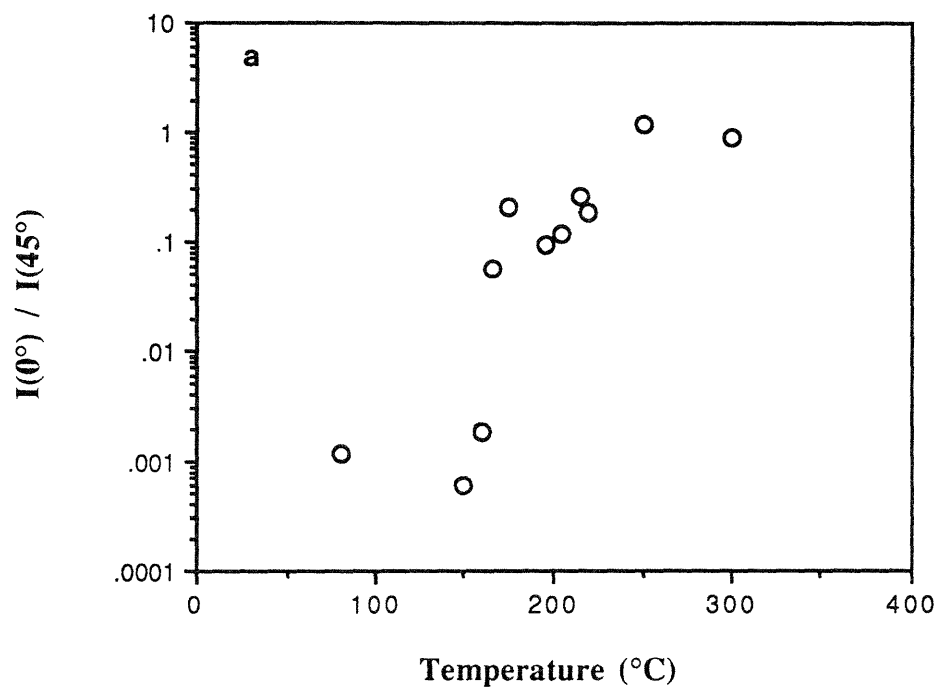


Figure 5.19. $I(0^\circ)/I(45^\circ)$ vs. post-brush cure temperature for liquid crystal alignment cells produced with brushed PMDA-APB alignment films. a.) PMDA-APB poly(amic acid) softbaked only.

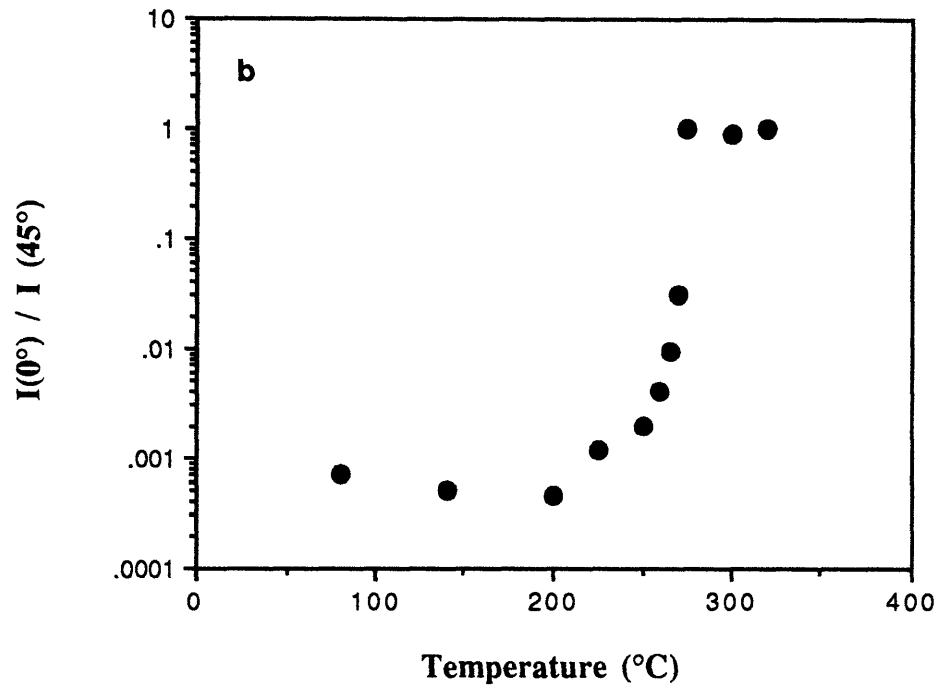


Figure 5.19. continued. b.) PMDA-APB hard baked 275°C 1 hour.

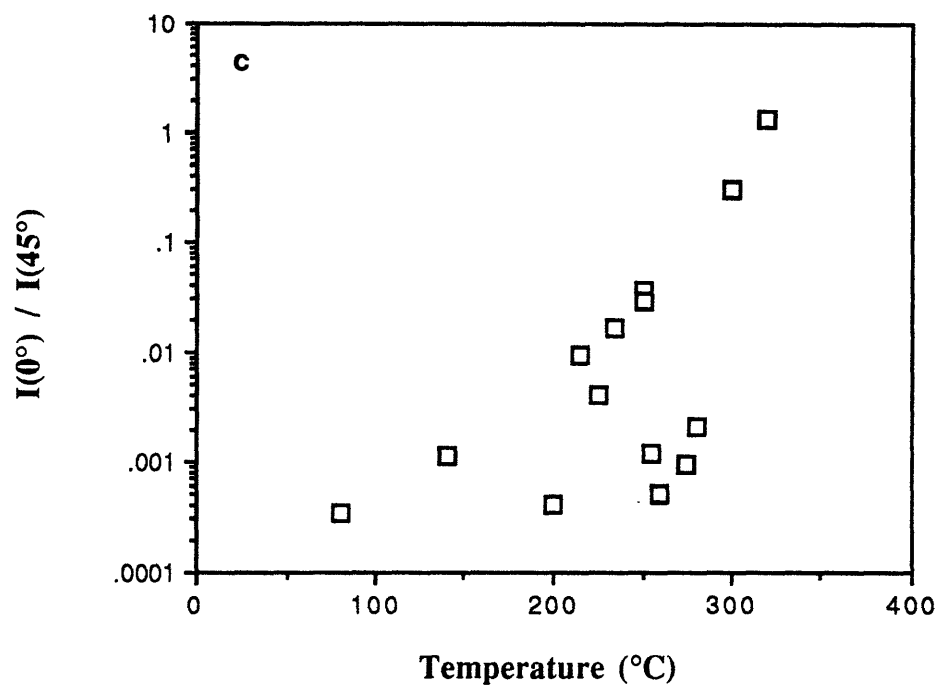


Figure 5.19. continued. c.) PMDA-APB cured at 221 $^\circ\text{C}$ for 30 minutes.

Poly(vinyl alcohol)

Poly(vinyl alcohol) has strong liquid crystal aligning properties. PVA is also known to be a highly crystalline polymer. Based on that fact, it seems less likely that the orientation of amorphous chains could be associated with alignment on PVA layers. 115,000 molecular weight PVA was dissolved at around 80°C as 3 wt% solids content in water. The solution was spin coated onto glass as films for liquid crystal alignment cells.

The relaxation of the alignment is shown in Figure 5.20. There appears to be a transition from aligned to unaligned which begins at around 200°C and appears to be complete at around 225°C. This “thermoalignment” transition is consistent with the melting temperature previously reported by Cebe [36]. Thus, it appears that for PVA, the alignment is associated with the orientation of crystalline material. As the crystals melt, the orientation introduced by the brushing process is destroyed. This data suggests that alignment of liquid crystals on brushed polymer layers is a “phase-neutral” process in the sense that it does not matter whether the polymeric film is crystalline or amorphous.

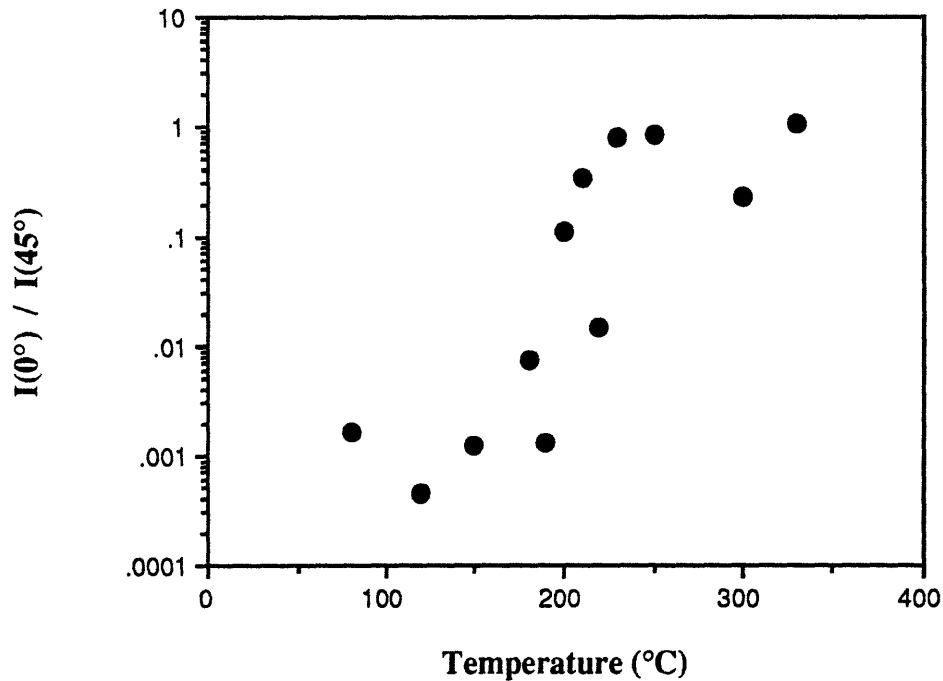


Figure 5.20. $I(0^\circ)/I(45^\circ)$ vs. post-brush cure temperature for liquid crystal alignment cells produced with poly(vinyl alcohol) alignment layers.

5.4. Experimental error

Experimental error was managed by several techniques, some of which have already been discussed. First, systematic error due to twist distortions was minimized by use of the adjustment technique described previously in Section 5.2.2. Error due to variations in cell thickness from sample to sample was minimized by use of the alignment parameter $A=I(0^\circ)/I(45^\circ)$ which should not be a function of cell thickness.

Still, statistical error can arise from variation in both the alignment strength and cell thickness from spot to spot within the sample. This error was minimized by a two-fold strategy. First, many data points were taken for each cell as previously explained in Section 5.2.2. Second, many cells were constructed throughout the course of the research, as is evident by the many data points in Chapters 5 and 6.

For $I(0^\circ)$ and $I(45^\circ)$ measurements of individual cells, the standard deviations of the means were on the order of 50% or less. In order to calculate the alignment parameter $A=I(0^\circ)/I(45^\circ)$ for an individual cell, two mean intensities were divided. The propagated standard deviation, S_w , for this mathematical manipulation of the data is given by [37]:

$$S_w^2 = (1/y^2) S_x^2 + (x^2/y^4) S_y^2 \quad (6)$$

where x is $I(0^\circ)$, y is $I(45^\circ)$, and S_x and S_y are the standard deviations in x and y respectively. For 50% error in $I(0^\circ)$ and $I(45^\circ)$, the propagated error is approximately 71% for $I(0^\circ)/I(45^\circ)$.

The change in $I(0^\circ)/I(45^\circ)$ from a state of strong alignment to a state of no alignment is approximately three orders of magnitude, as $I(0^\circ)/I(45^\circ)$ changes from about 10^{-3} to 10^0 . The error in a single data point is approximately 7% of that change. This clearly supports the conclusion that the transmission method is, in a real and meaningful way, able to distinguish aligned liquid crystals from unaligned liquid crystals.

By taking many data points, the uncertainty in the alignment measurements was reduced. The alignment parameter $A=I(0^\circ)/I(45^\circ)$ was shown to be $1.04 \times 10^{-3} \pm 2.8 \times 10^{-4}$ for brushed polyamide-imide aligned cells. The standard deviation in this measurement is about 27% of A , and only 3% of the change in A that occurs during the transition from the aligned to unaligned state.

To determine whether the measured transition from the aligned to unaligned state is significant, a t-test is performed for the cells produced from softbaked polyamide-imide alignment films (Figure 5.15). For aligned cells with post-brush cure temperatures 265°C and below, the average of the $I(0^\circ)/I(45^\circ)$ values is $1.0 \times 10^{-3} \pm 2.8 \times 10^{-4}$. On the other

hand, for unaligned cells with post-brush cure temperatures 300°C and above, the average of the $I(0^\circ)/I(45^\circ)$ values is 0.98 ± 0.20 .

The quantity t can be calculated according to [37]:

$$t = (x - y) / [(S_x^2/N_x) + (S_y^2/N_y)]^{1/2} \quad (7)$$

where x and y are the two means compared, S_x and S_y are the standard deviations in x and y respectively, and N_x and N_y are number of measurements in x and y . For comparing the data sets of the aligned and unaligned specimens in Figure 5.13, the calculated value of t is about 8.6. According to tabulated critical values of t [37], t would have to be greater than 2.45 in order to conclude that there is a significant difference between these two data sets with 95% certainty, and above 5.96 in order to conclude that there is a significant difference between these two data sets with 99.9% certainty. Thus, clearly, with $t=8.6$, there is a significant difference between the aligned (post-brush cure $\leq 265^\circ\text{C}$) and unaligned (post-brush cure $\geq 300^\circ\text{C}$) data sets with greater than 99.9% certainty.

In conclusion, it is clear that the techniques described in this chapter provide a very real and meaningful measure of the parallel alignment of the liquid crystals. Error in the intensity measurements should not seriously affect the validity of the results.

5.5. Conclusions

Brushed layers of Probimide 32 polyamide-imide parallel-aligned E7 nematic liquid crystals effectively. The main chains of the polyamide-imide are oriented during the brushing process. Also, 450Å films of the preimidized Probimide 32 resin appear to be free of solvent after a 110°C cure.

Polyimide, poly(amic acid), poly(vinyl alcohol), and poly(phenylene ether sulfone) also parallel-align E7 liquid crystals effectively. Empirically speaking, all of these polymers are yellow in color and have highly polar backbones. Polycarbonate and poly(methyl methacrylate) do not appear to produce parallel alignment of the liquid crystals.

The “relaxation of alignment layers” has been introduced as a technique for evaluating thermal transitions in surface layers. When brushed polyamide-imide, PMDA-APB poly(amic acid), PMDA-APB polyimide, and poly(phenylene ether sulfone) layers are treated above their glass transition temperatures, their ability to align liquid crystals is irreversibly lost. This phenomenon has been taken advantage of in order to investigate processing / structure / property relationships in polymer surface layers. In addition, it was found that the ability of brushed layers of highly crystalline poly(vinyl alcohol) to align

liquid crystals was destroyed at its melting temperature, suggesting that polymer surface alignment can involve the orientation of either amorphous or crystalline chains, depending upon the polymer.

5.6. References

1. D. Berreman, *Phys. Rev. Lett.*, **28(26)**, 1683 (1972).
2. D. Berreman, *Mol. Cryst. Liq. Cryst.*, **23**, 215 (1973).
3. U. Wolff, W. Greubel, and H. Kruger, *Mol. Cryst. Liq. Cryst.*, **23**, 187 (1973).
4. E. Lee, Y. Saito, and T. Uchida, *Jpn. J. Appl. Phys.*, **32(12B)**, L1822 (1993).
5. Y. Zhu, L. Wang, Z. Lu, and Y. Wei, X. Chen, and J. Tang, *Appl. Phys. Lett.*, **65(1)**, 49 (1994).
6. D. Seo, H. Matsuda, T. Oh-ide, and S. Kobayashi, *Mol. Cryst. Liq. Cryst.*, **224**, 13 (1993).
7. D. Seo, T. Oh-ide, H. Matsuda, T. Isogami, K. Muroi, Y. Yabe, and S. Kobayashi, *Mol. Cryst. Liq. Cryst.*, **231**, 95 (1993).
8. S. Ishihara, H. Wakemoto, K. Nakazima, Y. Matsuo, *Liquid Crystals*, **4(6)**, 669 (1989).
9. E. Lee, P. Vetter, T. Miyashita, T. Uchida, M. Kano, M. Abe, and K. Sugawara, *Jpn. J. Appl. Phys.*, **32(10A)**, L1436 (1993).
10. Y. Kawata, K. Takatoh, M. Hasegawa, and M. Sakamoto, *Liquid Crystals*, **16(6)**, 1027 (1994).
11. H. Aoyama, Y. Yamazaki, N. Matsuura, H. Mada, and S. Kobayashi, *Mol. Cryst. Liq. Cryst.*, **72**, 127 (1981).
12. N. van Aerle and J. Tol, *Macromol.*, **27**, 6520 (1994).

13. J.M. Geary, J.W. Goodby, A.R. Kmetz, and J.S. Patel, *J. Appl. Phys.*, **62(10)**, 4100 (1987).
14. E. Lee, P. Vetter, T. Miyashita, and T. Uchida, *Jpn. J. Appl. Phys.*, **32**, L1339 (1993).
15. S. Kuniyasu, H. Fukuro, S. Maeda, K. Nakara, M. Nitta, N. Ozaki, and S. Kobayashi, *Jpn. J. Appl. Phys.*, **27(5)**, 827 (1988).
16. N. van Aerle, *J. of the SID*, **2(1)**, 41 (1994).
17. D. Seo, H. Matsuda, T. Oh-Ide, and S. Kobayashi, *Mol. Cryst. Liq. Cryst.*, **224**, 13 (1993).
18. N. van Arle, M. Barmantlo, and R. Hollering, *J. Appl. Phys.*, **74(5)**, 3111 (1993).
19. T. Russell, *MRS Bulletin*, **21(1)**, 49 (1996).
20. M. Ree, T.L. Nunes, and D.P. Kirby, *Polym. Prep.*, **33(1)**, 309 (1992).
21. B. Factor, T. Russell, and M.F. Toney, *Phys. Rev. Lett.*, **66(9)**, 1181 (1991).
22. H. Fukuro and S. Kobayashi, *Mol. Cryst. Liq. Cryst.*, **163** 157 (1988)..
23. Y. Nakajima, K. Saito, M. Murata, and M. Uekita, *Mol. Cryst. Liq. Cryst.*, **237** 111 (1993).
24. D. Seo and S. Kobayashi, *Appl. Phys. Lett.*, **66(10)**, 1202 (1995).
25. D. Seo, S. Kobayashi, and M. Nishikawa, *Appl. Phys. Lett.*, **61(20)**, 1202 (1992).
26. M. Nishikawa, K. Sano, T. Miyamoto, Y. Yokoyama, M. Bessho, D. Seo, Y. Imura, and S. Kobayashi, *Jpn. J. Appl. Phys.*, **33(7A)**, 4152 (1994).

27. S. Ishibashi, M. Hirayama, and T. Matsuura, *Mol. Cryst. Liq. Cryst.*, **225**, 99 (1993).
28. Amoco Ultradel 7100 series photosensitive polyimides, product information.
29. Personal communication, Dr. T. Gardner and Dr. R. Wenz, 3M Corporation.
30. J. Cognard, *Mol. Cryst. Liq. Cryst.*, **78**, Suppl. 1 (1982).
31. Merck E7 nematic liquid crystals, product information.
32. P.G. de Gennes, *The Physics of Liquid Crystals*, Ch. 3, Oxford Press, London, (1975).
33. C. Gooch and H. Tarry, *J. Phys. D: Appl. Phys.*, **8**, 1575 (1975).
34. Scientific Polymer Products, Inc., product information guide.
35. T.L. St. Clair, in *Polyimides*, p. 58, D. Wilson, H.D. Stenzenberger, and P.M. Hergenrother, Eds., Blackie, Glasgow (1990).
36. P. Cebe, Ph.D. Thesis, Cornell University (1984).
37. *Laboratory Techniques Manual*, Ch. 3, Department of Chemistry, Massachusetts Institute of Technology (1979).

Chapter 6. Alignment of Liquid Crystals on Photo-irradiated Polyamide-imide Layers.

6.1. Introduction

In the previous chapter, the alignment of nematic liquid crystals on brushed polymer layers was discussed. As mentioned in Chapter 1, there is demand for techniques of alignment which do not require the surface to undergo a contact treatment. Techniques have been investigated to accomplish this, one of which is the exposure of a polymer layer to linearly polarized light. In this chapter, it is shown that the Probimide 32 polyamide-imide can be processed as a photo-induced surface alignment material.

Schadt *et al.* [1] previously showed that films of poly(vinyl methoxycinnamate) (PVMC) exposed to linearly polarized ultraviolet light were effective as surface alignment agents for nematic liquid crystals. The authors used a preferential crosslink argument to explain the phenomenon. One serious disadvantage of using a cinnamate polymer for alignment, however, is that it is a relatively obsolete photoresist material. It is not produced today in large, commercial quantities, nor does it sell at low cost.

Hasegawa and Taira [2] recently showed that an aromatic/aliphatic polyimide produced liquid crystal surface alignment upon exposure of the films to linearly polarized short wave ($\lambda=257$ nm) ultraviolet. This result was quite interesting because the polymer was not specifically designed for photosensitivity. The authors used a depolymerization argument, discussed in Chapter 1, to explain the alignment. One disadvantage of the technique was that the alignment was attained only in a very narrow range of exposure dosage, above and below which, no alignment was achieved. This could present difficulties, for example, in reproducing the alignment scheme should any processing conditions change.

In this chapter, a technique of alignment which uses the photo-irradiation of polyamide-imide films is introduced. The photo-alignment process is compared to the rubbing process. Information is also sought about the mechanism of alignment.

6.2. Experimental Section

6.2.1. The photo-alignment technique

The Probimide 32 polyamide-imide films and liquid crystal cells were produced as described in the experimental section of the previous chapter, section 5.2.1. The brushing

alignment was replaced here, however, with the linearly polarized ultraviolet (LP-UV) exposure process shown in Figure 6.1. The films were irradiated under a Spectroline Model R-51A short wavelength ($\lambda=254\text{ nm}$) ultraviolet lamp. The UV was passed through an Ealing UV polarizer prior to incidence upon the bare alignment films. The films were irradiated at a constant two inch distance from the lamp. The area-normalized exposure rate was approximately $1\text{ mW}/\text{cm}^2$. The alignment was evaluated by the qualitative approach and laser optical transmission technique discussed in section 5.2.2.

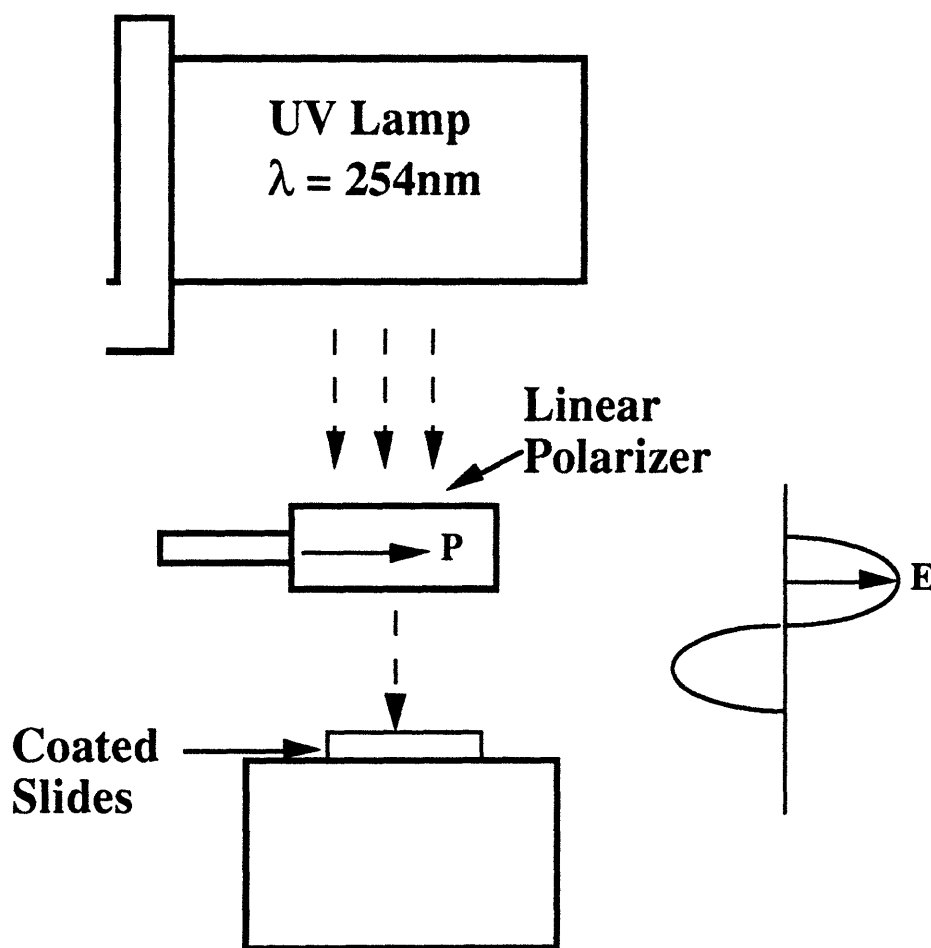


Figure 6.1. Exposure technique for irradiating alignment films with linearly polarized ultraviolet light (LP-UV).

6.2.2. Comments regarding the methodology by which PAI was selected

It would be appropriate here to make some brief remarks regarding the way in which photo-alignment in the polyamide-imide was discovered. The Probimide 32 polyamide-imide was not selected as a candidate for photo-alignment studies with any foreknowledge of its ability to align liquid crystals. In fact, many non-contact alignment techniques were attempted before a successful technique was found. Producing liquid crystal alignment by exposure of short wavelength LP-UV to virtually every alignment material discussed in Chapter 5 was attempted. Exposure of inherently photosensitive polyimide materials, discussed in Chapters 1 and 3, to LP-UV of i-line wavelength, which crosslinks the material, was also tried. A non-contact, air jet brushing approach, and many variations of it, were also attempted. However, the only technique which produced the desired effect of inducing alignment was exposure of the polyamide-imide to 254 nm LP-UV. In conclusion, the discovery of the photo-aligning properties in the Probimide 32 polyamide-imide was a culmination of an almost Edisonian style attack. Often, however, this is the only effective way of attaining a desired result.

6.3. Results and Discussion

6.3.1. Evidence of liquid crystal alignment upon LP-UV exposure

Qualitatively, it was apparent that the LP-UV exposure to the polyamide-imide films induced parallel alignment of the E7 liquid crystals. Cells produced from LP-UV exposed polyamide-imide films exhibited a pattern of 90° extinctions consistent with an aligned material, while cells produced from unexposed and unbrushed films were bright, i.e., exhibited no extinctions, when placed between crossed polarizers.

The alignment was therefore investigated by laser optical transmission. A liquid crystal cell with the alignment films irradiated with LP-UV for 25 minutes was rotated between the polarizer and analyzer with the alignment axis representing the 0° reference axis. For a given rotation angle ϕ , the optical transmission $I(\phi)$ for a perfectly aligned system is expected to follow the equation:

$$I(\phi)/I(45^\circ) = \sin^2(2\phi) \quad (1)$$

which is plotted in Figure 1.13 in Chapter 1. In Figure 6.2, the normalized optical transmission $I(\phi)/I(45^\circ)$ is plotted against ϕ for the LP-UV aligned cell. The curve closely approximates the theoretical curve from Figure 1.13, thus indicating the the LP-UV irradiated polyamide-imide films effectively align the liquid crystals. The minimum $I(\phi)/I(45^\circ)$ at the 0° , 90° , and 180° extinction angles, though greater than the theoretical zero, is near 10^{-3} , which is comparable to brush aligned cells.

The alignment parameter $A=I(0^\circ)/I(45^\circ)$ is plotted in Figure 6.3 as a function of LP-UV exposure dosage to the polyamide-imide layers. For very small dosages A is near unity, indicating the absence of alignment. As exposure time increases, however, A declines, indicating that the LP-UV treatment to the polyamide-imide is inducing alignment in the liquid crystals. The alignment is very strong after about 25 minutes of exposure, where $I(0^\circ)/I(45^\circ)$ is comparable to the $I(0^\circ)/I(45^\circ) \approx 10^{-3}$ obtained in Chapter 5 for brush-aligned liquid crystal cells. The alignment remains strong for long exposure times. Hence, it is shown that the window of exposure time required to produce alignment is quite wide.

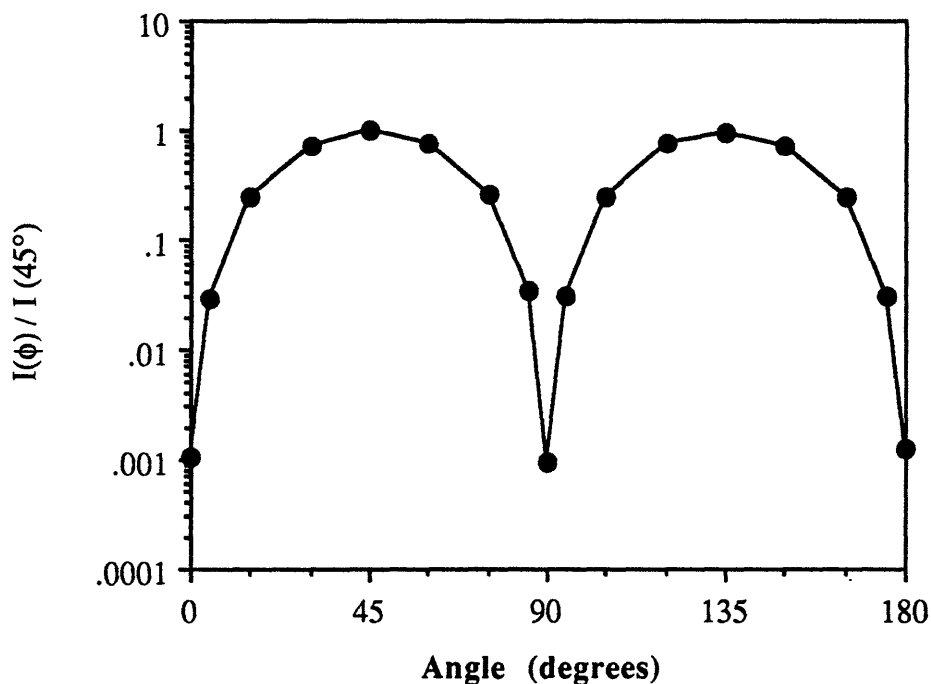


Figure 6.2. $I(\phi)/I(45^\circ)$ vs. rotation angle for liquid crystal alignment cell produced with polyamide-imide alignment layers that have been irradiated with LP-UV for 25 minutes.

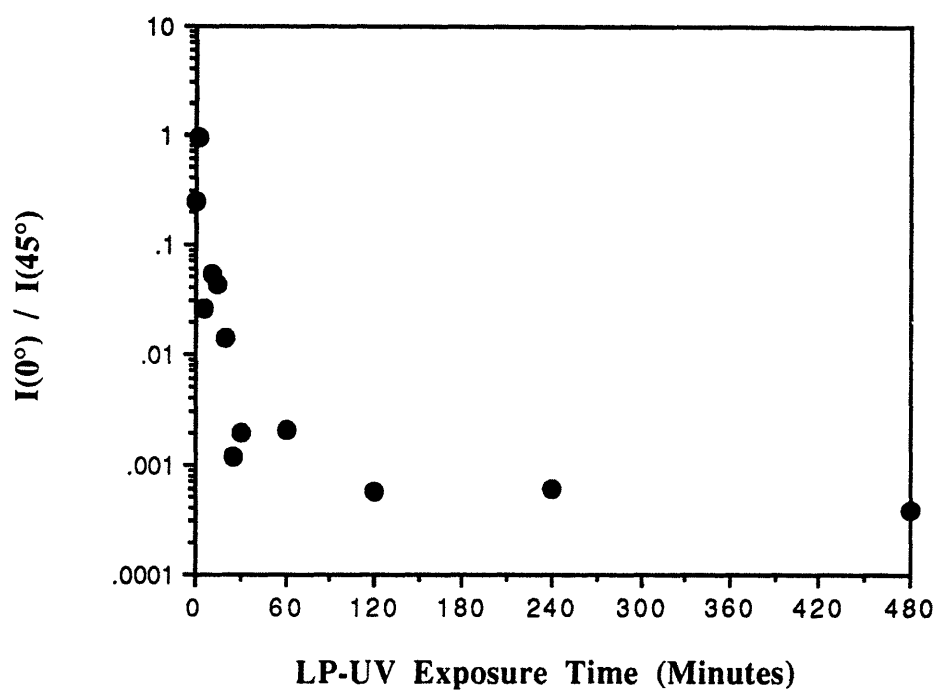


Figure 6.3. $I(0^\circ)/I(45^\circ)$ vs. LP-UV exposure time for liquid crystal cells produced with LP-UV irradiated polyamide-imide alignment films.

6.3.2. Effects of unpolarized UV exposure

Fourier transform infrared spectroscopy

It was desired to understand how the ultraviolet irradiation affects the polyamide-imide alignment film. FTIR spectra of unexposed and UV exposed polyamide-imide films are shown in Figure 6.4. The region in which changes can clearly be seen is in the 1200-1900 cm^{-1} range. The unexposed polyamide-imide film (Figure 6.4(a)) was irradiated with unpolarized UV for one hour with an area-normalized exposure rate of approximate $7\text{mW}/\text{cm}^2$ (Figure 6.4(b)). The most apparent change is the reduction in C=C phenyl stretching near 1500 cm^{-1} which declines about 50% in peak height relative to C=O stretching at 1720 cm^{-1} from the unexposed to exposed samples. Also, the N-C imide vibration at 1370 cm^{-1} declines in height about 25% relative to the 1720 cm^{-1} peak. In addition, the amide carbonyl band at 1680 cm^{-1} recedes into a shoulder upon UV exposure. These changes suggest that there are bond degradation reactions occurring in the polymer upon exposure to UV with the phenyl rings the primary site.

Alignment layer relaxation

Upon exposing a polymeric material to extreme conditions, such as to high temperatures or to irradiation, bond breaking, and possibly bond reformations, often occur. The net effect on structure and properties will often depend upon whether crosslinking or chain scission dominate the process. In Chapter 4, for example, it was found that upon heating the bulk films to high temperatures in air, chemical changes lead to a net increase in molecular weight. This was indicated by an increase in T_g and reinforcement of the rubbery modulus that was apparent in the bulk dynamic mechanical spectra.

The effect of UV on the alignment films is difficult to measure, however, via conventional bulk film measurements. For spin coated films $4\mu\text{m}$ thick, several hours of UV lamp exposure has no apparent effect on the FTIR spectra of the material. Kambe [3] reports that very long UV lamp exposure times, on the order of hundreds of hours, are required to degrade the bulk mechanical properties of aromatic polyimides, polyamides, and polyamide-imides. In any case, it may not be reasonable to assume that the effects of long term exposure on bulk films are similar to the changes that occur in the surface layers upon shorter exposures.

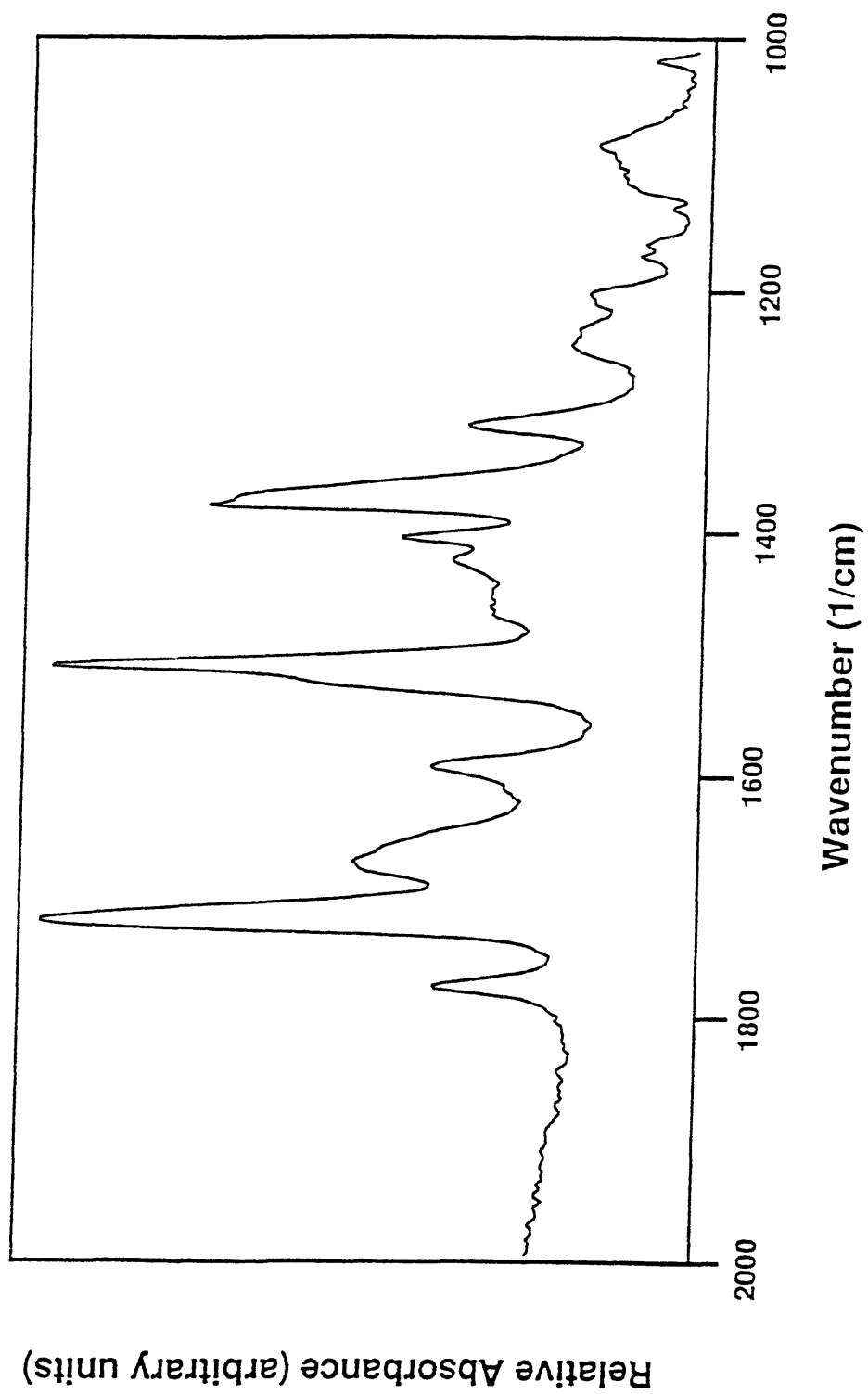


Figure 6.4. Relative absorbance vs. wavenumber for a Probimide 32 polyamide-imide film. a.) unexposed to UV, and

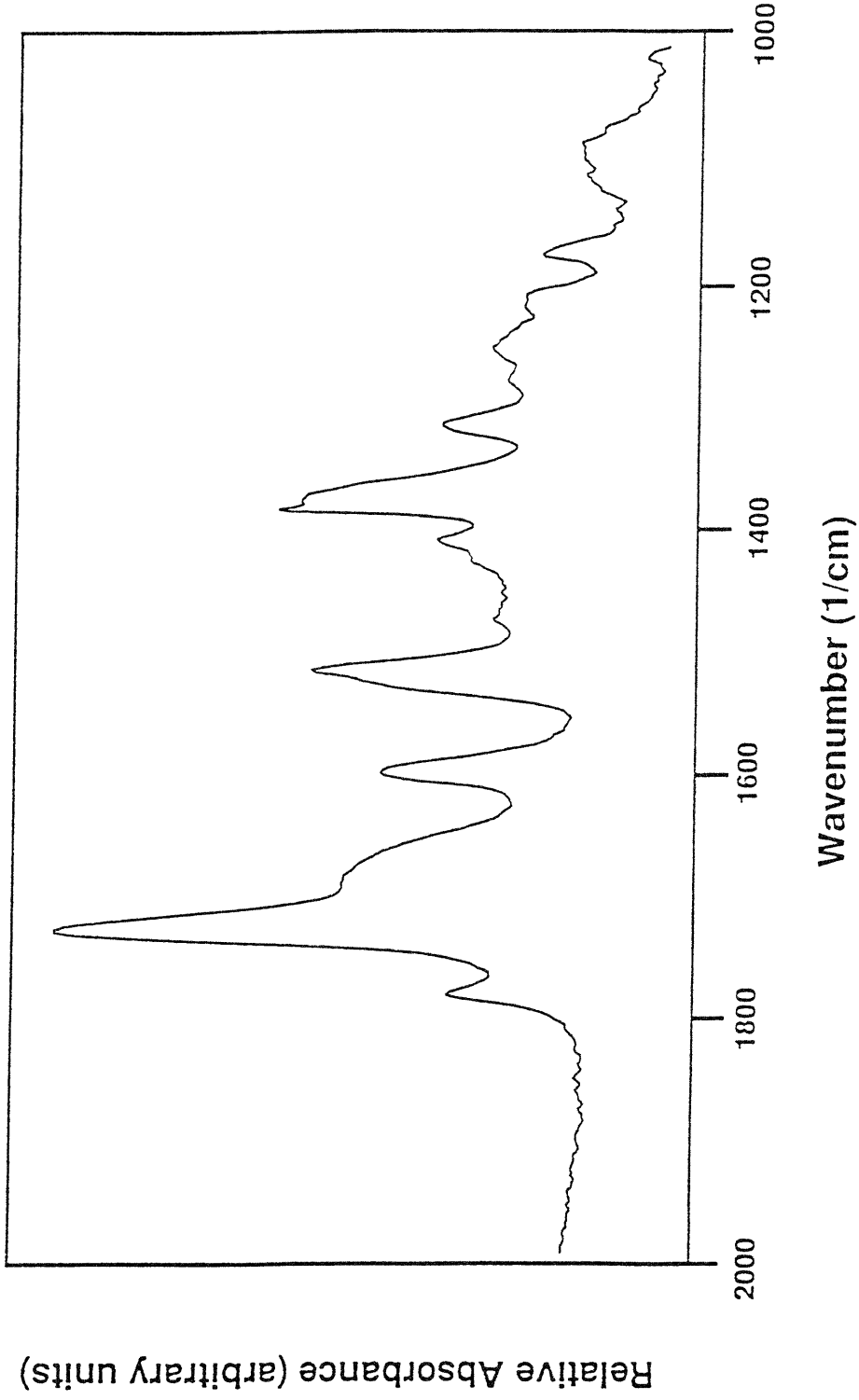


Figure 6.4. continued. b.) exposed to UV.

Fortunately, a technique called alignment layer relaxation, through which the thermal stability of surface layers can be investigated, was introduced in Chapter 5. This method was used here to evaluate the changes in thermal stability of UV irradiated polyamide-imide surfaces. Polyamide-imide alignment films on glass were exposed to unpolarized UV for 2 hours. The films were brushed with rayon, and consequently cured at an array of temperatures. Liquid crystal cells were built, and $I(0^\circ)/I(45^\circ)$ for the cells was plotted against post-brush cure temperature. The results, shown in Figure 6.5, indicate that the UV exposure reduces the T_g of the surface layers. This suggests that chain scission reactions dominate upon exposure to short wavelength UV. This furthermore suggests that the photo-aligning process in the polyamide-imide is associated with depolymerization rather than with crosslinking.

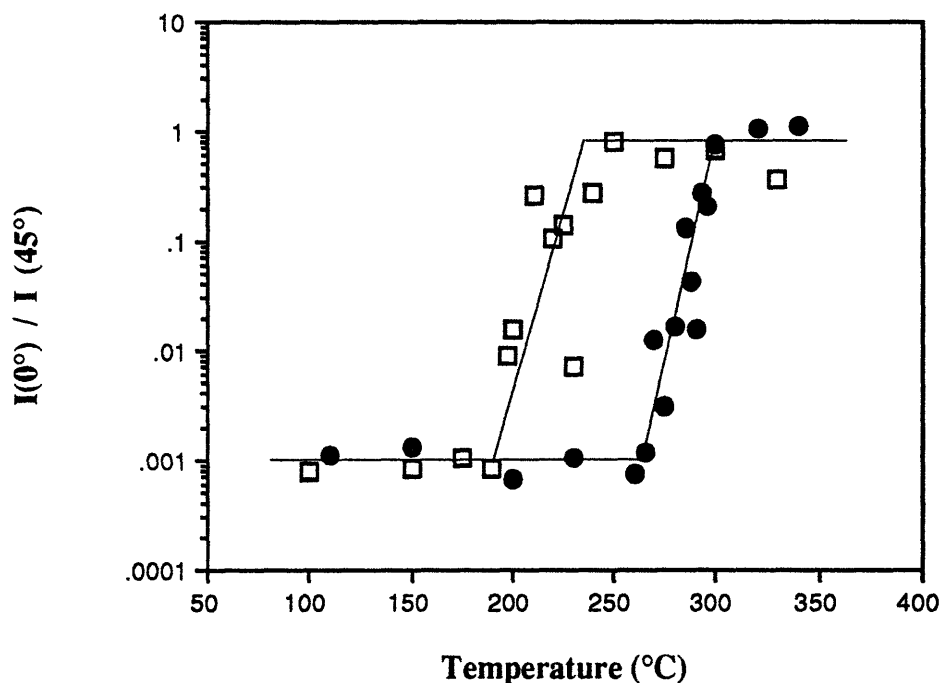


Figure 6.5 $I(0^\circ)/I(45^\circ)$ vs. post-brush curing temperature for liquid crystal cells produced with UV exposed (squares) and unexposed (circles) polyamide-imide alignment layers.

6.3.3. Effects of linearly polarized UV exposure

Fourier transform infrared spectroscopy

Linearly polarized UV and unpolarized UV appear to affect the polyamide-imide in a similar way. Furthermore, dichroic FTIR spectra of LP-UV exposed material in Figure 6.5, in contrast with brushed layers, do not indicate the development of anisotropy. The linearly polarized UV appears to reduce the height of the absorption at 1500 cm^{-1} after 2 hours of LP-UV exposure (Figure 6.6(a,b)), and even more after 4 hours of LP-UV exposure (Figure 6.6(c,d)). This change was also observed previously as a result of the unpolarized UV treatment.

FTIR spectra taken with the incident IR axis polarized parallel to the LP-UV axis (Figure 6.6(a,c)) appear to be identical to those taken with the incident IR perpendicular to the LP-UV axis (Figure 6.6(b,d)). This is dissimilar to dichroic FTIR data for the brushed polyamide-imide which indicated that the main chains were oriented in the direction of the brushing. These data of the LP-UV exposed sample suggest that the linearly polarized UV, unlike the brushing, does not physically move the polymer chains with respect to the LP-UV axis. It is also possible that the dichroism produced is too small to detect by conventional FTIR. This could be the case, for example, if orientation exists in only the first monolayer. Because the mechanism of liquid crystal alignment on polymer surfaces is not entirely understood, it is difficult to speculate as to what exactly is the mechanism of the UV-induced surface alignment for the polyamide-imide.

Alignment layer relaxation

The alignment layer relaxation method was applied for liquid crystal cells aligned with unbrushed, but LP-UV exposed, polyamide-imide layers. Many films were exposed to 2 hours of LP-UV, a treatment which was shown previously (see Figure 6.3) to produce strong liquid crystal alignment. The films were cured at an array of temperatures, and liquid crystal cells were built. The value of $I(0^\circ)/I(45^\circ)$ is plotted against post-UV-alignment curing temperature in Figure 6.7. It is apparent that the LP-UV exposed layers do in fact show a thermal transition. This result indicates that, though ordering in the LP-UV exposed alignment layers was not detected by FTIR, the relaxation of the film surface reverses the liquid crystal aligning properties introduced by the LP-UV. It is also apparent that chain scission caused by exposure to the LP-UV reduces the glass transition temperature of the polyamide-imide surface layer.

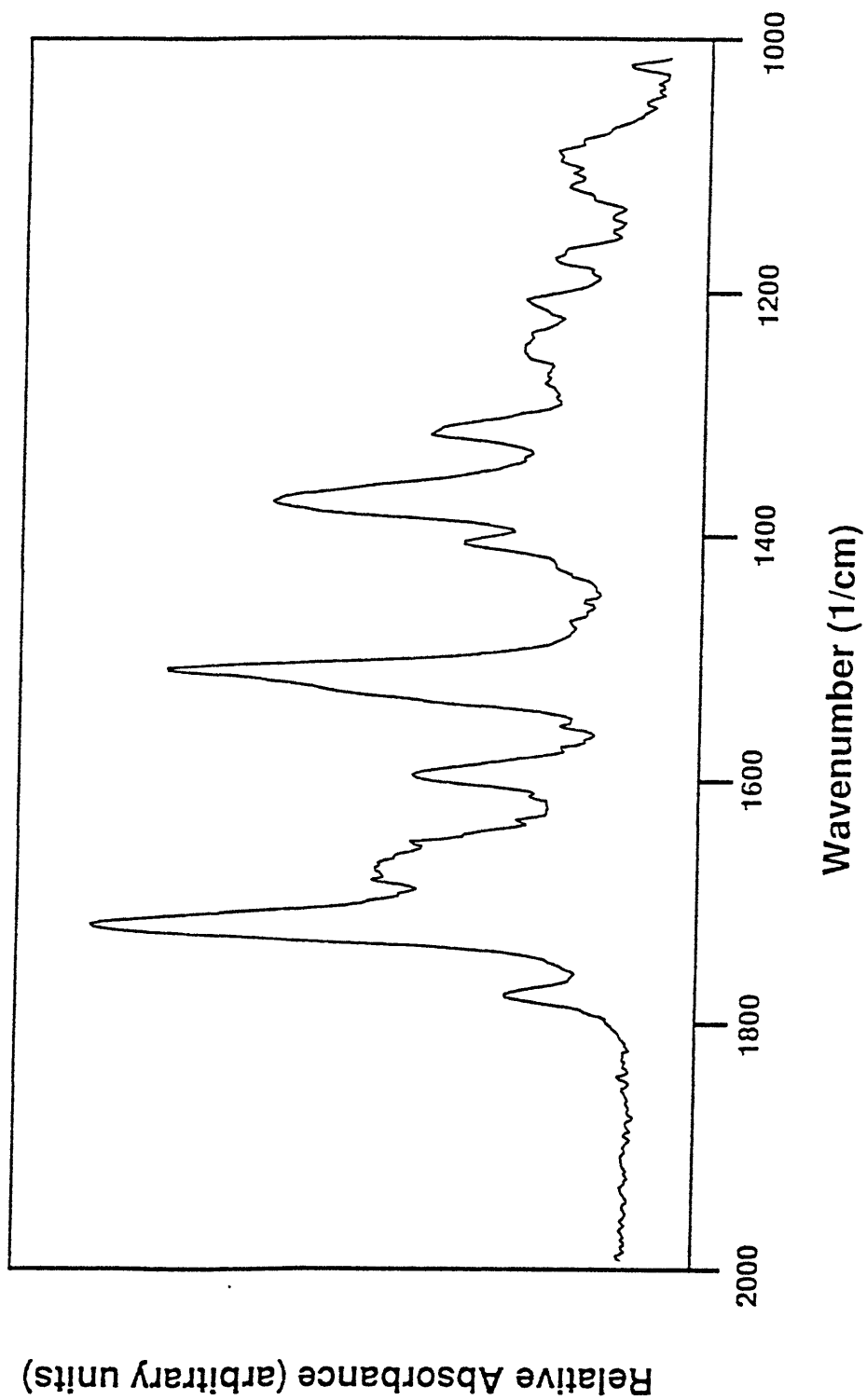


Figure 6.6. Relative absorbance vs. wavenumber for polyamide-imide layers exposed to linearly polarized ultraviolet ($\lambda=245$ nm). a.) 2 hour exposure, UV axis parallel to incident IR axis,

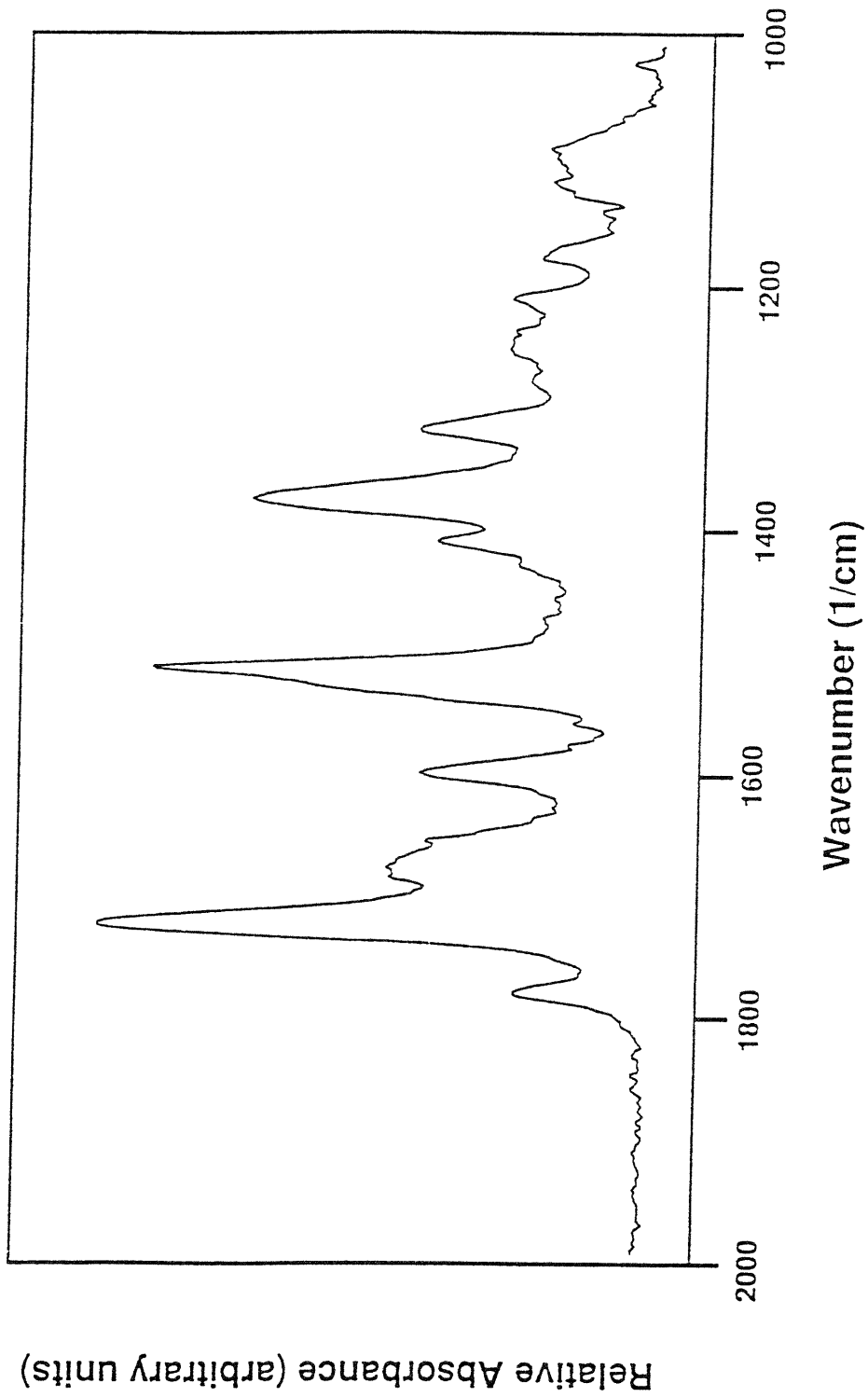


Figure 6.6. continued. b.) 2 hour exposure, UV axis perpendicular to incident IR axis,

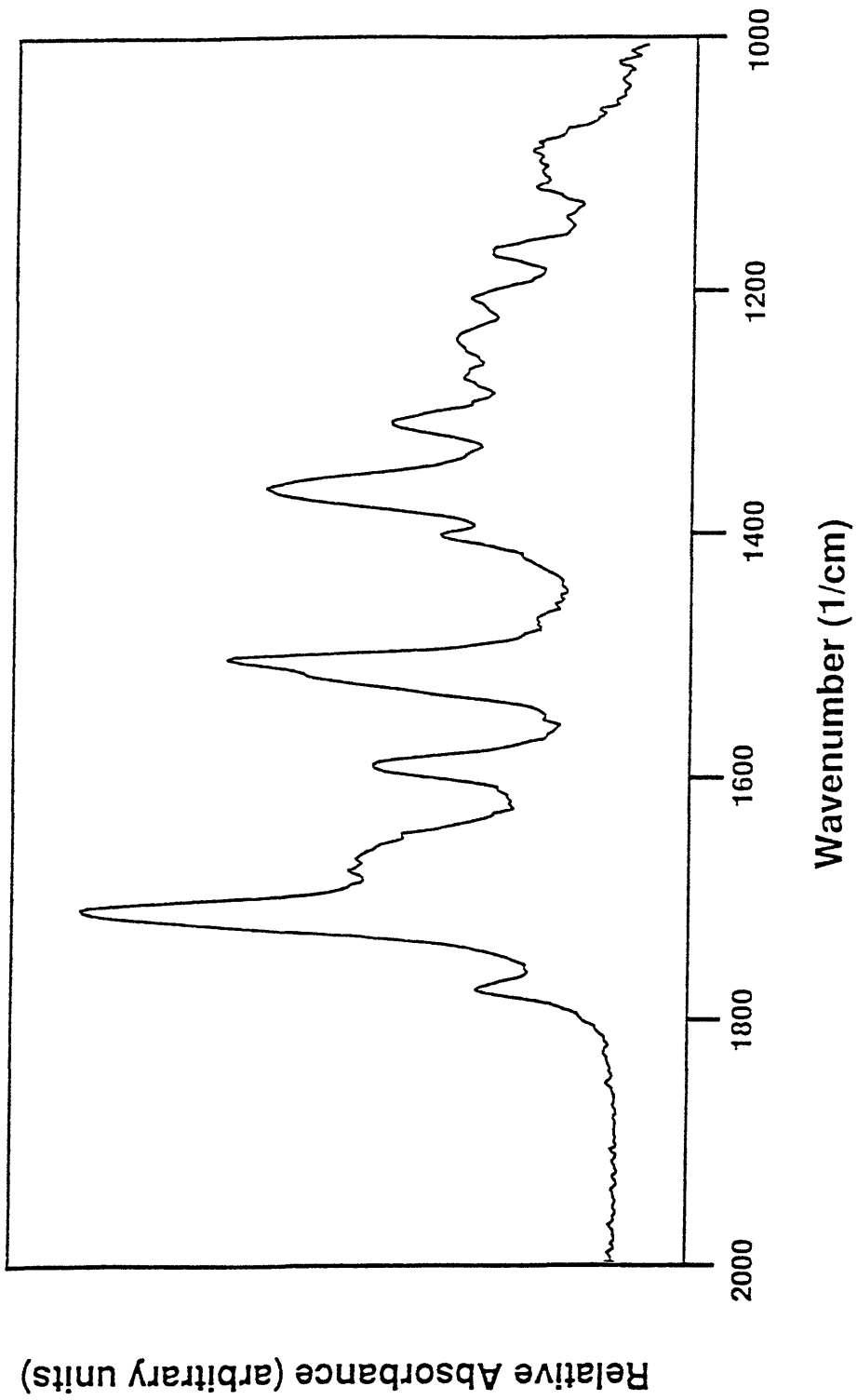


Figure 6.6. continued. c.) 4 hour exposure, UV axis parallel to incident IR axis,

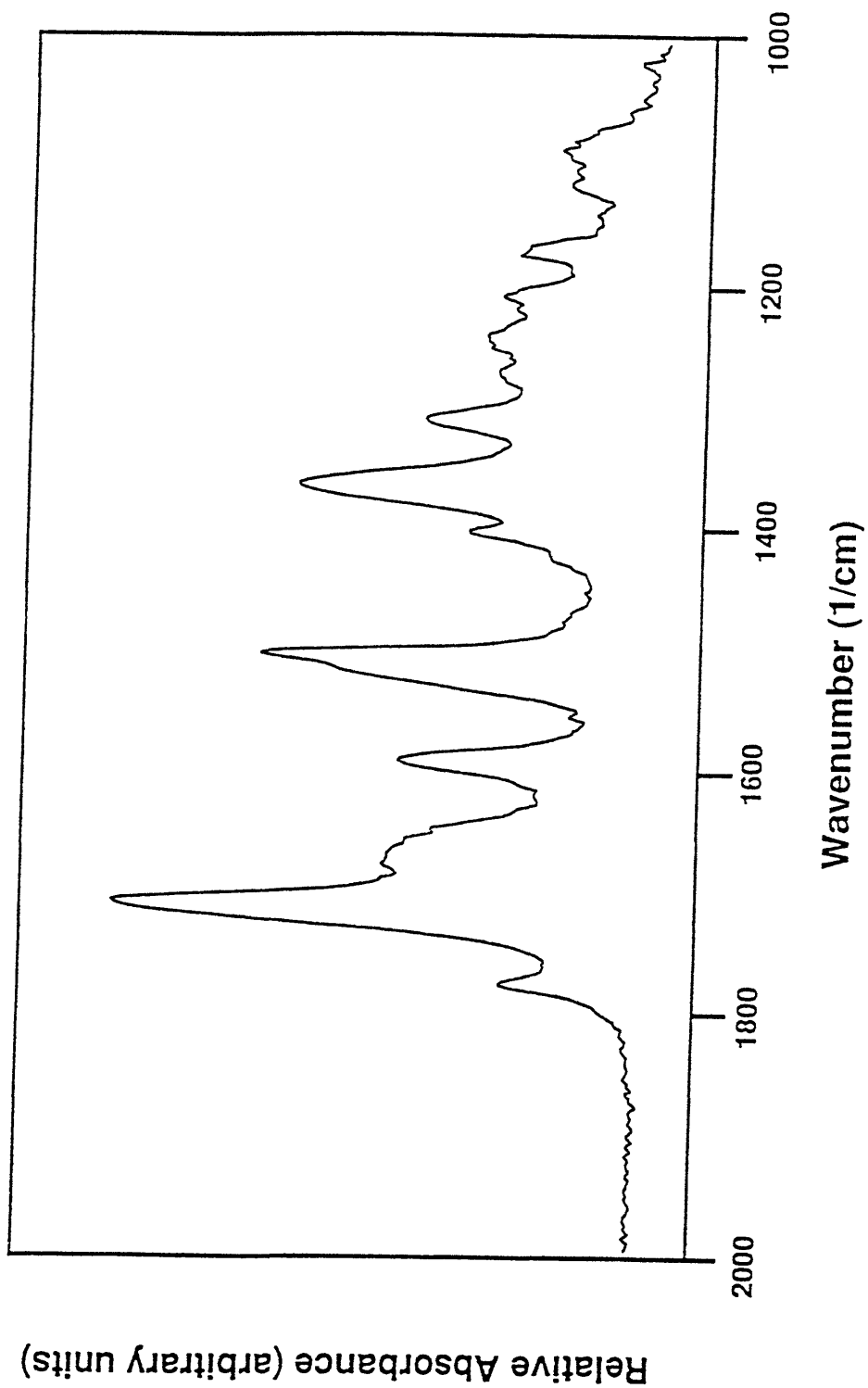


Figure 6.6. continued. d.) 4 hour exposure, UV axis perpendicular to incident IR axis.

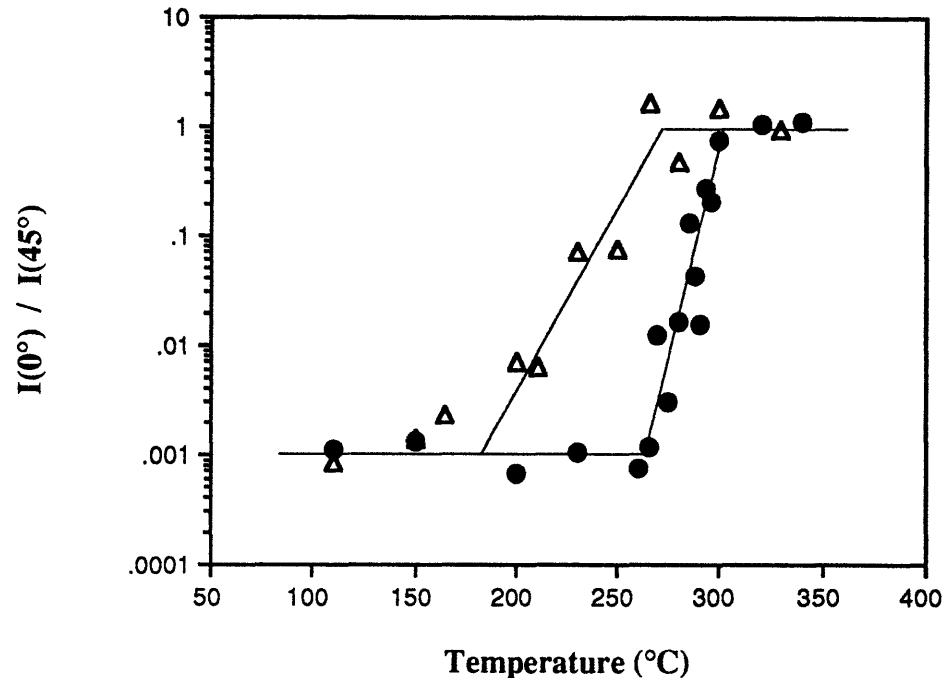


Figure 6.7 $I(0^\circ)/I(45^\circ)$ vs. post-aligning cure temperature for liquid crystals cells produced with polyamide-imide alignment films that have been exposed to LP-UV (triangles) or brushed (circles).

Atomic Force Microscopy

An atomic force microscopy (AFM) image of a Probimide 32 polyamide-imide film irradiated 2 hours with LP-UV is shown in Figure 6.8. There appear to be no microscopic effects of the UV when compared to the AFM of pristine material shown in Chapter 5, Figure 5.13(b). This is in contrast to the brushed films, shown in Figure 5.13(a), which had a rough surface and grooves running in the direction of the brushing.

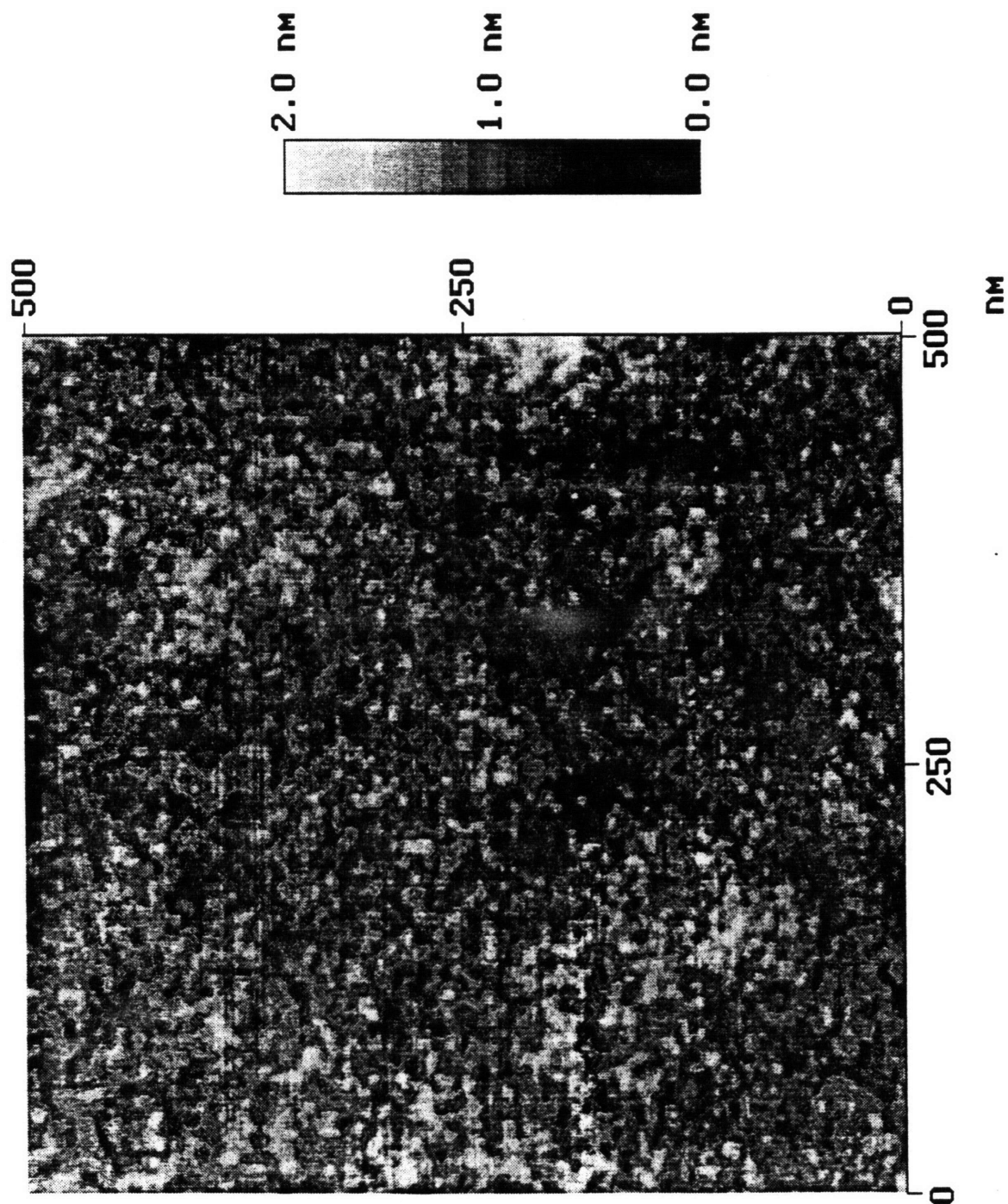


Figure 6.8. Atomic force microscopy (AFM) image of LP-UV irradiated polyamide-imide films.

UV stability of the alignment

The UV stability of the liquid crystal alignment was tested by the following procedure:

1. Many polyamide-imide films were treated with an alignment inducing process, i.e., brushing or LP-UV exposure.
2. The films were then exposed to unpolarized UV, approximately 7mW/cm^2 , for an array of exposure times, at least two films per exposure time.
3. Liquid crystal cells were constructed.
4. $I(0^\circ)/I(45^\circ)$ was measured and plotted vs. post-aligning UV dosage.

Measured values of $I(0^\circ)/I(45^\circ)$ are plotted against post-aligning UV dosage in Figure 6.9. The brushed films did not lose much of their aligning properties for any post-brush UV exposure. This is most likely because the alignment in the brushing alignment process is associated with the physical movement of main chains in the alignment film. Exposure to UV was apparently not sufficient to destroy the aligning characteristics of the film.

For the LP-UV aligned layers, however, subsequent unpolarized UV exposure appears to damage the ability of the polyamide-imide films to align the liquid crystals. This experiment indicates that the LP-UV does not align the liquid crystals via the physical movement of main chains. If that were the case, the unpolarized UV should not be able to reverse the alignment, as it did not in the case of brushed films. Alternatively, if the LP-UV exposure produces alignment by scissioning the polymer preferentially along one axis, it is possible that further exposure of the material to unpolarized UV might act to deplete the groups that are otherwise unaffected by the LP-UV, thus mitigating the aligning impact of the LP-UV.

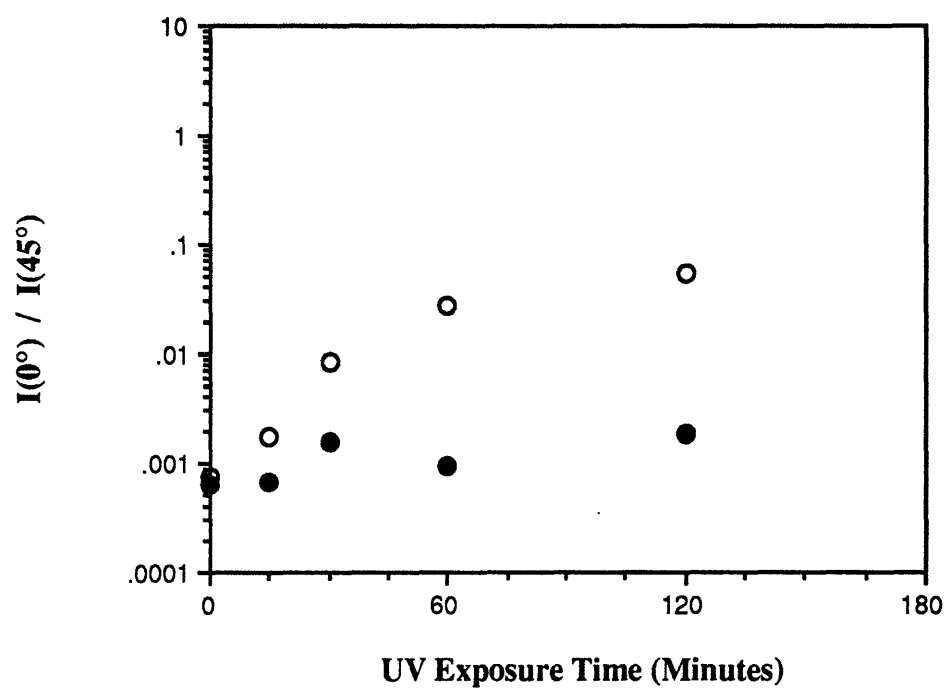


Figure 6.9. $I(0^\circ)/I(45^\circ)$ vs. post-aligning unpolarized UV exposure time for liquid crystal cells produced from polyamide-imide alignment films that were exposed to LP-UV (open circles) or brushed (filled circles).

6.4. Conclusions

The parallel alignment of nematic liquid crystals has been accomplished by use of a polyamide-imide alignment film that has been exposed to linearly polarized short wavelength ultraviolet ($\lambda = 254$ nm). Alignment was produced within minutes of exposure and was maintained with very long exposures. Alignment layer relaxation and Fourier transform infrared spectroscopy studies suggest that the short wavelength UV causes chain scission in the polyamide-imide, though it is difficult to speculate at this time as to the mechanism of alignment. Unlike the brushing technique, neither macroscopic grooves nor bulk orientation of the main chains are produced in the polymer films by the LP-UV. While brushing-induced alignment appears to be stable upon exposure to unpolarized short wavelength UV, the UV-induced alignment appears to be damaged by subsequent exposure of the bare alignment films to unpolarized short wavelength UV.

6.5. Subjects for further work

It was the goal of this research to demonstrate a new way of aligning liquid crystals and to gain some better understanding into the science of liquid crystal alignment. Though these goals were accomplished, this research has opened doors to topics for further investigation. They are listed below, and are divided between the practical and scientific questions. It will be quite interesting to see whether or not, over the next 5-10 years, these questions are answered.

Can effective commercial devices be produced in an economical way via a photo-alignment process? This raises many questions.

1. Can adequate surface pretilt be produced by a photo-aligning technique? And how might one go about producing surface pretilt by a photo-aligning process? Might alkyl side groups added to the repeat unit of the polymer or oblique irradiation of the alignment film produce pretilt?
2. Can the speed of the photo-alignment process be improved such that it is comparable to brushing? And how might one go about speeding it up? Will increasing the intensity or adding a radical initiator work?

3. Can a commercial display with adequate switching speed and device lifetime be manufactured via a photo-alignment technique?
4. If other polymers can be used in photo-alignment processes, how do they compare to the polyamide-imide in terms of the alignment strength produced and the window of exposure dosage required?
5. Will the photo-alignment work with other types of nematic liquid crystals or in other liquid crystal technologies? Can it be used to align smectic or ferroelectric liquid crystals? Can the photo-alignment approach be used in polymer dispersed liquid crystal displays?

What is the mechanism of photo-alignment? This is probably a more difficult question which probably also requires more insight into how the brushing-induced alignment works. This raises the following questions:

1. What types of polymers produce liquid crystal alignment by the brushing process, and which ones do not? Why?
2. What polymers have liquid crystal *photo-aligning* properties? What, then, are the characteristics of these polymers?
3. How do liquid crystals interact with brushed polymer surfaces, and how does this compare with the way they interact with LP-UV exposed polymer surfaces? Can this be investigated by molecular modeling, second harmonic generation experiments, or other surface sensitive techniques?
4. If brush-induced alignment has been suggested to be associated with crystallization, is it possible that the UV produces surface crystallization?
5. Though the dichroic FTIR experiments could not detect anisotropy in LP-UV exposed films, might there be other techniques that can? Is the orientation too small to detect? Does it occur in only the first monolayer? Or might there be no dipolarity at all?

6.6. References

1. M. Schadt, K. Schmitt, V. Kozinkov, and V. Chigrinov, *Jpn. J. Appl. Phys.*, **31(7)**, 2155 (1992).
2. M. Hasegawa and Y. Taira, *Rec. SID Int. Disp. Res. Conf.*, 213 (1994).
3. H. Kambe, in *Aspects of Degradation and Stabilization of Polymers*, Ch. 8, H. Jellinek, Ed., Elsevier, Amsterdam (1978).

Appendix A. Description of Nematic Alignment in Terms of the Poincare Sphere

A.1. The Poincare sphere

The Poincare sphere [1,2] is a geometrical construction upon which any polarization state can be described. Every latitudinal / longitudinal coordinate represents a different polarization state. As shown in Figure A.1, the lines of latitude describe the handedness and ellipticity (β) of the electric field vector. Light in the northern hemisphere is left handed, while light in the southern hemisphere is right handed. The closer to the equator, the lower is β . At the equator, $\beta = 0$, and the light is linearly polarized. At the poles, $|\beta| = 1$, the north pole representing left circularly polarized light, and the south pole representing right circularly polarized light. The equator is defined as 0° latitude, the south pole $+90^\circ$ latitude, the north pole -90° latitude. The ellipticity β is related to latitude (\mathbf{l}) by equation (1).

$$\mathbf{l} = 2 \arctan \beta \quad (1)$$

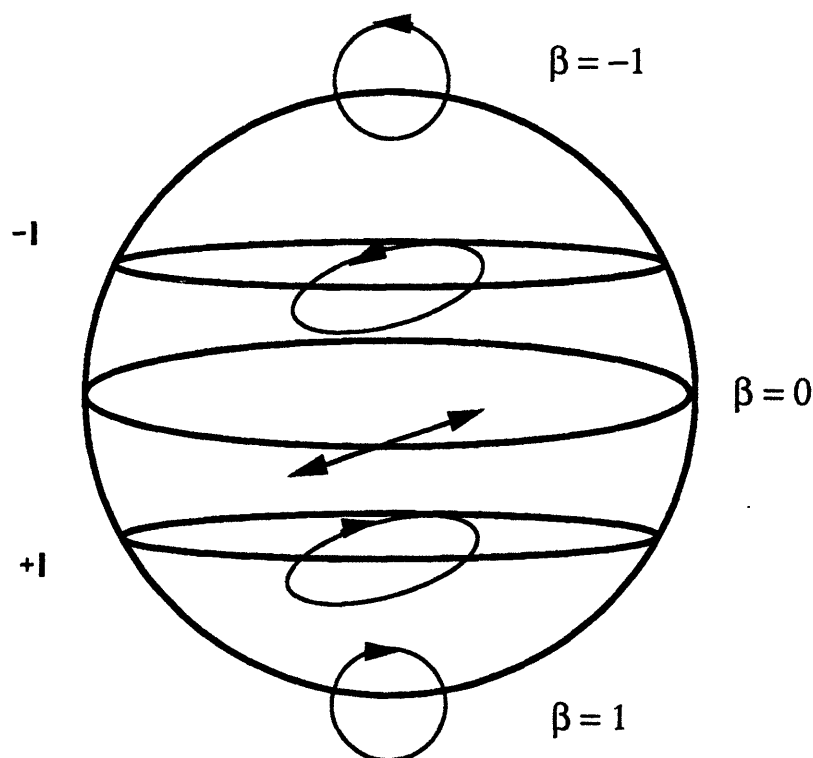


Figure A.1. Lines of latitude (\mathbf{l}) on the Poincare sphere representing ellipticity (β).

As shown in Figure A.2, the lines of longitude represent different azimuthal angles. The prime meridian, 0° longitude, is the point where the azimuthal angle is 0° , i.e., parallel to the axis of reference. The azimuth (α) increases as we travel clockwise from 0° longitude, as described in equation (2), where L represents degrees longitude.

$$L = 2 \alpha \quad (2)$$

Thus, two points along the equator separated by 180° longitude represent two linearly crossed polarized states.

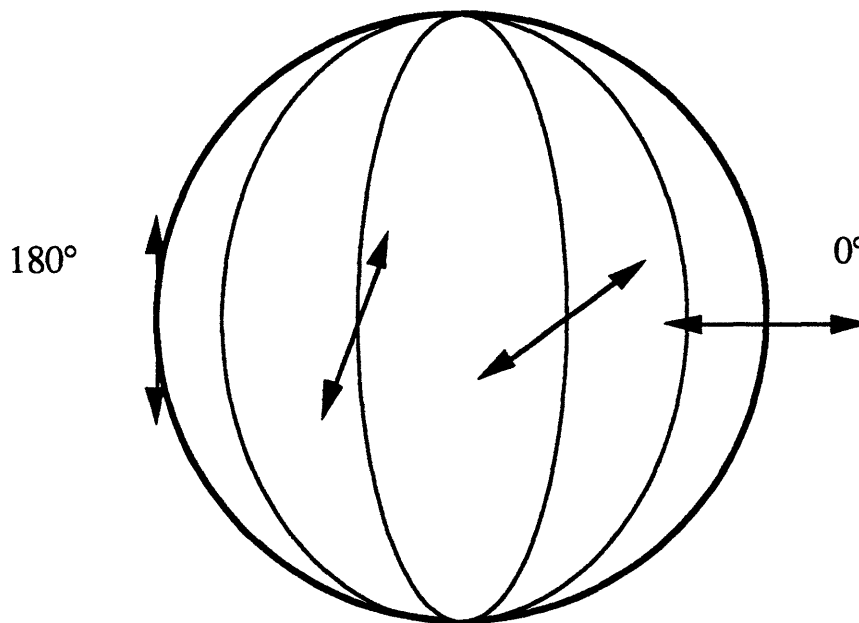


Figure A.2. Lines of longitude (L) on the Poincaré sphere representing azimuth (α).

A.2. Changes in polarization state on the Poincaré sphere

As light passes through a substance, the state of polarization of the light can change. Such a change can be represented by a relative positional change along the surface of the Poincaré sphere. If the light transverses multiple layers, the construction can be repeated as many times as needed to determine the final polarization state. We begin at a given point on the sphere. Movement on the sphere proceeds, in general, along an appropriate circle on the surface of the sphere. (Equivalently, we can fix the initial point and rotate the sphere along an appropriate axis.)

The polarization state of the light passing through the polarizer is quite easy to find on the Poincare sphere. The emerging light is linearly polarized, and thus, rests on the equator. For convenience, we can define this as zero azimuth, and place the initial state at 0° latitude and 0° longitude.

The change in polarization state as the light passes through a birefringent sample, i.e., an aligned LC film, is found as shown in Figure A.3. First, we locate the point P which represents the polarization state of the light before it enters the sample, that is, linearly polarized light. Having chosen point P as our point of reference, movement along the sphere proceeds as follows. We locate the point S which represents the fast vibration axis of the retarding material. In the parallel aligned liquid crystal cell, this would be the location on the equator which is perpendicular to the nematic director. Then, we draw the small circle on the surface of the Poincare sphere which intersects P and is normal to OS, the radial vector through S. The polarization state of the light after it has passed through the sample is found by traveling from P clockwise (looking from S) along the circle an arc length equal to δ given in equation (24) of Chapter 1. We can, of course, produce the same result by fixing the initial point in space and rotating the sphere about OS.

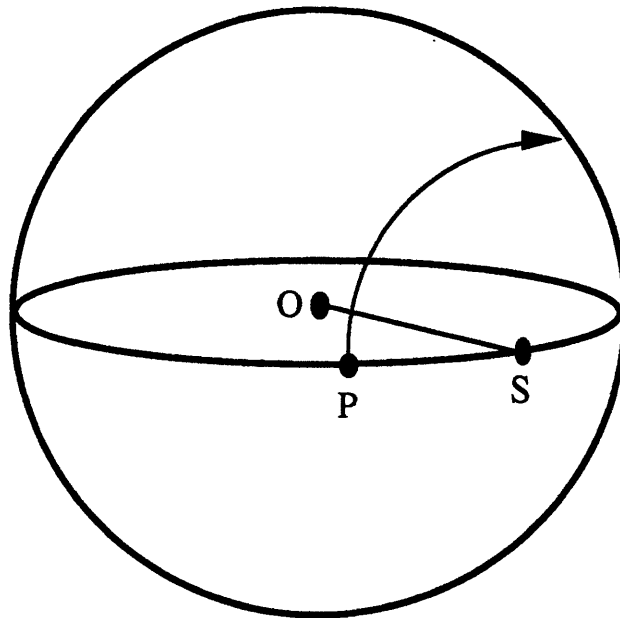


Figure A.3. Movement along the Poincare sphere from reference point P along the small circle of the sphere centered on OS, where O is the center of the sphere and S represents the azimuthal angle parallel to the fast vibration axis of the crystal.

As shown in Figure A.4, the change in polarization state as the light passes through the analyzer is found by moving along the small circle on the surface of the sphere which is in the plane normal to the pole-to-pole axis. In other words, we make purely a longitudinal shift along a line of latitude. The arc length moved is twice the azimuthal angle of the analyzer. We can, equivalently, fix the initial point and rotate the sphere about the polar axis.

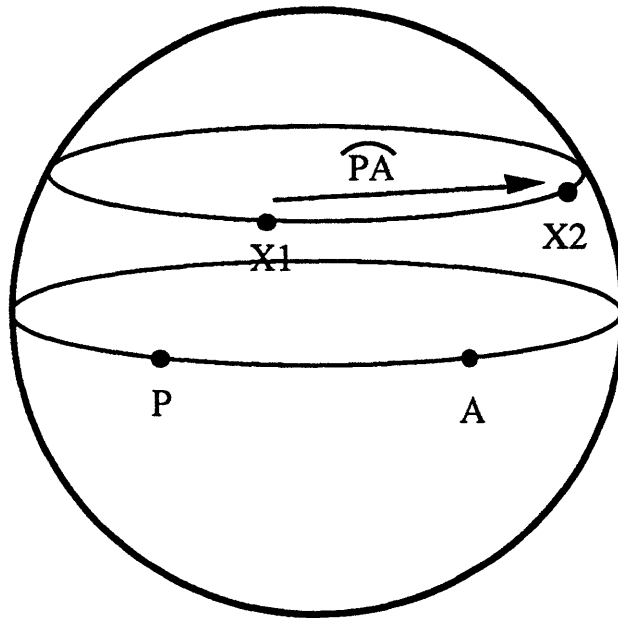


Figure A.4. The relative change in polarization state induced by the analyzer is a longitudinal shift through the arc length between the analyzer (A) and the point of reference (P). X1 moves to X2.

In Figure A.5, we suppose the position on the Poincaré sphere to have moved from P1, position of the polarizer, to P2, after having passed through the sample, and then to P3, after passing through the analyzer. The intensity of the light leaving the analyzer I/E^2 is shown by Jerrard [2] to be given by the simple expression in equation (2).

$$I/E^2 = \cos^2 \rho \quad (2)$$

In equation (2), 2ρ is the arc length between the reference point (P1) and final point (P3).

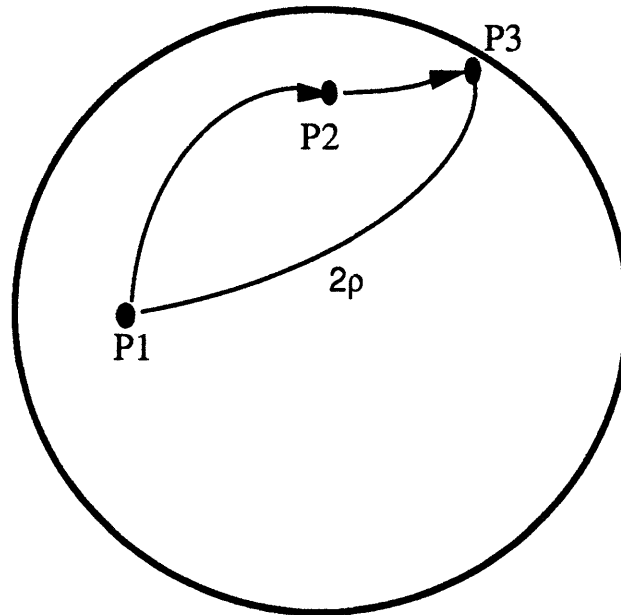


Figure A.5. The arc length from reference state P1 to final state P3 is given by 2ρ . The intensity transmitted by the system is $\cos^2\rho$ where full intensity is unity.

A.3. Examples of LC nematic orientation

Figure A.6 depicts the case in which the polarizer and analyzer are crossed, and the liquid crystal plate is oriented with the nematic vector parallel to the polarizer. Points P, A, and S represent the axes of the polarizer, analyzer, and fast vibration axis respectively. There is no change in polarization state as the light passes through the sample because S is diametrically opposed to P. Because the polarization state remains diametrically opposed to A, position of the analyzer, no light is transmitted. In other words, the analyzer in azimuth 90° imposes a 180° longitudinal shift. The arc length π represents 2ρ , and by equation (2), the intensity transmitted by the analyzer is zero, i.e. $\cos^2(\pi/2)$.

Figure A.7 depicts the case in which the nematic vector is 45° with respect to the polarizer. While the circle in Figure A.7 represents the equator, the line through the middle represents the prime meridian. As light from the polarizer is transmitted through the sample, the polarization state of the light moves from the linearly polarized state at point P to the elliptically polarized state at point E. In this geometry, light is permitted to pass with the intensity given by equation (2). Note that a 45° sample orientation has the unique property of imposing no change in the azimuth of the light ray.

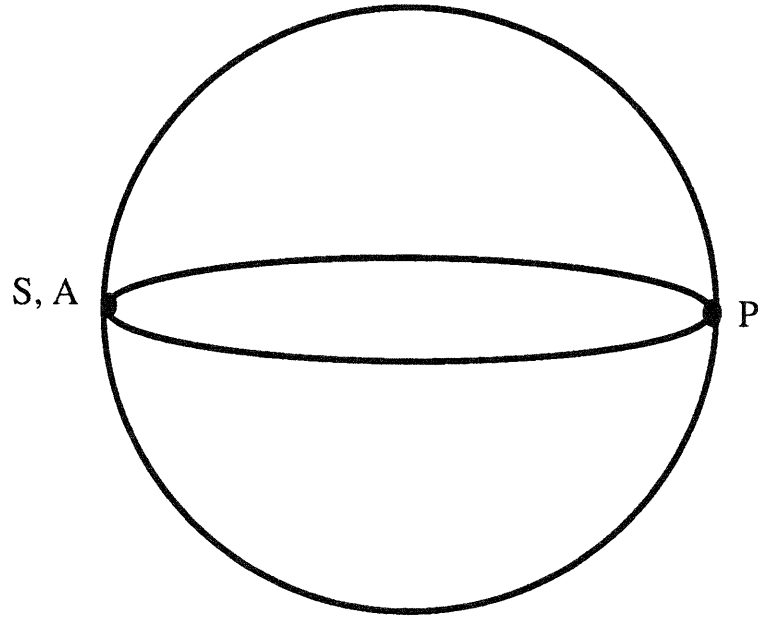


Figure A.6. Parallel aligned LC plate with nematic vector parallel to P.

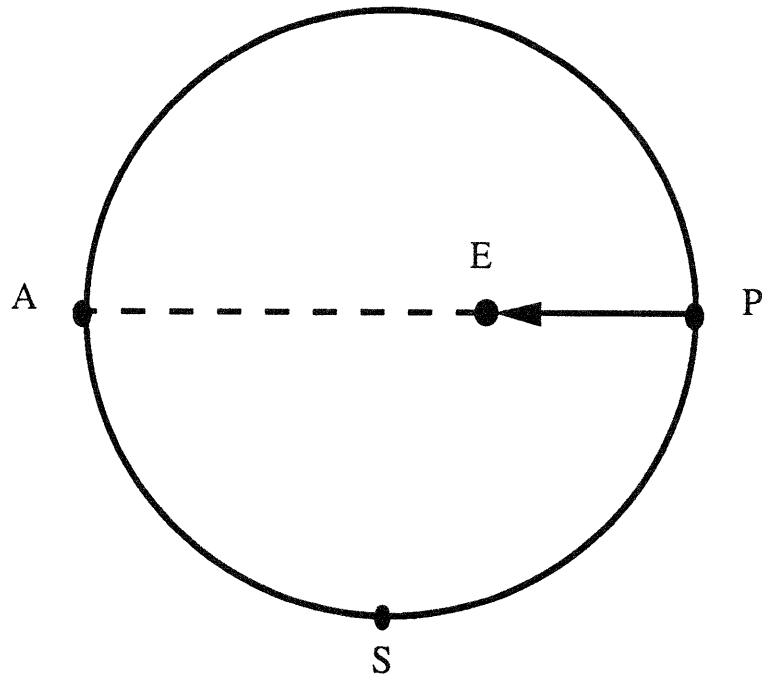


Figure A.7. LC cell with nematic vector 45° with respect to P and A. The light is elliptically polarized by the sample as it moves along the prime meridian to point E.

A.4. Effect of misalignment of the liquid crystals

Figure A.8 demonstrates the effect of inhomogeneous phases on the polarization state of light as represented on the Poincaré sphere. In Figure A.8, the alignment director is parallel to the polarizer. In an ideally aligned system, the final polarization state will be a single point A with reference to end point arc length $2\rho = 180^\circ$ (and $\cos^2\rho = 0$). Unique inhomogeneous phases, on the other hand, will create a distribution of polarization states on the surface of the sphere deviating from the single point A. Hence, the observed intensity will be greater than $\cos^2(90^\circ)$.

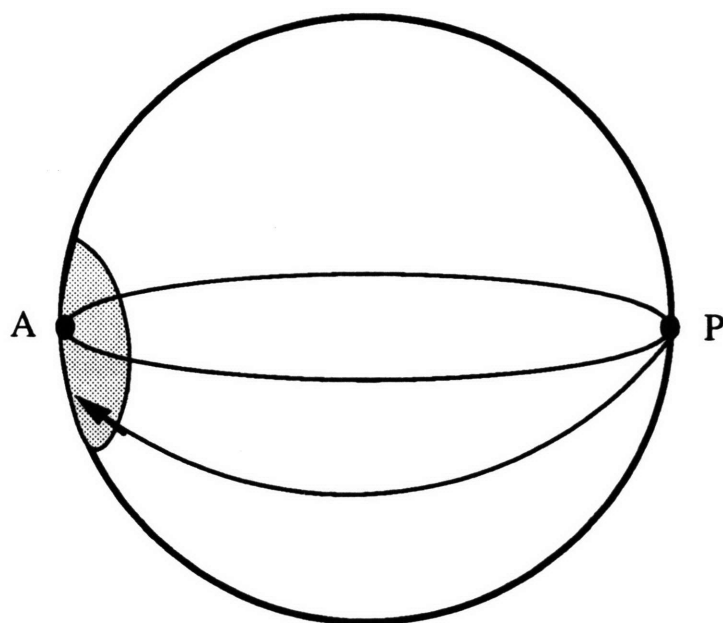


Figure A.8. Effect of random inhomogeneous region on the Poincaré sphere analysis. The shaded region represents a distribution of polarization states deviating from A.

A.5. References

1. C. Viney, *Transmitted Polarised Light Microscopy*, McRone Research Institute, Chicago (1990).
2. H. Jerrard, *J. Opt. Soc. Am.*, **44**(8), 634 (1954).